Multifaceted Engineering of Adhesive Hydrogel Devices

Zhenwei Ma

Department of Mechanical Engineering

McGill University, Montreal

April 2022

A thesis submitted to McGill University in partial fulfillment

of the requirements for the degree of Doctor of Philosophy

Abstract

Hydrogel adhesion with both synthetic biomaterials and biological tissues has significant implications in biomedical device functionalization and regenerative medicine. Devices strongly bonded with tough yet soft tissue-mimetic hydrogels, when interfaced with tissues in human body, can remedy the damage and irritation caused by the mechanically mismatched stiff biomaterials. The robust integration of such hydrogels with damaged or degenerated tissues can further serve as a functional interface and therapeutic intervention strategy to potentially accelerate tissue healing and rehabilitation.

However, it remains a major challenge to achieve tough wet adhesion between hydrogels and other materials. In clinical settings, even more hurdles need to be overcome considering the stringent regulations on the biocompatibility of the hydrogels/devices and the complex biomechanical environment they may encounter in vivo. To this end, this thesis focuses on the multifaceted design and engineering of tough adhesion between hydrogels, tissues, and biomedical devices, and explores the functionalization of the hybrid devices for advanced wound management.

First, we propose a new paradigm to engineer tough bioadhesion of hydrogels with unprecedented controllability. Our strategy leverages low-frequency ultrasound (US) and various anchoring primer materials (nanoparticles, proteins and polymers) to form tough adhesion between hydrogels and tissues spatiotemporally without any chemical reactions. We discover that the highly localized and transient effects of US-induced cavitation enable spatial control of tough bioadhesion, validated by both experiments and finite element simulations. We further demonstrate the on-demand removal of bioadhesives using US and their applications for sustained transdermal drug delivery.

Next, inspired by tendon endotenon sheath, we propose a versatile strategy to functionalize fiber-based devices such as sutures. This strategy seamlessly unites surgical sutures, tough gel sheath, and various functional materials. Robust modification is demonstrated with their strong interfacial adhesion. The surface stiffness, friction, and drag of the suture when contacted with tissues can be markedly reduced, without compromising the tensile strength. Versatile functionalization of the suture for infection prevention, wound monitoring, drug delivery, and near-infrared imaging is then presented.

The last part of the thesis proposes a novel design of gel adhesive puncture-sealing (GAPS) suture device for tissue closure and sealing. Applied at its dry state, the GAPS suture device can rapidly swell and adhere to the surrounding tissues to seal the puncture hole. We study the constrained swelling of hydrogels and the achieved tissue adhesion energy with experimental analysis. We further highlight various advantages of the GAPS sutures for the repair of mechanically active meniscus tissues ex vivo, by preventing gap formation, stress concentration and local tissue damage owing to the achieved strong integration of tissue, hydrogel, and biomaterial.

Résumé

L’adhérence d'hydrogels avec des biomatériaux synthétiques et des tissus biologiques a des implications importantes dans l’utilisation des dispositifs biomédicaux mais également en médecine régénérative. L’utilisation d’hydrogels mimant des tissus résistants et souples, lorsque mis en interaction avec les tissus du corps humain, peuvent remédier aux dommages et à l'irritation causée par les biomatériaux trop rigides et mécaniquement incompatibles. L'interaction robuste de ces hydrogels avec des tissus endommagés ou dégénérés peut en outre servir d'interface fonctionnelle et d’agent thérapeutique pour potentiellement accélérer la guérison et la réhabilitation des tissus humais sous-jacent.

Cependant, il persiste un défi majeur pour obtenir une adhérence efficace, en milieu humide, entre les hydrogels et d'autres matériaux. En milieu clinique, encore plus d'obstacles doivent être surmontés compte tenu des réglementations strictes sur la biocompatibilité des hydrogels, des dispositifs et de l'environnement biomécanique complexe que l’on rencontre *in vivo*. Dans le but de répondre à ce défi, cette thèse se concentre sur la conception et l'ingénierie des multiples facettes d’adhérence robuste entre les hydrogels, les tissus et les dispositifs biomédicaux, et explore la fonctionnalité des dispositifs hybrides pour la gestion avancée des plaies.

Tout d'abord, nous proposons un nouveau paradigme pour concevoir, avec un contrôle sans précédent, une bioadhésif d’hydrogel robuste. Notre stratégie utilise des ultrasons (US) à basse fréquence et divers matériaux d'amorce d'ancrage (nanoparticules, protéines et polymères) pour former une adhérence solide entre les hydrogels et les tissus de manière spatio-temporelle sans aucune réaction chimique. Ceci permettant une adhérence au niveau de l’interface pouvant atteindre plus de 1500 J/m^2. Nous découvrons que les effets hautement localisés et transitoires de la cavité induite par les US permettent un contrôle aisé de la bioadhérence, ceci étant prouvé à la fois par des expériences et à la fois par des simulations sur éléments finis. De plus, nous démontrons l'élimination à la demande des bioadhésifs à l'aide des US et leurs applications en terme d'administration transdermique progressive de médicaments.

Ensuite, nous proposons une stratégie polyvalente inspirés de l’endotenon pour améliorer les dispositifs à base de fibres tels que les sutures. Cette stratégie unit de façon harmonieuse des sutures chirurgicales, une gaine de gel résistante et divers matériaux fonctionnels. Une modification plus robuste est démontrée au niveau de l’interface avec une amélioration majeure

de l’adhérence. La rigidité de surface, la friction et la traînée de la suture lorsqu'elle est en contact avec les tissus peuvent être considérablement réduites, sans compromettre la résistance à la traction. Les fonctions polyvalentes de la suture en matière de prévention des infections, de maintien des plaies, de libération de médicaments ainsi que son imagerie dans le proche infrarouge sont ensuite présentées.

La dernière partie de la thèse propose un nouveau concept de dispositif de suture GAPS (gel adhésif puncture-sealing) pour la fermeture et le colmatage des tissus. Appliqué à l'état sec, le dispositif de suture GAPS peut rapidement s’expandre par la suite et adhérer aux tissus environnants pour sceller et remplir le trou de ponction de l’anguille utilisée. Nous étudions donc le gonflement limité des hydrogels et l’énergie d'adhésion tissulaire obtenue avec d’une part une analyse expérimentale et d’autre part une modélisation analytique.

Nous rapportons également divers avantages des sutures GAPS pour la réparation du tissus méniscal, possédant une biomécanique toute particulière, en *ex vivo*. En effet, les GAPS diminue la formation d'espaces au site lésionnel, mais aussi la concentration de stress et les dommages tissulaires locaux en raison de la forte interaction obtenue entre les tissus, l'hydrogel et les biomatériaux.

Acknowledgements

The last four years are simply joyful and remarkable. In Montréal, this unique and magical city, and at McGill, the adventurous and conservative bubble, I got to meet and work with so many brilliant minds.

First and foremost, I would like to thank my advisor and mentor, Prof. Jianyu Li. It's an utmost pleasure and honor, and almost a privilege to be your first PhD student. It has been such a splendid journey with unexpected (and expected!) discoveries, delightful achievements, and persistent growth. Thanks for being the best mentor I could ever ask for. "*What's past is prologue."* I can't wait to see what we'll achieve in the upcoming years.

To my office buddies in MD352, Zhen, Ran, Chris, Alex, Xuan, Shiyu, Yin, and David-Michael, thanks for making our tiny space the backyard of the lab, where I can layback and have some fun. To Zhen, thanks for teaching me everything mechanics and always be there for me. To Ran, thanks for all the work-out tips and being my best desk mate. To my I2I gang, Chris, Alex and Ran, thanks for making my first attempt in entrepreneurship such a wonderful experience. I wish I could spend some more time with you boys. To Xuan and Yin, thanks for always being so considerate and helping calmly neutralize the sometimes oversaturated "boy energy" in the office. To Shiyu, thanks for your help with all my bloody experiments. To David-Michael, thanks for providing so much positivity and fun in my life. I truly miss our Friday afternoon hangouts.

To my other friends in the Li lab, Guangyu, Shuaibing, and Farshid, thanks so much for all the help and supports over the years. I really enjoyed discussing with you about research ideas, future career goals or just venting on anything Covid-related.

To my collaborators at ETH Zurich, Outi and Claire, thanks for opening my mind and giving me the exposure to the intriguing world of ultrasound and cavitation bubbles. Thanks Outi for your patience in a layman like me, your shared enthusiasm, and your courage for your career and life choices. You're simply inspiring. And to my Zoom-pal Claire, thanks for experimenting all the crazy ideas we had and allowing me to take a peek at a life in Europe. I'll for sure meet you somewhere there, hopefully soon.

On the clinical side, I'd like to thank Qiman, for helping me establish the animal studies in our lab, and being so knowledgeable in all the exciting clinical applications and available resources at

McGill. Thanks Dr. Zu-Hua Gao for your support and trust in me, a passionate yet not that experienced young researcher, even we haven't met that many times. Your humbleness and diligence will be the characters I'm looking up to for life. To our collaborators at CHU Sainte-Justine, Drs. Nault, Mazy and Lamer, thanks for introducing me to the fascinating field of meniscus repair. Dr. Nault, thanks so much for letting me observe your surgeries and patiently teaching me everything related to meniscus. Dr. Lamer, thanks for driving back and forth early in the morning to help getting the bovine meniscus. Dr. Mazy, thanks for being such a compassionate and open-minded surgeon and friend. I really enjoyed all the time we spent in the lab, and of course all the Chinese restaurants. Let's "save the meniscus" together.

To all the undergrads I helped mentor, Tristan, Kieran, Alex (Nguyen), Celia, Anne and Xinyu, I hope that you've learnt something from me, but it won't be as much as I learnt from you. Tristan, thanks for being so true to yourself and embracing a life you dreamt to have. I wish to see your concert very soon. Kieran, thanks for taking the courage to explore a foreign yet intriguing field of quantitative mechanobiology. Thank Alex for being the model undergrad in the lab. You've achieved so much in such a short summer. Have fun in Tokyo. Celia, Anne, and Xinyu, I'm really impressed by your knowledge, diligence, and team spirits, you'll do great things and I can't wait to witness your growth.

To our collaborators at INRS, especially Prof. Ma and Dr. Yang. Thanks for your generosity and guidance to make our bioimaging demonstration possible. Thanks to Prof. Mongeau and everyone in Mongeau lab for their help over the year. I'm very lucky to work in our shared lab space.

Thanks to my friends outside the lab for making my life full of memorable adventures and exclusive details, and for exploring "*une vie ailleurs*" with me.

Most of all, thanks Mom and Dad. Words can't express how much I love you and miss you so dearly. You're my everything.

"So we beat on, boats against the current, borne back ceaselessly into the past."

- F. Scott Fitzgerald

Thesis Organization

This thesis is written and presented in a manuscript-based style, divided into 7 chapters as follows.

Chapter 1 serves as a high-level introduction of the thesis, including a brief overview of my research motivations, rationale and philosophy behind the study design, and a summary of main objectives.

Chapter 2 presents a comprehensive review of relevant literatures in the field of tissue adhesives and their emerging applications. Existing adhesion mechanisms, design considerations, and design strategies are summarized. Their limitations and disadvantages are identified. Future directions for multifaceted engineering and functionalization of bioadhesives are proposed.

Chapter 3 through 5 serve as the main body of the thesis. Chapter 3 proposes a paradigm-shifting technology to enable the unprecedented spatiotemporal controllability of tough adhesion between hydrogels and biological tissues by leveraging low-frequency ultrasound. Chapter 4 proposes a robust and versatile design of tough hydrogel sheath, demonstrating strong integration with diverse biomaterials and facile surface functionalization for various biomedical applications. Chapter 5 proposes a novel hybrid medical device, named gel adhesive puncture sealing (GAPS) sutures, showing promise for effective tissue sealing and enhanced meniscus wound management.

Chapter 6 provides a comprehensive discussion of all the findings, limitations of the reported technologies and future opportunities for improvement.

Finally, Chapter 7 provides final conclusion and remarks, comprising a conclusion encompassing all research findings of this thesis and recommendations for future work.

Contributions to Original Knowledge

The body of work presented in the thesis contains 3 main original contributions to the field of bioadhesives design:

1. ***I proposed a new bioadhesives technology based on low-frequency ultrasound (US) to precisely manipulate tough bioadhesion in strength, location, and time.*** This universal strategy is applicable to different anchoring primers and hydrogels on diverse tissues. This work greatly expands the material repertoire for tough bioadhesion and opens new avenues for bioadhesive technologies with high-level controllability.

   This work is currently in revision for ***Science***:

   Zhenwei Ma, Claire Bourquard, Qiman Gao, Shuaibing Jiang, Tristan De Iure-Grimmel, Ran Huo, Xuan Li, Zixin He, Zhen Yang, Galen Yang, Yixiang Wang, Edmond Lam, Zu-Hua Gao, Outi Supponen*, Jianyu Li*, Controlled tough bioadhesion mediated by ultrasound, ***Science*** (in revision) (2022)
2. ***I proposed a new bioinspired design to enable robust and versatile surface functionalization of fiber-based devices.*** This platform is an important step toward integration of hydrogel technologies, functional materials and fiber-based devices to develop next-generation multifunctional materials. This work would open new avenues for the development of surgical tools, wearable and implantable devices, soft robotics, fiber and textile materials.

   This work is published in ***Science Advances*** in 2021:

   Zhenwei Ma, Zhen Yang, Qiman Gao, Guangyu Bao, Amin Valiei, Fan Yang, Ran Huo, Chen Wang, Guolong Song, Dongling Ma, Zu-Hua Gao, Jianyu Li*. Bioinspired tough gel sheath for robust and versatile surface functionalization. *Science Advances* 7.15 (2021): eabc3012.
3. ***I developed a new biomedical device to enable effective tissue sealing and enhanced wound management of mechanically active tissues.*** The hybrid material system achieves strong adhesion between suture, hydrogel and tissues, presents a novel controlled swelling-adhesion mechanism. This technology validates the proposed bioadhesive design and demonstrates great translational potential for wound closure and regenerative medicine.

   This work is under preparation for submission:

Zhenwei Ma, Alex Nguyen, David Mazy, Christopher Chung-Tze-Cheong, Stéphanie Lamer, Farshid Ghezelbash, Zhen Yang, Yin Liu, Shiyu Liu, Benjamin Freedman, Marie-Lyne Nault*, Jianyu Li*. Gel adhesive puncture-sealing sutures for wound closure. (Under preparation) (2022)

In addition, I have contributed to the following published works during my Ph.D. study (unpublished works are not included here):

1. Zhen Yang, **Zhenwei Ma**, Shiyu Liu, Jianyu Li*. Tissue adhesion with tough hydrogels: Experiments and Modeling. ***Mechanics of Materials*** (2021): 103800.
2. Shiyu Liu, Guangyu Bao, **Zhenwei Ma**, Christian J. Kastrup, Jianyu Li*, Fracture mechanics of human blood clots: Measurements of toughness and critical length scales, ***Extreme Mechanics Letters***, 101444 (2021).
3. Guangyu Bao, Ran Huo, **Zhenwei Ma**, Mitchell Strong, Amin Valiei, Shuaibing Jiang, Shiyu Liu, Luc Mongeau, Jianyu Li*, Ionotronic tough adhesives with intrinsic multifunctionality, ***ACS Applied Materials and Interfaces***, 13 (31), 37849-37861 (2021).
4. Guangyu Bao, Tao Jiang, Hossein Ravanbakhsh, Alicia Reyes, **Zhenwei Ma**, Mitchell Strong, Huijie Wang, Joseph M. Kinsella, Jianyu Li*, Luc Mongeau*, Triggered micropore-forming bioprinting of porous viscoelastic hydrogels, ***Materials Horizons***, 7, 2336-2347 (2020).

Contribution of Authors

The completion of the thesis would not have been possible without the collaborative and supportive research efforts of excellent colleagues and collaborators with diverse backgrounds. This section outlines the scientific contributions of authors for each of the thesis chapters presented herein. Of note, all of the work presented in this thesis greatly benefitted from the inputs provided by and discussions with my Ph.D. advisor and mentor, Prof. Jianyu Li. Both Prof. Li and I conceived the ideas leading to the presented thesis and together we designed the research.

In Chapter 2, most of the work involving initial conceptualization, literature survey, and manuscript writing was done by myself. Guangyu Bao contributed to part of the literature search, data collection and revision regarding one case study and literature survey related to topical applications of tissue adhesives.

This work was published in ***Advanced Materials*** in 2021:

Zhenwei Ma, Guangyu Bao, Jianyu Li*. Multifaceted design and emerging applications of tissue adhesives. ***Advanced Materials*** (2021): 2007663

In Chapter 3, most of the work involving the conceptualization, implementation, characterization, and analysis of the US-mediated tough bioadhesion was done by myself. Prof. Outi Supponen and Dr. Claire Bourquard from ETH Zurich contributed significantly to the in-depth understanding and deciphering of the underlying mechanisms, especially regarding the parts involving US-induced cavitation. Prof. Supponen advised on the experimental characterization design of US-induced microbubble clouds, which was later conducted by me and Dr. Qiman Gao at McGill. Dr. Bourquard carried out the laser induced single-bubble cavitation, its interactions with tissues, and analytic modeling of the pressure field under US transducer. Dr. Qiman Gao and I conducted the animal studies. Shuaibing Jiang contributed significantly to the introduction of a new class of nanomaterials into the materials system compatible with US-mediated bioadhesion. Tristan De Iure-Grimmel assisted with studies regarding the temporal control of bioadhesion and related mechanical testing. Ran Huo assisted with the studies involving the US-induced thermal effects. Xuan Li helped with imaging part of transdermal drug delivery studies. Zixin He characterized the displacement of the US transducer, which was used to support the finite element modeling. Prof. Yixiang Wang provided the valuable cellulose nanocrystals

materials used in the studies. Prof. Edmond Lam provided the valuable chitosan nanocrystals materials used in the studies. Prof. Zu-Hua Gao analyzed all the histological samples. The manuscript for this work was largely written by myself, Dr. Bourquard, Profs. Li and Supponen, with minor modifications from all other contributing authors.

This work is in revision for ***Science*** in 2022:

Zhenwei Ma, Claire Bourquard, Qiman Gao, Shuaibing Jiang, Tristan De Iure-Grimmel, Ran Huo, Xuan Li, Zixin He, Zhen Yang, Galen Yang, Yixiang Wang, Edmond Lam, Zu-Hua Gao, Outi Supponen*, Jianyu Li*, Controlled tough bioadhesion mediated by ultrasound, ***Science*** (in revision) (2022)

In Chapter 4, most of the work involving material design, experimental characterization, application, and demonstration was done by myself. Zhen Yang performed the finite element modeling and analysis. Dr. Qiman Gao and I performed the in vivo studies. Guangyu Bao carried out experiments involving atomic force microscope measurement and scanning electron microscopy characterization. Amin Valiei and I conducted the antibacterial studies. Ran Huo and I designed and implemented the tissue friction and drag measurements. Prof. Dongling Ma and her team members (Dr. Fan Yang, Chen Wang, and Guolong Song) from INRS were in charge of the synthesis of fluorescent nanoparticles; together we demonstrated our platform for bioimaging. Prof. Zu-Hua Gao analyzed all the histological samples. The manuscript for this work was largely written by myself and Prof. Li, with edits by Profs. Zu-Hua Gao and Dongling Ma.

This work was published in ***Science Advances*** in 2021:

Zhenwei Ma, Zhen Yang, Qiman Gao, Guangyu Bao, Amin Valiei, Fan Yang, Ran Huo, Chen Wang, Guolong Song, Dongling Ma, Zu-Hua Gao, Jianyu Li*. Bioinspired tough gel sheath for robust and versatile surface functionalization. *Science Advances* 7.15 (2021): eabc3012.

In Chapter 5, most of the work involving conceptualization, experimental design, and data analysis was conducted by myself. Alex Nguyen contributed tremendously to the generation of the preliminary data for this project. Drs. David Mazy, Stéphanie Lamer, Prof. Marie-Lyne Nault from CHU Sainte-Justine and Christopher Chung are all involved in the ex vivo studies of surgical sutures for meniscus repair. The current version of the manuscript for this work was largely written by me, with edits by Prof. Li.

This work is in preparation for submission in 2022:

Zhenwei Ma, Alex Nguyen, David Mazy, Christopher Chung-Tze-Cheong, Stéphanie Lamer, Farshid Ghezelbash, Zhen Yang, Yin Liu, Shiyu Liu, Benjamin Freedman, Marie-Lyne Nault*, Jianyu Li*. Gel adhesive puncture-sealing sutures for wound closure. (Under preparation) (2022)

Table of Contents

Abstract i

Résumé iii

Acknowledgements v

Thesis Organization viii

Contributions to Original Knowledge ix

Table of Contents xiv

Chapter 1 Introduction 1

1.1 Thesis Motivation 1

1.2 Thesis Rationale 2

1.3 Thesis Objectives 3

Preface to Chapter 2 5

Chapter 2 Background and Literature Review 6

2.1 Introduction 6

2.2 Design Principles of Biomaterials Bioadhesion 8

2.3 Delivery Approaches 24

2.4 Degradability 30

2.5 Emerging Applications of Bioadhesives and Devices 31

References 52

Preface to Chapter 3 85

Chapter 3 Controlled Tough Bioadhesion with Ultrasound 86

Abstract 86

3.1 Introduction 86

3.2 Results and Discussion 86

3.3 Materials and Methods 96
3.4 Supporting Information 103
References 110
Preface to Chapter 4 113
Chapter 4 Bioinspired Tough Gel Sheath for Biomaterials Surface Functionalization 114
Abstract 114
4.1 Introduction 114
4.2 Design and Fabrication of Tough Gel Sheathed (TGS) Sutures 117
4.3 Experimental Investigation of Strong Suture-Sheath Bonding 119
4.4 Finite Element Modeling of Suture-Sheath Adhesion 121
4.5 Wide Applicability of TGS Design 121
4.6 Characterization of TGS Suture Biomechanical Properties 123
4.7 In Vivo Biocompatibility and Wound Closure 126
4.8 Versatile Functionalization of TGS Sutures 127
4.9 Discussions and Conclusions 130
4.10 Conclusions 132
4.11 Materials and Methods 133
References 156
Preface to Chapter 5 160
Chapter 5 Gel Adhesive Puncture-Sealing Sutures for Wound Closure 161
5.1 Introduction 161
5.2 Results and Discussions 163
5.3 Conclusion 172
5.4 Materials and Methods 172

Reference 175
Chapter 6 Discussions 180
6.1 Adhesive Substrate 180
6.2 Adhesive Layer 181
6.3 Adhesive Matrix 182
6.4 External Apparatus 183
6.5 Translational Potential 184
6.6 Future Work 185
Chapter 7 Conclusion and Remarks 188
References 189

Chapter 1 Introduction

1.1 Thesis Motivation

Most human tissues are soft, wet, and bioactive; yet existing traditional biomaterials, including metals, plastics, and elastomers, for topical and implantable usage are often stiff, dry, and biologically inert. Achieving the ultimate biointegration of native tissues and man-made materials is of imminent significance in addressing grand societal challenges in healthcare, sustainability, and beyond. However, interfacing human and synthetic materials is long bottlenecked by their fundamentally incompatible mechanical, chemical and biological properties.

Hydrogel adhesives are emerging material innovations that can potentially serve as a biomimetic interface between biological tissues and synthetic biomaterials, since they can be designed to be soft, wet, and bioactive (*1*). The engineered hydrogel bioadhesion thus has potentially significant implications in biomedical device functionalization and regenerative medicine (*2*). Despite the recent surge of interests in bioadhesion (*3*–*8*), it remains a vital challenge to integrate diverse synthetic biomaterials, hydrogels, and biological tissues easily and robustly. Markedly enhanced biomechanical and biochemical compatibility of these bioadhesives with native tissues are anticipated, but they are yet to be validated and demonstrated for the repair of mechanically active musculoskeletal tissues, such as IVD and meniscus.

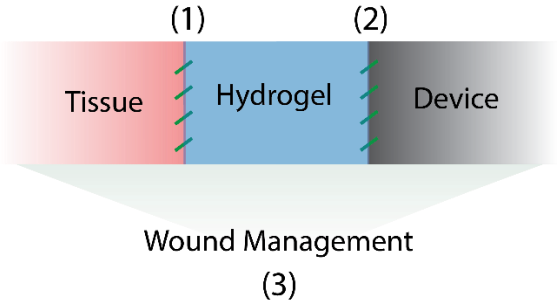

Figure 1.1 Schematic high-level overview of the thesis.

To this end, this thesis focuses on the multifaceted design and engineering of tough adhesion between hydrogels, tissues, and biomedical devices, and explores the functionalization of the hybrid devices for advanced wound management (Figure 1.1).

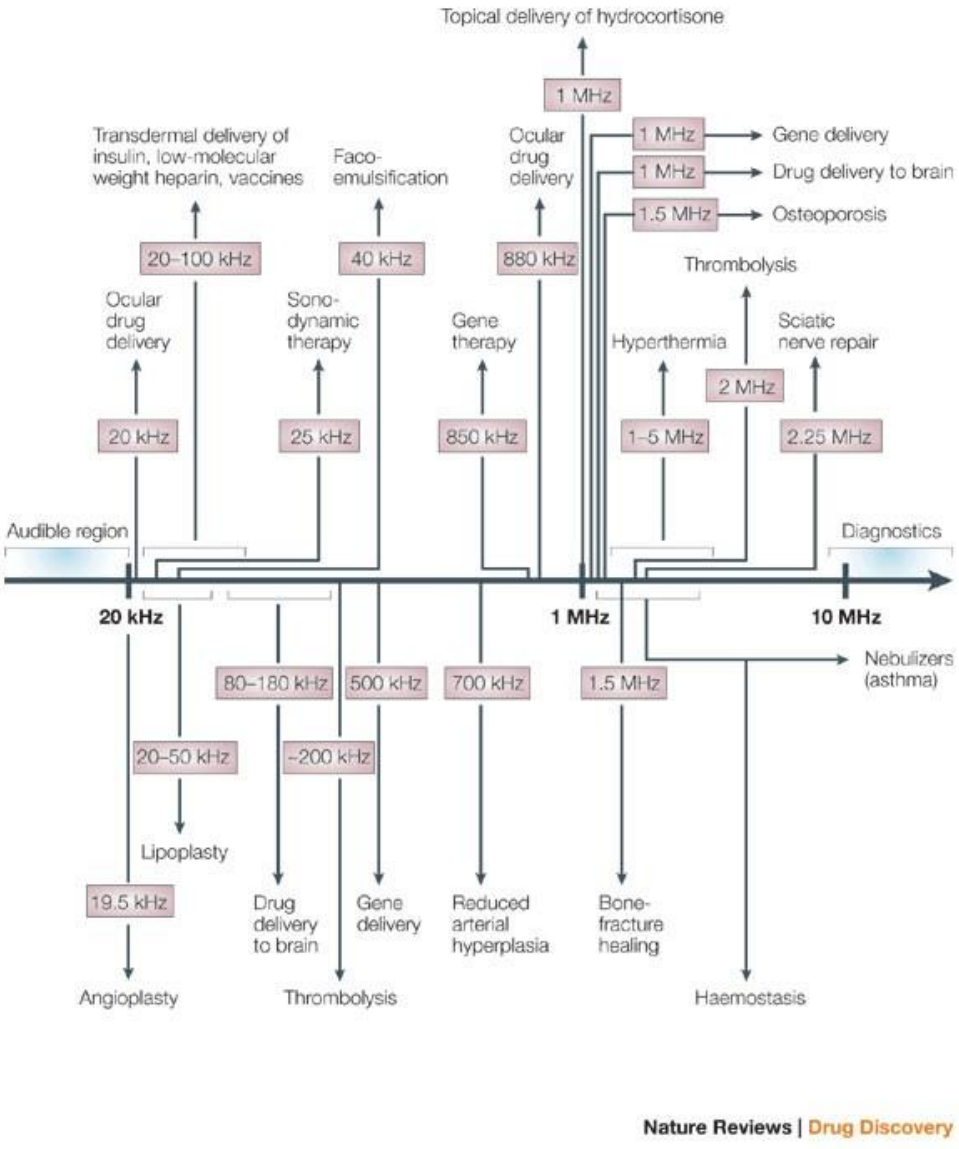

Figure 1.2 A partial summary of ultrasound frequencies used for medical applications. (*9*)

1.2 Thesis Rationale

To expand the material repertoire and toolbox available for designing tough adhesive hydrogels, one needs to understand and/or reinvent the fundamental interfacial adhesion mechanisms and design principles. With a final goal of fabricating complex multifunctional bioadhesive hydrogel devices for tissue repair, a bottom-up approach will be adopted to deconstruct bioadhesives design elements, and reverse-engineer tough adhesion between hydrogels, other biomaterials and biological tissues. Multifunctionality will be finally introduced by incorporating functional materials at various length scales.

1.3 Thesis Objectives

By merging disciplines of mechanics, chemistry and biology, through bioinspired and biomimetic materials innovation, this thesis focuses on (1) developing a platform technology and material system to manipulate hydrogel adhesion with biological tissues with unprecedented controllability; (2) developing a platform technology and material system to engineer tough adhesion and functionalization of various sutures and hydrogel; (3) developing a swellable adhesive hydrogel coated suture device for wound management of meniscal tear. They're detailed as follows:

(1) Tough adhesion of bioadhesives and biological tissues has been long bottlenecked by the limited passive diffusion due to the recognized barrier effects of various tissues. Apart from being traditionally used for diagnostic imaging, ultrasound (US) has found various new forms of therapeutic applications for treating thrombosis, skin wounds, bone fractures, cancer diabetes, stroke, cardiovascular diseases, and infections (*9*) (Figure 1.2). The US in a range of kHz range has been suggested to induce prominent non-invasive mechanical effects to breach the natural barrier within our human body (*10*). We thus hypothesize that these low-frequency US could potentially facilitate the enhanced diffusion and anchoring of adhesives to achieve robust interfacial adhesion between hydrogels and biological tissues with mitigated barrier.

We propose a new paradigm to engineer hydrogel tough bioadhesion with unprecedented controllability. Our strategy leverages low-frequency US and various anchoring primer materials (nanoparticles, proteins and polymers) to form tough adhesion between hydrogels and tissues spatiotemporally without any chemical reactions. We discover that the highly localized and transient effects of US-induced cavitation enable spatial control of tough bioadhesion, validated by both experiments and finite element simulations. We further demonstrate the on-demand removal of bioadhesives using US and their applications for sustained transdermal drug delivery.

(2) Tough adhesion between hydrogels and fiber-based biomedical devices, such as surgical sutures, can potentially mitigate the mechanical mismatch, damage and wear to the native soft tissues caused by the stiff suture fibers. These integrated robust hydrogel sheath can also potentially be further engineered with diverse multifunctions for the advanced diagnostic, monitoring, and therapeutic intervention of the closed wound bed.

Inspired by tendon endotenon sheath, we propose a versatile strategy to functionalize fiber-based devices such as sutures. This strategy seamlessly unites surgical sutures, tough gel sheath, and

various functional materials. Robust modification is demonstrated with their strong interfacial adhesion. The surface stiffness, friction, and drag of the suture when contacted with tissues can be markedly reduced, without compromising the tensile strength. Versatile functionalization of the suture for infection prevention, wound monitoring, drug delivery, and near-infrared imaging is then presented.

(3) Tough adhesion between biomedical devices, such as sutures, and biological tissues has been a critical challenge to fully realize the therapeutic potential of the implanted devices for regenerative medicine. Considering the indispensable role of surgical suture for repairing mechanically active tissues, including musculoskeletal and gastrointestinal tissues, we hypothesize that by engineering an adhesive hydrogel layer between sutures and tissues of interest could enable the intimate biointegration for effective sealing and assistive mechanotherapy.

The last part of the thesis proposes a novel design of gel adhesive puncture-sealing (GAPS) suture device for wound closure and sealing. Applied at its dry state, the GAPS suture device can rapidly swell and adhere to the surrounding tissues to seal a puncture hole. We study the constrained swelling of hydrogels and the achieved tissue adhesion energy with experimental investigations. We further demonstrate various advantages of the GAPS sutures for the repair of mechanically active meniscus tissues ex vivo, by preventing gap formation, stress concentration and local tissue damage owing to the achieved strong integration of tissue, hydrogel, and sutures.

Preface to Chapter 2

Although surgical suturing remains to be the gold-standard wound closure materials, as alternatives, bioadhesives have been applied in certain clinical settings as sealants and dressings. However, they usually suffer from disadvantages such as weak cohesive, adhesive mechanical properties and limited therapeutic functions. With the new understanding of biomaterials chemistry and mechanics, and how biomaterials can be applied to biomechanically, biochemically and bioelectronically interface with biological tissues, a roster of novel adhesive hydrogel devices has been actively developed recently.

In Chapter 2, we propose multifaceted design strategies of tissue adhesives, by identifying the three key elements of the adhesives material system: the adhesive substrate, the adhesive surface, and the adhesive matrix, and thoroughly discussing their contribution and design principles. Apart from tissue sealing and on-demand detachment, emerging applications of the tissue adhesives are introduced, including advanced wound management, musculoskeletal tissue repair, and cardiovascular system interface. Future directions toward next-generation tissue adhesives are also discussed.

This chapter has been published as a *Progress Report* in ***Advanced Materials***:

Zhenwei Ma, Guangyu Bao, Jianyu Li*. Multifaceted design and emerging applications of tissue adhesives. ***Advanced Materials*** (2021): 2007663

Chapter 2 Background and Literature Review

Abstract

Tissue adhesives, or bioadhesives, can form appreciable adhesion with biological tissues and have found clinical use in a variety of medical settings such as wound closure, surgical sealants, regenerative medicine, and device attachment. The advantages of bioadhesives include ease of implementation, rapid application, mitigation of tissue damage, and compatibility with minimally invasive procedures. The field of tissue adhesives is rapidly evolving, leading to tissue adhesives with superior mechanical properties and advanced functionality. Such adhesives enable new applications ranging from mobile health to cancer treatment.

To provide guidelines for the rational design of tissue adhesives, this chapter synthesizes existing strategies for tissue adhesives into a *multifaceted* design, which comprises three design elements: the tissue, the adhesive surface, and the adhesive matrix. We review the mechanical, chemical, and biological considerations associated with each design element. Throughout the literature review, we discuss the limitations of existing tissue adhesives and immediate opportunities for improvement. We highlight the recent progress of tissue adhesives in topical and implantable applications and then outline future directions toward next-generation tissue adhesives. The development of tissue adhesives will fuse disciplines and make broad impacts in engineering and medicine.

2.1 Introduction

Tissue adhesives can adhere to biological tissues (*1–5*) and are widely used for a variety of medical applications such as wound closure, surgical sealants, device attachment, repair and regeneration of injured or degenerated tissues. Since the introduction of fibrin glues in the 1940s, the roster of tissue adhesives has expanded with a number of formulations and delivery approaches (e.g., preformed patches, glues, paste, sprays) (*6*). Meanwhile, the associated annual global market is rapidly increasing with a growth rate of 9.7% and is expected to exceed 15 billion US dollars by 2024 (*7*). In clinical settings, the primary function of tissue adhesives is currently to complement sutures, stitches, and staples for wound closure. Apart from providing mechanical support, tissue adhesives are under intense development to integrate advanced functionality for emerging applications, including bleeding control (*1*, *8*), regenerative medicine (*9–11*), cancer therapy (*12*, *13*), and health monitoring (*14*).

The advantages of tissue adhesives are manifold, compared to other surgical techniques like suturing. Many tissue adhesives are soft and hydrated, and thus well-positioned to match biological tissues mechanically and biochemically. By eliminating mechanical mismatch, tissue adhesives can lower stress concentration and better facilitate healing. They are easy to implement and compatible with minimally invasive procedures. They can also mitigate postoperative complications such as body fluid/air leakage, infection, nerve damage, and inflammation. These salient features make tissue adhesives appealing for the applications where suturing is challenging to implement or prone to failure. Arthroplasty surgery, for instance, encounters small and complex spacing in joints, posing challenges for orthopedic surgeons to perform proper suturing (*15*). Despite the preceding attributes, existing tissue adhesives are far from ideal. Clinically used tissue adhesives are vulnerable to rupture and debonding, and thus cannot be applied independently of sutures and staples and raise safety concerns in the applications interfacing with dynamic tissues. One exception is cyanoacrylate-based adhesives with sufficient strength. But they are cytotoxic and not compatible with wet surfaces, and thus limited to topical wound closure by regulation (*16*–*18*). Another major limitation of tissue adhesive is the lack of functionality to monitor and regulate the healing process.

Recently, transformative advances have been made in the field of tissue adhesives. Newly developed tissue adhesives achieve unprecedented adhesion on diverse tissues, as tough as the interface between cartilage and bone. Some adhesives can not only help monitor wound conditions but also deliver therapeutics to regulate the healing process. The application scope of tissue adhesives is expanded to include wearable electronics, precision medicine, cardiovascular surgery, and cancer treatment (*2*, *12*, *19*, *20*). The driving force underlying such advances is the fusion of disciplines, including materials chemistry, mechanics, polymer science, clinical medicine, tissue, and cell biology. A *multifaceted design* of tissue adhesives has emerged, highlighting a holistic understanding of mechanical, chemical, and biological properties of tissue adhesives and their interplay with the human body.

Whereas s*ingle-faceted* designs such as surface chemistry (*21*), material composition (*22*), clinical translation (*7*) have been reviewed elsewhere, there is no review focusing on the multifaceted design of tissue adhesives. To fill this gap, this literature review aims to provide up-to-date guidelines for the development of tissue adhesives (Fig. 2.1). Three key elements of the multifaceted design will be formulated: the tissues, the adhesive surface, and the adhesive matrix.

The fundamental understanding, design principles, and technologies associated with each design element will then be discussed. Recent important advances of tissue adhesives in the topical (interfacing with skin) and implantable applications with examples that achieve enhanced properties and advanced functionality will also be promoted. I will then highlight remaining challenges and immediate opportunities, and delineate future directions for next-generation tissue adhesives, which are expected to open new avenues in broad areas, ranging from tissue repair, precision medicine to mobile health.

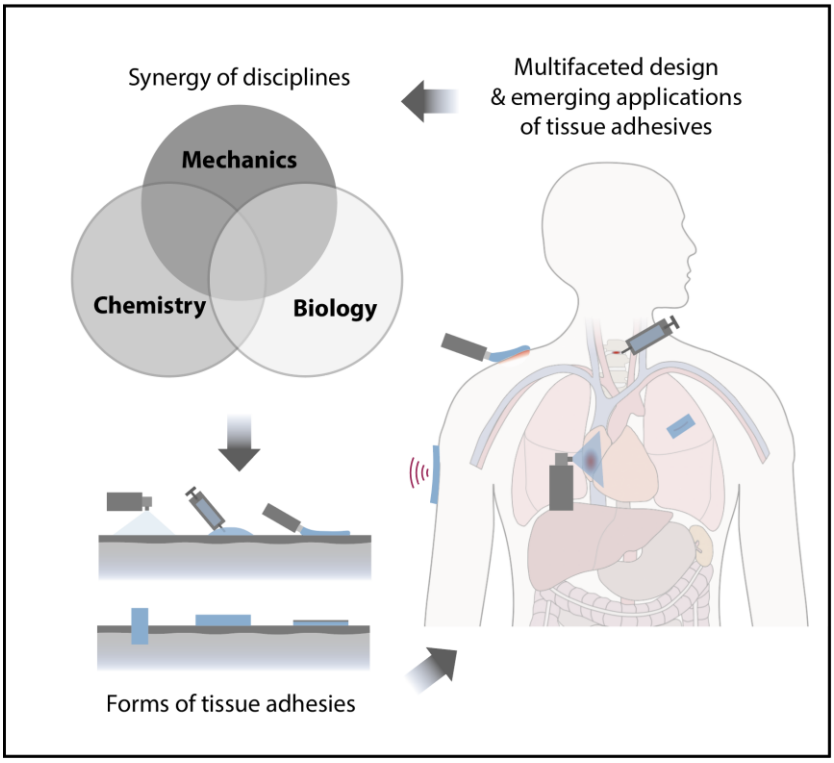

Figure 2.1. Multifaceted design and emerging applications of tissue adhesives.

2.2 Design Principles of Biomaterials Bioadhesion

An ideal bioadhesive could bear large forces and absorb substantial mechanical energies before failure. The amount of energy required to debond an adhesive is often quantified as the adhesion energy (Γ). To achieve such strong and tough adhesion, one must rationally design both the surface and matrix properties of the adhesive. Besides the considerations of tissue properties, the surface and matrix of adhesives are key design elements to account for. Considering a crack propagating

at an adhesive-tissue interface, there are three key contributors for the overall adhesion energy: the energy (i.e., intrinsic toughness) required to break interfacial bonds between the tissue and adhesive (Γ_0) (*23*), energy dissipation in the adhesive matrix (Γ_A) and the tissue (Γ_T). Their roles are revealed with an equation below:

$$G = G_0 + G_A + G_T ,$$

While the effect of Γ_T is pre-determined by the tissues, one can in principle tune Γ_0 and Γ_A through the surface and matrix designs of the tissue adhesive, respectively. They can be either integrated within a polymer network design or made separately in bilayered adhesives. Γ_0 (1-10 J m^{-2}) is typically much smaller than Γ_A (100-1000 J m^{-2}), when a tough hydrogel is used (*3*). Recent studies have shown the value of Γ_0 determines the amplification effect from energy dissipation of the bulk material, which can be expressed as a simple scaling(*24*):

$$\Gamma = \frac{G_0}{1-ah_{max}},$$

where h_{max} denotes the maximum hysteresis ratio, a is the Ogden parameter, which are all intimately correlated with the mechanical properties (e.g. elastic modulus and energy-dissipation capacity) of the tissue and the adhesive. Little is known quantitatively about the tissue contribution Γ_T as it has not been measured experimentally or modelled theoretically. In principle, Γ_T can be caused by the viscous dissipation of the tissue, as well as other rate-independent processes (e.g., breaking of polymers and chemical bonds) in the tissue. While the tissue and the associated Γ_T are largely pre-determined in specific applications, G_0 and G_A are key design factors for achieving high adhesion energy (*23*). Below discussed are the fundamental understanding and design strategies to tune Γ_0 and Γ_A.

2.2.1 Considerations of substrate mechanics, chemistry and topology

Biological tissues consist of cells and extracellular matrix (ECM), serving as a basis for the design of tissue adhesives. They vary greatly in biology, chemistry, mechanics, and topology. Such diversity and complexity of biological tissues lead to multifaceted requirements in the development of tissue adhesives. Although it is common to pursue one-fit-all adhesives, the diverse tissue microenvironments demand tissue-specific designs to maximize the performance and therapeutic outcomes. While internal tissues are covered with mucus and other body fluids,

the skin surface is wet sometimes due to sweats, bleeding, or exposure to water from the outer environment (Fig. 2.2A). The wet adhesion represents a long-lasting challenge in the field of adhesive materials, particularly tissue adhesives.

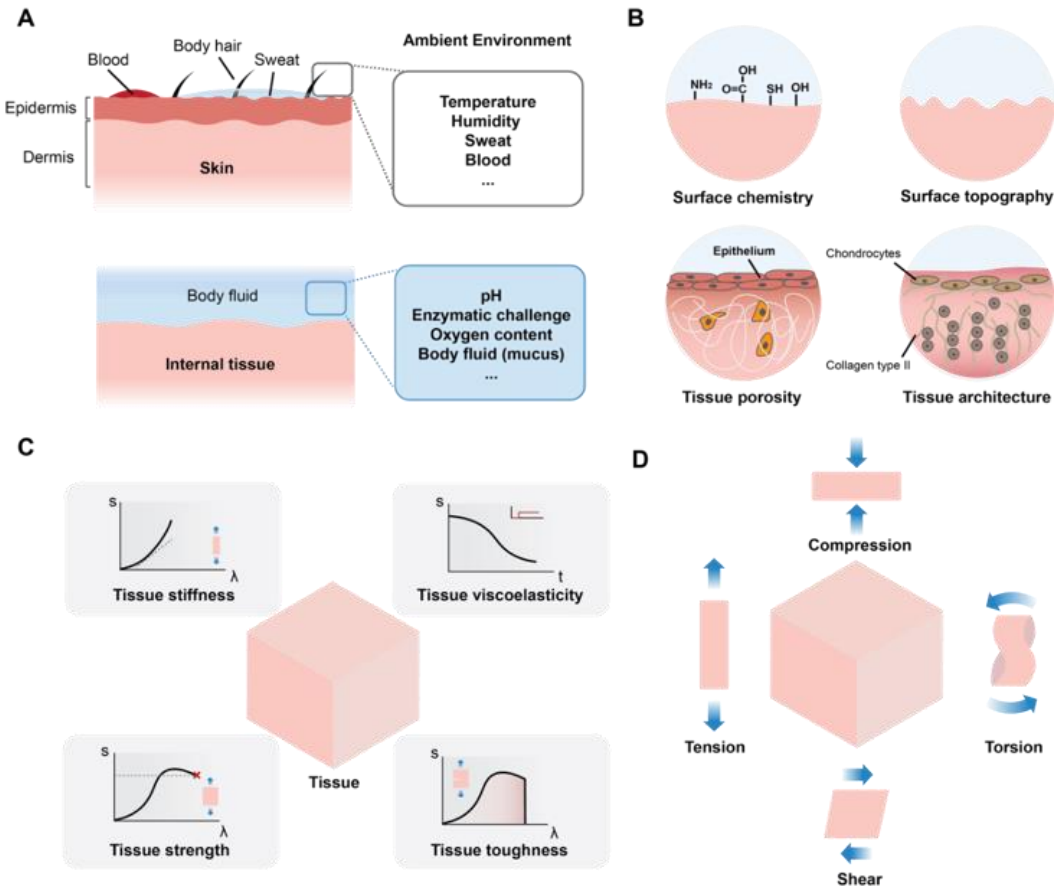

Figure 2.2. Design considerations of biological tissues. (A) Schematics of the microenvironments of skin and internal tissues. (B) Chemical and structural considerations of biological tissues. (C) Mechanical properties of tissues, including stiffness, viscoelasticity, strength, and toughness. (D) Mechanical loading applied onto or exerted by tissues, including tension, compression, shear, and torsion.

Tissue-specific considerations are central to the tissue adhesive design. They can be deconstructed into three aspects: chemistry, topology, and mechanics. The chemistry and topology of the tissue surface govern the formation of the bonds at the interface, linking the adhesive and the tissue. The

mechanics of tissues has twofold effects. First, the tissue is part of the adhesive-tissue system and thus inevitably contributes to the adhesion performance. Second, the mechanical loading of the tissue microenvironment gives rise to a driving force to cause debonding (adhesion failure). These considerations will be elaborated below.

2.2.1.1 Tissue chemistry. Tissues are composed of liquid (e.g., water and solutes) and solid matter (e.g., proteins and minerals). While the liquid components are hardly exploitable for adhesion, the solid matter is pivotal for adhesion. Among them, proteins constitute 20% dry mass of the human body and are structural elements to provide mechanical supports for cells and ECM(*25*). Examples include interlinking protein filaments in cytoskeletons (e.g. actin, myosin) (*26*, *27*), glycoproteins in cell membranes, and fibrous proteins in the ECM (e.g. collagen, elastin) (*28*, *29*). Among them, the focus is on collagen, which is the most abundant protein accounting for 25% of the entire proteins in the human body. The proteins are made of amino acids, some of which carry functional groups employable for tissue adhesion (*30*). Such functional groups include carboxylic acid/carboxylate (-COOH), amine ($-NH_2$), and thiol groups (-SH) (Fig. 1B). They appear on glutamic acid, hydroxylysine, lysine, aspartic acid, and cysteine. These amino acids constitute >20% collectively of the total amino acids (*31–34*). Glutamic acid (with residue carboxylic acid) and lysine (with residue primary amine) were found to occur in 10% and 6% of amino acids in the human body (*31*). In comparison, the occurrence of cysteine (with residue thiol) presentation is much lower (around 1%) (*34*), thus less explored as reactive groups for tissue adhesion. It should be noted that the quantitative characterization of the functional groups on different tissue surfaces is missing in the literature. Considering the importance of surface functional groups on tissues, information obtained via Fourier-transform infrared spectroscopy, proteomics, and Raman spectroscopy could greatly inform the design and development of tissue-specific adhesives (*35*, *36*).

Hydrogen bonds (-OH) are also major players to enable strong intermolecular interactions, which are ubiquitously presented on most amino acids. Tissue surfaces also feature net negative charges and hydrophobicity due to lipid bilayers of cell membranes (*1*, *37*). Altogether, these characteristics define the intrinsic surface properties of tissues.

The tissue chemistry is crucial for designing the bonds between the tissue and the adhesive. A set of chemical reactions have been established for this purpose, including carbodiimide (*3*), aldehyde

(*38*), catechol (*39*), azide (*13*), and enzymatic reactions like transglutaminase (*40*). The carbodiimide chemistry is commonly used to trigger the amide bond formation between -COOH and -NH_2 in aqueous environments. The reactivity of collagen enables enzymatic reactions via transglutaminase to crosslink amine groups or the Factor XIII used in fibrin clot formation (*41*). Recent studies proved that chemical variances between tissues affect the strength and retention of tissue adhesives (*42–44*). A notable example is a dextran aldehyde-based tissue adhesive, which elicits tissue-dependent adhesive strength and immune response (*38*). Leveraging the Schiff-base reaction between amine groups on tissues and aldehyde groups in adhesives, different levels of adhesion strength were observed on various tissues. Among the tissue tested, the highest adhesion modulus was reported on duodenum (part of the small intestine), while it was much lower on lungs. The moduli for liver and heart are comparatively intermediate (*38*). A recently developed tough adhesive based on carbodiimide crosslinking between the carboxylic acid groups on tissues and primary amine groups within the adhesives also demonstrated tissue-dependent adhesion performance, showing robust adhesion on skin, heart, cartilage, and relatively lower adhesion on liver (*3*). A similar trend was observed with a recently reported double adhesive tape leveraging amide and hydrogen-bond formation at the interface (*2*). The interfacial reaction efficiency can also greatly affect the matrix formation of certain adhesive glues, where competition is expected between adhesive and cohesive bond formation. Following adhesive application, the immediate unreacted adhesive residue not depleted by interfacial and matrix reactions or byproducts resulting from long-term degradation can potentially cause various levels of inflammation (*38*). The bonding strength realized via tissue-specific chemistry can also drastically affect their degradation profile.

The surface chemistry of tissues can be modified for high-level control over tissue adhesion, for example, by priming the tissue surface with additional functional groups. The priming treatment can base on bioconjugation, physical interpenetration with bridging polymers (*3*, *45*), or even genetic engineering of cells to express specific proteins for adhesion reactions (*46*). The benefit of the priming treatment has been shown before. When the native surface of cartilage doesn't facilitate adhesion, pretreating the defect with a surface-degrading enzymatic to remove interfacial proteoglycans can significantly increase the adhesion strength of a chitosan-based adhesive (*47*).

Local tissue microenvironments are also relevant to adhesive performance. The factors from ambient environments include temperature, humidity, and UV exposure (*48*). Other chemical factors include pH (*49–51*), oxygen (*52–54*), and enzyme (*55*, *56*) (Fig. 1A). These factors have

implications in the formation and long-term stability of tissue adhesion. Take the pH as an example. The pH levels vary greatly among tissues, and even between physiological or pathological conditions of the same tissue. The pH of tumor tissues is often more acidic than healthy tissues (*57*). The pH of a wound bed changes considerably with infection or healing (*50*). For ingestible adhesives, the drastic pH change in the gastrointestinal environment should be accounted for (*58*). While the polymers and chemistries used in tissue adhesives are sensitive to pH, one needs to consider the local pH of the target tissue. The pH-dependent tissue adhesion is demonstrated by adhesives based on the pH-sensitive imine-bond formation which achieves the highest adhesion strength at neutral pH (*38*). Also, topological adhesion relying on pH-induced molecular stitching shows a tissue-specific behavior (*5*). In addition, adhesives could actively alter the local pH for cancer therapy (*12*). The oxygen at the application sites can directly inhibit the reaction efficiency of adhesives in-situ formed via free-radical polymerization, leaving sometimes toxic unreacted monomers/precursors (*59*). When exposed to oxidants such as oxygen, catechol-based adhesives can undergo oxidation resulting in a loss of adhesiveness (*60*). Certain specific enzymes (e.g. collagenase and hyaluronidase) can significantly affect the degradation profiles of adhesives composed of naturally derived polymers (e.g. collagen and hyaluronan). The degradation of some synthetic polymers (e.g. polyurethanes and polyetherurea-urethanes) can also be triggered by cholesterol esterase, an enzyme found in monocyte-derived macrophages. Apart from the degradation of the bulk matrix, these external chemical stimuli could also be leveraged to enable on-demand detachment of the applied adhesives. For example, sodium bicarbonate solutions were recently used to neutralize the bioadhesive-tissue interface, leading to the cleavage of hydrogen-bond enabled physical crosslinking, while the covalently crosslinked disulfide bonds can be de-crosslinked with glutathione (*62*).

2.2.1.2 Tissue topology. Topological elements such as pore size and surface roughness matter in the tissue adhesive design (Fig. 2.2B) (*63–67*). Pores are defined as apertures on the surface or within the tissues that enable the input or output of gases or fluids (*68, 69*). They are related to the available area for chemical and physical bondings. Tissue roughness, commonly evaluated using Arithmetical mean deviation (Ra), represents the texture of a tissue surface on or below the microscale (*70*). The pore size determines the permeability of tissues (especially for skin, blood-brain barrier, and mucosa) (*71–73*). This factor further regulates macromolecule interpenetration and cell infiltration, which have implications in tissue adhesion (*74*) and drug and cell delivery

(*75–77*). To promote adhesion, the approaches developed in the field of drug delivery (e.g. ultrasound, microneedle, and chemical enhancers) could be repurposed to upregulate the tissue permeability for strong interpenetration (*77–79*). On the other hand, high roughness impairs the formation of intimate contact between pre-formed adhesives and the tissues. But they can serve as anchors for mechanical interlocking to increase adhesion and prevent sliding (*6*, *80*).

Connective tissues such as annulus fibrosus (AF) in IVD (*81*, *82*), cartilage (*83*, *84*), and tendons (*85–87*) are highly anisotropic. For example, the unique depth-dependent tissue architecture of cartilage features unidirectionally oriented collagen type II fibers at the superficial layer, while randomly organized meshes are observed approaching the bone-cartilage interface (Fig. 2.2B)(*84*). A heterotypic cellular environment also exhibits drastically different orientations and phenotypes, similar to the distinct shift in a tissue matrix organization. These architectural features significantly contribute to normal tissue functions (*88*). Failing to deliver or recover these anisotropic properties can lead to scar formation and tissue degeneration; while even only partially recapitulating these topographical characteristics has been shown to optimize the bio-integration of implanted materials and enhanced regeneration outcome (*89*).

Another factor that has profound effects on the properties of tissues is the renewing and regeneration of living tissues, especially after an injury. This would potentially disturb the formed adhesion, therefore long-term retention. Considering an adhesive bonded to skin, the outer layer of the skin where the adhesive anchors on may shed off. For healthy skin, the turn-over rate is 4-8 weeks. It varies up to months for injured skins, and even longer for patients with diabetic ulcers (*90*).

2.2.1.3 Tissue mechanics. The effect of tissue mechanics on adhesion is twofold: mechanical properties of the tissues and mechanical loading that the tissue experiences or exerts. The stiffness of tissues determines the intimate contact between the tissue and the adhesive, as well as the adhesion energy achievable through crack blunting and background hysteresis (Fig. 2.2C). The strength and toughness of tissues govern the failure modes of tissue adhesives. If a tissue is brittle, cohesion failure of the tissue is dominant. Otherwise, the failure occurs at the interface or in the adhesive matrix. The viscoelasticity of tissues also contributes to the adhesion energy achieved with the adhesives.

Mechanical loading exerted by tissues plays a critical role (Fig. 2.2D). Endogenous forces can deform the adhesive and drive crack growth, causing detachment. For blood vessels and other liquid-containing organs, shear stress and hydraulic pressure are important. For musculoskeletal tissues such as tendon and intervertebral disc (IVD), (*91–93*) there is significant mechanical loading of varying magnitudes, modes, and frequencies (*94*). For instance, the tensile force applied onto the Achilles tendon is as much as 9 kN, and the inner core of IVD (nucleus pulposus) is subjected to a hydrostatic pressure of 2.9 MPa during heavy lifting(*95*). The mechanical loading can be either static or cyclic. The static loading can be pre-strains of skin (10-30%)(*96*), as manifested by the skin tension lines. The pre-strain varies among locations of the body and is considered an important design variable for wound dressings and cardiac patches (*20*). Cyclic deformation is common among heart, lung, and blood vessels. A lung gets inflated and deflated 500 to 800 million times in one's life. While the existing adhesives and implants are often stress-free and assessed under monotonic loading, the effects of pre-strain and cyclic loading need further investigation.

Besides adhesion, the bulk mechanical properties of tissue adhesives should meet tissue-specific requirements to restore the function of target tissues. Adhesive materials could provide instructive cues to promote tissue repair and regeneration (*97–99*). These cues can be biochemical, cellular, or mechanical. The strategies to design adhesives to match tissue mechanics have been thoroughly reviewed elsewhere (*10*, *67*, *89*). The biomechanical cues are known to regulate pathogenesis, such as fibrosis(*100*). The undesirable mechanical cues (such as high stiffness) are believed to hamper the regeneration process and cause scar formation (*101–103*). Therefore, it is reasonable to match the tissue and the adhesive in terms of mechanical properties, such as stiffness, strength (*104*, *105*), viscoelasticity (*106–109*), and toughness (*24*, *110*, *111*). It would be particularly beneficial for the applications associated with load-bearing tissues such as cartilage, tendon, meniscus, and IVD. It should be noted that tissue mechanics could and most likely change due to pathological conditions (degeneration, genetic disease, or trauma) and aging (*105*, *108*, *109*, *112*). Also, achieving some exceptional properties of tissues may be very challenging, for instance, the tensile strength of the tendon. These challenges call for a fundamental understanding of tissue mechanics and strategies to modulate the properties of adhesive materials.

Although recent studies have investigated the hydrogel adhesion on rigid substrates experimentally and computationally (*3*, *6*, *113*), the role of tissue mechanics on the adhesion of tissue adhesives

remains elusive. It is well documented that the performance of tissue adhesives varies with the types of tissues and that the tissues exhibit complex mechanical responses (Mullins effect and viscoelasticity), which are believed to contribute to the interfacial fracture process and thus the adhesion performance of the adhesives. To comprehend and predict the complex coupling between the adhesion and tissue mechanics, researchers need to develop new simulation platforms and experimental methods.

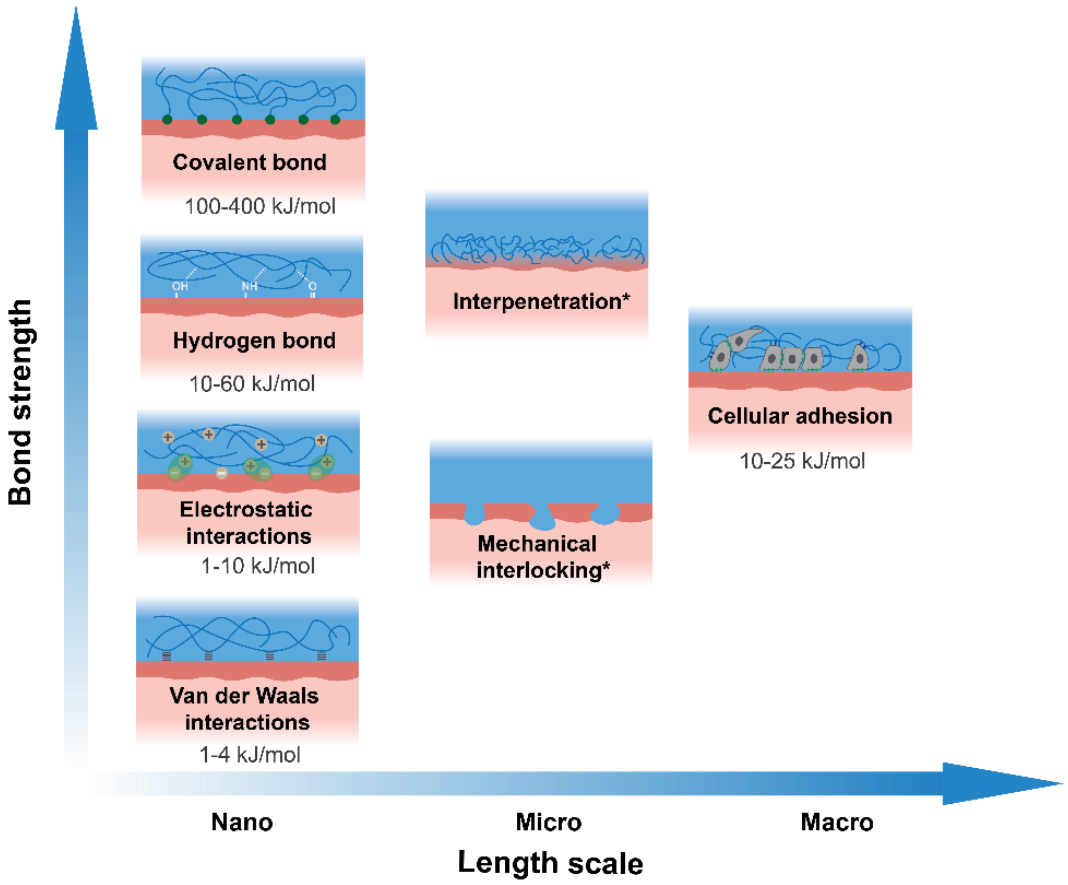

Figure 2.3. Various interactions exploitable at the interface of the tissue (red) and the adhesive (blue). They are positioned relative to each other in terms of bond strength and length scale (*6*, *16*, *114*, *115*). A bridging polymer (solid line) links the adhesive and the underlying tissue together. *The bond strength of mechanical interlocking or interpenetration is strongly dependent on the nature of material's crosslinking mechanism.

2.2.2 Adhesive surface design

The adhesive surface is key to the integration of the tissues and tissue adhesives. The surface design is also multifaceted, involving mechanics, chemistry, physics, and biology. Fig. 2.3 illustrates a variety of interfacial bonding mechanisms at different length scales (*6*, *16*, *114*, *115*). At the nanoscale, atomic and molecular bonds have been widely exploited with a library of chemistries (*114*). The polymer interpenetration on the order of 100 nanometers is resulted from diffusing a bridging polymer at the tissue-adhesive interface (*3*). At the microscale and beyond, cell adhesion based on cellular adhesion ligands like arginylglycylaspartic acid (RGD) peptides can play a critical role in bio-integration (*116*); mechanical interlocking with the microscale roughness is common for rigid adhesives. Often, a tissue adhesive leverages more than one mechanism for strong adhesion. Features at different length scales ubiquitously observed in biological materials has inspired the multiscale design of artificial materials with exceptional structural and mechanical properties (*41*, *117*, *118*). A systemic understanding of material interactions across length scales underpins our ability to comprehend, predict and control the properties and performance of tissue adhesives. Importantly, the crack tip field involved in cohesive and adhesive failures of tissue adhesives is strongly length-dependent, potentially involving various interactions at multi-scales (e.g., breaking of bonds and pull-out of chains) (*6*).

2.2.2.1 Molecular interactions. A number of functional groups present on tissue surfaces, including primary amine, carboxylic acid, hydroxyl, and thiol. They are readily available to react with the adhesive. A "toolbox" of chemical reactions has been developed or repurposed for tissue adhesion. To react with primary amine, one can choose cyanoacrylate (*119*), aldehyde (*38*, *120–122*), urethane (*123*, *124*) or *o*-quinone (*17*, *39*, *125–127*) chemistries. Carbodiimide chemistry is often used to form amide bonds between the tissue and the tissue adhesives containing polysaccharides, such as chitosan (*3*, *128*), alginate (*129*), and hyaluronic acid (*130*). Adhesives carrying thiol groups can form mucoadhesion through disulfide bonds with cystines-containing mucus (*74*). Other strategies are inspired by nature, including catechol chemistry and bacterial-derived mechanisms (*127*, *131*). A notable example inspired by mussel adhesion is catechol, a benzene ring and two neighboring hydroxyl groups (*60*). The catechol can facilitate a set of adhesion mechanisms such as hydrogen bonding, hydrophobic interactions, and covalent bonding, and is amenable to tissue adhesive applications (*39*).

The aforementioned chemical strategies are sensitive to the surface chemistry of tissues (*38*), thus can be tailored for specific tissues, leading to tissue-specific adhesives. It is exemplified with an adhesive that can base on surface proteins to target certain tissues, enabling local therapy with high precision and prolonged retention (*12*, *132*). Besides the functional groups inherent in tissues, their surfaces could be primed with exogenous functional groups. As such, one has more freedom to select chemical reactions of designed kinetics and efficiency (*3*, *6*). Herein, a set of click chemistry reactions are appealing due to their advantages of high efficiency, specificity, and biorthogonality (i.e., no crosstalk with biomolecules and biological processes).

Some tissue bonding strategies are learned from blood clotting. Components of blood clots (e.g., fibrinogen, platelets, and coagulation factors) are capable of binding with collagen, cells, and ECM. They are intrinsically biocompatible and biodegradable. Derived from the hemostatic cascades is the fibrin glue, which is extensively used in various surgical procedures. Another example is a hyaluronic acid (HA) hydrogel adhesive, crosslinked by a blood coagulation Factor XIII. This adhesive adhered well to cartilage and can deliver and support chondroprogenitors to stiffen the adhesive matrix to a level of native cartilage in vivo (*40*).

Unlike the chemical reactions producing permanent bonds, physical interactions can yield reversible bonds, due to relatively low bond strengths. A set of physical interactions exploitable for tissue adhesion include electrostatic attraction, hydrogen bonding, hydrophobic association, and Van der Waals forces (*21*, *133*, *134*). They are feasible given the intrinsic surface properties of tissues (i.e., negatively charged surface, hydrophobic lipids in cell membranes). A variety of bioadhesive polymers are found to form physical interactions with tissues, particularly mucoadhesive that are studied extensively for nasal and oral drug delivery. Based on the hydrogen bonding, polyacrylic acid can adhere to tissues instantly (*2*, *131*, *134*). Carrying a high density of primary amine groups, chitosan can form electrostatic interaction and physical interpenetration with tissues (*128*). To enhance tissue affinity, one can modify the polymers with hydrophobic chains such as alkyl chains and lipids, which can fuse into the cell membrane via hydrophobic association (*124*).

Due to the reversible nature, the physical interactions allow for re-positioning and re-use of the adhesives. However, the reversibility also concerns the strength and stability of the adhesion. In

line with this, researchers can combine physical interactions with chemical bonding strategies to realize instant and stable adhesion (*2*).

2.2.2.2 Physical interlocking. Alternative to chemical reactions, physical interlocking can anchor the adhesive onto tissues via steric hindrance. There are two main mechanisms: one is polymer interlocking, and the other is mechanical interlocking with rough surfaces (Fig. 2.3) (*6*). For the polymer interlocking, a diffusing polymer interpenetrates the tissue and the adhesive, forming an interlocking network across the interface (*135*). They are like macromolecule stitches, enabling adhesion (*5*). Herein, the topology of the tissue, particularly pore size, dictates the amount and rate of diffusion, thus the adhesion strength. The charge density of tissues also matters as they define the affinity between the diffusing polymer and the tissue (*37*). A representative diffusing polymer is chitosan, which is shown to easily penetrate tissues, due to the positive charges at neutral pH. Also, the chitosan can form an interlocking network via hydrogen bonding (*5*) or covalent crosslinking via carbodiimide chemistry (*3*). A limitation of this strategy is the relatively slow adhesion, as the diffusion of polymers is limited kinetically. This limitation could be overcome by physical and chemical approaches to expedite the diffusion, which has yet been reported.

Mechanical interlocking works in a fashion of lock-key interactions. This mechanism requires an adhesive to infiltrate the surface irregularities and then solidify (*6*). Thus, it is mission-critical to balance the liquid- and solid-like properties. There are two common strategies. One strategy is to leverage sol-gel transition (in the case of cyanoacrylate): liquid precursors polymerize in situ to form rigid solids. The other strategy is reliant on the viscoelasticity of the adhesive material, which can flow viscously into the irregularities under pressure while maintaining elasticity. These viscoelastic adhesives are found to comply with the Dahlquist criterion: the elastic modulus is generally lower than 0.1 MPa. Such adhesives are also known as pressure-sensitive adhesives (e.g. *BAND-AID®* from Johnson & Johnson). Because of the viscoelastic nature, the adhesion performance of pressure-sensitive adhesives is rate-dependent.

Compared to the polymer interlocking applicable to most permeable surfaces, the mechanical interlocking is insensitive to the tissue permeability but limited to rough tissue surfaces. Wet and smooth surfaces would pose challenges. A straightforward remedy is roughening of the tissue surface (rasping). This approach is applied by rasping meniscus surfaces, which has been used in clinical practice to improve meniscus healing potential.

Apart from the microscopic interactions, bioinspired mechanisms for physical interlocking have been explored. A biphasic hydrogel microneedle (polystyrene-*block*-polyacrylic acid), inspired by endoparasitic spiny-headed worms, swells upon contact with water and mechanically interlocks itself with local tissue (*136*). Snail Epiphragm inspired a recent finding on polyhydroxyethyl methacrylate hydrogel, which can conform to rough surfaces when soft and hydrated, and stiffen dramatically upon dehydration, resulting in mechanical interlocking (*137*). Adhesives mimicking fibrillar array covering the bottom of gecko feet (*133*, *138*), protuberances in suction cups of octopi (*139*, *140*), and clingfish (*141*) have been extensively explored as reversible wet adhesives.

2.2.2.3. **Cell adhesion.** Cells adhere to ECM (collagen, fibronectin, and laminin) and other substrates via integrin and other transmembrane proteins (Fig. 2.3). They also adhere to other cells via cellular adhesion molecules such as cadherin and desmosome. The energy of cellular adhesion is on the order of 10 kJ mol^{-1}, comparable with physical interactions; the integrin-RGD binding energy, for instance, was measured at 25 kJ mol^{-1} (*116*). Although lower than covalent bonds, cell adhesion can contribute to tissue adhesion.

Cell adhesion is living and dynamic. Its kinetics and strength are dependent on cell types and substrates (*142–144*). It takes minutes to hours for cells to adhere to a substrate or form cell clusters (spheroids) (*145*). Also, the matrix deposition of cells such as collagen and mineral can diffuse and penetrate the adhesive matrix, enhancing the structural integrity of the tissue-adhesive interface and adhesive matrix by forming an interpenetrating network, subsequently reinforcing the adhesion. This phenomenon was observed when a double network gel was isolated from cartilage sites after weeks (*4*). Importantly, the cell adhesion formed with neighboring cells and the ECM can also facilitate intercellular crosstalk and impact intracellular mechanotransduction, thus regulate the fate and activities of cells (either endogenous or transplanted with the adhesives) such as migration, proliferation, matrix deposition, and differentiation (*97*, *146–149*). On the other hand, the adhesion of immune cells (e.g. neutrophils and macrophages) on adhesive scaffolds have a significant impact on the degradation profile of the adhesives and inflammatory response (*150*). Along with other biochemical signaling, these factors together determine disease progression and tissue regeneration. Combining adhesive engineering with carefully designed cell-cell and cell-ECM (adhesive) interactions can lead to next-generation translational cell-based therapy.

The coupling between mechanics, materials, and biology highlights the importance of the multifaceted design of tissue adhesives.

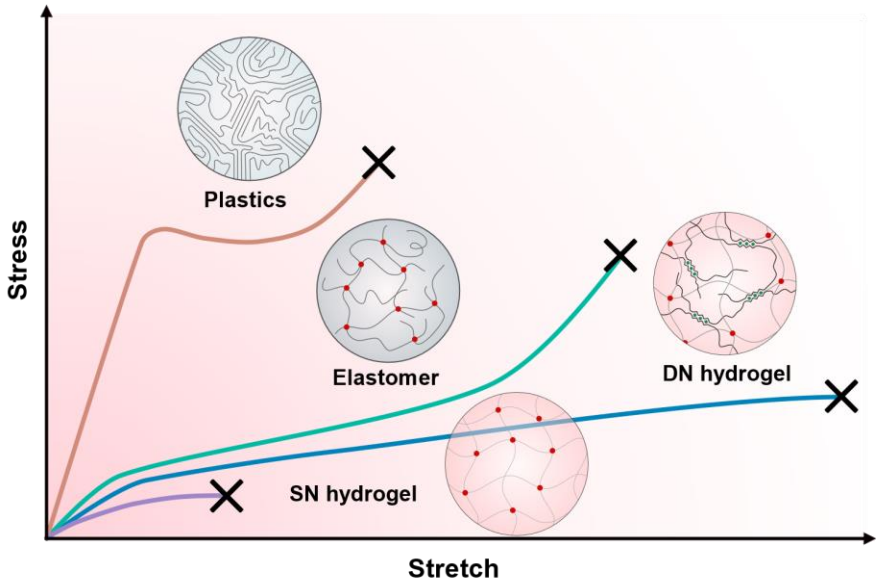

Figure 2.4. **Representative stress-stretch relations and schematics of the four adhesive matrices, including plastics, elastomers, single- (SN) and double-network (DN) hydrogels**. Crosses denote rupture points.

2.2.3 Adhesive matrix design

The cohesive properties of tissue adhesives govern the adhesion performance and other biological functions. They encompass strength, toughness, stiffness, as well as bioactive functions such as drug delivery capacity. When the adhesive matrix is brittle, an interfacial crack is prone to kink into the adhesive, resulting in cohesive failure. Fig. 2.4A showcases the main four classes of materials used to form adhesive matrices, which are reviewed below.

2.2.3.1 Plastics. Tissue adhesives can be made with plastics such as cyanoacrylate and polyesters, including poly(glycolide) (PGA), poly(lactide) (PLA), poly(ε-caprolactone) (PCL) and poly(lactic-co-glycolic acid) (PLGA). The polyesters are biodegradable via hydrolysis of the ester bonds, but their degradation products may locally decrease the pH and cause inflammation (*151*). They form weaker adhesion than the cyanoacrylate adhesive. There exist many commercial

products based on cyanoacrylate and its derivatives. A representative product is *Dermabond®* (from Johnson & Johnson) used for topical wound closure (*119*). Another product named *Omnex®* was recently received FDA approval for internal use. The liquid cyanoacrylate monomers exhibit high reactivity and polymerize in seconds upon exposure to water. Impressively, the resulting matrix alone gives rise to many adhesion mechanisms, ranging from mechanical interlocking (as the liquid monomers fill the rough tissue surface), covalent bonding with tissue proteins (e.g., primary amines of the lysine side chains), to physical interactions (e.g., hydrogen bonds).

Despite the salient features, cyanoacrylate adhesives have several limitations. First, this adhesive is incompatible with wet surfaces, as it solidifies rapidly upon exposure to body fluids. The rapid solidification of cyanoacrylate concerns some practical applications, making repositioning difficult. Second, the polycyanoacrylate is in a glassy state, and thus stiff and rigid (modulus 50-500 MPa). The rigidity causes the inability to close large wounds, incompatibility with dynamic tissues due to the mechanical constraint (*152*). This issue could be mitigated by organic co-solvents to soften the polycyanocrylate (*153*), but its biocompatibility remains a concern. Extensive studies conclude that the cyanoacrylate monomers are cytotoxic, and the degradation products after hydrolysis (cyanoacetate and formaldehyde) induces substantial fibrosis, inflammation, and other immune responses in vivo (*154*). The cytotoxicity can be reduced with longer alkyl side chains (e.g., 2-octyl cyanoacrylate), since they degrade more slowly than the counterparts of shorter alkyl chains (e.g., ethyl-2-cyanoacrylate) (*155*).

2.2.3.2 Elastomers. Because of the low glassy transition temperature, elastomers exhibit lower stiffness (on the order of 1 MPa) and higher deformability (>100%) than plastics (Fig. 3B). They are thus more suitable for the applications interfacing with soft and dynamic tissues. Elastomer tissue adhesives are extensively used in daily life and the clinic. The elastomers include acrylic elastomers (VHB®), polydimethylsiloxane (PDMS), polyurethanes (*TissuGlu®*, *Sylys®*) (*156*), styrene-butadiene rubber (SBT) (*157*), and newly developed poly(glycerol sebacate acrylate) (*1*, *138*). They are also known as pressure-sensitive adhesives (PSA), reflective of the need for applied pressure to form appreciable adhesion (See the discussion on physical interlocking). The adhesion mechanisms of existing elastomer adhesives are mainly two-fold. First, their surfaces comprise reactive functional groups (e.g., aldehyde in VHB) to react with tissues chemically, as well as other groups to build physical interactions like hydrogen bonding. Second, the highly viscoelastic matrix

enables mechanical interlocking with the substrate and helps dissipate energy for high adhesion energy. However, the adhesion energy remains relatively low (lower than cyanoacrylate). Immediate opportunities remain to achieve stronger adhesion with elastomer-based adhesives.

2.2.3.3 Hydrogels. Hydrogels contain a large content of water (typically >90%). Because of this property, hydrogels feature good biocompatibility and the lowest stiffness (~10 kPa) among existing adhesive matrices (Fig. 2.4B). These features make hydrogels the current focus for the development of tissue adhesives (*130*, *158*). A large number of hydrogel systems, either synthetic and naturally derived, are available. The design principles of hydrogels have been discussed thoroughly in recent reviews (*22*), leading to a short discussion here focusing on the network configuration of hydrogels and its mechanical consequences. The network configuration of choice includes conventional single-network (SN) hydrogels, double-network (DN) hydrogels that contain two or more interpenetrating networks.

Conventionally, the SN hydrogels (either synthetic or protein-based) are used in tissue adhesives. One of the widely used systems is polyethylene glycol (PEG) hydrogels (*159*, *160*), which come in different formulations such as chemically functionalized linear or branched PEG molecules. A few PEG hydrogels have been FDA-approved and used clinically, for instance, *Coseal*® (two four-arm PEGs) (*161*), and *Duraseal*® *(*PEG ester and trilysine amine). Their indication is primarily sealing suture lines or as an adjunct to dural closure (*162*). The simple composition is advantageous in terms of fabrication and regulation. But the matrix is typically weak and brittle, limiting their application on load-bearing tissues. Another concern is on the significant swelling ratio in vivo (up to 400% of the original volume), especially under circumstances of closed spaces and pressure-sensitive tissues like spinal cord.

Protein-based adhesives are derived from biological materials. A benchmark material system is the fibrin glue, which is formed by the crosslinking of tissue-adhesive fibrinogen. Thanks to the advantages such as fast curing, biocompatibility, and biodegradability, fibrin glues are exploited as sealants in cardiovascular surgery, as well as in neurosurgery to seal cerebrospinal fluid postoperatively. Another notable family of tissue adhesive is based on glutaraldehyde-crosslinked albumin, such as *GlueBran 2*®and *BioGlue*®, for topical applications. These commercial products possess high strength and strong adhesion with skin when concentrated albumin is used. However, the cytotoxicity of glutaraldehyde is a major safety concern. Another family of gelatin-based glues,

forming covalent bonds with the tissue surface with the aid of aldehyde or carbodiimide agents, are also commercially available (*120*, *163*, *164*). A general limitation of protein adhesives is the potential risks of blood-borne disease and allergic reactions (*152*).

Whereas the SN hydrogels suffer from limited mechanical performance, the DN hydrogels achieve better mechanical strength, toughness, and adhesion properties. The DN hydrogels were first invented by Jianping Gong and coworkers in 2003 (*165*), and have evolved into a big library of materials. The fracture energy of DN hydrogels can reach up to 10,000 J m^{-2}, compared to 1-10 J m^{-2} of SN hydrogels. The superior mechanical performance of DN hydrogels is attributed to the synergy of two polymeric networks: one for crack bridging and the other for energy dissipation (*3*, *153*). The two networks can be both covalently crosslinked [e.g. poly (2-acrylamido, 2-methyl, 1-propanesulfonic acid) (PAMPS) and polyacrylamide (PAAm) (*165*)], or a combination of covalently and physically crosslinked networks (e.g. alginate and PAAm (*166*), hyaluronic acid, and semi-interpenetrating collagen[121]). The design principles and examples of DN hydrogels have been thoroughly reviewed (*117*, *167*). Due to high toughness, the DN hydrogel can contribute to extremely high adhesion energy on wet tissues (*3*, *6*). The resulting tough tissue adhesives emerged recently as promising biomaterials to repair/substitute load-bearing tissues such as IVD and tendon (*168*).

Besides the mechanical properties, the advantages of hydrogel adhesives include mild gelation conditions, transparency, biocompatibility, and tunable biodegradability. The unique combination of properties is well-positioned for cornea repair. For instance, a transparent tissue adhesive (*GelCORE*), composed of chemically modified gelatin and photoinitiators, can gel in situ under visible light (450-550 nm), which prevents the potential retinal damage and complications caused by UV-initiated crosslinking (*169*). By matching the adhesive stiffness with that of the native cornea, researchers improved the retention and efficacy of the adhesive in repairing cornea defects.

2.3 Delivery Approaches

The design of the delivery approach is key to adhesive applications but is largely overlooked in previous reviews. The mechanical properties of tissue adhesives are often benchmarked in their equilibrium state. However, their initial form and mechanical properties determine their applications scenarios and how they are implemented in clinical settings, especially when used in combination with other surgical tools (e.g. guide wire, endoscopic/vascular catheter, trocar, etc.)

and techniques (e.g. microfracture, etc.), and when minimally invasive procedures are preferred. The choice of delivery approach depends on the mechanical and flow properties of the adhesives, including storage/loss modulus, viscosity, shear-thinning behavior, gelation kinetics, as well as the biocompatibility of the adhesive precursors. Given toxic precursors or harsh gelation conditions, the adhesives typically have to be pre-formed into certain shapes (patch or plug) and sterilized before implementation. The constraint is lessened for the systems with biocompatible precursors and mild gelation conditions. For certain delivery approaches, researchers also need to refine the flow properties, for instance, by adding inclusions for shear-thinning behavior for pasting (*11*). The compatibility with surgical techniques should also be considered, especially for the knee and IVD surgeries using trocar (*170*), and gastric intestinal wound dressing using endoscopy (*171*).

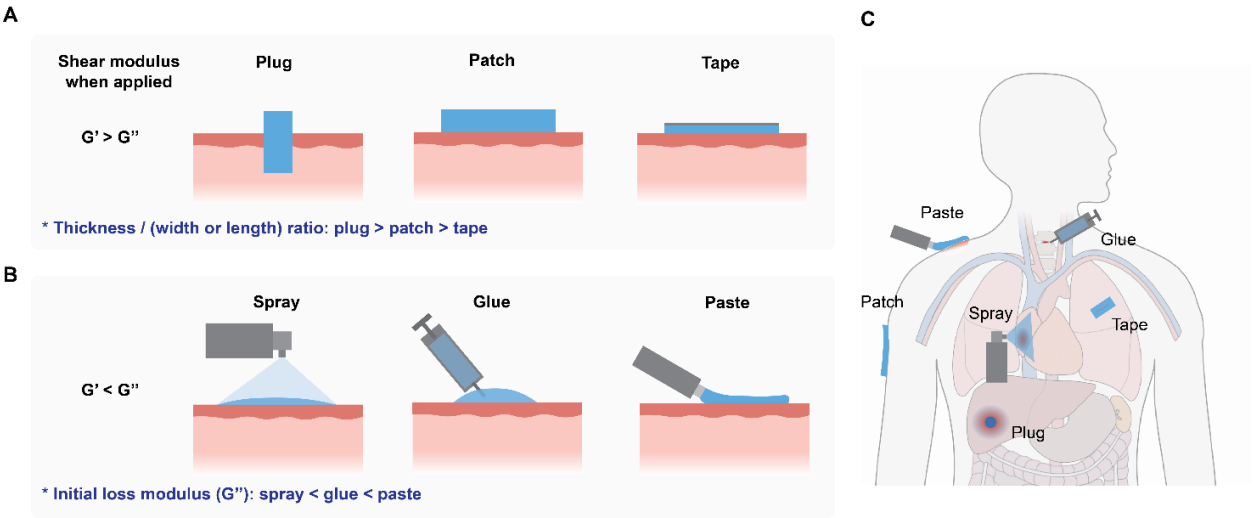

Figure 2.5. Delivery approaches and physical forms of tissue adhesives. (A) solid-like preformed adhesives. (B) liquid-like in-situ forming adhesives. The storage and loss modulus are denoted as G' and G'', respectively. (C) Examples of application scenarios of various forms of adhesives.

Shear modulus is one of the key parameters to define the formation kinetics of the adhesives and/or their performance under different conditions (*22*). It is often measured with time-sweep, frequency-sweep, or temperature-sweep rheological tests. In particular, the storage modulus G' is closely correlated to the elasticity and the crosslink density of the adhesive matrix, while the loss

modulus G'' reflects the liquid-like, viscous properties. When the storage modulus G' is higher than the loss modulus G'', the elastic portion prevails, suggesting that a solid-like matrix is formed (*97*). The values of G' and G'' can be modulated, for instance, through tuning the type and amount of crosslinks, and the polymer molecular weight (*75*). According to the shear modulus of adhesives before application, there are two main categories of tissue adhesives: pre-formed (G' > G'') and in-situ forming (G' < G'') adhesives. The curing/crosslinking mechanisms for the adhesives have been thoroughly reviewed elsewhere (*125*, *168*, *172*).

2.3.1 Pre-formed adhesives. Pre-formed adhesives with solid matrix and defined geometry are often used when a large delivery route is available, e.g. in topical applications, traumatic incidents, and/or when open surgery is acceptable. They are common in the clinic and daily life. They can be patched onto the tissue surface or shaped into a specific geometry to plug into a tissue defect (*2–4*, *173*). Motivated by their proposed application settings, these adhesives are pre-formed into various geometries with drastically different aspect ratios, which could be further categorized as plugs, tapes, and patches (Fig. 2.5A).

Adhesive plugs are often designed to be cylindrical/cuboid matrix insertable to holes/defects in tissues. They differ from the patches in terms of aspect ratios (height >> width). An important design rule is to control the geometry of the plug (e.g. diameter, thickness) to fit tightly the defect site. The application scenarios of adhesive plugs include tissue repair (i.e. annulus fibrosus (AF) repair in IVD surgeries (*174*)) and wound management (*173*). In particular, they're positioned to treat traumatic wounds as a first-aid rescue. Because the pre-formed plugs possess initially elasticity and strength and provide a readily available sealing capability, with sometimes additionally incorporated hemostatic, blood absorbing, antiseptic functions (*173*). Despite their successful implementation in emergencies, the adhesive plugs might sometimes cause severe inflammation, especially when used in large quantities, if not removed in time. The swelling ratio of the adhesive plugs also needs to be well controlled. The induced pressure on epithelial surfaces and tissues resulted from the excessive swelling of adhesives could lead to severe complications, such as the compression of the spinal cord by dura sealants (*175*, *176*).

Adhesive tapes are thin films (i.e., large width/length to height ratio) designed to approximate tissues or to attach devices to tissues (*2*). They could be readily used to seal small incisions on tissues to prevent air/liquid leakage. Due to their film-like structure, the adhesive tapes can adapt

to the roughness and irregularity of tissue surface, providing additional favorable sensitivity and conformity for anchoring of flexible and even stretchable wearable devices onto tissues. Rigid backings such as polyethylene terephthalate films are usually incorporated to enhance its mechanical strength and to regulate the permeability of the adhesive. Examples include pressure-sensitive tapes for wound management and device fixation on skin.

Adhesives patches are sheets of hydrogels or elastomers, applicable on smooth and flat surfaces such as skin or surgical sites where the wound area can be re-shaped. Adhesive patches refer to geometrical designs in between a plug and a tape. They are a popular choice for open wound dressing applications, particularly for large and chronic wounds such as ulcers. They can act as a synthetic barrier to the outer environment and can be engineered with therapeutic and monitoring functions. The patch shape design can provide adequate tissue adhesion, reliable matrix strength, and customizable functions. They can retain moisture, prevent body fluid leakage, and potentially deliver therapeutics locally to the targeted sites. These pre-formed matrices endow them with advantages such as well-controlled material homogeneity, pre-defined geometry, and user-friendly design. However, some limitations remain regarding the incompatibility with irregular defects and the need for compressive forces on the adhesive to be conformable to the tissue. A remedy to this issue is to lower the elastic modulus and thickness of the adhesives. Although adhesive patches are good candidates for topical applications, minimally invasive delivery of these materials with well-defined geometry inside the human body is challenging. Proper deposition inside the body often necessitates invasive procedures. Adhesive patches with shear-thinning or shape-memory properties could be potentially injected via a needle (*20*). Porous design could allow the pre-formed constructs for needle injection, which has been demonstrated for hydrogels (*177*), but not for tissue adhesives.

The pre-formed nature of these adhesives entails them well-controlled and homogenous matrix formation before application, however, their delivery via intricate delivery devices with tight delivery routes for internal usage can be very challenging, especially when minimally invasive surgeries are often preferred. Shape memory and shape morphing polymers that can be delivered via surgical tools and reverse to their original geometry could be appealing future directions to pursue (*177–179*).

2.3.2 In situ forming adhesives. As the pre-formed adhesives are difficult to apply onto irregular surfaces or delicate tissues that cannot be compressed, these issues motivate the development of in situ forming adhesives. They behave as a liquid upon implementation (i.e., the storage modulus G' is smaller than the loss modulus G''), and thus can form seamless contact with the tissue while requiring no compression; in-situ solidification then occurs overtime or via external stimuli such as humidity, temperature, pH and light exposure (*11*, *119*, *169*, *180*). An ideal in-situ forming adhesive should readily cover the target tissue surface, but not flow out of the target site, causing peritoneal adhesion. Following these goals, the design rule underscores the wetting ability, flow, and gelation properties of the adhesive precursor. The wetting ability is often quantified as the contact angle of the adhesive droplet formed on the tissue. According to Young's Equation, when the contact angle is small, the adhesive precursor tends to spread and wet the substrates (*181*). The flow properties such as viscosity and shear-thinning property determine how the in-situ forming adhesives could be delivered. Fig. 4B illustrates that highly viscous liquids can only be pasted onto the target tissue (*182*), and the liquids of low viscosity are amenable to spraying via pressured gas (*12*, *183*, *184*). Injection through a syringe and other tube-like devices is the most common approach compatible with the liquids of low-to-medium viscosity (*126*, *185–187*).

Injectable tissue adhesive glues are ideal for minimally invasive procedures such as laparoscopic surgery, where the access and space of operative sites are limited. They are also desirable for other application scenarios where suturing or stapling is difficult to implement or prone to leakage (*182*, *183*), and for non-compressible tissue surfaces. The curing/crosslinking mechanism often relies on the mixing of multiple ingredients and/or the application of light (either visible or UV lights). Cyanoacrylate is a unique example that polymerizes instantaneously upon contact with water/moisture in the ambient environment and the tissue surface. Many glues are implemented by mixing two or more compounds upon injection (*13*, *126*, *188*). Another widely used glue is fibrin glue, which can slowly solidify post-mixing without the need for external stimulation, yielding lower strength than the cyanoacrylate (*163*). Herein, refining the gelation kinetics is critical for the successful delivery. Because too fast gelation/polymerization could cause clotting of the delivery device, whereas slow gelling systems could diffuse out of the target tissues. To deal with the trade-off, the use of stimuli-triggered reactions is beneficial. For instance, UV light has been used to trigger the crosslinking of a poly(glycerol sebacate acrylate) based surgical glue to

enable on-demand adhesion and hemostatic seal within seconds of light application (*1*). However, the additional stimulus apparatus for minimally invasive procedures would raise some concerns.

Other delivery approaches for in-situ forming adhesives include pasting and spray. Although not as common as the injectable tissue adhesives, they find merits for specific materials systems and applications. The pasting method is preferred when the precursor solution is very viscous. Viscosity modifiers can be added to make the adhesive paste-like. Such adhesives exhibit finite yielding stresses so that they can hold the shape and be applied onto dynamic surfaces, where precursors of adhesives glue or spray would flow away. A notable example of this kind is a chondroitin sulfate-based adhesive, which can be pasted and adhere to a cartilage defect, exhibiting efficacy in cartilage repair.

The sprayable adhesives, sometimes referred to as "liquid bandage spray", are liquid adhesive precursors delivered as aerosol sprays to cover irregular tissue surface. The motivations for the sprayable adhesives are the need to cover a large surface of target tissues within a short duration. To achieve these goals, a spray gun is often used to activate, vaporize, and deposit the compressed precursors rapidly to the target surface. Thus, they're easy to implement without the need for mixing or stimulation. Regarding the design rules of sprayable adhesives, the precursor solution should exhibit a low viscosity (low G'') and is easy to form microdroplets under compressed air. Also, due to the low viscosity, a rapid polymerization kinetics is a must.

Due to the aforementioned features, the sprayable adhesives are particularly appealing for hemostatic use, particularly in battlefields, reinforcement of suture lines in vascular repair, and tissue reconstructions. Recently, a sprayable hydrogel adhesive was developed to avoid peritoneal adhesion (*184*). To achieve a homogenous and defect-free film, one needs to optimize the spraying conditions such as the spraying distance and gas flow rate. Ideally, the precursors used as adhesive spray should form instant adhesion with the underlying substrate and possess acceptable cohesive properties to guarantee retention right after their application. They also need to be stable in pressurized conditions and compatible with antifoaming agents to inhibit foam formation during agitation or occasional shaking. Plasticizers are often added to reduce the brittleness, ensure flexibility, enhance the resistance and tear strength of the polymer film formed after spraying (*189*). Various materials have been adapted as tissue adhesive sprays, including silicon-, cyanoacrylate- and fibrin-based polymer precursors. However, they're notoriously difficult to clean after each use

to prevent blockage of the spray nozzle. They're also predominantly used for topical applications and only used for internal organs when no other resources are available.

2.4 Degradability

Similar to surgical sutures for wound closure, where both non-degradable and degradable sutures are under clinical use in various settings, the degradation requirements for tissue adhesive design are also application- and tissue-specific. For load-bearing tissues with limited regeneration capability, non-degradable adhesives are preferred to provide long-term mechanical functions (both adhesive and cohesive strength) until a treatment is completed. In other application scenarios, degradable adhesives are generally desired to mitigate the need for secondary surgeries or post-operative procedures to retrieve the implanted materials. With a proper design of the polymeric network and crosslinks, a tissue adhesive to facilitate regeneration should degrade in accordance with the tissue regeneration process, eliminating the need for adhesive removal and associated complications (*190*). The degradation profile of tissue adhesive is sensitive to physical (e.g. mechanical loadings, flow rate), chemical (e.g. pH), and biological (e.g. enzymes) factors presented in the microenvironments where the adhesives reside. Also, the geometry and topology of the adhesive matrix impact mass transport, and thus the mechanism (bulk versus surface erosion) and rate of degradation (*191*). All these factors are coupled with the mechanical function of the tissue adhesive over time.

2.4.1 Degradation mechanism. Degradation can occur at the polymer backbone and/or the crosslink sites. The design of degradable adhesives favors the hydrogel matrix due to their highly tunable degradability (*192*). A variety of degradation mechanisms have been explored, for instance, the inclusion of degradable moieties (to the polymer backbone or the crosslinks) such as anhydrides (*193*), esters (*194*), thioesters (*195*), amide (*196*), urea (*197*), urethane (*61*), imine (*198*), peptide sequences (*199*). They can respond to hydrolysis, pH, enzyme, or light(*48*). A recent study showed that alginate-PAAm tough adhesives containing disulfide crosslinkers for PAAm network were fully degraded at physiological conditions within 5 weeks (*192*). A PAAc-gelatin-based tissue adhesive is degraded after 4-week implantation (*2*) due to the enzymatic degradation of the gelatin. The hydrolysis is particularly appealing due to the abundance of body fluid and relatively predictable degradation profile. The hydrolytic degradation can be modulated by the porosity, hydrophobicity, and geometry of the adhesive matrix, along with outer environmental factors such

as pH and temperature. Other mechanisms can base upon the breaking of chemical bonds under mechanical triggers such as ultrasound (*200*) and mechanical loading (*201-203*). These strategies can be utilized for temporal and spatial control over the degradation profile and the adhesion performance.

***2.4.2 Clearance pathways*.** The biocompatibility and immune response of the tissue adhesives in vivo are important considerations for the adhesive design. Since adhesives may elicit foreign body reactions, the (attempted) clearance of these materials can be initiated shortly following their placement. Small fragments (less than 10 μm) from fragmented or residue adhesive materials could be readily phagocytosed and subsequently digested by neutrophils and macrophages (*204*). Particles between 10 and 100 μm could be engulfed by multinucleated body giant cells, formed via macrophages fusion (*205*). Materials large enough to avoid phagocytosis are eventually encapsulated by a fibrotic tissue layer if not degraded in time (*206*). Most degradation products, including polymers with lower molecular weight and small molecule by-products, can be cleared from the body through the renal pathway, with a cut-off molecular weight around 70 kDa (*207*). These cleaved molecules from degraded adhesives are found to induce different levels of immune response. Some of them can cause serious inflammation or even carcinogenesis. Examples include cyanoacrylate based adhesives (*208*) and those containing glutaraldehyde (*209*). Tissue-dependent immune response and local reactions to the degradable products of an albumin-glutaraldehyde based adhesive was also observed, showing high-grade inflammatory response when applied on lung and liver, and only low- or medium-grade inflammation on aortic tissues (*210*). To this end, long-chain alky cyanoacrylate has been shown to effectively lower the degradation rate and slow down the build-up of toxic compounds, contributing to milder inflammation (*211*). Lowering the concentration of cytotoxic compounds (e.g. aldehyde) used in the adhesive led to thinner fibrotic capsules, indicating less severe inflammation (*38*).

2.5 Emerging Applications of Bioadhesives and Devices

Tissue adhesives with unprecedented mechanical properties have been recently developed to enhance their traditional functions for wound closure and mechanical support. By further engineering adhesion with native tissues and advanced functional matrix design, tissue adhesives have emerged as mechanically, chemically, and biologically instructive materials for regenerative medicine. The mechanical integration enabled by tissue adhesives also allows intimate reciprocal

signaling and transmission, which shed light on their promising applications in health monitoring and management. Below the recent progress and emerging applications of tissue adhesives are reported.

2.5.1 Tissue sealing and on-demand detachment

2.5.1.1 Pressure-sensitive adhesives (PSAs). As the most widely used topical adhesives, PSAs are primarily biochemically inert, mechanically passive devices to adhere to skin given applied pressure. They are commonly seen as medical tapes for fixing life-sustaining and -monitoring devices to the body, or as skin bandages for wound care (*215, 216*). PSAs typically consist of an adhesive layer and a backing (*216*). The adhesives are made with a number of elastomers, including acrylic, natural rubber, silicone, and polyurethane(*217*). They are preformed and tacky to both dry and moist skins. However, the adhesion energy is modest (10-100 J m^{-2}) and rate-dependent due to weak interfacial bonding and viscoelasticity of PSA (*218*). However, repeated changing of PSAs at the same site can indeed damage the stratum corneum and cause skin injuries, especially for neonates and people with sensitive skin (*216, 219*). In addition, the stiff backing of PSA may constraint mechanically the underlying skin.

Recent efforts have been made to minimize some complications associated with PSAs. As an example, polydimethylsiloxane (PDMS) adhesives are optimized for attachment of epidermal electronics to the skin(*220, 221*). Such adhesives are designed with low elastic modulus and small thickness to conform and adhere to skin surfaces, sustaining normal motions (Fig. 2.6A, B). The adhesives can integrate the skin with electrodes for real-time monitoring of vital signals, such as electroencephalograms (EEGs), electrocardiograms (ECGs), electromyograms (EMGs), and photoplethysmograms (PPGs)(*212, 222*). Importantly, the adhesion is repeatable and detachable, resulting in minimal adverse effects on the skin. Under circumstances that necessitate strong adhesion, covalent bonding can be introduced by coating tissue-bonding reagents such as oxidized dextran (carrying aldehyde groups) to the adhesive surface. But this approach would sacrifice repeatability.

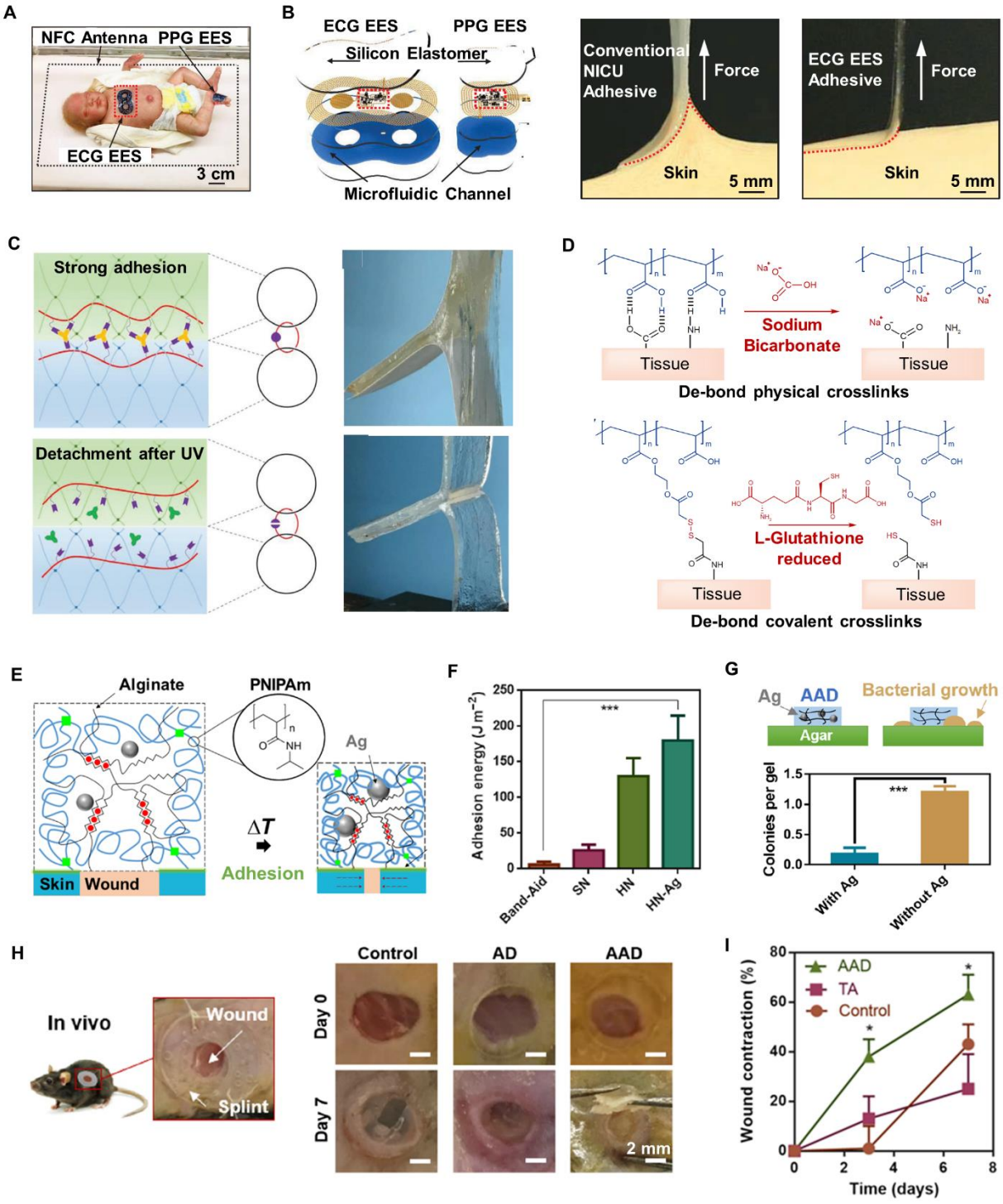

Figure 2.6. Applications of topical tissue adhesives. **(**A) A neonatal intensive care unit (NICU) setting of an epidermal electronic system (EES) configured with a binodal (chest and foot) deployment of skin-like wireless devices. (B) Peeling off a conventional NICU adhesive (left) and the EES adhesive (right) from the skin of a healthy adult. Reproduced with permission.(*212*) (C)

Design of topological adhesion. Two hydrogels adhere strongly when stitching polymer chains form a topological entanglement between the adherents and disassociate when UV light breaks the stitching polymer network.(*213*) (D) Schematic illustrations for the de-crosslinking process of cleavable physical and covalent crosslinks by sodium bicarbonate and L-Glutathione reduced. Reproduced with permission.(*62*) (E) Schematics of a temperature-triggered transition of active adhesive dressing (AAD), which consist of PNIPAm (blue lines), alginate (black lines), and silver nanoparticles (Ag; grey spheres). AAD forms strong adhesion (green lines) with the wounded skin. (F) Adhesion energy measured on porcine skin of Band-Aid and AAD composed of either single-network gel (SN) or hybrid-network gel with and without Ag (HN, HN-Ag). (G) Antimicrobial function of AAD with and without Ag. (H) Digital images of the initial wounds and those after 7 days with no hydrogel treatment (control), with treatment with non-active dressing (AD), and with treatment with AAD. (I) Wound contraction as a function of time and treatment conditions.(*214*)

Microstructured surface design inspired by nature has been recently explored to potentiate the elastomer adhesives. The surface microstructures are proposed to increase the adhesive-tissue interactions, while reducing the effective surface modulus even when the bulk modulus exceeds the upper limit of the Dahlquist criterion (*218*). In line with this design principle, a gecko-inspired micropillar design was applied to promote Van der Waals forces and adhesion performance (*138*, *223*). In octopus-inspired adhesives, microscale dome-like arrays are constructed to mimic the protuberances of octopi suction cups (*139*). Suction force induced by a negative pressure can be formed through squeezing the air out of the micro-domes.

2.5.1.2 Tough hydrogel adhesives. A major advance in the field of tissue adhesives is the development of tough hydrogel-based adhesives, exhibiting the best adhesion performance so far. The key mechanism is to synergize strong interfacial bonding and tough hydrogel matrix. The tough hydrogel matrix features extremely high toughness (10^3-10^4 J m^{-2}), even overperforming skin and cartilage (*224*, *225*). Such adhesives are usually composed of both a strong and weak polymeric network within the matrices. When the adhesive is peeled off from tissue, the weakly crosslinked network will break and dissipate energy within the hydrogel matrix, converting to high adhesion energy. The first demonstration of this design principle is a tough hydrogel adhesive, made of alginate-polyacrylamide hydrogel surface-activated with chitosan and carbodiimide

chemistry for tissue bonding(*3*). Such adhesives achieved high adhesion energy >1000 J m^{-2} on diverse tissues, including skin, cartilage, and blood vessels. In line with this design principle, dry double-sided tapes (DSTs) were recently reported to achieve high adhesion within seconds(*2*). The DST is a dry tough gel made of covalently crosslinked poly(acrylic acid) network grafted with N-hydroxysuccinimide esters (NHS), which react with the primary amine of tissues for covalent bonding. The instantaneous adhesion performance is attributed to a dry crosslinking mechanism, as well as poly(acrylic acid) network capable of forming hydrogen bonds with tissues rapidly. Moreover, tough hydrogel-based adhesives can bond firmly with metals and elastomers, are well-positioned for use in wearable electronics for mobile health (*23*, *226*).

2.5.1.3 Transdermal patches. The skin adhesives can encapsulate and release drugs to the skin. The transdermal patches can realize painless transdermal drug administration (*77*). Compared to oral delivery, transdermal delivery could mitigate first-pass effects and liver damage(*218*). Based on PSAs, most transdermal patches contain either a drug-laden elastomeric matrix or a drug reservoir sandwiched between a rate-controlling membrane and a backing (*227*). The drugs compatible with this strategy are mainly small-molecule drugs, such as buprenorphine, clonidine, methylphenidate, and testosterone. Because hydrophilic and high molecular weight drugs suffer from limited permeability through the skin barrier (*228*). For high skin permeability, rigid sharp miniaturized needles (microneedles) are constructed on patch surfaces to pierce the outermost layer and to deliver the drugs directly into the dermis layer (*229*, *230*). As a result, macromolecules drugs such as proteins and vaccines can overcome the skin barrier. When coated with swellable polymers, the microneedle patches can leverage swelling to facilitate mechanical interlocking with the tissues (*231*, *232*).

2.5.1.4 On-demand detachment. When a medical treatment completes, the tissue adhesives might need to be removed. Other circumstances include drug refilling, adhesive repositioning, medical examination, and antimicrobial treatment (*233*, *234*). Even for adhesives with weak adhesion, the repeated change could cause trauma to sensitive skin or damage the newly formed tissues or peri-wound skin (*219*). For cyanoacrylate adhesives, it is challenging to remove the adhesive prematurely and substantial residues are often left on the skin (*235*).

A quick, easy, and damage-free removal (i.e., on-demand detachment) is desirable but currently cannot be met with existing adhesives. There is progress to overcome this challenge. A solution

for medical tapes is to add a low-adhesion intermediary layer between the adhesive layer and the backing layer, leading to "quick-release" medical tapes (*216*). After the backing layer is peeled off, such tapes leave a large volume of adhesive behind, instead of residue islands from conventional medical tapes. The thick adhesive residues can be easily rolled and removed with minimized dermal strains. This method is amenable to adhesives with moderate adhesion strength. When one wants strong adhesion and no residues, it is imperative to realize on-demand detachment. To this end, a common strategy is to engineer the adhesives to lose adhesion and detach upon an external trigger (*236*). For the cases of polymer interlocking, one can dissociate the interpretation network of the stitching polymers with external stimuli. Take the chitosan-based adhesives as an example.

The resulting network at the interface can dissolve at an acidic condition (pH<6.5), resulting in adhesive detachment (*237*). Following a similar design principle, researchers utilized UV light to switch off the adhesion enabled by poly(acrylic acid)/iron stitching polymer system (*213*, *238*). Upon exposure to UV light, Fe^{3+} ions are reduced to Fe^{2+} ions and dissociate with the carboxyl groups from the PAA chains, thereby turning off the adhesion (Fig. 2.6C). The demonstrated adhesion energy between two alginate-polyacrylamide hydrogels was reduced from 1400 to 10 J m^{-2} upon the UV exposure.

For the adhesion enabled with molecular interactions, one can target the interfacial bonds directly with external triggers (*236*). For instance, cleavable disulfide bonds can be introduced between adhesive functional groups (e.g., NHS ester groups) and polymeric chains of the bioadhesives (*62*). Such bonds break upon the exposure of biocompatible reducing agents (e.g. L-Glutathione reduced), leading to cleavage of covalent crosslinks between the bioadhesives and the tissue. Bioadhesives relying on the physical crosslinks of hydrogen bonds can also be cleaved by adjusting pH (Fig. 2.6D). In vivo biocompatibility of a triggering solution, containing L-Glutathione reduced and sodium bicarbonate, has been demonstrated in a rat model with benign bioadhesive detachment and low level of inflammation.

2.5.2 Wound management

Unlike adhesion-only applications involving intact tissues, wound management is to treat open or internal wounds with tissue adhesives (i.e., wound dressings). Wound variables include thickness, size, tissue loss (versus incision), and wound types (chronic, acute wounds, burn) (*234*, *239*). An ideal wound dressing should not only provide stable adhesion but also account for the wound

healing process and the potential risk of tissue trauma during the removal of adhesives (See discussion on on-demand detachment) (*219*). Specific considerations include therapeutics delivery, wound monitoring, maintaining high humidity, gaseous exchange, removal of wound exudates, and avoiding infection. The global market for wound management is US$19.8 billion in 2019 and is projected to reach US$23.8 billion by 2025 (*240*). The general process of implementation includes (i) filling/closure of the wound to form adhesion and avoid infection; (ii) exerting biochemical and physical cues to promote the healing; (iii) providing additional functionality to monitor the wound conditions; (iv) detachment or degradation. The design considerations and examples at each step will be elaborated below.

2.5.2.1 Antimicrobial function. Open wounds are prone to infection due to a favorable environment for pathogenic organisms, which may lead to necrosis and sepsis (*183*, *241*). A post-surgery infection rate of 3.9-8.2% exists, even if standard sanitization measures are taken, such as the use of povidone-iodine, isopropyl alcohol, and chlorhexidine to disinfect the wounds (*241*). Around 1.6-4.4 species of bacteria are found in ulcer wounds (*242*), and many bacteria produce toxic metabolites, leading to patients' morbidity and mortality (*183*). Therefore, the integration of antimicrobial functions into skin adhesives is critical for wound management, especially for chronic and burn wounds that demand extensive medical care (*241*, *243*).

To combat infections at wound sites, a common approach is to deliver antibiotics from the wound dressings directly. Antibiotics can be easily loaded into hydrogel-based skin adhesives. For example, a dopamine-hyaluronic acid adhesive dressing encapsulates and releases doxycycline in an extended manner (*185*). The antibacterial dressing inhibits the growth of *E. coli* for 9 days and *S. aureus* for 15 days. Despite the success of antibiotics, increasing risks emerge with antibiotic-resistant pathogens (*244*). Another approach is to employ heavy metal nanoparticles (NPs) as antibacterial agents. The toxicity of those nanoparticles depends on their shape, size, surface charge, composition, and dosage (*245*). Nanoparticles such as silver (Ag) and titanium have been approved by the FDA for antibacterial indications. The AgNPs laden into hydrogel-based active adhesive dressing inhibited bacteria growth effectively compared to dressings without AgNPs (Fig. 2.6E-G) (*214*). As an alternative to antimicrobial reagent release, an adhesive matrix with intrinsic antimicrobial polymers is attractive for long-term antibacterial function. The inclusion of polymers functionalized with bioactive groups can provide dressing matrices with permanent biocides (*244*, *245*). For instance, quaternized chitosan exhibits enhanced antibacterial activity at all pH

conditions compared to the unmodified chitosan (*186*). An in vivo rabbit tibial fracture model shows that quaternized chitosan-loaded polymethylmethacrylate (PMMA) bone cement exhibited excellent antimicrobial performance against methicillin-resistant *staphylococcus epidermidis* infection (*246*). The treatment group using quaternized chitosan-loaded PMMA resulted in significantly reduced bacteria colonies (over 4-fold reduction), white blood cell counts, and intramedullary abscesses compared to groups with antibiotic-loaded PMMA treatment, an established procedure for treatment of infections of severe open tibial fractures(*247*). Aldehyde functionalized polysaccharides and block copolymers also lead to enhanced antibacterial function (*248*, *249*).

Physical approaches like photothermal treatment are also developed(*185*, *238*, *250*, *251*). Near-infrared (NIR) light-absorbing additives can be incorporated into the adhesive matrix. Examples include gold nanorods (AuNRs) and graphene oxide (GO). Such materials can convert the NIR light into localized heat to destroy the pathogens (*250*). Studies show that 10-min NIR exposure at low intensity (2 W cm^{-2}) can effectively reduce the viability of multiple bacteria types such as *E. coli*, *E. faecalis*, and *S. epidermidis*. Carbon nanotubes (CNTs) are added into hydrogel wound dressings for photothermal function (*186*). With a similar radiation dosage, the dressing temperature can be raised to above 50℃ to denature the bacteria protein and membrane lipids, which results in bacterial death. A CNT concentration-dependent killing ratio between 92-100% can be achieved for *S. aureus*, *E. coli*, and *P. aeruginosa*.

2.5.2.2 Controlled drug delivery. Tissue adhesives can encapsulate and release bioactive reagents such as small-molecule and macromolecular drugs to wound sites locally. The drug-eluting adhesives have been shown to accelerate and promote wound healing effectively (*252*). Reagents to deliver are often growth factors that directly mediate different phases of wound healing (*253*). For instance, vascular endothelial growth factor (VEGF), fibroblast growth factors (FGFs), and PDGF can guide the migration and proliferation of endothelial cells toward wound sites to form new blood vessels; insulin-like growth factor (IGF), FGFs, TGFs, keratinocyte growth factor (KGF), and matrix metalloproteinases (MMP) can promote fibroblasts proliferation, ECM deposition, and wound contraction (*239*, *252–254*).

These bioactive reagents are compatible with hydrogel-based adhesives. Thanks to the tunable physical properties and controllable degradability, hydrogel adhesives enable spatiotemporal

control over the drug release (*75*). A simple strategy is to load the drugs inside the polymeric network and release them through diffusion. This strategy is demonstrated on tough hydrogel-based DST, in which a mock drug (FITC-gelatin) releases continuously out of the adhesive matrix over 12 hours (*2*). Another strategy is to engineer appropriate drug-polymer interactions for a higher degree of controlled release. The affinity of drugs is based on covalent conjugation, electrostatic interactions, or hydrophobic association. A PNIPAm hydrogel adhesive containing graphene oxide and quadruple hydrogen ureidopyrimidinone is developed for doxorubicin hydrochloride (DOX) delivery(*255*). The physical and electrostatic interactions between DOX and graphene oxide lead to a slow and sustained drug release profile.

An emerging direction is designing tissue adhesives for on-demand drug release. This attempt is to reduce side effects associated with burst release and to enable digital control over the drug administration (*256*, *257*). The function can be realized with stimuli-responsive polymeric networks. For instance, a smart skin dressing exploits the thermosensitive PNIPAm for on-demand drug release (*258*, *259*). Drug-laden PNIPAm microparticles are encapsulated inside the wound dressing while a PET film containing a 3D printed temperature sensor and flexible thin heater is placed as the dressing backing. When the abnormal change of wound temperature is detected as a result of microbial infection, the heater will be activated and trigger the shrinkage of the encapsulated microparticles, leading to the on-demand release of pre-loaded antimicrobial drugs. Although the PNIPAm has been extensively used, opportunities remain for other systems sensitive to pH (*260*), light (*261*), or ultrasound (*262*).

2.5.2.3 Electrical and sensing function. Besides the therapeutic function, tissue adhesives under development are gaining electrical and sensing function. Consideration of electrical properties is mission-critical for some applications such as cardiac tissue engineering and bioelectronics. When applied for myocardial infarction treatment, the adhesives with improved electrical conductivity has been shown to elevate cardiac pump function and to prevent negative left ventricle dilation compared to the nonconductive adhesives (*182*, *263*).

An emerging trend is to engineer the monitoring of wound conditions such as temperature, hydration status, and pH. The quantitative data are important indicators of inflammations, infections, and wound healing processes to inform the professional assessment (*221*, *241*). The benefits can be seen in a recent work (Fig. 6A,B), showing a soft epidermal electronics system

(EES) contains fractal layouts of microscale metal traces to map the temperature and hydration status of the skin near the wounds (*212*, *221*). This system is very compliant and slim, allowing seamless contact and intimate coupling with the skin via Van der Waals interactions alone. Another design of smart bandage further integrated stimuli-responsive dressings, temperature and pH sensors, and a flexible heater within a wound bandage (*259*). Through a wireless communication module, the bandage can transmit temperature and pH data continuously to a program. When an infection is detected, the controller will use the heater to trigger the thermosensitive dressing to release antibiotics.

Strain-dependent electrical properties of adhesives have also been exploited to develop soft wearable sensors for health monitoring. When attached to motion-active body parts, the adhesives report electrical signal change, which can be correlated to physical or physiological motions such as finger moving, wrist bending, and breathing (*264, 265*). Diode-like electrical characteristics of ionically conductive hydrogel adhesives have also been explored to sense force, strain, and humidity, mimicking the sensation of skin (*266*). Conductive hydrogel adhesive sensors have also been demonstrated to monitor dynamic motions of organs wirelessly in real time (*267*). Such abilities enable the possibility to monitor wound healing progress without repetitive invasive procedures for internal organs. Conductive materials are commonly incorporated into the tissue adhesives to improve conductivity. Examples include carbon nanotubes, graphene, organic conductive polymers such as pyrrole, and choline-based bio-ionic liquid.

2.5.2.4 Actuation. Conventionally, tissue adhesives are mechanically passive devices. They can be mechanically active to promote wound healing. This concept was recently demonstrated with an active adhesive dressing (AAD) for wound management (*214*). The AAD matrix comprises PNIPAm and alginate tough double-network hydrogels. PNIPAm is a widely used biocompatible thermoresponsive polymer that repels water and shrinks at around 32°C. When the AAD is applied to the open wound, the body temperature-triggered contraction can apply contractile strains to the wound edges. The active matrix shows a significantly quicker wound closure rate compared to non-active wound dressings (Fig. 2.6E-I). This design echoes a modern wound treatment method, termed topical negative pressure therapy, in which a localized negative pressure is applied under the wound dressing to promote wound healing (*234*).

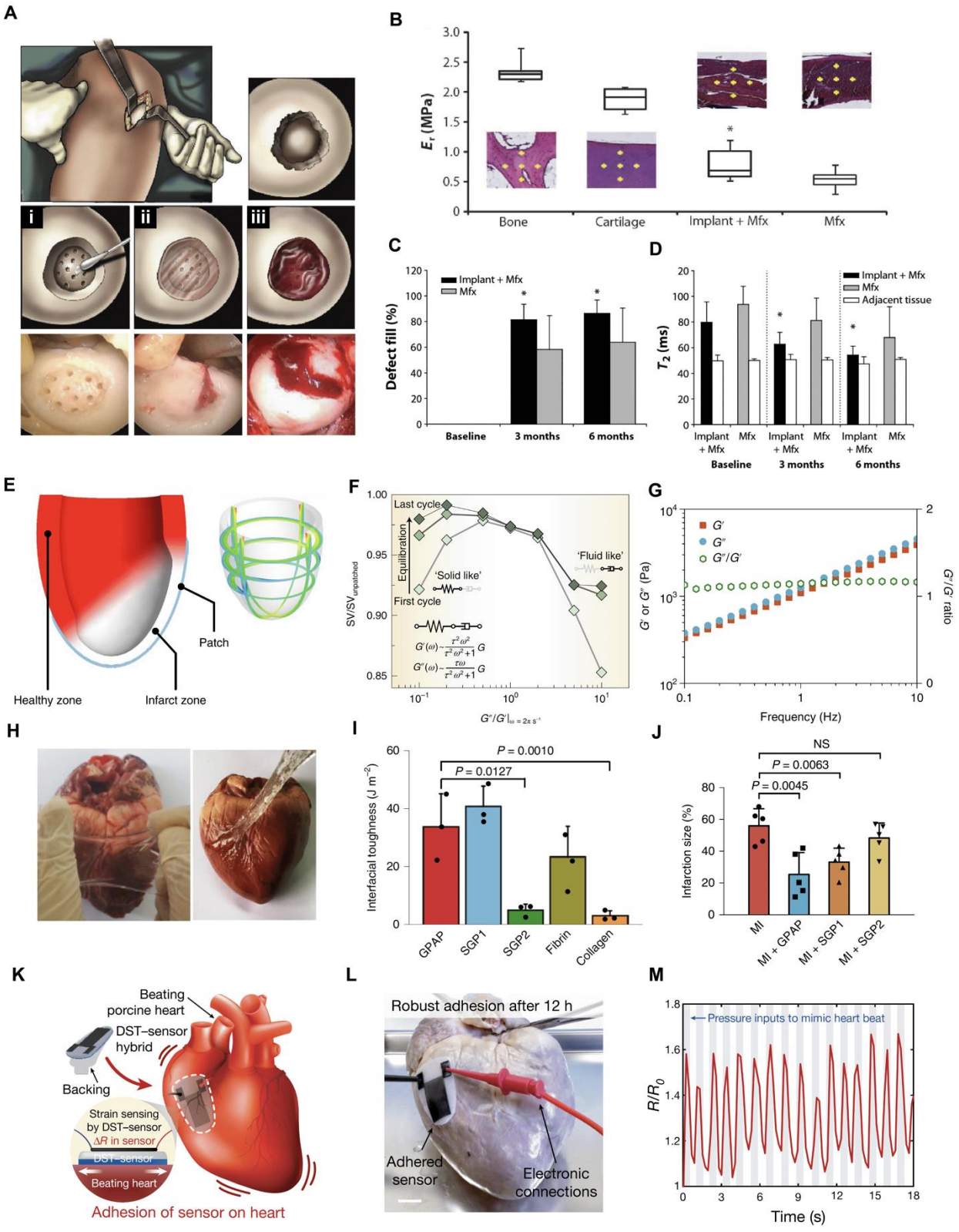

Figure 2.7. Examples of implantable adhesive design. (A-D) Adhesive-hydrogel composite for cartilage repair. (A) Clinical procedure for adhesive-hydrogel implantation into a cartilage defect.

(i) Surgical microfracture creation; (ii) adhesive application; (iii) hydrogel precursor injection and in situ polymerization. (B) Elastic moduli and histological sections of bone, cartilage, and cartilage with implants and microfracture (mfx) or with mfx alone in a goat model. (C) Enhanced defect fill for patients treated with hydrogel implants compared with patients receiving microfracture alone. (D) T_2 relaxation time, indicative of tissue organization and water content, was significantly lower compared with baseline measurement for patients with hydrogel implants treatment, but no difference of statistical significance was observed with microfractured patients.(*11*) (E-J) A viscoelastic adhesive epicardial patch for treating myocardial infarction. (E) Simulation guided epicardial patch design. (F) Effect of patch viscoelasticity and cyclic deformation during equilibrium on stroke volume in a simulation. (G) Oscillation frequency dependence of the gel-point adhesive patch (GPAP). (H) A stretched GPAP film (left) adhering to a pig epicardium (right). (I) Material/epicardium interfacial toughnesses of SGP (starch gel patch), fibrin glues, and collagen gels. (J) Decreased infarction size was observed in GPAP treated groups after acute myocardial infarction (MI).(*20*) (K-M) Adhesion of a dry double-sided tape (DST)-strain-sensor hybrid on a beating porcine heart ex vivo. (M) Normalized electrical resistance of the DST-adhered strain sensor over time to measure the deformation of a beating heart.(*2*)

2.5.2.5 Hemostasis. As hemostasis is the first step towards wound healing, the consideration of hemostatic function is relevant to tissue adhesive design. There are generally two strategies to provide hemostatic functions. One is to use hemostatic reagents to trigger or facilitate the innate clotting mechanism (*268*). The other strategy is to use adhesives to physically block the bleeding sites, especially for patients with bleeding disorders (*7*). Nanoparticles, such as nanoclay, bioglass, and ion oxide, have been explored as hemostatic adhesives. They can bridge lacerated wounds through electrostatic interactions or hydrogen bonds and cause coagulation to stop the bleeding (*269*). However, their ability is limited due to their low intrinsic adhesion energy (~10 J m^{-2}). The unintended coagulations caused by the invasion of hemostatic nanoparticles into the bloodstream is another concern (*270*).

Polymer-based adhesive sponges have demonstrated excellent hemostatic effect. Lyophilized oxidized-dextran sponges can quickly absorb the blood on the wound and form stable adhesion through Schiff base reaction (*271*). The increased concentrations of red blood cells and platelets

after serum removal can trigger the coagulation pathway. However, the matrix of sponge adhesives is generally weak and cannot provide long-term barrier functions. Hydrogel-based hemostatic glues have also been explored in hemostasis studies. Such glues comprise methacrylated polymers, such as gelatin, hyaluronic acid, or tropoelastin, in conjunction with photoinitiators for in situ light crosslinking (*173*, *183*, *187*). Nonetheless, those glues also share the problem of limited adhesion strength and may not be suitable for the mechanically active tissue parts.

2.5.3 Musculoskeletal tissues repair

Implantable tissue adhesives are implanted into the human body for wound closure, sealing, regenerative medicine, or to avoid undesirable postoperative tissue adhesion (*272*). Wet and dynamic internal organs pose a challenge to form strong adhesion, which should endure complex loading of the tissue microenvironment. Compared to topical adhesives, implantable adhesives should meet additional requirements on the delivery, retention, and clearance. Among them, important considerations include the delivery approaches (enabling invasive or minimally invasive procedures), immune response (i.e., host-biomaterial interactions), degradation profile, and clearance pathway. Those considerations have been addressed with recently developed implantable adhesives. Notable advances in the applications of musculoskeletal and cardiovascular systems will be highlighted and discussed below.

Musculoskeletal system is where tissue adhesives can make great impacts. It is associated with a number of diseases and injuries, such as low back pain and arthritis, which becomes prevalent among the aging population and result in huge socioeconomic burdens. Tissue adhesives are appealing as they can avoid tissue microtrauma (caused by suturing and stapling) and help reduce the stress concentration by matching the tissues mechanically. They can complement current treatment and potentially revolutionize regeneration intervention strategies. Also, they can serve as a versatile platform to provide additional biomechanical and biochemical cues to facilitate tissue repair and regeneration. The musculoskeletal tissues such as cartilage and IVD suffer limited regenerative capacity due to their low cellularity, vasculature, and exposure to stringent mechanical loading. To ensure healing outcomes, the adhesives should exhibit superior mechanical properties to accommodate the loading and deformation of the tissues, while instructing and accelerating the regeneration process.

Cartilage repair with tissue adhesives has received much attention. Suturing in cartilage has been linked with microcracks and local inflammation due to the stress concentration effect of the suture (*273*). This issue could be overcome with tissue adhesives. Besides, the adhesives can fill cartilage defects as acellular scaffolds. The acellular approach is illustrated with chondroitin sulfate (CS) based adhesives, showing efficacy in repairing cartilage defects. Such adhesives carry methacrylate and aldehyde groups to enable covalent bonding between the cartilage and PEG hydrogel (*45*). The integrated hydrogel-cartilage constructs survived the mechanically harsh joints environments, and suggested enhanced cartilage regeneration and increased area of tissue fill in small and large animal models.

The acellular approach can be combined with microfracture to allow bone marrow stimulation in the defect site to accelerate healing. In a clinical study, the CS-based adhesive was applied along with a microfracture procedure, which is commonly practiced to expose bone-marrow-derived progenitor cells at cartilage defects (Fig. 2.7A)(*11*). The adhesives showed good compatibility with the blood and blood clotting processes. Good integration of clot-hydrogel and native tissue was confirmed with imaging techniques. The cartilages treated with both microfracture and adhesive-hydrogel showed increased elastic modulus and defect filling, and enhanced tissue organization compared to those treated with microfracture alone (Fig. 2.7B-D). Despite the encouraging results, the mechanical property of the repaired tissue remained much lower than the native cartilage (Fig. 2.7B). Other concerns include the cytotoxicity of aldehyde, the use of UV light, and the brittle hydrogel in use. Strategies to fully restore a defected cartilage mechanically remain to be explored. Alternatively, cell delivery with adhesives can be applied to replenish the cell population. As such, the lack of integration with grafted tissues and complications associated with retention of transplanted cells could be addressed.

Repair of other musculoskeletal tissues such as tendon and IVD also calls for tissue adhesives. For tendon repair, commercially available adhesives are shown to improve the healing outcomes of suturing procedures (*274*). The tissue adhesives are believed to reduce stress concentration and distribute mechanical loading across the tendon. For IVD repair, a recent advance is a new strategy to fill the NP cavity after discectomy with HA hydrogel and, simultaneously, seal the defect in the AF with a light-crosslinked collagen hydrogel. This hybrid strategy can preserve native IVD morphology and restore NP content based on histological evaluation in a 6-week study of a caprine model, indicative of the prevention of acute IVD degeneration of IVD (*275*). Mechanical

characterization also showed that the repaired IVD restored the mechanics of native tissue. Although the implant-tissue adhesion was not measured, a certain level of biointegration is achieved by interpenetration via in situ crosslinking, which is necessary to sustain the high pressure within the IVD space. This study also demonstrated that the implantable materials should be refined for appropriate mechanical and biochemical properties to match target tissues to fulfill their distinct functions.

Despite some successes, the development of tissue adhesives for tensile load-bearing tissues such as tendon is lagging. Mounting evidence shows the benefits of tissue adhesives alone or as an ancillary method to suturing, but the healing outcomes remain limited (*276*, *277*). A reason for the unsatisfactory results is the mechanical mismatch between the implantable adhesives and the target tissues. For instance, fibrin glues used in previous studies were much softer and more brittle than the musculoskeletal tissues. Further development is foreseen to precisely tailor biomechanical properties of the adhesives to recreate a biomimetic or instructive niche. Biointegration enabled by the advanced tissue adhesive allows intimate interactions of the implanted materials and the native tissues, apart from their traditional wound closure functions to replace sutures. Local tissue development and disease development could be altered or guided by the restored mechanical environments enabled with the adhesives.

Toughness and strength of the implantable adhesives are critical, as many musculoskeletal tissues bear mechanical loading. For high toughness and strength, implantable adhesives based on double network hydrogels have been developed and tested. For example, a PEGDA-alginate-cellulose fiber hydrogel was developed to form in situ and adhere to several load-bearing musculoskeletal tissues, including subchondral bone, articular cartilage, and lateral meniscus (*278*). This study presented ex vivo mechanical testing to corroborate the immediate effects of enhancing tissue adhesion with a tough hydrogel matrix for orthopedic applications. Immediate adhesion was demonstrated, but the long-term adhesion in vivo remains elusive. Besides the long-term evaluation, future work could focus on shortening the UV exposure for gelation.

2.5.4 Cardiovascular system interface

The cardiovascular system is a wet, dynamic, and pressurized system. When degenerated or injured (which might be fatal), the cardiovascular system requires surgical intervention to seal the defect and to restore the proper function. While suturing remains prevalent in cardiovascular

surgeries, the use of tissue adhesives is emerging into three applications: (1) suture supplements to avoid fluid leakage; (2) hemostats to control bleeding; (3) mechanical supports to reinforce degenerated cardiovascular tissues. To supplement sutures, several tissue adhesives are approved by FDA and used clinically, including *BioGlue®*, *CoSeal®*, and *Tisseel®*. The inability to replace sutures is attributed to lower mechanical strength than the target tissues and the suboptimal adhesion performance. For the use of hemostats, tissue adhesives form mechanical barriers to stop the blood flow. This principle is illustrated with a tough adhesive capable of controlling hemorrhage condition in a rodent laceration model(*3*). Besides, the adhesives can exert hemostatic function by directly participating in the hemostatic cascade or by releasing blood clotting agents (such as thrombin and fibrinogen). Examples include the widely used fibrin glue (part of the native hemostatic cascade) and a composite gelatin hydrogel containing silicate nanoparticles (*279*).

Tissue adhesives also find use in the cardiovascular system without open wounds. Their deployment is to reinforce mechanically diseased cardiovascular tissues such as infarcted myocardium and aneurysm (bulging blood vessels). A recent advance in this area is a highly viscoelastic adhesive hydrogel patch for treating myocardial infarction (*20*). A finite element modeling of the epicardial patch concluded that an adhesive patch with fluid-like properties near the gel-point (i.e., storage and loss moduli are equivalent) would be ideal for the cardiac functions, compatible with the heart's constantly beating movements (Fig. 2.7E, F). This adhesive patch is an ionically crosslinked starch hydrogel with fluid-like properties near the gel-point (Fig. 2.7G). The adhesion of the patch is based on hydrogen bonds at the adhesive-tissue interface and a highly viscous hydrogel matrix for energy dissipation (Fig. 2.7H, I). The adhesive showed no significant degradation after 1.5-year implantation. Its therapeutic efficacy outperformed many other acellular patches and some drug-eluting patches in a rodent model (Fig. 2.7J). In comparison, cyanoacrylate glue caused a 100% death rate due to their high stiffness, which failed to accommodate the cyclic deformation of a beating heart. This study highlights the significance of a carefully designed adhesive matrix and a compliant tissue-adhesive interface in fulfilling and augmenting the function of native tissues. The proposed material design strategy to computationally simulate adhesive-tissue interactions and accurately predict and analyze the treatment outcome also presents an efficient approach for proof-of-concept analysis before the time-consuming and expensive ex vivo/in vivo experiments.

Those adhesives as cardiac patches can also deliver cells or drugs, offering a potential treatment for severe myocardium infarction (MI). The approach was recently exemplified with a fibrin adhesive dressing, which can adhere to the heart without suturing, and encapsulate and deliver mesenchymal stromal/stem cells epicardially. This work showed the adhesive matrix can promote MSC's function and that the technique enhanced cardiac function recovery with improved myocardial tissue repair in a rat ischemic cardiomyopathy model(*280*).

In addition to the mechanical and biological considerations, electrical functions are also within the tissue adhesive design. First, electrical conductivity is intrinsic to the heart activity. This design consideration is included in the design of a conductive adhesive cardiac patch for MI treatment (*182*). The main component of the hydrogel matrix is a hyperbranched polymer containing dopamine and pyrrole end-cap and gelatin. Upon adding Fe^{3+} as the curing agent, pyrrole is in situ polymerized as conductive polypyrrole nanoparticles. Meanwhile, the formed catechol-Fe^{3+} complexation can enable wet adhesion of the hydrogels. The paste-like adhesive hydrogel can be painted and rapidly bond to beating hearts, and enhance the conduction of electrophysiological signals and revascularization of the infarcted myocardium. Another type of electrical function is monitoring the electrical activities of target tissues. Given an intimate and stable interface with the heart, the adhesives are advantageous to directly monitor the electrogram signals from a beating heart. The requirement is the integration of flexible electrodes. An exemplar work shows an adhesive tape developed recently can adhere to a stretchable strain sensor and a beating heart with a dynamic and curved surface (Fig. 2.7K-M)(*2*). Another work reports an adhesive hydrogel containing polydopamine and an array of electrodes demonstrated substantially improved recording efficiency due to the enhanced adhesion between the elastrode (elastic electrode) array and epicardium (*281*).

2.6 Discussion and Conclusions

Despite the rapid advances in the field of tissue adhesives, many challenges and unmet clinical needs remain. We will next discuss the limitations of existing tissue adhesives and shed light upon future directions toward next-generation tissue adhesives.

Whereas many design factors have been considered, the pathological condition of tissues has been largely overlooked. Diseased/injured tissues could differ substantially from healthy tissues mechanically and biochemically (*282–284*). The difference also includes the change of local

immune microenvironment (e.g., inflammatory cytokines, macrophages) (*205*, *206*). They would inevitably impact the property and performance of tissue adhesives. Arguably, the coupling between the material and the biological system is complex and deserves an in-depth investigation. The recent surge of the research of biomaterial-immune system interactions could motivate the study focusing on the in vivo response of tissue adhesives (*285*). The understanding could in turn inform the creation of bio-instructive tissue adhesives capable of instructing the immune response for better healing.

Mechanical properties of tissue adhesives require further improvement, particularly tensile strength and fatigue resistance. Although tough tissue adhesion has been recently demonstrated, the tensile strength of most adhesives (on the order of 0.1 MPa) is much lower than that of surgical sutures (1 GPa) (*286*, *287*) and load-bearing tissues such as cartilage and tendon (~10 MPa)(*10*). Due to the lack of mechanical strength, commercialized tissue adhesives such as fibrin glues and *Bioglue®* suffer from limited outcomes in repairing tendon (*276*, *277*). The mismatch of mechanical properties is a major constraint that disqualifies tissue adhesives as a stand-alone repair technique to replace suturing. Another mechanical concern is about the loss of adhesion under cyclic loading, i.e., interfacial fatigue fracture. It is critical as a recent study highlights that a tissue adhesive is, despite high adhesion energy (~500 J m^{-2} under monotonic load), susceptible to debond at small cyclic load (~20 J m^{-2}) (*288*). Strategies to improve the fatigue resistance of tissue adhesives are currently missing. In the future, tissue adhesives should bear a large tensile load without rupture and be immune against cyclic loading. As such, they could replace suturing, enabling suture-free procedures that have been proposed for years.

A critical intellectual advance is the recognized role of tissue adhesives in promoting tissue regeneration actively, either independently or in adjunction to therapeutic agents (*289*, *290*). This concept challenges the traditional concept that a tissue adhesive serves as a passive mechanical device for wound closure. The regenerative capacity of tissue adhesives is critical in applications associated with poorly regenerative tissues such as cartilage and IVD and in patients with compromised healing potential due to disease conditions such as diabetics and autoimmune diseases (*10*, *291*). Cell and drug delivery with tissue adhesives are attractive to pursue (*292*). By doing so, the adhesives can release bioactive agents directly to wound sites. Adhesives with selective affinity to certain tissues could be utilized as drug depots, to deliver therapeutic agents

on sites with improved efficiency and efficacy (*75*). It could also be refilled to achieve sustained drug eluting (*293*). This approach can overcome the limitations of conventional drug administration such as low efficacy, high dosage, and poor targeting (*13*). Additionally, stem cells (such as human mesenchymal stem cells) could be hosted in hydrogel adhesives with fine-tuned chemical and physical properties before differentiating and/or migrating to targeted tissues (*97*). This could be particularly beneficial for the healing of acellular tissues with low regenerative capacity (e.g. IVD, tendon) or patients with diabetes.

Another trending application category exploiting the tissue adhesion is health monitoring and diagnosis with wearable or implantable electronics. Exciting progress has been made in epidermal electronics or wearables, capable of sensing mechanical signals, such as EEG and ECG, from the outermost layer of skin (*212*, *294*). There are many endeavors to expand the detectable vital signals for better monitoring and diagnosis, for instance, by incorporating biosensing abilities to these devices. Recent works have demonstrated the capability to collect and analyze bio-signals from sweat in situ, which can inform fast and non-invasive diagnosis (*295*, *296*). Such bio-signals from sweat include sodium and chloride (dehydration and cystic fibrosis), blood glucose concentration (diabetes), pH (kidney disease), and sweat rate (autonomic regulation disorders and stroke)(*297*). In this regard, the strong and stable tissue adhesion, despite the sweat, is mission-critical. The adhesion is also relevant for implantable electronics that are developed to sense bio-signals from dynamically moving tissues, such as heart and lung, which are associated with wound healing status and health conditions (*267*). The integration of tough adhesives can also strengthen the electronical signal sensing stability (*298*). When wireless communication technologies are integrated, the adhesive biosensors can be used for remote health monitoring with high fidelity signals.

The future adhesives could be tissue-specific and meet the requirements of certain tissues. In the future, smart adhesives could be leveraged to enable selected adhesion on specific tissue types(*5*). The optimal design condition continues to be sought for different applications. A common strategy is biomimetics, that is, matching the mechanical and biochemical properties of the adhesive and the target tissue. As such, the function and homeostasis of the tissues could be restored. Various strategies have been established to tune the mechanical properties of biomaterials such as hydrogels over a wide range, encompassing most biological tissues. The biochemical features could be engineered by loading the adhesives with tissue-specific compounds (e.g., cells, ECM,

growth factors, cytokines)(*19*, *75*, *299*). While the majority of tissue adhesives are currently homogenous, the tissue adhesives may in the future recapitulate the structural properties of target tissues. To do so, one can leverage the recent surge of additive manufacturing techniques such as 3D bioprinting to fabricate or in situ deposit the adhesives of customized structures (*300*). The development of biomimetic tissue adhesives would benefit from the advances in biomechanics and biological analysis, such as proteomic characterization of tissues, and eventually enable personalized and precision medicine in the future (*301*).

Assessing long-term adhesion in vivo remains a big challenge in the field, due to the high cost of animal studies, the complexity of living tissue environments, and the lack of widely accepted testing protocols. Many biological tissues require a prolonged healing time (*158*). Evaluation of the retention and stability of tissue adhesives in vivo over a long term is thus critical. In lieu of the challenges of in vivo experiments, theoretical and computational tools are alternatives (*18*, *20*). Theoretical modeling has been explored for in vivo drug release (*302*), but the modeling of in vivo adhesion has not been explored. If successful, these tools could allow one to predict the adhesion performance in silicon and guide the material design.

An ideal tissue adhesive must be translational and easy to implement. The procedure should be compatible with the current surgical tools and procedures, meanwhile straightforward for surgeons to practice in clinics. A counterexample is *Focal Seal*, an FDA-approved adhesive for sealing air leaks during lung surgery (*303*), which has been discontinued due to the multiple-step application process. Whereas mixing more than one ingredient is mandatory for many commercialized adhesives, next-generation tissue adhesives are expected to be implemented readily. An example of this kind is the recently reported DST, which can be applied after removing the backing (*2*). Other practical considerations include storage and shelf-life time. Many tissue adhesives that are commercially available and under development involve water-sensitive reagents such as NHS. They need to be kept in dry conditions and have to be used once upon opening. A tissue adhesive with a long shelf-life and simple storage conditions would be well-positioned for translation and commercialization.

The development of tissue adhesives has been fueled by advances in material chemistry, mechanics, biomaterials, and fundamental understanding of tissue and cell biology. In this progress report, we presented the multifaceted design of tissue adhesives to provide guidelines for the

rational design and future development of tissue adhesives. When designing a tissue adhesive, one needs to take a holistic approach by taking three key design elements into consideration, namely the tissue, and the surface and matrix of the adhesives. In each design element, there are a variety of design considerations ranging from chemistry, mechanics, topology to biology. To synthesize the design principles, we conducted two case studies of newly developed tissue adhesives for the treatment of gastric ulcers and cell/drug delivery, respectively. We reviewed the recent progress with examples for the device attachment to skin, wound management, repair and regeneration of musculoskeletal and cardiovascular tissues. We highlighted the emerging applications ranging from the mobile health to cancer treatment. With an expanding arsenal of material systems and target applications, the impact of tissue adhesives is anticipated to increase in importance for years to come. Next-generation tissue adhesives are likely to further change the paradigm of clinical medicine, and continue to improve human healthcare.

References

1. N. Lang, M. J. Pereira, Y. Lee, I. Friehs, N. V. Vasilyev, E. N. Feins, K. Ablasser, E. D. O'Cearbhaill, C. Xu, A. Fabozzo, R. Padera, S. Wasserman, F. Freudenthal, L. S. Ferreira, R. Langer, J. M. Karp, P. J. del Nido, A Blood-Resistant Surgical Glue for Minimally Invasive Repair of Vessels and Heart Defects. *Sci. Transl. Med.* **6**, 218ra6-218ra6 (2014).

2. H. Yuk, C. E. Varela, C. S. Nabzdyk, X. Mao, R. F. Padera, E. T. Roche, X. Zhao, Dry double-sided tape for adhesion of wet tissues and devices. *Nature*. **575**, 169–174 (2019).

3. J. Li, A. D. Celiz, J. Yang, Q. Yang, I. Wamala, W. Whyte, B. R. Seo, N. V. Vasilyev, J. J. Vlassak, Z. Suo, D. J. Mooney, Tough adhesives for diverse wet surfaces. *Science*. **357**, 378–381 (2017).

4. T. Nonoyama, S. Wada, R. Kiyama, N. Kitamura, M. T. I. Mredha, X. Zhang, T. Kurokawa, T. Nakajima, Y. Takagi, K. Yasuda, J. P. Gong, Double-Network Hydrogels Strongly Bondable to Bones by Spontaneous Osteogenesis Penetration. *Adv. Mater.* **28**, 6740–6745 (2016).

5. J. Yang, R. Bai, Z. Suo, Topological Adhesion of Wet Materials. *Adv. Mater.* **30**, 1800671 (2018).

6. J. Yang, R. Bai, B. Chen, Z. Suo, Hydrogel Adhesion: A Supramolecular Synergy of Chemistry, Topology, and Mechanics. *Adv. Funct. Mater.* **30**, 1901693 (2020).

7. G. M. Taboada, K. Yang, M. J. N. Pereira, S. S. Liu, Y. Hu, J. M. Karp, N. Artzi, Y. Lee, Overcoming the translational barriers of tissue adhesives. *Nat. Rev. Mater.* **5**, 310–329 (2020).

8. K. S. Vyas, S. P. Saha, Comparison of hemostatic agents used in vascular surgery. *Expert Opin. Biol. Ther.* **13**, 1663–1672 (2013).

9. M. W. Grinstaff, Designing hydrogel adhesives for corneal wound repair. *Biomaterials*. **28**, 5205–5214 (2007).

10. B. R. Freedman, D. J. Mooney, Biomaterials to Mimic and Heal Connective Tissues. *Adv. Mater.* **31**, 1806695 (2019).

11. B. Sharma, S. Fermanian, M. Gibson, S. Unterman, D. A. Herzka, B. Cascio, J. Coburn, A. Y. Hui, N. Marcus, G. E. Gold, J. H. Elisseeff, Human Cartilage Repair with a Photoreactive Adhesive-Hydrogel Composite. *Sci. Transl. Med.* **5**, 167ra6-167ra6 (2013).

12. Q. Chen, C. Wang, X. Zhang, G. Chen, Q. Hu, H. Li, J. Wang, D. Wen, Y. Zhang, Y. Lu, G. Yang, C. Jiang, J. Wang, G. Dotti, Z. Gu, In situ sprayed bioresponsive immunotherapeutic gel for post-surgical cancer treatment. *Nat. Nanotechnol.* **14**, 89 (2019).

13. S. Yu, C. Wang, J. Yu, J. Wang, Y. Lu, Y. Zhang, X. Zhang, Q. Hu, W. Sun, C. He, X. Chen, Z. Gu, Injectable Bioresponsive Gel Depot for Enhanced Immune Checkpoint Blockade. *Adv. Mater.* **30**, 1801527 (2018).

14. H. Yuk, B. Lu, X. Zhao, Hydrogel bioelectronics. *Chem. Soc. Rev.* **48**, 1642–1667 (2019).

15. J. Pajarinen, T.-H. Lin, T. Sato, Z. Yao, S. B. Goodman, Interaction of materials and biology in total joint replacement – successes, challenges and future directions. *J. Mater. Chem. B.* **2**, 7094–7108 (2014).

16. S. Rose, A. Prevoteau, P. Elzière, D. Hourdet, A. Marcellan, L. Leibler, Nanoparticle solutions as adhesives for gels and biological tissues. *Nature*. **505**, 382–385 (2014).

17. D. G. Barrett, G. G. Bushnell, P. B. Messersmith, Mechanically Robust, Negative-Swelling, Mussel-Inspired Tissue Adhesives. *Adv. Healthc. Mater.* **2**, 745–755 (2013).

18. A. K. Dastjerdi, M. Pagano, M. T. Kaartinen, M. D. McKee, F. Barthelat, Cohesive behavior of soft biological adhesives: Experiments and modeling. *Acta Biomater.* **8**, 3349–3359 (2012).

19. B. A. Aguado, J. C. Grim, A. M. Rosales, J. J. Watson-Capps, K. S. Anseth, Engineering precision biomaterials for personalized medicine. *Sci. Transl. Med.* **10** (2018), doi:10.1126/scitranslmed.aam8645.

20. X. Lin, Y. Liu, A. Bai, H. Cai, Y. Bai, W. Jiang, H. Yang, X. Wang, L. Yang, N. Sun, H. Gao, A viscoelastic adhesive epicardial patch for treating myocardial infarction. *Nat. Biomed. Eng.* **3**, 632–643 (2019).

21. A. H. Hofman, I. A. van Hees, J. Yang, M. Kamperman, Bioinspired Underwater Adhesives by Using the Supramolecular Toolbox. *Adv. Mater.* **30**, 1704640 (2018).

22. C. Ghobril, M. W. Grinstaff, The chemistry and engineering of polymeric hydrogel adhesives for wound closure: a tutorial. *Chem. Soc. Rev.* **44**, 1820–1835 (2015).

23. H. Yuk, T. Zhang, S. Lin, G. A. Parada, X. Zhao, Tough bonding of hydrogels to diverse non-porous surfaces. *Nat. Mater.* **15**, 190–196 (2016).

24. C. Gokgol, C. Basdogan, D. Canadinc, Estimation of fracture toughness of liver tissue: Experiments and validation. *Med. Eng. Phys.* **34**, 882–891 (2012).

25. P. Lengyel, D. Söll, Mechanism of protein biosynthesis. *Bacteriol. Rev.* **33**, 264–301 (1969).

26. D. A. Fletcher, R. D. Mullins, Cell mechanics and the cytoskeleton. *Nature*. **463**, 485–492 (2010).

27. Y. Cai, O. Rossier, N. C. Gauthier, N. Biais, M.-A. Fardin, X. Zhang, L. W. Miller, B. Ladoux, V. W. Cornish, M. P. Sheetz, Cytoskeletal coherence requires myosin-IIA contractility. *J Cell Sci*. **123**, 413–423 (2010).

28. C. Frantz, K. M. Stewart, V. M. Weaver, The extracellular matrix at a glance. *J Cell Sci*. **123**, 4195–4200 (2010).

29. J. K. Kular, S. Basu, R. I. Sharma, The extracellular matrix: Structure, composition, age-related differences, tools for analysis and applications for tissue engineering. *J. Tissue Eng.* **5**, 2041731414557112 (2014).

30. D. L. Bocobo, M. Skellenger, C. E. Shaw, B. F. Steele, Amino acid composition of some human tissues. *Arch. Biochem.* **40**, 448–452 (1952).

31. M. H. Smith, The amino acid composition of proteins. *J. Theor. Biol.* **13**, 261–282 (1966).

32. G. R. Reeck, L. Fisher, A Statistical Analysis of the Amino Acid Compositions of Proteins. *Int. J. Pept. Protein Res.* **5**, 109–117 (1973).

33. T. Ohta, M. Kimura, Amino Acid Composition of Proteins as a Product of Molecular Evolution. *Science*. **174**, 150–153 (1971).

34. R. C. Fahey, J. S. Hunt, G. C. Windham, On the cysteine and cystine content of proteins. Differences between intracellular and extracellular proteins. *J. Mol. Evol.* **10**, 155–160 (1977).

35. F. Pati, J. Jang, D.-H. Ha, S. Won Kim, J.-W. Rhie, J.-H. Shim, D.-H. Kim, D.-W. Cho, Printing three-dimensional tissue analogues with decellularized extracellular matrix bioink. *Nat. Commun.* **5**, 3935 (2014).

36. G. S. Hussey, J. L. Dziki, S. F. Badylak, Extracellular matrix-based materials for regenerative medicine. *Nat. Rev. Mater.* **3**, 159–173 (2018).

37. A. Vedadghavami, C. Zhang, A. G. Bajpayee, Overcoming negatively charged tissue barriers: Drug delivery using cationic peptides and proteins. *Nano Today*. **34**, 100898 (2020).

38. N. Artzi, T. Shazly, A. B. Baker, A. Bon, E. R. Edelman, Aldehyde-Amine Chemistry Enables Modulated Biosealants with Tissue-Specific Adhesion. *Adv. Mater.* **21**, 3399–3403 (2009).

39. H. Zhang, L. P. Bré, T. Zhao, Y. Zheng, B. Newland, W. Wang, Mussel-inspired hyperbranched poly(amino ester) polymer as strong wet tissue adhesive. *Biomaterials*. **35**, 711–719 (2014).

40. N. Broguiere, E. Cavalli, G. M. Salzmann, L. A. Applegate, M. Zenobi-Wong, Factor XIII Cross-Linked Hyaluronan Hydrogels for Cartilage Tissue Engineering. *ACS Biomater. Sci. Eng.* **2**, 2176–2184 (2016).

41. A. E. X. Brown, R. I. Litvinov, D. E. Discher, P. K. Purohit, J. W. Weisel, Multiscale Mechanics of Fibrin Polymer: Gel Stretching with Protein Unfolding and Loss of Water. *Science*. **325**, 741–744 (2009).

42. D. Emig, M. Albrecht, Tissue-Specific Proteins and Functional Implications. *J. Proteome Res.* **10**, 1893–1903 (2011).

43. Pinto Alexander R., Ilinykh Alexei, Ivey Malina J., Kuwabara Jill T., D'Antoni Michelle L., Debuque Ryan, Chandran Anjana, Wang Lina, Arora Komal, Rosenthal Nadia A., Tallquist Michelle D., Revisiting Cardiac Cellular Composition. *Circ. Res.* **118**, 400–409 (2016).

44. E. M. Culav, C. H. Clark, M. J. Merrilees, Connective Tissues: Matrix Composition and Its Relevance to Physical Therapy. *Phys. Ther.* **79**, 308–319 (1999).

45. D.-A. Wang, S. Varghese, B. Sharma, I. Strehin, S. Fermanian, J. Gorham, D. H. Fairbrother, B. Cascio, J. H. Elisseeff, Multifunctional chondroitin sulphate for cartilage tissue–biomaterial integration. *Nat. Mater.* **6**, 385–392 (2007).

46. C. R. Shurer, M. J. Colville, V. K. Gupta, S. E. Head, F. Kai, J. N. Lakins, M. J. Paszek, Genetically Encoded Toolbox for Glycocalyx Engineering: Tunable Control of Cell Adhesion, Survival, and Cancer Cell Behaviors. *ACS Biomater. Sci. Eng.* **4**, 388–399 (2018).

47. J. Gittens, A. M. Haleem, S. Grenier, N. A. Smyth, C. P. Hannon, K. A. Ross, P. A. Torzilli, J. G. Kennedy, Use of novel chitosan hydrogels for chemical tissue bonding of autologous chondral transplants. *J. Orthop. Res.* **34**, 1139–1146 (2016).

48. R. Raman, T. Hua, D. Gwynne, J. Collins, S. Tamang, J. Zhou, T. Esfandiary, V. Soares, S. Pajovic, A. Hayward, R. Langer, G. Traverso, Light-degradable hydrogels as dynamic triggers for gastrointestinal applications. *Sci. Adv.* **6**, eaay0065 (2020).

49. S. Ono, R. Imai, Y. Ida, D. Shibata, T. Komiya, H. Matsumura, Increased wound pH as an indicator of local wound infection in second degree burns. *Burns*. **41**, 820–824 (2015).

50. S. Schreml, R.-M. Szeimies, S. Karrer, J. Heinlin, M. Landthaler, P. Babilas, The impact of the pH value on skin integrity and cutaneous wound healing. *J. Eur. Acad. Dermatol. Venereol.* **24**, 373–378 (2010).

51. L. A. Schneider, A. Korber, S. Grabbe, J. Dissemond, Influence of pH on wound-healing: a new perspective for wound-therapy? *Arch. Dermatol. Res.* **298**, 413–420 (2007).

52. C. K. Sen, Wound healing essentials: Let there be oxygen. *Wound Repair Regen.* **17**, 1–18 (2009).

53. N. Chang, W. H. Goodson, F. Gottrup, T. K. Hunt, Direct measurement of wound and tissue oxygen tension in postoperative patients. *Ann. Surg.* **197**, 470–478 (1983).

54. A. A. Tandara, T. A. Mustoe, Oxygen in Wound Healing—More than a Nutrient. *World J. Surg.* **28**, 294–300 (2004).

55. D. M. Yourtee, R. E. Smith, K. A. Russo, S. Burmaster, J. M. Cannon, J. D. Eick, E. L. Kostoryz, The stability of methacrylate biomaterials when enzyme challenged: Kinetic and systematic evaluations. *J. Biomed. Mater. Res.* **57**, 522–531 (2001).

56. R. V. Ulijn, Enzyme-responsive materials: a new class of smart biomaterials. *J. Mater. Chem.* **16**, 2217–2225 (2006).

57. E. Boedtkjer, S. F. Pedersen, The Acidic Tumor Microenvironment as a Driver of Cancer. *Annu. Rev. Physiol.* **82**, 103–126 (2020).

58. C. Steiger, A. Abramson, P. Nadeau, A. P. Chandrakasan, R. Langer, G. Traverso, Ingestible electronics for diagnostics and therapy. *Nat. Rev. Mater.* **4**, 83–98 (2019).

59. J.-S. Kim, Y.-H. Choi, B.-H. Cho, H.-H. Son, I.-B. Lee, C.-M. Um, C.-K. Kim, Effect of light-cure time of adhesive resin on the thickness of the oxygen-inhibited layer and the microtensile bond strength to dentin. *J. Biomed. Mater. Res. B Appl. Biomater.* **78B**, 115–123 (2006).

60. J. Yu, W. Wei, E. Danner, R. K. Ashley, J. N. Israelachvili, J. H. Waite, Mussel protein adhesion depends on interprotein thiol-mediated redox modulation. *Nat. Chem. Biol.* **7**, 588–590 (2011).

61. J. P. Santerre, R. S. Labow, D. G. Duguay, D. Erfle, G. A. Adams, Biodegradation evaluation of polyether and polyester-urethanes with oxidative and hydrolytic enzymes. *J. Biomed. Mater. Res.* **28**, 1187–1199 (1994).

62. X. Chen, H. Yuk, J. Wu, C. S. Nabzdyk, X. Zhao, Instant tough bioadhesive with triggerable benign detachment. *Proc. Natl. Acad. Sci.*, 202006389 (2020).

63. M. C. Prewitz, F. P. Seib, M. von Bonin, J. Friedrichs, A. Stißel, C. Niehage, K. Müller, K. Anastassiadis, C. Waskow, B. Hoflack, M. Bornhäuser, C. Werner, Tightly anchored tissue-mimetic matrices as instructive stem cell microenvironments. *Nat. Methods*. **10**, 788–794 (2013).

64. J. Kim, J. R. Staunton, K. Tanner, Independent Control of Topography for 3D Patterning of the ECM Microenvironment. *Adv. Mater.* **28**, 132–137 (2016).

65. S. S. Rao, M. T. Nelson, R. Xue, J. K. DeJesus, M. S. Viapiano, J. J. Lannutti, A. Sarkar, J. O. Winter, Mimicking white matter tract topography using core–shell electrospun nanofibers to examine migration of malignant brain tumors. *Biomaterials*. **34**, 5181–5190 (2013).

66. R. M. A. Domingues, S. Chiera, P. Gershovich, A. Motta, R. L. Reis, M. E. Gomes, Enhancing the Biomechanical Performance of Anisotropic Nanofibrous Scaffolds in Tendon Tissue Engineering: Reinforcement with Cellulose Nanocrystals. *Adv. Healthc. Mater.* **5**, 1364–1375 (2016).

67. T. G. Kim, H. Shin, D. W. Lim, Biomimetic Scaffolds for Tissue Engineering. *Adv. Funct. Mater.* **22**, 2446–2468 (2012).

68. B. Young, P. Woodford, G. O'Dowd, *Wheater's Functional Histology E-Book: a Text and Colour Atlas* (2013).

69. F. Flament, G. Francois, H. Qiu, C. Ye, T. Hanaya, D. Batisse, S. Cointereau-Chardon, M. D. G. Seixas, S. E. Dal Belo, R. Bazin, Facial skin pores: a multiethnic study. *Clin. Cosmet. Investig. Dermatol.*, 85 (2015).

70. R. Ohtsuki, T. Sakamaki, S. Tominaga, Analysis of skin surface roughness by visual assessment and surface measurement. *Opt. Rev.* **20**, 94–101 (2013).

71. R. J. Scheuplein, I. H. Blank, Permeability of the skin. *Physiol. Rev.* **51**, 702–747 (1971).

72. N. J. Abbott, Astrocyte–endothelial interactions and blood–brain barrier permeability*. *J. Anat.* **200**, 629–638 (2002).

73. K. D. Crissinger, P. R. Kvietys, D. N. Granger, Pathophysiology of gastrointestinal mucosal permeability. *J. Intern. Med.* **228**, 145–154 (1990).

74. V. V. Khutoryanskiy, Advances in Mucoadhesion and Mucoadhesive Polymers. *Macromol. Biosci.* **11**, 748–764 (2011).

75. J. Li, D. J. Mooney, Designing hydrogels for controlled drug delivery. *Nat. Rev. Mater.* **1**, 16071 (2016).

76. A. Ahuja, R. K. Khar, J. Ali, Mucoadhesive Drug Delivery Systems. *Drug Dev. Ind. Pharm.* **23**, 489–515 (1997).

77. M. R. Prausnitz, R. Langer, Transdermal drug delivery. *Nat. Biotechnol.* **26**, 1261–1268 (2008).

78. M. R. Prausnitz, V. G. Bose, R. Langer, J. C. Weaver, Electroporation of mammalian skin: a mechanism to enhance transdermal drug delivery. *Proc. Natl. Acad. Sci.* **90**, 10504–10508 (1993).

79. T. M. Allen, P. R. Cullis, Drug Delivery Systems: Entering the Mainstream. *Science*. **303**, 1818–1822 (2004).

80. M. D. Kern, Y. Qi, R. Long, M. E. Rentschler, Characterizing adhesion between a micropatterned surface and a soft synthetic tissue. *Langmuir*. **33**, 854–864 (2017).

81. H. A. L. Guerin, D. M. Elliott, Degeneration affects the fiber reorientation of human annulus fibrosus under tensile load. *J. Biomech.* **39**, 1410–1418 (2006).

82. H.-C. Wu, R.-F. Yao, Mechanical behavior of the human annulus fibrosus. *J. Biomech.* **9**, 1–7 (1976).

83. E. B. Hunziker, T. M. Quinn, H.-J. Häuselmann, Quantitative structural organization of normal adult human articular cartilage. *Osteoarthritis Cartilage*. **10**, 564–572 (2002).

84. J. Rieppo, M. M. Hyttinen, E. Halmesmaki, H. Ruotsalainen, A. Vasara, I. Kiviranta, J. S. Jurvelin, H. J. Helminen, Changes in spatial collagen content and collagen network architecture in porcine articular cartilage during growth and maturation. *Osteoarthritis Cartilage*. **17**, 448–455 (2009).

85. S. Thomopoulos, J. P. Marquez, B. Weinberger, V. Birman, G. M. Genin, Collagen fiber orientation at the tendon to bone insertion and its influence on stress concentrations. *J. Biomech.* **39**, 1842–1851 (2006).

86. P. P. Purslow, T. J. Wess, D. W. Hukins, Collagen orientation and molecular spacing during creep and stress-relaxation in soft connective tissues. *J. Exp. Biol.* **201**, 135–142 (1998).

87. N. J. B. Driessen, G. W. M. Peters, J. M. Huyghe, C. V. C. Bouten, F. P. T. Baaijens, Remodelling of continuously distributed collagen fibres in soft connective tissues. *J. Biomech.* **36**, 1151–1158 (2003).

88. I. Calejo, R. Costa-Almeida, R. L. Reis, M. E. Gomes, A Physiology-Inspired Multifactorial Toolbox in Soft-to-Hard Musculoskeletal Interface Tissue Engineering. *Trends Biotechnol.* **38**, 83–98 (2020).

89. T. Courtney, M. S. Sacks, J. Stankus, J. Guan, W. R. Wagner, Design and analysis of tissue engineering scaffolds that mimic soft tissue mechanical anisotropy. *Biomaterials*. **27**, 3631–3638 (2006).

90. K.-P. Wilhelm, J. C. Saunders, H. I. Maibach, Increased stratum corneum turnover induced by subclinical irritant dermatitis. *Br. J. Dermatol.* **122**, 793–798 (1990).

91. D. L. Bader, P. Bowker, Mechanical characteristics of skin and underlying tissues in vivo. *Biomaterials*. **4**, 305–308 (1983).

92. K. M. Myers, A. P. Paskaleva, M. House, S. Socrate, Mechanical and biochemical properties of human cervical tissue. *Acta Biomater.* **4**, 104–116 (2008).

93. F. Guilak, W. R. Jones, H. P. Ting-Beall, G. M. Lee, The deformation behavior and mechanical properties of chondrocytes in articular cartilage. *Osteoarthritis Cartilage*. **7**, 59–70 (1999).

94. H. Saraf, K. T. Ramesh, A. M. Lennon, A. C. Merkle, J. C. Roberts, Mechanical properties of soft human tissues under dynamic loading. *J. Biomech.* **40**, 1960–1967 (2007).

95. H.-J. Wilke, P. Neef, M. Caimi, T. Hoogland, L. E. Claes, New In Vivo Measurements of Pressures in the Intervertebral Disc in Daily Life. *Spine*. **24**, 755–762 (1999).

96. C. Deroy, M. Destrade, A. M. Alinden, A. N. Annaidh, Non-invasive evaluation of skin tension lines with elastic waves. *Skin Res. Technol.* **23**, 326–335 (2017).

97. K. H. Vining, D. J. Mooney, Mechanical forces direct stem cell behaviour in development and regeneration. *Nat. Rev. Mol. Cell Biol.* **18**, 728–742 (2017).

98. L. Li, J. Eyckmans, C. S. Chen, Designer biomaterials for mechanobiology. *Nat. Mater.* **16**, 1164–1168 (2017).

99. P. C. D. P. Dingal, D. E. Discher, Combining insoluble and soluble factors to steer stem cell fate. *Nat. Mater.* **13**, 532–537 (2014).

100. D. Duscher, Z. N. Maan, V. W. Wong, R. C. Rennert, M. Januszyk, M. Rodrigues, M. Hu, A. J. Whitmore, A. J. Whittam, M. T. Longaker, G. C. Gurtner, Mechanotransduction and fibrosis. *J. Biomech.* **47**, 1997–2005 (2014).

101. A. M. Kloxin, J. A. Benton, K. S. Anseth, In situ elasticity modulation with dynamic substrates to direct cell phenotype. *Biomaterials*. **31**, 1–8 (2010).

102. K. M. Mabry, R. L. Lawrence, K. S. Anseth, Dynamic stiffening of poly(ethylene glycol)-based hydrogels to direct valvular interstitial cell phenotype in a three-dimensional environment. *Biomaterials*. **49**, 47–56 (2015).

103. J. Herrera, C. A. Henke, P. B. Bitterman, Extracellular matrix as a driver of progressive fibrosis. *J. Clin. Invest.* **128**, 45–53 (2018).

104. C. J. Doillon, M. G. Dunn, E. Bender, F. H. Silver, Collagen Fiber Formation in Repair Tissue: Development of Strength and Toughness. *Coll. Relat. Res.* **5**, 481–492 (1985).

105. H. J. Steiger, R. Aaslid, S. Keller, H.-J. Reulen, Strength, elasticity and viscoelastic properties of cerebral aneurysms. *Heart Vessels*. **5**, 41–46 (1989).

106. R. W. Chan, Measurements of vocal fold tissue viscoelasticity: Approaching the male phonatory frequency range. *J. Acoust. Soc. Am.* **115**, 3161–3170 (2004).

107. T. Ebihara, N. Venkatesan, R. Tanaka, M. S. Ludwig, Changes in Extracellular Matrix and Tissue Viscoelasticity in Bleomycin–induced Lung Fibrosis. *Am. J. Respir. Crit. Care Med.* **162**, 1569–1576 (2000).

108. I. Sack, B. Beierbach, J. Wuerfel, D. Klatt, U. Hamhaber, S. Papazoglou, P. Martus, J. Braun, The impact of aging and gender on brain viscoelasticity. *NeuroImage*. **46**, 652–657 (2009).

109. M. Muller, J.-L. Gennisson, T. Deffieux, M. Tanter, M. Fink, Quantitative Viscoelasticity Mapping of Human Liver Using Supersonic Shear Imaging: Preliminary In Vivo Feasability Study. *Ultrasound Med. Biol.* **35**, 219–229 (2009).

110. K. Comley, N. A. Fleck, The toughness of adipose tissue: measurements and physical basis. *J. Biomech.* **43**, 1823–1826 (2010).

111. D. Taylor, N. O'Mara, E. Ryan, M. Takaza, C. Simms, The fracture toughness of soft tissues. *J. Mech. Behav. Biomed. Mater.* **6**, 139–147 (2012).

112. J. C. Kohn, M. C. Lampi, C. A. Reinhart-King, Age-related vascular stiffening: causes and consequences. *Front. Genet.* **6** (2015), doi:10.3389/fgene.2015.00112.

113. R. Bai, J. Yang, Z. Suo, Fatigue of hydrogels. *Eur. J. Mech. - ASolids*. **74**, 337–370 (2019).

114. R. Hołyst, Some features of soft matter systems. *Soft Matter*. **1**, 329–333 (2005).

115. T. Steiner, The Hydrogen Bond in the Solid State. *Angew. Chem. Int. Ed.* **41**, 48–76 (2002).

116. S. Goennenwein, M. Tanaka, B. Hu, L. Moroder, E. Sackmann, Functional Incorporation of Integrins into Solid Supported Membranes on Ultrathin Films of Cellulose: Impact on Adhesion. *Biophys. J.* **85**, 646–655 (2003).

117. X. Zhao, Multi-scale multi-mechanism design of tough hydrogels: building dissipation into stretchy networks. *Soft Matter*. **10**, 672–687 (2014).

118. M. J. Buehler, Multiscale mechanics of biological and biologically inspired materials and structures. *Acta Mech. Solida Sin.* **23**, 471–483 (2010).

119. A. J. Singer, J. V. Quinn, J. E. Hollander, The cyanoacrylate topical skin adhesives. *Am. J. Emerg. Med.* **26**, 490–496 (2008).

120. J. M. Albes, C. Krettek, B. Hausen, R. Rohde, A. Haverich, H.-G. Borst, Biophysical properties of the gelatin-resorcinformaldehyde/glutaraldehyde adhesive. *Ann. Thorac. Surg.* **56**, 910–915 (1993).

121. T. M. Shazly, N. Artzi, F. Boehning, E. R. Edelman, Viscoelastic adhesive mechanics of aldehyde-mediated soft tissue sealants. *Biomaterials*. **29**, 4584–4591 (2008).

122. J. M. G. Reyes, S. Herretes, A. Pirouzmanesh, D.-A. Wang, J. H. Elisseeff, A. Jun, P. J. McDonnell, R. S. Chuck, A. Behrens, A Modified Chondroitin Sulfate Aldehyde Adhesive for Sealing Corneal Incisions. *Invest. Ophthalmol. Vis. Sci.* **46**, 1247–1250 (2005).

123. N. Sheikh, A. A. Katbab, H. Mirzadeh, Isocyanate-terminated urethane prepolymer as bioadhesive base material: synthesis and characterization. *Int. J. Adhes. Adhes.* **20**, 299–304 (2000).

124. F. N. Habib, S. S. Kordestani, F. Afshar-Taromi, Z. Shariatinia, A Novel Topical Tissue Adhesive Composed of Urethane Prepolymer Modified with Chitosan. *Int. J. Polym. Anal. Charact.* **16**, 609–618 (2011).

125. P. K. Forooshani, B. P. Lee, Recent approaches in designing bioadhesive materials inspired by mussel adhesive protein. *J. Polym. Sci. Part Polym. Chem.* **55**, 9–33 (2017).

126. M. Mehdizadeh, H. Weng, D. Gyawali, L. Tang, J. Yang, Injectable citrate-based mussel-inspired tissue bioadhesives with high wet strength for sutureless wound closure. *Biomaterials*. **33**, 7972–7983 (2012).

127. S. Moulay, Dopa/Catechol-Tethered Polymers: Bioadhesives and Biomimetic Adhesive Materials. *Polym. Rev.* **54**, 436–513 (2014).

128. N. Mati-Baouche, P.-H. Elchinger, H. de Baynast, G. Pierre, C. Delattre, P. Michaud, Chitosan as an adhesive. *Eur. Polym. J.* **60**, 198–212 (2014).

129. B. Cohen, O. Pinkas, M. Foox, M. Zilberman, Gelatin–alginate novel tissue adhesives and their formulation–strength effects. *Acta Biomater.* **9**, 9004–9011 (2013).

130. C. B. Highley, G. D. Prestwich, J. A. Burdick, Recent advances in hyaluronic acid hydrogels for biomedical applications. *Curr. Opin. Biotechnol.* **40**, 35–40 (2016).

131. D. Gan, W. Xing, L. Jiang, J. Fang, C. Zhao, F. Ren, L. Fang, K. Wang, X. Lu, Plant-inspired adhesive and tough hydrogel based on Ag-Lignin nanoparticles-triggered dynamic redox catechol chemistry. *Nat. Commun.* **10**, 1487 (2019).

132. R. Feiner, L. Engel, S. Fleischer, M. Malki, I. Gal, A. Shapira, Y. Shacham-Diamand, T. Dvir, Engineered hybrid cardiac patches with multifunctional electronics for online monitoring and regulation of tissue function. *Nat. Mater.* **15**, 679–685 (2016).

133. H. Lee, B. P. Lee, P. B. Messersmith, A reversible wet/dry adhesive inspired by mussels and geckos. *Nature*. **448**, 338–341 (2007).

134. P. Rao, T. L. Sun, L. Chen, R. Takahashi, G. Shinohara, H. Guo, D. R. King, T. Kurokawa, J. P. Gong, Tough Hydrogels with Fast, Strong, and Reversible Underwater Adhesion Based on a Multiscale Design. *Adv. Mater.* **30**, 1801884 (2018).

135. C.-M. Lehr, J. A. Bouwstra, F. Spies, J. Onderwater, J. van het Noordeinde, C. Vermeij-Keers, C. J. van Munsteren, H. E. Junginger, Visualization studies of the mucoadhesive interface. *J. Controlled Release*. **18**, 249–260 (1992).

136. S. Y. Yang, E. D. O'Cearbhaill, G. C. Sisk, K. M. Park, W. K. Cho, M. Villiger, B. E. Bouma, B. Pomahac, J. M. Karp, A bio-inspired swellable microneedle adhesive for mechanical interlocking with tissue. *Nat. Commun.* **4**, 1702 (2013).

137. H. Cho, G. Wu, J. C. Jolly, N. Fortoul, Z. He, Y. Gao, A. Jagota, S. Yang, Intrinsically reversible superglues via shape adaptation inspired by snail epiphragm. *Proc. Natl. Acad. Sci.* **116**, 13774–13779 (2019).

138. A. Mahdavi, L. Ferreira, C. Sundback, J. W. Nichol, E. P. Chan, D. J. D. Carter, C. J. Bettinger, S. Patanavanich, L. Chignozha, E. Ben-Joseph, A. Galakatos, H. Pryor, I. Pomerantseva, P. T. Masiakos, W. Faquin, A. Zumbuehl, S. Hong, J. Borenstein, J. Vacanti, R. Langer, J. M. Karp, A biodegradable and biocompatible gecko-inspired tissue adhesive. *Proc. Natl. Acad. Sci.* **105**, 2307–2312 (2008).

139. S. Baik, D. W. Kim, Y. Park, T.-J. Lee, S. Ho Bhang, C. Pang, A wet-tolerant adhesive patch inspired by protuberances in suction cups of octopi. *Nature*. **546**, 396–400 (2017).

140. H. Lee, D.-S. Um, Y. Lee, S. Lim, H. Kim, H. Ko, Octopus-Inspired Smart Adhesive Pads for Transfer Printing of Semiconducting Nanomembranes. *Adv. Mater.* **28**, 7457–7465 (2016).

141. P. Rao, T. L. Sun, L. Chen, R. Takahashi, G. Shinohara, H. Guo, D. R. King, T. Kurokawa, J. P. Gong, Tough Hydrogels with Fast, Strong, and Reversible Underwater Adhesion Based on a Multiscale Design. *Adv. Mater.* **30**, 1801884 (2018).

142. J. T. Parsons, A. R. Horwitz, M. A. Schwartz, Cell adhesion: integrating cytoskeletal dynamics and cellular tension. *Nat. Rev. Mol. Cell Biol.* **11**, 633–643 (2010).

143. S. V. Plotnikov, A. M. Pasapera, B. Sabass, C. M. Waterman, Force Fluctuations within Focal Adhesions Mediate ECM-Rigidity Sensing to Guide Directed Cell Migration. *Cell*. **151**, 1513–1527 (2012).

144. Z. Ma, L. Sagrillo-Fagundes, R. Tran, P. K. Parameshwar, N. Kalashnikov, C. Vaillancourt, C. Moraes, Biomimetic Micropatterned Adhesive Surfaces To Mechanobiologically Regulate Placental Trophoblast Fusion. *ACS Appl. Mater. Interfaces*. **11**, 47810–47821 (2019).

145. S. Schlie, M. Gruene, H. Dittmar, B. N. Chichkov, Dynamics of Cell Attachment: Adhesion Time and Force. *Tissue Eng. Part C Methods*. **18**, 688–696 (2012).

146. U. S. Schwarz, M. L. Gardel, United we stand – integrating the actin cytoskeleton and cell–matrix adhesions in cellular mechanotransduction. *J. Cell Sci.* **125**, 3051–3060 (2012).

147. Y. A. Miroshnikova, H. Q. Le, D. Schneider, T. Thalheim, M. Rübsam, N. Bremicker, J. Polleux, N. Kamprad, M. Tarantola, I. Wang, M. Balland, C. M. Niessen, J. Galle, S. A. Wickström, Adhesion forces and cortical tension couple cell proliferation and differentiation to drive epidermal stratification. *Nat. Cell Biol.* **20**, 69–80 (2018).

148. O. Chaudhuri, L. Gu, D. Klumpers, M. Darnell, S. A. Bencherif, J. C. Weaver, N. Huebsch, H. Lee, E. Lippens, G. N. Duda, D. J. Mooney, Hydrogels with tunable stress relaxation regulate stem cell fate and activity. *Nat. Mater.* **15**, 326 (2016).

149. R. Sunyer, V. Conte, J. Escribano, A. Elosegui-Artola, A. Labernadie, L. Valon, D. Navajas, J. M. García-Aznar, J. J. Muñoz, P. Roca-Cusachs, X. Trepat, Collective cell durotaxis emerges from long-range intercellular force transmission. *Science*. **353**, 1157–1161 (2016).

150. B. O. O. Boni, L. Lamboni, T. Souho, M. Gauthier, G. Yang, Immunomodulation and cellular response to biomaterials: the overriding role of neutrophils in healing. *Mater. Horiz.* **6**, 1122–1137 (2019).

151. L. N. Woodard, M. A. Grunlan, Hydrolytic Degradation and Erosion of Polyester Biomaterials. *ACS Macro Lett.* **7**, 976–982 (2018).

152. M. Mehdizadeh, J. Yang, Design Strategies and Applications of Tissue Bioadhesives. *Macromol. Biosci.* **13**, 271–288 (2013).

153. D. Wirthl, R. Pichler, M. Drack, G. Kettlguber, R. Moser, R. Gerstmayr, F. Hartmann, E. Bradt, R. Kaltseis, C. M. Siket, S. E. Schausberger, S. Hild, S. Bauer, M. Kaltenbrunner, Instant tough bonding of hydrogels for soft machines and electronics. *Sci. Adv.* **3**, e1700053 (2017).

154. H. V. Vinters, K. A. Galil, M. J. Lundie, J. C. E. Kaufmann, The histotoxicity of cyanoacrylates. *Neuroradiology*. **27**, 279–291 (1985).

155. J. J. Sohn, T. M. Gruber, J. L. Zahorsky-Reeves, G. W. Lawson, Comparison of 2-ethyl-cyanoacrylate and 2-butyl-cyanoacrylate for use on the calvaria of cd1 mice. *J. Am. Assoc. Lab. Anim. Sci.* **55**, 5 (2016).

156. K. J. Walgenbach, H. Bannasch, S. Kalthoff, J. P. Rubin, Randomized, Prospective Study of TissuGlu® Surgical Adhesive in the Management of Wound Drainage Following Abdominoplasty. *Aesthetic Plast. Surg.* **36**, 491–496 (2012).

157. C. A. Midgley, J. B. Rea, in *Handbook of Adhesives*, I. Skeist, Ed. (Springer US, Boston, MA, 1990; https://doi.org/10.1007/978-1-4613-0671-9_12), pp. 227–238.

158. B. R. Freedman, D. J. Mooney, Biomaterials to Mimic and Heal Connective Tissues. *Adv. Mater.* **0**, 1806695.

159. L. Yu, J. Ding, Injectable hydrogels as unique biomedical materials. *Chem. Soc. Rev.* **37**, 1473–1481 (2008).

160. N. A. Peppas, J. Z. Hilt, A. Khademhosseini, R. Langer, Hydrogels in Biology and Medicine: From Molecular Principles to Bionanotechnology. *Adv. Mater.* **18**, 1345–1360 (2006).

161. D. G. Wallace, G. M. Cruise, W. M. Rhee, J. A. Schroeder, J. J. Prior, J. Ju, M. Maroney, J. Duronio, M. H. Ngo, T. Estridge, G. C. Coker, A tissue sealant based on reactive multifunctional polyethylene glycol. *J. Biomed. Mater. Res.* **58**, 545–555 (2001).

162. W. D. Spotnitz, S. Burks, Hemostats, sealants, and adhesives: components of the surgical toolbox. *Transfusion (Paris)*. **48**, 1502–1516 (2008).

163. D. H. Sierra, Fibrin Sealant Adhesive Systems: A Review of Their Chemistry, Material Properties and Clinical Applications. *J. Biomater. Appl.* **7**, 309–352 (1993).

164. C. M. Elvin, T. Vuocolo, A. G. Brownlee, L. Sando, M. G. Huson, N. E. Liyou, P. R. Stockwell, R. E. Lyons, M. Kim, G. A. Edwards, G. Johnson, G. A. McFarland, J. A. M. Ramshaw, J. A. Werkmeister, A highly elastic tissue sealant based on photopolymerised gelatin. *Biomaterials*. **31**, 8323–8331 (2010).

165. J. P. Gong, Y. Katsuyama, T. Kurokawa, Y. Osada, Double-Network Hydrogels with Extremely High Mechanical Strength. *Adv. Mater.* **15**, 1155–1158 (2003).

166. J.-Y. Sun, X. Zhao, W. R. K. Illeperuma, O. Chaudhuri, K. H. Oh, D. J. Mooney, J. J. Vlassak, Z. Suo, Highly stretchable and tough hydrogels. *Nature*. **489**, 133–136 (2012).

167. S. Fuchs, K. Shariati, M. Ma, Specialty Tough Hydrogels and Their Biomedical Applications. *Adv. Healthc. Mater.* **9**, 1901396 (2020).

168. C. W. Peak, J. J. Wilker, G. Schmidt, A review on tough and sticky hydrogels. *Colloid Polym. Sci.* **291**, 2031–2047 (2013).

169. E. S. Sani, A. Kheirkhah, D. Rana, Z. Sun, W. Foulsham, A. Sheikhi, A. Khademhosseini, R. Dana, N. Annabi, Sutureless repair of corneal injuries using naturally derived bioadhesive hydrogels. *Sci. Adv.* **5**, eaav1281 (2019).

170. E. T. Roche, M. A. Horvath, I. Wamala, A. Alazmani, S.-E. Song, W. Whyte, Z. Machaidze, C. J. Payne, J. C. Weaver, G. Fishbein, J. Kuebler, N. V. Vasilyev, D. J. Mooney, F. A. Pigula, C. J. Walsh, Soft robotic sleeve supports heart function. *Sci. Transl. Med.* **9** (2017), doi:10.1126/scitranslmed.aaf3925.

171. X. Xu, X. Xia, K. Zhang, A. Rai, Z. Li, P. Zhao, K. Wei, L. Zou, B. Yang, W.-K. Wong, P. W.-Y. Chiu, L. Bian, Bioadhesive hydrogels demonstrating pH-independent and ultrafast gelation promote gastric ulcer healing in pigs. *Sci. Transl. Med.* **12** (2020), doi:10.1126/scitranslmed.aba8014.

172. Y. S. Zhang, A. Khademhosseini, Advances in engineering hydrogels. *Science*. **356**, eaaf3627 (2017).

173. Y. Hong, F. Zhou, Y. Hua, X. Zhang, C. Ni, D. Pan, Y. Zhang, D. Jiang, L. Yang, Q. Lin, Y. Zou, D. Yu, D. E. Arnot, X. Zou, L. Zhu, S. Zhang, H. Ouyang, A strongly adhesive hemostatic hydrogel for the repair of arterial and heart bleeds. *Nat. Commun.* **10**, 2060 (2019).

174. T. J. DiStefano, J. O. Shmukler, G. Danias, T. Di Pauli von Treuheim, W. W. Hom, D. A. Goldberg, D. M. Laudier, P. R. Nasser, A. C. Hecht, S. B. Nicoll, J. C. Iatridis, Development of a two-part biomaterial adhesive strategy for annulus fibrosus repair and ex vivo evaluation of implant herniation risk. *Biomaterials*. **258**, 120309 (2020).

175. S. l. Blackburn, M. D. Smyth, Hydrogel-induced cervicomedullary compression after posterior fossa decompression for Chiari malformation: Case report. *J. Neurosurg. Pediatr.* **106**, 302–304 (2007).

176. S.-H. Lee, C.-W. Park, S.-G. Lee, W.-K. Kim, Postoperative cervical cord compression induced by hydrogel dural sealant (duraseal®). *Korean J. Spine*. **10**, 44 (2013).

177. S. A. Bencherif, R. W. Sands, D. Bhatta, P. Arany, C. S. Verbeke, D. A. Edwards, D. J. Mooney, Injectable preformed scaffolds with shape-memory properties. *Proc. Natl. Acad. Sci.* **109**, 19590–19595 (2012).

178. A. Lendlein, R. Langer, Biodegradable, Elastic Shape-Memory Polymers for Potential Biomedical Applications. *Science*. **296**, 1673–1676 (2002).

179. N. Kalashnikov, C. Moraes, Morphodynamic Tissues via Integrated Programmable Shape Memory Actuators. *Adv. Funct. Mater.* **29**, 1903327 (2019).

180. M. D. Brigham, A. Bick, E. Lo, A. Bendali, J. A. Burdick, A. Khademhosseini, Mechanically Robust and Bioadhesive Collagen and Photocrosslinkable Hyaluronic Acid Semi-Interpenetrating Networks. *Tissue Eng. Part A*. **15**, 1645–1653 (2008).

181. D. Singh, R. Baier, in *Advances in Contact Angle, Wettability and Adhesion* (John Wiley & Sons, Ltd, 2018; https://onlinelibrary.wiley.com/doi/abs/10.1002/9781119459996.ch15), pp. 349–372.

182. S. Liang, Y. Zhang, H. Wang, Z. Xu, J. Chen, R. Bao, B. Tan, Y. Cui, G. Fan, W. Wang, W. Wang, W. Liu, Paintable and Rapidly Bondable Conductive Hydrogels as Therapeutic Cardiac Patches. *Adv. Mater.* **30**, 1704235 (2018).

183. N. Annabi, D. Rana, E. Shirzaei Sani, R. Portillo-Lara, J. L. Gifford, M. M. Fares, S. M. Mithieux, A. S. Weiss, Engineering a sprayable and elastic hydrogel adhesive with antimicrobial properties for wound healing. *Biomaterials*. **139**, 229–243 (2017).

184. P. Qi, Y. G. Zheng, S. Ohta, N. Kokudo, K. Hasegawa, T. Ito, In Situ Fabrication of Double-Layered Hydrogels via Spray Processes to Prevent Postoperative Peritoneal Adhesion. *ACS Biomater. Sci. Eng.* **5**, 4790–4798 (2019).

185. Y. Liang, X. Zhao, T. Hu, B. Chen, Z. Yin, P. X. Ma, B. Guo, Adhesive hemostatic conducting injectable composite hydrogels with sustained drug release and photothermal antibacterial activity to promote full‐thickness skin regeneration during wound healing. *Small*. **15**, 1900046 (2019).

186. X. Zhao, B. Guo, H. Wu, Y. Liang, P. X. Ma, Injectable antibacterial conductive nanocomposite cryogels with rapid shape recovery for noncompressible hemorrhage and wound healing. *Nat. Commun.* **9**, 2784 (2018).

187. N. Annabi, Y.-N. Zhang, A. Assmann, E. S. Sani, G. Cheng, A. D. Lassaletta, A. Vegh, B. Dehghani, G. U. Ruiz-Esparza, X. Wang, S. Gangadharan, A. S. Weiss, A. Khademhosseini, Engineering a highly elastic human protein–based sealant for surgical applications. *Sci. Transl. Med.* **9**, eaai7466 (2017).

188. S. T. Koshy, R. M. Desai, P. Joly, J. Li, R. K. Bagrodia, S. A. Lewin, N. S. Joshi, D. J. Mooney, Click-Crosslinked Injectable Gelatin Hydrogels. *Adv. Healthc. Mater.* **5**, 541–547 (2016).

189. A. Radhakrishnan, G. Kuppusamy, V. V. S. R. Karri, Spray bandage strategy in topical drug delivery. *J. Drug Deliv. Sci. Technol.* **43**, 113–121 (2018).

190. S. Mandla, L. Davenport Huyer, M. Radisic, Review: Multimodal bioactive material approaches for wound healing. *APL Bioeng.* **2**, 021503 (2018).

191. F. von Burkersroda, L. Schedl, A. Göpferich, Why degradable polymers undergo surface erosion or bulk erosion. *Biomaterials*. **23**, 4221–4231 (2002).

192. H. Yang, C. Li, J. Tang, Z. Suo, Strong and degradable adhesion of hydrogels. *ACS Appl. Bio Mater.* **2**, 1781–1786 (2019).

193. L. Erdmann, B. Macedo, K. E. Uhrich, Degradable poly(anhydride ester) implants: effects of localized salicylic acid release on bone. *Biomaterials*. **21**, 2507–2512 (2000).

194. J. L. Ifkovits, J. A. Burdick, Review: Photopolymerizable and Degradable Biomaterials for Tissue Engineering Applications. *Tissue Eng.* **13**, 2369–2385 (2007).

195. T. E. Brown, B. J. Carberry, B. T. Worrell, O. Y. Dudaryeva, M. K. McBride, C. N. Bowman, K. S. Anseth, Photopolymerized dynamic hydrogels with tunable viscoelastic properties through thioester exchange. *Biomaterials*. **178**, 496–503 (2018).

196. K. R. Stevens, J. S. Miller, B. L. Blakely, C. S. Chen, S. N. Bhatia, Degradable hydrogels derived from PEG-diacrylamide for hepatic tissue engineering. *J. Biomed. Mater. Res. A.* **103**, 3331–3338 (2015).

197. H. Ying, J. Yen, R. Wang, Y. Lai, J.-L.-A. Hsu, Y. Hu, J. Cheng, Degradable and biocompatible hydrogels bearing a hindered urea bond. *Biomater. Sci.* **5**, 2398–2402 (2017).

198. N. Boehnke, C. Cam, E. Bat, T. Segura, H. D. Maynard, Imine Hydrogels with Tunable Degradability for Tissue Engineering. *Biomacromolecules*. **16**, 2101–2108 (2015).

199. S. B. Anderson, C.-C. Lin, D. V. Kuntzler, K. S. Anseth, The performance of human mesenchymal stem cells encapsulated in cell-degradable polymer-peptide hydrogels. *Biomaterials*. **32**, 3564–3574 (2011).

200. J. Kost, K. Leong, R. Langer, Ultrasound-enhanced polymer degradation and release of incorporated substances. *Proc. Natl. Acad. Sci.* **86**, 7663–7666 (1989).

201. G. D. Nicodemus, K. A. Shiplet, S. R. Kaltz, S. J. Bryant, Dynamic compressive loading influences degradation behavior of PEG-PLA hydrogels. *Biotechnol. Bioeng.* **102**, 948–959 (2009).

202. P. M. Kharkar, K. L. Kiick, A. M. Kloxin, Designing degradable hydrogels for orthogonal control of cell microenvironments. *Chem. Soc. Rev.* **42**, 7335–7372 (2013).

203. M. K. Beyer, H. Clausen-Schaumann, Mechanochemistry: The Mechanical Activation of Covalent Bonds. *Chem. Rev.* **105**, 2921–2948 (2005).

204. J. A. Champion, A. Walker, S. Mitragotri, Role of Particle Size in Phagocytosis of Polymeric Microspheres. *Pharm. Res.* **25**, 1815–1821 (2008).

205. Z. Xia, J. T. Triffitt, A review on macrophage responses to biomaterials. *Biomed. Mater.* **1**, R1–R9 (2006).

206. C. E. Witherel, D. Abebayehu, T. H. Barker, K. L. Spiller, Macrophage and Fibroblast Interactions in Biomaterial-Mediated Fibrosis. *Adv. Healthc. Mater.* **8**, 1801451 (2019).

207. P. Caliceti, F. M. Veronese, Pharmacokinetic and biodistribution properties of poly(ethylene glycol)–protein conjugates. *Adv. Drug Deliv. Rev.* **55**, 1261–1277 (2003).

208. P. A. Leggat, D. R. Smith, U. Kedjarune, Surgical Applications of Cyanoacrylate Adhesives: A Review of Toxicity. *ANZ J. Surg.* **77**, 209–213 (2007).

209. C. W. Hewitt, S. W. Marra, B. R. Kann, H. S. Tran, M. M. Puc, F. A. Chrzanowski, J.-L. V. Tran, S. D. Lenz, J. H. Cilley, V. A. Simonetti, A. J. DelRossi, BioGlue surgical adhesive for thoracic aortic repair during coagulopathy: efficacy and histopathology. *Ann. Thorac. Surg.* **71**, 1609–1612 (2001).

210. W. Fürst, A. Banerjee, Release of Glutaraldehyde From an Albumin-Glutaraldehyde Tissue Adhesive Causes Significant In Vitro and In Vivo Toxicity. *Ann. Thorac. Surg.* **79**, 1522–1528 (2005).

211. V. Bhagat, M. L. Becker, Degradable Adhesives for Surgery and Tissue Engineering. *Biomacromolecules*. **18**, 3009–3039 (2017).

212. H. U. Chung, B. H. Kim, J. Y. Lee, J. Lee, Z. Xie, E. M. Ibler, K. Lee, A. Banks, J. Y. Jeong, J. Kim, C. Ogle, D. Grande, Y. Yu, H. Jang, P. Assem, D. Ryu, J. W. Kwak, M. Namkoong, J. B. Park, Y. Lee, D. H. Kim, A. Ryu, J. Jeong, K. You, B. Ji, Z. Liu, Q. Huo, X. Feng, Y. Deng, Y. Xu, K.-I. Jang, J. Kim, Y. Zhang, R. Ghaffari, C. M. Rand, M. Schau, A. Hamvas, D. E. Weese-Mayer, Y. Huang, S. M. Lee, C. H. Lee, N. R. Shanbhag, A. S. Paller, S. Xu, J. A. Rogers, Binodal, wireless epidermal electronic systems with in-sensor analytics for neonatal intensive care. *Science*. **363**, eaau0780 (2019).

213. Y. Gao, K. Wu, Z. Suo, Photodetachable Adhesion. *Adv. Mater.*, 1806948 (2018).

214. S. O. Blacklow, J. Li, B. R. Freedman, M. Zeidi, C. Chen, D. J. Mooney, Bioinspired mechanically active adhesive dressings to accelerate wound closure. *Sci. Adv.* **5**, eaaw3963 (2019).

215. S. Venkatraman, R. Gale, Skin adhesives and skin adhesion 1. Transdermal drug delivery systems. *Biomaterials*. **19**, 1119–1136 (1998).

216. B. Laulicht, R. Langer, J. M. Karp, Quick-release medical tape. *Proc. Natl. Acad. Sci.* **109**, 18803–18808 (2012).

217. I. Webster, Recent developments in pressure-sensitive adhesives for medical applications. *Int. J. Adhes. Adhes.* **17**, 69–73 (1997).

218. I. Hwang, H. N. Kim, M. Seong, S.-H. Lee, M. Kang, H. Yi, W. G. Bae, M. K. Kwak, H. E. Jeong, Multifunctional smart skin adhesive patches for advanced health care. *Adv. Healthc. Mater.* **7**, 1800275 (2018).

219. K. F. Cutting, Impact of adhesive surgical tape and wound dressings on the skin, with reference to skin stripping. *J. Wound Care*. **17**, 157–162 (2008).

220. D.-H. Kim, N. Lu, R. Ma, Y.-S. Kim, R.-H. Kim, S. Wang, J. Wu, S. M. Won, H. Tao, A. Islam, K. J. Yu, T. -i. Kim, R. Chowdhury, M. Ying, L. Xu, M. Li, H.-J. Chung, H. Keum, M. McCormick, P. Liu, Y.-W. Zhang, F. G. Omenetto, Y. Huang, T. Coleman, J. A. Rogers, Epidermal electronics. *Science*. **333**, 838–843 (2011).

221. Y. Hattori, L. Falgout, W. Lee, S.-Y. Jung, E. Poon, J. W. Lee, I. Na, A. Geisler, D. Sadhwani, Y. Zhang, Y. Su, X. Wang, Z. Liu, J. Xia, H. Cheng, R. C. Webb, A. P. Bonifas, P. Won, J.-W. Jeong, K.-I. Jang, Y. M. Song, B. Nardone, M. Nodzenski, J. A. Fan, Y. Huang, D. P. West, A. S. Paller, M. Alam, W.-H. Yeo, J. A. Rogers, Multifunctional skin-like electronics for quantitative, clinical monitoring of cutaneous wound healing. *Adv. Healthc. Mater.* **3**, 1597–1607 (2014).

222. Z. Lei, P. Wu, Adaptable polyionic elastomers with multiple sensations and entropy-driven actuations for prosthetic skins and neuromuscular systems. *Mater. Horiz.* **6**, 538–545 (2019).

223. M. K. Kwak, H.-E. Jeong, K. Y. Suh, Rational design and enhanced biocompatibility of a dry adhesive medical skin patch. *Adv. Mater.* **23**, 3949–3953 (2011).

224. J. P. Gong, Y. Katsuyama, T. Kurokawa, Y. Osada, Double-Network Hydrogels with Extremely High Mechanical Strength. *Adv. Mater.* **15**, 1155–1158 (2003).

225. J.-Y. Sun, X. Zhao, W. R. K. Illeperuma, O. Chaudhuri, K. H. Oh, D. J. Mooney, J. J. Vlassak, Z. Suo, Highly stretchable and tough hydrogels. *Nature*. **489**, 133–136 (2012).

226. J. Yang, R. Bai, J. Li, C. Yang, X. Yao, Q. Liu, J. J. Vlassak, D. J. Mooney, Z. Suo, Design molecular topology for wet–dry adhesion. *ACS Appl. Mater. Interfaces*. **11**, 24802–24811 (2019).

227. H. A. E. Benson, J. E. Grice, Y. Mohammed, S. Namjoshi, M. S. Roberts, Topical and transdermal drug delivery: from simple potions to smart technologies. *Curr. Drug Deliv.* **16**, 444–460 (2019).

228. J. D. Bos, M. M. H. M. Meinardi, The 500 Dalton rule for the skin penetration of chemical compounds and drugs. *Exp. Dermatol.* **9**, 165–169 (2000).

229. Y. Zhang, G. Jiang, W. Yu, D. Liu, B. Xu, Microneedles fabricated from alginate and maltose for transdermal delivery of insulin on diabetic rats. *Mater. Sci. Eng. C*. **85**, 18–26 (2018).

230. S. N. Economidou, C. P. P. Pere, A. Reid, Md. J. Uddin, J. F. C. Windmill, D. A. Lamprou, D. Douroumis, 3D printed microneedle patches using stereolithography (SLA) for intradermal insulin delivery. *Mater. Sci. Eng. C*. **102**, 743–755 (2019).

231. S. Y. Yang, E. D. O'Cearbhaill, G. C. Sisk, K. M. Park, W. K. Cho, M. Villiger, B. E. Bouma, B. Pomahac, J. M. Karp, A bio-inspired swellable microneedle adhesive for mechanical interlocking with tissue. *Nat. Commun.* **4**, 1702 (2013).

232. E. Y. Jeon, J. Lee, B. J. Kim, K. I. Joo, K. H. Kim, G. Lim, H. J. Cha, Bio-inspired swellable hydrogel-forming double-layered adhesive microneedle protein patch for regenerative internal/external surgical closure. *Biomaterials*. **222**, 119439 (2019).

233. M. Rippon, R. White, P. Davies, Skin adhesives and their role in wound dressings. *Wounds UK*. **3**, 76–86 (2007).

234. K. Vowden, P. Vowden, Wound dressings: principles and practice. *Surg. Oxf.* **35**, 489–494 (2017).

235. A. J. Singer, J. V. Quinn, J. E. Hollander, The cyanoacrylate topical skin adhesives. *Am. J. Emerg. Med.* **26**, 490–496 (2008).

236. W. Li, X. Liu, Z. Deng, Y. Chen, Q. Yu, W. Tang, T. L. Sun, Y. S. Zhang, K. Yue, Tough bonding, on‐demand debonding, and facile rebonding between hydrogels and diverse metal surfaces. *Adv. Mater.* **31**, 1904732 (2019).

237. G. Bao, T. Jiang, H. Ravanbakhsh, A. Reyes, Z. Ma, M. Strong, H. Wang, J. M. Kinsella, J. Li, L. Mongeau, Triggered micropore-forming bioprinting of porous viscoelastic hydrogels. *Mater. Horiz.* **7**, 2336–2347 (2020).

238. P. Chen, X. Li, J. Ma, R. Zhang, F. Qin, J. Wang, T. S. Hu, Y. Zhang, Q. Xu, Bioinspired photodetachable dry self-cleaning surface. *Langmuir*. **35**, 6379–6386 (2019).

239. J. S. Boateng, K. H. Matthews, H. N. E. Stevens, G. M. Eccleston, Wound healing dressings and drug delivery systems: a review. *J. Pharm. Sci.* **97**, 2892–2923 (2008).

240. Wound care market global forecast. *Res. Engine* (2020), (available at marketresearchengine.com/wound-care-market).

241. J. C. Lawrence, Dressings and wound infection. *Am. J. Surg.* **167**, 21–24 (1994).

242. B. R. Swenson, T. L. Hedrick, R. Metzger, H. Bonatti, T. L. Pruett, R. G. Sawyer, Effects of preoperative skin preparation on postoperative wound infection rates a prospective study of 3 skin preparation protocols. *Infect. Control Hosp. Epidemiol.* **30**, 964–971 (2009).

243. R. S. Howell-Jones, M. J. Wilson, K. E. Hill, A. J. Howard, P. E. Price, D. W. Thomas, A review of the microbiology, antibiotic usage and resistance in chronic skin wounds. *J. Antimicrob. Chemother.* **55**, 143–149 (2005).

244. L. Timofeeva, N. Kleshcheva, Antimicrobial polymers: mechanism of action, factors of activity, and applications. *Appl. Microbiol. Biotechnol.* **89**, 475–492 (2011).

245. S. Fernando, T. Gunasekara, J. Holton, Antimicrobial nanoparticles: applications and mechanisms of action. *Sri Lankan J. Infect. Dis.* **8**, 2 (2018).

246. H. Tan, H. Ao, R. Ma, W. Lin, T. Tang, *In vivo* effect of quaternized chitosan-loaded polymethylmethacrylate bone cement on methicillin-resistant staphylococcus epidermidis infection of the tibial metaphysis in a rabbit model. *Antimicrob. Agents Chemother.* **58**, 6016–6023 (2014).

247. S. J. Melvin, D. G. Dombroski, J. T. Torbert, S. J. Kovach, J. L. Esterhai, S. Mehta, Open tibial shaft fractures: i. evaluation and initial wound management: *Am. Acad. Orthop. Surg.* **18**, 10–19 (2010).

248. J. Qu, X. Zhao, Y. Liang, T. Zhang, P. X. Ma, B. Guo, Antibacterial adhesive injectable hydrogels with rapid self-healing, extensibility and compressibility as wound dressing for joints skin wound healing. *Biomaterials*. **183**, 185–199 (2018).

249. X. Zhao, H. Wu, B. Guo, R. Dong, Y. Qiu, P. X. Ma, Antibacterial anti-oxidant electroactive injectable hydrogel as self-healing wound dressing with hemostasis and adhesiveness for cutaneous wound healing. *Biomaterials*. **122**, 34–47 (2017).

250. C. Li, R. Ye, J. Bouckaert, A. Zurutuza, D. Drider, T. Dumych, S. Paryzhak, V. Vovk, R. O. Bilyy, S. Melinte, M. Li, R. Boukherroub, S. Szunerits, Flexible nanoholey patches for

antibiotic-free treatments of skin infections. *ACS Appl. Mater. Interfaces*. **9**, 36665–36674 (2017).

251. K. Turcheniuk, C.-H. Hage, J. Spadavecchia, A. Y. Serrano, I. Larroulet, A. Pesquera, A. Zurutuza, M. G. Pisfil, L. Héliot, J. Boukaert, R. Boukherroub, S. Szunerits, Plasmonic photothermal destruction of uropathogenic E. coli with reduced graphene oxide and core/shell nanocomposites of gold nanorods/reduced graphene oxide. *J. Mater. Chem. B.* **3**, 375–386 (2015).

252. G. Gainza, S. Villullas, J. L. Pedraz, R. M. Hernandez, M. Igartua, Advances in drug delivery systems (DDSs) to release growth factors for wound healing and skin regeneration. *Nanomedicine Nanotechnol. Biol. Med.* **11**, 1551–1573 (2015).

253. T. N. Demidova-Rice, M. R. Hamblin, I. M. Herman, Acute and impaired wound healing: pathophysiology and current methods for drug delivery, part 1: normal and chronic wounds: biology, causes, and approaches to care. *Adv. Skin Wound Care*. **25**, 304–314 (2012).

254. H. S. Kim, X. Sun, J.-H. Lee, H.-W. Kim, X. Fu, K. W. Leong, Advanced drug delivery systems and artificial skin grafts for skin wound healing. *Adv. Drug Deliv. Rev.* **146**, 209–239 (2019).

255. Y. Chen, W. Cheng, L. Teng, M. Jin, B. Lu, L. Ren, Y. Wang, Graphene oxide hybrid supramolecular hydrogels with self-healable, bioadhesive and stimuli-responsive properties and drug delivery application. *Macromol. Mater. Eng.* **303**, 1700660 (2018).

256. B. L. Li, R. Li, H. L. Zou, K. Ariga, N. B. Li, D. T. Leong, Engineered functionalized 2D nanoarchitectures for stimuli-responsive drug delivery. *Mater. Horiz.* **7**, 455–469 (2020).

257. A. Zhang, K. Jung, A. Li, J. Liu, C. Boyer, Recent advances in stimuli-responsive polymer systems for remotely controlled drug release. *Prog. Polym. Sci.* **99**, 101164 (2019).

258. S. Bagherifard, A. Tamayol, P. Mostafalu, M. Akbari, M. Comotto, N. Annabi, M. Ghaderi, S. Sonkusale, M. R. Dokmeci, A. Khademhosseini, Dermal patch with integrated flexible heater for on demand drug delivery. *Adv. Healthc. Mater.* **5**, 175–184 (2016).

259. P. Mostafalu, A. Tamayol, R. Rahimi, M. Ochoa, A. Khalilpour, G. Kiaee, I. K. Yazdi, S. Bagherifard, M. R. Dokmeci, B. Ziaie, S. R. Sonkusale, A. Khademhosseini, Smart bandage for monitoring and treatment of chronic wounds. *Small*. **14**, 1703509 (2018).

260. Y. Wang, S. Song, J. Liu, D. Liu, H. Zhang, *Angew. Chem. Int. Ed.*, in press, doi:10.1002/anie.201409519.

261. G. Yang, X. Sun, J. Liu, L. Feng, Z. Liu, Light-responsive, singlet-oxygen-triggered on-demand drug release from photosensitizer-doped mesoporous silica nanorods for cancer combination therapy. *Adv. Funct. Mater.* **26**, 4722–4732 (2016).

262. S. Mitragotri, Healing sound: the use of ultrasound in drug delivery and other therapeutic applications. *Nat. Rev. Drug Discov.* **4**, 255–260 (2005).

263. B. W. Walker, R. P. Lara, C. H. Yu, E. S. Sani, W. Kimball, S. Joyce, N. Annabi, Engineering a naturally-derived adhesive and conductive cardiopatch. *Biomaterials*. **207**, 89–101 (2019).

264. L. Han, L. Yan, M. Wang, K. Wang, L. Fang, J. Zhou, J. Fang, F. Ren, X. Lu, Transparent, adhesive, and conductive hydrogel for soft bioelectronics based on light-transmitting polydopamine-doped polypyrrole nanofibrils. *Chem. Mater.* **30**, 5561–5572 (2018).

265. D. Zhao, Y. Zhu, W. Cheng, G. Xu, Q. Wang, S. Liu, J. Li, C. Chen, H. Yu, L. Hu, A dynamic gel with reversible and tunable topological networks and performances. *Matter*. **2**, 390–403 (2020).

266. B. Ying, Q. Wu, J. Li, X. Liu, An ambient-stable and stretchable ionic skin with multimodal sensation. *Mater. Horiz.* **7**, 477–488 (2020).

267. X. Pei, H. Zhang, Y. Zhou, L. Zhou, J. Fu, Stretchable, self-healing and tissue-adhesive zwitterionic hydrogels as strain sensors for wireless monitoring of organ motions. *Mater. Horiz.* **7**, 1872–1882 (2020).

268. Z. Li, A. Milionis, Y. Zheng, M. Yee, L. Codispoti, F. Tan, D. Poulikakos, C. H. Yap, Superhydrophobic hemostatic nanofiber composites for fast clotting and minimal adhesion. *Nat. Commun.* **10**, 5562 (2019).

269. A. Meddahi-Pellé, A. Legrand, A. Marcellan, L. Louedec, D. Letourneur, L. Leibler, Organ repair, hemostasis, and in vivo bonding of medical devices by aqueous solutions of nanoparticles. *Angew. Chem. Int. Ed.* **53**, 6369–6373 (2014).

270. E. Fröhlich, Action of nanoparticles on platelet activation and plasmatic coagulation. *Curr. Med. Chem.* **23**, 408–430 (2016).

271. C. Liu, X. Liu, C. Liu, N. Wang, H. Chen, W. Yao, G. Sun, Q. Song, W. Qiao, A highly efficient, in situ wet-adhesive dextran derivative sponge for rapid hemostasis. *Biomaterials*. **205**, 23–37 (2019).

272. L. M. Stapleton, A. N. Steele, H. Wang, H. Lopez Hernandez, A. C. Yu, M. J. Paulsen, A. A. A. Smith, G. A. Roth, A. D. Thakore, H. J. Lucian, K. P. Totherow, S. W. Baker, Y. Tada, J. M. Farry, A. Eskandari, C. E. Hironaka, K. J. Jaatinen, K. M. Williams, H. Bergamasco, C. Marschel, B. Chadwick, F. Grady, M. Ma, E. A. Appel, Y. J. Woo, Use of a supramolecular polymeric hydrogel as an effective post-operative pericardial adhesion barrier. *Nat. Biomed. Eng.* **3**, 611–620 (2019).

273. E. B. Hunziker, A. Stähli, Surgical suturing of articular cartilage induces osteoarthritis-like changes. *Osteoarthritis Cartilage*. **16**, 1067–1073 (2008).

274. S. W. Linderman, I. Kormpakis, R. H. Gelberman, V. Birman, U. G. K. Wegst, G. M. Genin, S. Thomopoulos, Shear lag sutures: Improved suture repair through the use of adhesives. *Acta Biomater.* **23**, 229–239 (2015).

275. S. R. Sloan, C. Wipplinger, S. Kirnaz, R. Navarro-Ramirez, F. Schmidt, D. McCloskey, T. Pannellini, A. Schiavinato, R. Härtl, L. J. Bonassar, Combined nucleus pulposus augmentation and annulus fibrosus repair prevents acute intervertebral disc degeneration after discectomy. *Sci. Transl. Med.* **12** (2020), doi:10.1126/scitranslmed.aay2380.

276. M. He, A. W. T. Gan, A. Y. T. Lim, J. C. H. Goh, J. H. P. Hui, E. H. Lee, A. K. S. Chong, The effect of fibrin glue on tendon healing and adhesion formation in a rabbit model of flexor tendon injury and repair. *J. Plast. Surg. Hand Surg.* **47**, 509–512 (2013).

277. M. C. Jordan, V. Schmitt, S. Dannigkeit, K. Schmidt, R. H. Meffert, S. Hoelscher-Doht, Surgical adhesive BioGlue^{TM} does not benefit tendon repair strength: an ex vivo study. *J. Hand Surg. Eur. Vol.* **40**, 700–704 (2015).

278. P. Karami, C. S. Wyss, A. Khoushabi, A. Schmocker, M. Broome, C. Moser, P.-E. Bourban, D. P. Pioletti, Composite Double-Network Hydrogels To Improve Adhesion on Biological Surfaces. *ACS Appl. Mater. Interfaces.* **10**, 38692–38699 (2018).

279. A. K. Gaharwar, R. K. Avery, A. Assmann, A. Paul, G. H. McKinley, A. Khademhosseini, B. D. Olsen, Shear-Thinning Nanocomposite Hydrogels for the Treatment of Hemorrhage. *ACS Nano*. **8**, 9833–9842 (2014).

280. K. Kobayashi, Y. Ichihara, N. Sato, N. Umeda, L. Fields, M. Fukumitsu, Y. Tago, T. Ito, S. Kainuma, M. Podaru, F. Lewis-McDougall, K. Yamahara, R. Uppal, K. Suzuki, On-site fabrication of Bi-layered adhesive mesenchymal stromal cell-dressings for the treatment of heart failure. *Biomaterials*. **209**, 41–53 (2019).

281. J. Liu, X. Zhang, Y. Liu, M. Rodrigo, P. D. Loftus, J. Aparicio-Valenzuela, J. Zheng, T. Pong, K. J. Cyr, M. Babakhanian, J. Hasi, J. Li, Y. Jiang, C. J. Kenney, P. J. Wang, A. M. Lee, Z. Bao, Intrinsically stretchable electrode array enabled in vivo electrophysiological mapping of atrial fibrillation at cellular resolution. *Proc. Natl. Acad. Sci.* **117**, 14769–14778 (2020).

282. T. R. Cox, J. T. Erler, Remodeling and homeostasis of the extracellular matrix: implications for fibrotic diseases and cancer. *Dis. Model. Mech.* **4**, 165–178 (2011).

283. M. C. Lampi, C. A. Reinhart-King, Targeting extracellular matrix stiffness to attenuate disease: From molecular mechanisms to clinical trials. *Sci. Transl. Med.* **10**, eaao0475 (2018).

284. J. M. Barnes, L. Przybyla, V. M. Weaver, Tissue mechanics regulate brain development, homeostasis and disease. *J Cell Sci*. **130**, 71–82 (2017).

285. H. Wang, D. J. Mooney, Biomaterial-assisted targeted modulation of immune cells in cancer treatment. *Nat. Mater.* **17**, 761–772 (2018).

286. R. E. Abhari, J. A. Martins, H. L. Morris, P.-A. Mouthuy, A. Carr, Synthetic sutures: Clinical evaluation and future developments. *J. Biomater. Appl.* **32**, 410–421 (2017).

287. Dennis Christopher, Sethu Swaminathan, Nayak Sunita, Mohan Loganathan, Morsi Yosry (Yos), Manivasagam Geetha, Suture materials — Current and emerging trends. *J. Biomed. Mater. Res. A.* **104**, 1544–1559 (2016).

288. X. Ni, C. Chen, J. Li, Interfacial fatigue fracture of tissue adhesive hydrogels. *Extreme Mech. Lett.* **34**, 100601 (2020).

289. X. Xu, X. Xia, K. Zhang, A. Rai, Z. Li, P. Zhao, K. Wei, L. Zou, B. Yang, W.-K. Wong, P. W.-Y. Chiu, L. Bian, Bioadhesive hydrogels demonstrating pH-independent and ultrafast gelation promote gastric ulcer healing in pigs. *Sci. Transl. Med.* **12** (2020), doi:10.1126/scitranslmed.aba8014.

290. E. S. Sani, A. Kheirkhah, D. Rana, Z. Sun, W. Foulsham, A. Sheikhi, A. Khademhosseini, R. Dana, N. Annabi, Sutureless repair of corneal injuries using naturally derived bioadhesive hydrogels. *Sci. Adv.* **5**, eaav1281 (2019).

291. V. Falanga, Wound healing and its impairment in the diabetic foot. *The Lancet*. **366**, 1736–1743 (2005).

292. J. Chen, D. Wang, L.-H. Wang, W. Liu, A. Chiu, K. Shariati, Q. Liu, X. Wang, Z. Zhong, J. Webb, R. E. Schwartz, N. Bouklas, M. Ma, An adhesive hydrogel with "load-sharing" effect as tissue bandages for drug and cell delivery. *Adv. Mater.*, 8 (2020).

293. Y. Brudno, M. J. Pezone, T. K. Snyder, O. Uzun, C. T. Moody, M. Aizenberg, D. J. Mooney, Replenishable drug depot to combat post-resection cancer recurrence. *Biomaterials*. **178**, 373–382 (2018).

294. H. U. Chung, A. Y. Rwei, A. Hourlier-Fargette, S. Xu, K. Lee, E. C. Dunne, Z. Xie, C. Liu, A. Carlini, D. H. Kim, D. Ryu, E. Kulikova, J. Cao, I. C. Odland, K. B. Fields, B. Hopkins, A. Banks, C. Ogle, D. Grande, J. B. Park, J. Kim, M. Irie, H. Jang, J. Lee, Y. Park, J. Kim, H. H. Jo, H. Hahm, R. Avila, Y. Xu, M. Namkoong, J. W. Kwak, E. Suen, M. A. Paulus, R. J. Kim, B. V. Parsons, K. A. Human, S. S. Kim, M. Patel, W. Reuther, H. S. Kim, S. H. Lee, J. D. Leedle, Y. Yun, S. Rigali, T. Son, I. Jung, H. Arafa, V. R. Soundararajan, A. Ollech, A. Shukla, A. Bradley, M. Schau, C. M. Rand, L. E. Marsillio, Z. L. Harris, Y. Huang, A. Hamvas, A. S. Paller, D. E. Weese-Mayer, J. Y. Lee, J. A. Rogers, Skin-interfaced biosensors for advanced wireless physiological monitoring in neonatal and pediatric intensive-care units. *Nat. Med.* **26**, 418–429 (2020).

295. A. Koh, D. Kang, Y. Xue, S. Lee, R. M. Pielak, J. Kim, T. Hwang, S. Min, A. Banks, P. Bastien, M. C. Manco, L. Wang, K. R. Ammann, K.-I. Jang, P. Won, S. Han, R. Ghaffari, U. Paik, M. J. Slepian, G. Balooch, Y. Huang, J. A. Rogers, A soft, wearable microfluidic device for the capture, storage, and colorimetric sensing of sweat. *Sci. Transl. Med.* **8**, 366ra165-366ra165 (2016).

296. J. Choi, Y. Xue, W. Xia, T. R. Ray, J. T. Reeder, A. J. Bandodkar, D. Kang, S. Xu, Y. Huang, J. A. Rogers, Soft, skin-mounted microfluidic systems for measuring secretory fluidic pressures generated at the surface of the skin by eccrine sweat glands. *Lab. Chip*. **17**, 2572–2580 (2017).

297. J. Choi, R. Ghaffari, L. B. Baker, J. A. Rogers, Skin-interfaced systems for sweat collection and analytics. *Sci. Adv.* **4**, eaar3921 (2018).

298. J. Deng, H. Yuk, J. Wu, C. E. Varela, X. Chen, E. T. Roche, C. F. Guo, X. Zhao, Electrical bioadhesive interface for bioelectronics. *Nat. Mater.* (2020), doi:10.1038/s41563-020-00814-2.

299. D. E. Discher, D. J. Mooney, P. W. Zandstra, Growth Factors, Matrices, and Forces Combine and Control Stem Cells. *Science*. **324**, 1673–1677 (2009).

300. K. S. Lim, F. Abinzano, P. N. Bernal, A. Albillos Sanchez, P. Atienza‐Roca, I. A. Otto, Q. C. Peiffer, M. Matsusaki, T. B. F. Woodfield, J. Malda, R. Levato, One‐step photoactivation of a dual‐functionalized bioink as cell carrier and cartilage‐binding glue for chondral regeneration. *Adv. Healthc. Mater.* **9**, 1901792 (2020).

301. D. Emig, M. Albrecht, Tissue-Specific Proteins and Functional Implications. *J. Proteome Res.* **10**, 1893–1903 (2011).

302. A. N. Ford Versypt, D. W. Pack, R. D. Braatz, Mathematical modeling of drug delivery from autocatalytically degradable PLGA microspheres — A review. *J. Controlled Release*. **165**, 29–37 (2013).

303. S. Ishida, F. Okamoto, S. Hoshi, S. Fukuda, Y. Sugiura, M. Arai, T. Hirose, T. Oshika, FocalSeal® for Closure of Sutureless Sclerotomies of Vitrectomy: An In Vivo and Histological Study. *Invest. Ophthalmol. Vis. Sci.* **55**, 2337–2337 (2014).

Preface to Chapter 3

As reviewed in Chapter 2, with multifaceted design, bioadhesives can form adhesion on biological tissues and have found emerging applications for tissue sealing, bleeding control, mobile health, bioelectronics, and regenerative medicine. However, due to the often weak interfacial adhesion, low fatigue fracture resistance, and limited spatiotemporal control of the formed adhesion, existing bioadhesives have yet to meet the stringent demand to amend highly tough and adhesive biological tissues. On the other hand, adhesion formed via physical attachment can only form very weak wet adhesion on tissues due to the van der Waals force involved. Complex nano- and micro-fabrication techniques are usually required to obtain patterned adhesives to tune the adhesion performance. Thus, new tough bioadhesion mechanisms continue to be sought to address the aforementioned challenges.

Ultrasound (US), referring to sound at frequencies greater than 20 kHz, have been widely used in the clinics and hospitals for health monitoring, tumor ablation, therapeutic administration and bioimaging. Particularly, the prominent mechanical effects of US have been leveraged to enable effective transdermal and gastrointestinal drug delivery. Therefore, we hypothesize that by controlling the mechanical effects of US, especially cavitation, we may create transient and localized delivery of anchoring primer reagents as a bridging matrix for spatiotemporally controlled bioadhesion.

In Chapter 3, we propose a facile and universal US mediated anchorage approach for tough bioadhesion without chemical reactions. We investigate the US-mediated adhesion mechanism using experimental analysis of US induced cavitation, US mediated bioadhesion energy, strength, and fatigue fracture threshold. We next show the potential of US for spatiotemporal manipulation of bioadhesion. Finally, we confirm the biocompatibility of the US-mediated bioadhesion in vivo and demonstrate its applications for transdermal drug delivery.

This work is in revision for ***Science*** in 2022:

Zhenwei Ma, Claire Bourquard, Qiman Gao, Shuaibing Jiang, Tristan De Iure-Grimmel, Ran Huo, Xuan Li, Zixin He, Zhen Yang, Galen Yang, Yixiang Wang, Edmond Lam, Zu-Hua Gao, Outi Supponen*, Jianyu Li*, Controlled tough bioadhesion mediated by ultrasound, ***Science*** (in revision) (2022)

Chapter 3 Controlled Tough Bioadhesion with Ultrasound

Abstract

Tough bioadhesion has significant implications in engineering and medicine, but remains challenging to form and control over space and time. Here, we report an ultrasound (US)-mediated bioadhesion technology to achieve tough bioadhesion with unprecedented controllability and fatigue resistance. Without chemical reactions, US amplifies the adhesion energy and interfacial fatigue threshold between hydrogels and skin by up to 100 and 10 times. Combined experiments and computation modeling identify the key mechanism to be US-induced cavitation, which propels and anchors primers into tissues with mitigated barrier effects. The US effects are potent yet localized to enable spatial patterning of tough bioadhesion, on-demand detachment, and transdermal drug delivery. This work greatly expands the material repertoire for tough bioadhesion and opens new avenues for bioadhesive technologies with high-level controllability.

3.1 Introduction

Bioadhesive technologies find significant use in wearable electronics, biomedical implants, wound management, anastomosis, regenerative medicine, and drug delivery (*1–5*). However, they have been long bottlenecked by barrier effects of biological tissues such as low permeability and limited functional groups. Skin, for instance, contains dense stratum corneum, limiting the interpenetration and bonding of bioadhesive agents (Fig. 3.1A). These issues are particularly critical for the bioadhesives based on physical interactions such as polymer interpenetration; the polymers are too slow and even impossible to diffuse and entangle with tissues (*6*), resulting in poor bioadhesion (*7*). Chemical strategies have thus far been inevitable for tough bioadhesion. Despite achieving high adhesion energy, they cannot allow high-level control over bioadhesion in space and time. Exceptions require sophisticated surface patterning, exogenous chemicals and external apparatus to remove interfacial bonding (*8, 9*). Other disadvantages include interference with payloads for drug delivery (*10*), low fatigue threshold (due to limited functional groups on tissue surfaces) (*11*), acute and/or chronic toxicity (caused by chemical reactions and their reagents) (*12*). Fundamentally solving these issues necessitates a paradigm-shifting strategy, leveraging physical interactions to overcome the barrier effects of tissues and enable tough bioadhesion with spatiotemporal controllability.

3.2 Results and Discussion

Here, we report a new strategy of ultrasound (US)-mediated bioadhesion to achieve tough bioadhesion with unprecedented controllability. The US has been extensively used in the clinics for imaging (*13*), monitoring (*14*), tumor ablation (*15*) and drug delivery (*16*). We hypothesize that the mechanical effects of US, particularly cavitation, could transiently permeate the tissue boundaries, potently propel and immobilize anchoring primers into tissues, which are otherwise impossible with passive diffusion (Fig. 3.1A, B); while anchoring to tissues, the primers can further interpenetrate and entangle with the hydrogel patch, leading to strong bioadhesion (*6*). This mechanism, called *US-triggered anchorage*, differentiates from existing strategies based on either passive diffusion or chemical reactions, as well as medical devices such as suture anchors and swellable microneedles (*17*) that rely on invasive mechanical interlocking (fig. S3.1). We demonstrate that our strategy is applicable to various anchoring primers (polymers, nanoparticles, and proteins), hydrogels (single- and double-network hydrogels), and biological tissues (skin, buccal mucosa, and aorta). The universal applicability supports technological impacts in broad areas ranging from wearable devices to drug delivery.

The US-mediated bioadhesion is achieved in two steps. We first apply the US to a primer solution/suspension of anchoring agents spread on tissue substrates (e.g., porcine skin) with an ultrasonic transducer (VWR 76193) for a short period of time. Sequentially, we cover the treated area with a hydrogel patch with gentle compression (Fig. 3.1B). As a model system, we deploy a chitosan (Chi) solution and a polyacrylamide-alginate (PAAm-alg) hydrogel as the primer and the hydrogel patch, respectively. We then measure the adhesion energy between the hydrogel and the tissue with peeling tests (Fig. 3.1C). Our results show extremely high adhesion energy of 1500 J m^{-2} obtained on porcine skin with the US treatment (20 kHz, 1 min, 116 W cm^{-2}), more than 15 times higher than that of the non-US control (Fig. 3.1D). We further validate the US-mediated bioadhesion with an ultrasonic scaler (20-35 kHz) routinely used in dental clinics, confirming tough adhesion (~ 800 J m^{-2}) on porcine skin after the US treatment (fig. S3.2).

The effectiveness of our strategy is demonstrated with a large repertoire of materials. First, we confirm the adhesion enhancement by US with other hydrogels, including another double-network poly(N-isopropylacrylamide)-alginate (PNIPAm-alg) hydrogel and a single-network PAAm hydrogel (fig. S3.3). Also, the same efficacy is observed with other anchoring agents such as proteins and nanoparticles (Fig. 3.1D), despite the fact that they vary greatly in chemistry and size and can otherwise form very weak bioadhesion (1-10 J m^{-2}) (*18*). Besides chitosan, gelatin can

lead to over 200 J m^{-2} of adhesion energy with US treatment. For nanoparticles, aldehyde-functionalized cellulose nanocrystals (CHO-CNC) with US treatment yield high adhesion energy (~ 180 J m^{-2}), whereas the non-US condition yields weak adhesion (< 15 J m^{-2}). Chitosan nanocrystals (ChsNCs) result in even higher adhesion energy exceeding 500 J m^{-2}, two orders of magnitude higher than the same material without US (~5 J m^{-2}). Notably, without the aid of US, the adhesion of ChsNCs remains weak even when coupling agents [i.e., 1-Ethyl-3-(3-dimethylaminopropyl)carbodiimide and N-Hydroxysuccinimide] are used to form amide bonds with tissues (fig. S3.4). The versatility of US-mediated bioadhesion and its indispensable role in nanoparticle bioadhesion unlock the potential of various materials for tough bioadhesion.

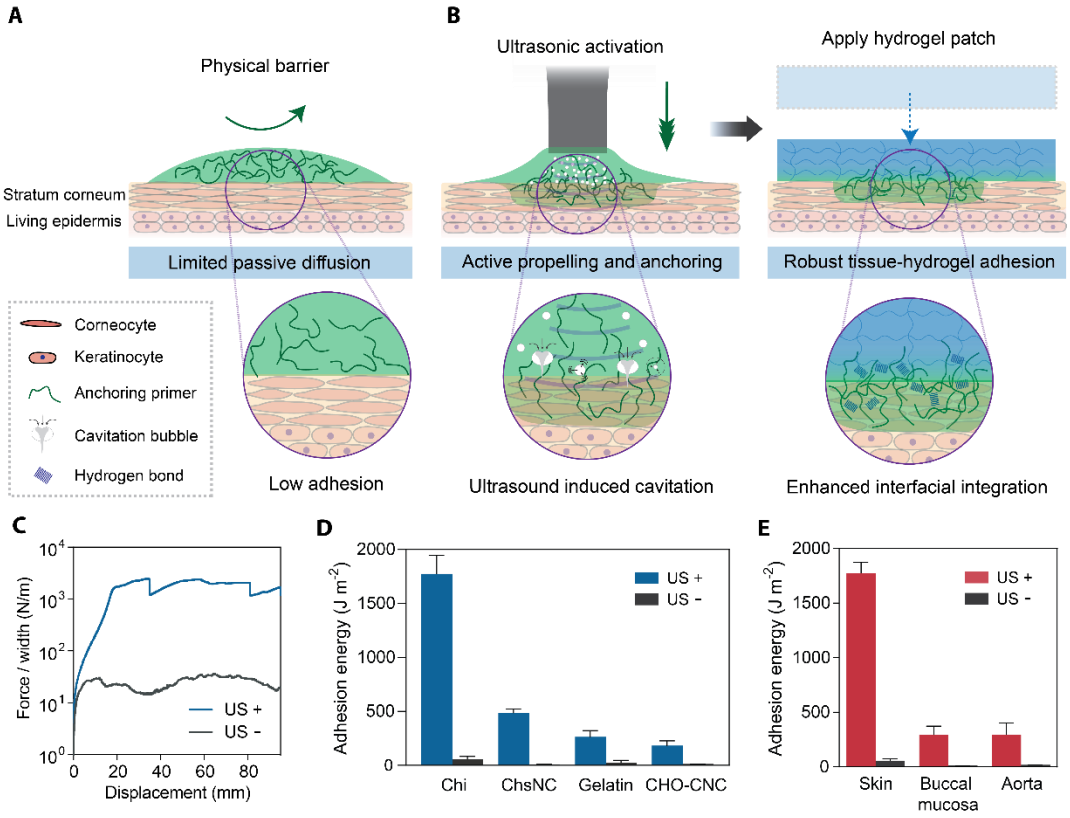

Figure 3.1. Robust and versatile US mediated tough bioadhesion. (A). Schematic of skin with barrier effects, limiting passive diffusion and impairing bioadhesion. (B). US actively propels and anchors primer agents into tissue substrate, forming spatially confined tough adhesion between hydrogel and tissue. (C). Representative force-displacement curves of hydrogel-tissue (porcine skin) hybrids with or without US treatment in peeling tests. (D). US enables diverse anchoring

agents for tough bioadhesion on skin. Chi: chitosan; ChsNC: chitosan nanocrystals; CHO-CNC: aldehyde functionalized cellulose nanocrystals. (E). Adhesion enhancement with US on diverse biological tissues, including skin, buccal mucosa and aorta. Chitosan was used as the anchoring primer. Data reported as means ± SD for n = 3 independent experiments.

In addition to skin, our strategy is applicable to various biological tissues, including those with recognized barrier effects (Fig. 3.1E). A manifestation of the adverse barrier effect of tissues is that the hydrogels with chitosan primer exhibit low adhesion energy, 11.8 J m^{-2} and 18.9 J m^{-2}, on buccal mucosa and aorta, respectively. In comparison, such tissues can adhere strongly to the hydrogel patch with the aid of US. The measured adhesion energy is ~ 295.2 J m^{-2} for buccal mucosa, and ~ 297.4 J m^{-2} for aorta. The tough bioadhesion is evidenced by the debonding of buccal membrane from the underlying tissues during peeling (fig. S3.5), indicating that the adhesion interface outperforms the native bonding between the mucosa epithelium lining and the underlying connective tissue.

After proving the universal applicability (fig. S3.6), we delve into the mechanism underlying US-mediated bioadhesion. Given the US intensity and the chemicals used in this study, the likelihood of triggering chemical reactions (e.g., generating radicals) by US is low (*19*). The effects of the US exerted on the primer and the tissue substrate are mainly thermal and mechanical. To evaluate the thermal effect, we monitor the temperature change by the US with a thermal camera. After 1-minute application of 32 W cm^{-2} US, the surface temperature of skin increases by 10 °C (fig. S3.7). To examine its consequence, we replicate the temperature change, with a temperature-controlled oven, to incubate hydrogel-primer-tissue hybrids. As no significant change of bioadhesion is found (fig. S3.8), we thus exclude the thermal effect. While the possible mechanical effects include cavitation, viscous stresses, acoustic streaming, and radiation force, we consider the low frequency US used here and conjecture US-induced cavitation as the key mechanism (*20*). To test this hypothesis, we combine experiments and computational modeling to substantiate the link between the US-mediated cavitation and bioadhesion below.

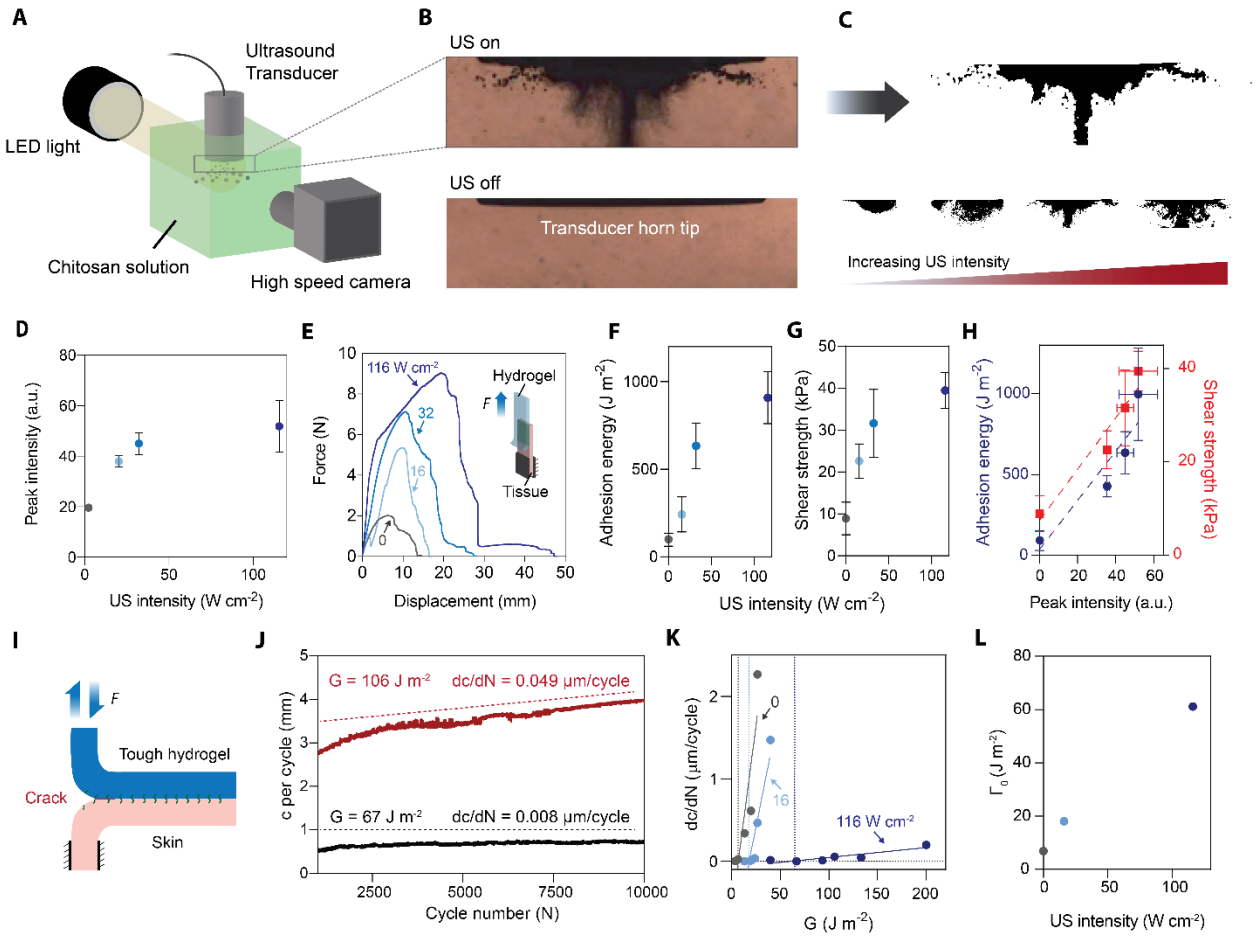

Figure 3.2. US-induced cavitation regulates bioadhesion. (A). Experimental setup for characterizing US-induced microbubble cavitation. (B). Digital images of the microbubble cloud at peak intensity in a cycle captured by the high-speed camera. (C). Processed binary images of the bubble clouds. (D). Normalized peak intensity of the induced microbubble clouds as a function of the US intensity. (E). Representative force-displacement curves of hydrogel-tissue hybrids in lap-shear tests. Correlation between applied US intensity and interfacial adhesion energy (F) and shear strength (G). (H). Correlation between peak intensity of bubble clouds, interfacial adhesion energy and shear strength. (I). Schematic illustration of the fatigue test of hydrogel-tissue hybrid. Data reported as means ± SD for n = 3 independent experiments. (J). Representative curves of the cycle number and crack extension *c* per cycle at two energy release rates for samples with US treatment. (K). Crack extension rate (dc/dN) versus applied energy release rate G = F/W for hydrogel adhesion on tissues after exposure of zero, low (16 W cm^{-2}), high (116 W cm^{-2}) intensity of US. The linear extrapolation to the G-axis (solid lines) gives the fatigue threshold Γ_0. (L). Correlation of US intensity and obtained fatigue threshold Γ_0.

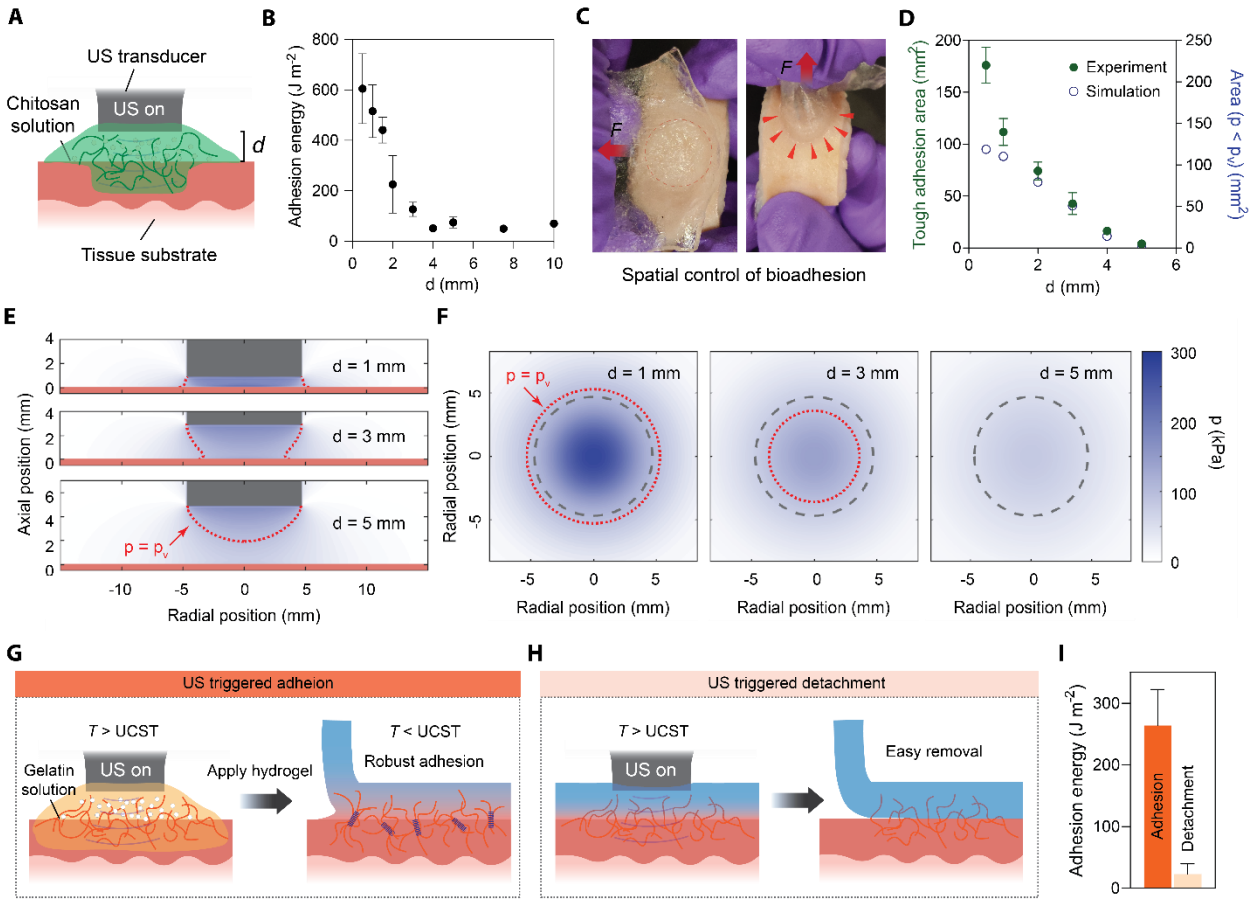

Figure 3.3 Spatiotemporal control of bioadhesion mediated with US. (A). Schematics of the US application at varying distances *d* between the US horn and the tissue substrate. (B). Correlation of *d* and adhesion energy characterized by lap shear tests. (C). Digital images of obtained spatial control of bioadhesion. (D). Correlation of *d* and tough adhesion area measured experimentally (green dot) and simulated (blue circle). (E). Side view of simulation fields with area where $p < p_v$ during part of the acoustic cycle delimited in red dashed line for *d* = 1, 3, and 5 mm. (F). Corresponding top view at substrate level for *d* = 1, 3, and 5 mm. Red arrowhead indicates the boundary of tough adhesion area. Blue areas are where total pressure p goes below vapor pressure p_v according to simulations. Schematic illustration of US-triggered adhesion (G) and detachment (H) with thermo-sensitive gelatin anchoring agent. (I). Adhesion energy characterized for US mediated on-demand adhesion and detachment. Data reported as means ± SD for n = 3 independent experiments.

To correlate US-induced cavitation and bioadhesion, we characterize the cavitation phenomenon and the adhesion performance as a function of US intensity. The cavitation is manifested with dynamic microbubble clouds present under the US transducer, visualized with a high-speed camera (Fig. 3.2A, B), showing oscillating vapor bubble cloud patterns and geometries in each cycle. Similar US-induced cavitation events are observed with the clinically used ultrasonic scaler (fig. S3.2). From the binary images of the bubble clouds, the peak cavitation intensity is quantified with the maximum area of microbubble cloud in each cycle (Fig. 3.2C). The measured peak intensity increases with the US intensity, and then plateaus when the US intensity is beyond 50 W cm^{-2} (Fig. 3.2D). Remarkably, a similar trend is obtained in modified lap-shear tests (Fig. 3.2E). The adhesion energy and shear strength between hydrogel and skin both increase with the US intensity and then plateau (Fig. 3.2F, G), and both are shown to correlate linearly with the peak bubble intensity (Fig. 3.2H). This correlation could be understood as follows. When the vapor bubbles grow, oscillate and collapse, a series of mechanical consequences, including acoustic streaming, local acoustic emissions, shock waves and micro-jetting, can propel, penetrate, and anchor the primer agent into the tissue, facilitating the tough bonding with hydrogels. In support of this point, we further visualize the single bubble dynamics with laser-induced cavitation experiments, showing that the laser-induced bubble collapses and jets towards the tissue substrate (fig. S3.9), which potentially permeate the tissue locally and form strong interfacial entanglement for tough bioadhesion. Also, the adhesion energy scales almost linearly with the duration of US treatment (fig. S3.10), further corroborating the correlation between cavitation and bioadhesion.

To further demonstrate that the US treatment results in strong interfacial bonding, we characterize the interfacial bonding with fatigue fracture tests. Such tests can screen the contributions of background hysteresis and pinpoint the interfacial bonding in cases of tough adhesion. They output interfacial fatigue threshold or intrinsic work of adhesion Γ_0, which scales with the density of interfacial bonds according to the Lake-Thomas theory (*21*). In the fatigue tests under 180-degree peeling configuration, we vary magnitudes of cyclic loads applied onto the specimens for different energy release rates G, and monitor the crack extension over cycles (dc/dN) (Fig. 3.2I, J). Consistent with prior works (*11*), the hydrogel-tissue adhesion suffers from fatigue and the crack growth rate increases with the loading G (Fig. 3.2K). The linear regression of the G-dc/dN curves informs the intrinsic work of adhesion (Γ_0). Remarkably, the US treatment raises Γ_0 from 5 J m^{-2} (non-US) to 65 J m^{-2} (Fig. 3.2L). The results substantiate the existence of strong interfacial bonding,

which resembles covalent bonds, in contrast to often weak physical interactions such as entanglement resulted from interdiffusion. Importantly, with the absence of covalent bonding at interface, the high Γ_0 is among the highest value reported for bioadhesion, and even exceeds the cases of forming interfacial amide bonds via carbodiimide chemistry (~25 J m^{-2}) (*11*). Free of chemical reactions with tissues, our strategy can bypass the limited functional groups on tissues, paving new ways for fatigue-resistant bioadhesives with high interfacial fatigue threshold.

In addition to the role of a key contributor, the US serves as a regulator for tough bioadhesion. As the US effects scale with the distance between the transducer and the tissue (*d*), we hypothesize controllability over bioadhesion in magnitude and space by simply maneuvering the US transducer (Fig. 3.3A). Indeed, we find that the adhesion energy is tightly regulated by *d*. Specifically, when the US horn (32 W cm^{-2}) is placed very close to the tissue substrate (0.5 mm), over 600 J m^{-2} adhesion energy is measured (Fig. 3.3B). When the transducer is positioned farther away from the substrate, the adhesion decreases eventually to the level of the control condition without US. The dependence further underscores the importance of cavitation activity close to the tissue surface and allows one to tune the adhesion performance without changing any material or chemistry.

The transducer-tissue distance *d* also mediates the adhesion area formed on porcine skin, defined by a clear boundary between tough adhesion and non-adhesion regions (Fig. 3.3C). The tough adhesion area decreases with the gap between the transducer and the tissue (Fig. 3.3D). To understand and predict the spatially controlled bioadhesion by US, we conduct computational modeling on the acoustic field produced by the US transducer between the horn and the substrate. We extract the area on the substrate where the absolute pressure drops below the vapor pressure in every acoustic cycle, thereby enabling the formation of cavitation bubbles (Fig. 3.3E, F). At various *d*, we obtain drastically different pressure profiles on the tissue substrate, from which the regions impacted by cavitation are estimated. According to our simulation, when d = 1 mm, cavitation can affect tissue size similar to the US transducer horn, while when d = 5 mm, no cavitation effect is expected on the tissue surface (Fig. 3.3D). The simulation results agree very well with the experimental measurements. The spatial resolution of the realized bioadhesion are expected to be further improved with focused-ultrasound devices (*22*). Instead of engineering the shape, geometry, or topography of the adhesive matrix, our strategy allows precise spatial control of adhesion, with the aid of US. This ability is particularly desired as current bioadhesives are

limited by isotropic adhesiveness, poor control over the diffusion of adhesive agents and complications associated with patterning adhesives (*2*, *8*, *9*).

Besides the spatial control, we further demonstrate that the US treatment could initiate debonding by leveraging its thermal effect (Fig. 3.3G, H). To show the temporal control of bioadhesion, we select a thermo-sensitive biopolymer gelatin, which gels below 30 - 35 °C and dissociates at the temperature above. Upon US application, the gelatin behaves as liquid to penetrate the epidermis layer of skin and the hydrogel matrix, then cools down to normal human skin temperature and undergoes sol-gel transition, forming tough bioadhesion (~ 250 J m^{-2}) (Fig. 3.3I). To remove the bioadhesives, one can apply US again above the hydrogel to trigger a localized temperature increase (fig. S3.11), followed by the dissociation of the gelatin matrix at elevated temperature. The adhesion energy is drastically decreased (~20 J m^{-2}) (Fig. 3.3I), which allows the hydrogel patch to be easily removed. While this demonstration is for topical applications, implantation applications are possible with other thermo-sensitive materials with an upper critical transition temperature (UCST) above 37°C.

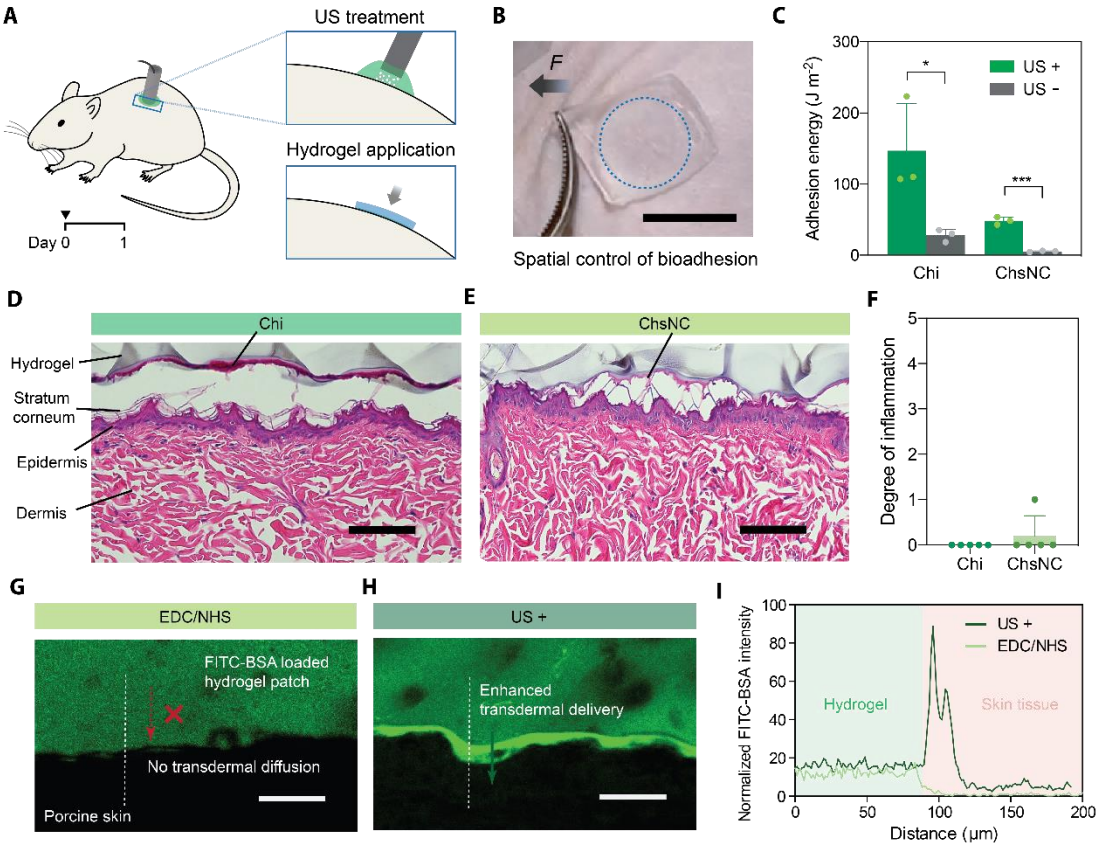

Figure 3.4. Biocompatibility and applications. (A). Schematics of the procedures of US mediated bioadhesion with a rodent model. (B). Spatial control of bioadhesion on rat skin. Blue dotted circle indicates the adhesion region. Scale bar is 1 cm. (C). Adhesion energy between rat skin and hydrogel with or without US treatment. Data reported as means ± SD for n = 3 independent experiments. Representative H&E images of hydrogel-rat skin hybrid using Chi (D) and ChsNC (E) as anchoring primer, respectively. Scale bar is 100 μm. (F). Degree of inflammation after 1-day hydrogel attachment mediated by US; 0, no inflammation; 1, very mild inflammation; 2, mild; 3, moderate; 4, severe; 5, very severe. (G). No transdermal diffusion of FITC-BSA (green) is observed using EDC/NHS chemistry to achieve bioadhesion. (H). Markedly enhanced FITC-BSA delivery into skin using US-mediated bioadhesion strategy. Dashed line indicates the region of interest analyzed for fluorescence intensity. Scale bar is 100 μm. (I). Characterization of the FITC-BSA signals at the skin-hydrogel interface using covalent bonding (EDC/NHS) and US-mediated tough bioadhesion. Statistical significance and *P* values are determined by two-sided Student's *t* test. "*" indicates $P < 0.05$; "***" indicates $P < 0.001$.

To evaluate the safety and efficacy of US-mediated bioadhesion *in vivo*, we validate its biocompatibility with a rodent model. The animal study is critical as the mechanical index for the high-frequency US safety criteria for imaging applications is not applicable for the low-frequency US used in this study (*16*). We test both Chi and ChsNCs to prove *in vivo* applicability. The US transducer is immersed in the primer solution and kept around 1 mm above the rat dorsal skin. After 30-second US treatment, a PAAm-alg hydrogel patch is placed and compressed gently on the treated skin (Fig. 3.4A). Tough bioadhesion forms within 10 minutes, selectively on a circular region treated with US, indicative of spatially controlled adhesion (Fig. 3.4B). By testing freshly excised rat skin, we confirm higher adhesion energy for both Chi and ChsNCs achieved *in vivo*. The adhesion is slightly weaker than that on porcine skin (Fig. 3.4C), which can be attributed to the difference in skin mechanics and anatomy (*21*). Histological assessments conclude no marked tissue damage by US (Fig. 3.4D and E). No acute inflammation is observed when the chitosan is applied, while only one exception of very mild inflammation is found with ChsNCs (Fig. 3.4F). Further validation with human skin is needed to establish the safety criteria for clinical application but outside the scope of this study.

Lastly, another advantage of our strategy is facilitating transdermal drug delivery, owing to the robust hydrogel-tissue biointegration and the delivery capacity of the hydrogel patch. In prior works, drug molecules were delivered in a solution concurrent with US application for transdermal drug delivery (*23*). Using FITC-BSA as a model drug, we show that tough adhesion realized by interfacial chemical reactions fail to deliver drug transdermally due to the extremely low permeability of skin (Fig. 3.4G), while US triggered anchorage approach successfully enhance the transdermal protein delivery from the drug-encapsulated hydrogel patch into the epidermis and dermis layer of the skin (Fig. 3.4H, I). The usage of tough hydrogels also guarantees the physical integrity of the hydrogel matrix, where single-network hydrogels (such as alginate) would undergo significant damage after each cycle of US stimulation (*24*). Compared to microneedle devices (*25*), our strategy combines strong adhesion performance, mitigated tissue damage and lowered infection risks.

In conclusion, we report the strategy of US-mediated bioadhesion to precisely control the spatial and temporal profiles of hydrogel adhesion on various tissues. Combining experimental and computational studies, our result imply that US-induced cavitation is the key contributor and regulator of the bioadhesion performance. The US-induced cavitation can anchor various primer materials into the tissue substrate, leading to strong interfacial bonding and tough adhesion with hydrogels. The proposed US-mediated anchorage is biocompatible and can provide additional therapeutic benefits such as transdermal drug delivery. Other immediate opportunities include the application of wearable devices and the development of non-contact, remotely applied, deep-in-tissue implantable bioadhesives. This work highlights the convergence of disciplines and opens new avenues to develop bioadhesive technologies with unprecedented controllability and performance.

3.3 Materials and Methods

Hydrogel synthesis. The PAAm-alg tough hydrogel was prepared following a modified protocol previously reported (*3, 26*). Briefly, sodium alginate (high molecular weight, I1G, Kimica Corporation) and acrylamide (Sigma-Aldrich) were first dissolved in deionized (DI) water at 2% w/w and 12% w/w, respectively. The mixture was stirred overnight until a clean solution was obtained. The solution of 20 mL was then syringe-mixed with 72 μL of 2% w/w covalent crosslinker N,N'-methylene bis(acrylamide) (MBAA; Sigma-Aldrich), 32 μL of accelerator tetramethyl-ethylenediamine (TEMED; Sigma-Aldrich), 452 μL 66 mg/mL ammonium persulfate

(APS; Sigma-Aldrich), and 250 µL of 15% w/w calcium sulfate slurry. The mixture was injected into a closed glass mold overnight to complete the reaction. The PAAm hydrogel was prepared by mixing the prepolymer solution, containing 20 mL 12% w/w acrylamide solution, 144 µL of 2% w/w MBAA, 32 µL of TEMED, and 452 µL 66 mg/mL APS, then injecting into a closed glass mold for more than 1 hour. To prepare PNIPAm-alg hydrogel. Sodium alginate and NIPAm was first dissolved in DI water at 2% w/w and 12.6% w/w respectively and stirred overnight. The solution of 20 mL was then syringe-mixed with 45 µL of 2% w/w MBAA, 23 µL of accelerator tetramethyl-ethylenediamine (TEMED; Sigma-Aldrich), 468 µL 66 mg/mL APS; Sigma-Aldrich, and 360 µL of 15% w/w calcium sulfate slurry. The mixture was injected into a closed glass mold overnight to complete the reaction at 4 °C.

Preparation of anchoring primer solutions. The anchoring materials tested in this study include chitosan (50-190 kDa, Sigma-Aldrich, 448869), gelatin (type B, Sigma-Aldrich), chitosan nanocrystals (ChsNCs; fabricated following a previously reported protocol (*27*)), and cellulose nanocrystals carrying CHO groups (CNC-CHO; gift from Prof. Yixiang Wang at McGill University). The solution of 2% Chitosan was prepared by dissolving chitosan powder into 0.1% HCl solution. The suspension of 2% ChsNCs was prepared by mixing 20 mg ChsNCs powder with 1 mL DI water, and dispersed in an ultrasonic cleaner for 10 minutes before usage. The solution of 2% gelatin was prepared by mixing 20 mg gelatin powder with 1 mL DPBS (Fisher Scientific) and heated at 50 °C to allow for complete dissolution. 2% CNC-CHO solution was prepared by mixing 20 mg CNC-CHO powder with 1 mL DI water, and dispersed in an ultrasonic cleaner for 10 minutes.

US-mediated bioadhesion. Porcine skin, buccal mucosa and aorta tissues were purchased from local slaughterhouse, preserved at -80 °C and thawed at 4 °C before usage. To form tough adhesion between PAAm-alginate hydrogel and porcine tissues, the anchoring primer solution was first spread on the tissue surface. The US transducer was then immersed in the primer solution on the tissue surface and imposed the US for a certain period. To characterize the effects of US transducer-tissue distance on bioadhesion, the US transducer was fixed with a lab stand at varying distances from the tissue. The US treatment was then initiated for 1 minute. The hydrogel patch was then placed on top of the region where anchoring agent and US was applied. The hydrogel-tissue hybrids prepared without US treatment was tested as control.

Characterization of US-induced microbubble clouds. A customized set-up was established to visualize and quantify the microbubble clouds induced by US. Briefly, the US transducer was immersed in a transparent glass beaker filled with 2% w/w chitosan solutions. An LED light was placed behind the container, while a high-speed camera (FASTCAM MC2.1, Photron, Japan) was placed in front. When the US and LED light were on, after the optimization of lighting conditions, the microbubbles were identified as non-transparent objects (shadowgraph) and captured by the high-speed camera. The obtained videos were converted into binary digital images, where dark pixels within the microbubble clouds in each cycle were quantified, by measuring the greyscale of each image and mass processed with a customized ImageJ Macro program. To normalize pixel intensity, a completely black image was set at 100, while a white image was set at 0. The obtained normalized peak bubble intensity can be compared between different US intensities.

Adhesion energy measurements. Both 180° peeling and modified lap shear tests were performed with an Instron machine to characterize the adhesion energy between the hydrogel and the tissue. For a 180° peeling test, a ribbon of hydrogel-tissue hybrid ($15 \times 1.5 \times 60$ mm^3) adhered using various anchoring primer materials with or without US treatment were prepared. An initial crack was created at one end of the hybrid. A rigid polyethylene terephthalate (PET) film was adhered on the top surface of hydrogel and tissues using Krazy glues to prevent their deformation during mechanical testing. The free end of the tissue is fixed with mechanical grips, while the hydrogel was gripped and connected to the load cell of the machine. Unidirectional tension was applied, while the force and displacement were recorded. The loading rate was kept constant at 0.5 mm/s. The adhesion energy was two times the plateau value of the ratio of the force and width. For lap shear testing, the hydrogel-tissue hybrid was prepared with an overlapping joint of 15 mm for adhesion and an initial crack of 5 mm at the interface. Unidirectional tension was applied on two free-ends of the hydrogel-tissue hybrid, while the force and displacement were recorded. The adhesion energy was calculated using the form: $G = W_g t_g + W_t t_t$, where t is the thickness of the specimen, W is the strain energy of the sheared region under a critical load. The subscriptions stand g and t stand for the gel and the tissue, respectively.

To quantify the interfacial fatigue threshold of the hydrogel adhesion to porcine skin with or without US treatment, we further performed the 180° peeling test under cyclic loading (force control mode). Cyclic peeling force with an amplitude of F_a ($F_a < F_s$) over N cycles was applied, and the interfacial crack extension c were recorded from the machine as a function of cycle number

N. Accordingly, the applied energy release rate was calculated as $G = F_a/W$, and the interfacial crack propagation rate as dc/dN. The multiple-cycle peeling test was performed at varied applied force amplitudes to give a plot of dc/dN versus G. By linearly extrapolating the plot of dc/dN versus G to the x-intercept, we obtained the interfacial fatigue threshold Γ_0.

Spatially controlled bioadhesion. The US transducer was fixed with a lab stand above the porcine skin tissue at varying distances during the US treatment. The interfacial adhesion energy was measured using the lap shear test with the same overlapping joint size of 15 × 15 mm^2. To characterize the area of tough adhesion and identify the tough adhesion boundaries, two arms of the hydrogel/tissue hybrid were stretched until a significant resistance was experienced. The tough adhesion area where the hydrogel and tissue still strongly attached was measured using a caliper.

Characterization of the US transducer displacement. The ultrasonic transducer displacement was characterized using both a microphone and a laser vibrometer in ambient air. The microphone (B&K Type 4939) amplified by a microphone conditioner (B&K Type 2690) has a linear response up to 100 kHz. The vibrometer controller and sensor head (Polytech OFV-5000 and OFV-534) is equipped with a displacement decoder (DD-900) which is sensitive up to 2.5 MHz. The vibrometer is configured to an output sensitivity of 2 μm/V, which allows a resolution of 0.6 nm and a maximum amplitude of 40 μm. The two instruments were placed facing the ultrasonic transducer 50 cm away. While the US transducer was operated at various intensities, the pressure and displacement was recorded from the instruments at a sampling rate of 160 kHz using LabVIEW (National Instruments, USA) and a data acquisition device (NI cDAQ-9172 with NI 9215) (Fig. S3.12).

Acoustic simulations. Simulations were carried out using an open-source K-WAVE acoustics toolbox for MATLAB (*28*). This toolbox allows the simulation of nonlinear acoustic propagation in a quiescent, isotropic and inviscid medium, including power-law modelling of acoustic absorption. For this purpose, the toolbox calculates the acoustic pressure and acoustic velocity field by solving a modified form of the Westervelt equation using k-space pseudospectral method. This modified Westervelt equation, valid for heterogeneous media with power law absorption, is given by:

$$\nabla^2 p - \frac{1}{c_0^2}\frac{\partial^2 p}{\partial t^2} - \frac{1}{\rho_0}\nabla\rho_0 \cdot \nabla p + \frac{\beta}{\rho_0 c_0^4}\frac{\partial^2 p}{\partial t^2} - L\nabla^2 p = 0,$$

with p the acoustic pressure, ρ_0 the medium density, c_0 the medium speed of sound, $\beta = 1 + B/2A$ the coefficient of nonlinearity and L a loss operator modelling power-law acoustic absorption of the medium. In the present case, the values used were ρ_0 = 994 kg/m3, c_0 = 1517 m/s and B/A = 5.2, corresponding to the values for water at 35°C. The axisymmetric assumption was made to reduce the problem to 2D to save the computation time. The setup consisted in wall boundary conditions (i.e. impedance jump where density and speed of sound are suddenly multiplied by a factor 20) at the bottom of the domain and at the horn side wall, the horn tip modelled as an acoustic velocity source of radius 4.7 mm, and dissipative (i.e., non-reflective) boundary conditions on all other boundaries. The grid size was 25 mm in the width, and 6.5 mm in height (except for the d = 5 mm case where the height was 13 mm). The cell size was 0.1 mm for all simulations except d = 0.5mm where the grid size was reduced to 0.05mm. The case for d=1 mm was tested both with larger grid height (13 mm) and smaller grid cell size (0.05 mm) to make sure the grid adaptation for computational efficiency did not have an influence on the result. The acoustic absorption coefficient fed into the loss operator L was set to α= 0.16 dB/cm/MHz^2. This value corresponds to that of human blood (*29*), since rheological tests showed that chitosan has a similar zero-shear viscosity and shear-thinning behavior as blood (fig. S3.13). From the computed acoustic fields, one can determine however that the shearing rates stay low in most of the domain, meaning that the fluid can be assumed to be Newtonian for the current application. The shielding effects of bubbles in the fluid are neglected (single-phase fluid). For the determination of the probable cavitation area on the substrate, the maximum amplitude of the pressure oscillations p' just above the bottom wall were extracted, and the total pressure $p = p_0 - p'$ (p_0 being the atmospheric pressure) compared to the water vapour pressure at 35°C, which is p_v = 5627 Pa.

Laser-induced single cavitation bubble. Laser-induced bubble experiment were conducted in order to verify that the microjets occurring during bubble collapse occur towards the skin. The bubble dynamics on the tissue surface cannot be easily captured, since the clouds obstruct the light source when the transducer-substrate distance is small. For this purpose, the following setup was used: a Litron Nano T 135-15 PIV laser shoots a single beam (5mm diameter, 8ns pulse duration, 532 nm wavelength) through a 10x beam expander (52-71-10X-532/1064, Special Optics). The expanded beam is aligned with a parabolic mirror (87-409, Edmund optics) focusing the laser beam on a single point at a 90° angle from the original beam. The focus point is set such that it lays around 1mm above the pork skin. The focused laser pulse creates an optical breakdown-

induced plasma which evolves into a single vapour bubble reaching a radius of up to 1.5mm. The inception and collapse of the bubble is imaged using a Shimadzu HPV-X2 high speed camera coupled to a Laowa 100mm f/2.8 2x ultra macro lens at 500 kFPS. The field of view is $11 \times 7 mm^2$. The front illumination is achieved through a Cordin flash lamp operated at 800V with a pulse width of 20 ms.

US mediated on-demand detachment. To demonstrate the temporal control of bioadhesion, 2% gelatin solution was used as the anchoring primer material. The tough bioadhesion was first validated using a 180-degree peeling test. To enable the detachment, the US transducer was placed on the hydrogel patch and the 30-second US treatment was applied. The adhesion energy for detachment of the hydrogel/tissue hybrid was then immediately characterized with a 180-degree peeling test.

In vivo biocompatibility of US-mediated bioadhesion. All animal surgical procedures were reviewed and approved by the Facility Animal Care Committees at McGill University and the Research Institute of McGill University Health Centre. Female Sprague Dawley rats (200 to 300 g, Charles River Laboratories) were used for all *in vivo* studies. All hydrogel precursors prepared for the PAAm-alg hydrogel patch fabrication and chitosan solutions were sterilized with 0.2-μm filters. Chitosan nanocrystal suspensions were sterilized with autoclaves. For *in vivo* biocompatibility assays of the topical application of US mediated bioadhesion, the dorsal hair of rats was first removed. Around 300 μl of either chitosan solution or chitosan nanocrystal suspensions were applied on the shaved skin surface. The US transducer was immersed in the solution/suspension and the US treatment was initiated for 30 seconds in total with 10-second intervals. The hydrogel patch (15×15 mm^2) was then placed on the treated region with gentle pressure applied. A Tegaderm film (3M) was also applied on top of the hydrogel patch to minimize its dehydration. A maximum of 4 hydrogel patches were applied on each rat. Rats were euthanized after 24 hours. Tissues with regions of interest were excised and fixed in 4% formalin for 24 hours before histological processing.

Histological processing. Fixed tissue samples were placed into 70% ethanol and submitted for histological processing and hematoxylin and eosin staining at the Histology Core of the Goodman Cancer Research Center at McGill University. Z.-H.G. is a Professor of the Department of

Pathology & Laboratory Medicine at the University of British Columbia and examined all histological sections.

Transdermal drug delivery. FITC-albumin (A9771, Sigma-Aldrich) was dissolved in PAAm-alg prepolymer solution at 10 mg/ml then fabricated as a drug-eluting hydrogel patch. The US-mediated tough bioadhesion between the hydrogel patch and porcine skin was formed as previously described. The hydrogel-tissue hybrids were then incubated at 37 °C for 3 hours, and immediately frozen at -80 °C before cryosectioning with a cryotome. The obtained hydrogel-tissue sections were analyzed under a fluorescent microscope to characterize the penetration depth of FITC-albumin into the skin.

3.4 Supporting Information

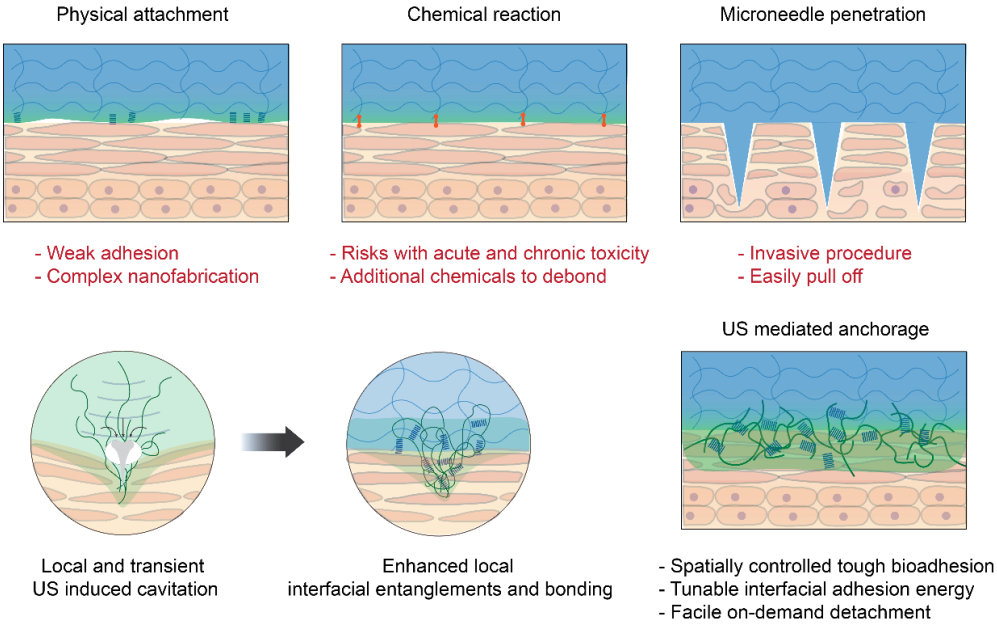

Figure S3.1. Comparison of existing adhesion mechanisms (top row) and the proposed mechanism - US mediated anchorage (bottom row).

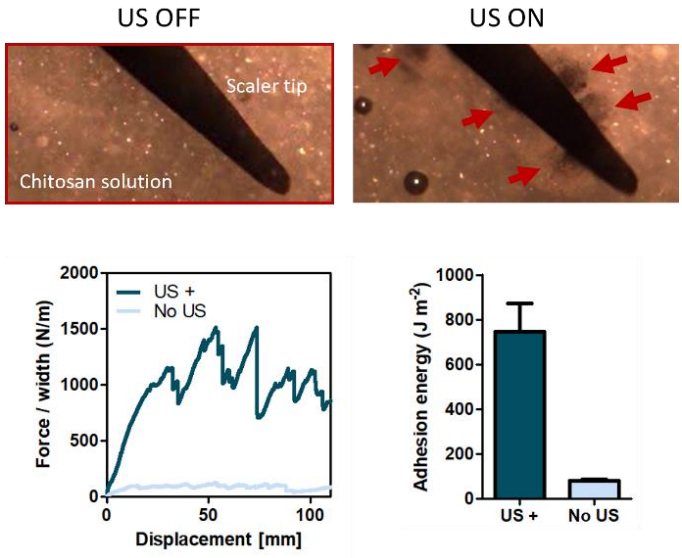

Figure S3.2. Images and characterization of US-mediated bioadhesion using a clinically used ultrasonic scaler. Red arrow indicates cavitation bubble clouds. (Top) Cavitation induced around the scaler tip; (Bottom) Force-displacement curves and adhesion energy of the hydrogel-skin hybrids with and without US. Red arrow indicates cavitation bubble clouds. Data reported as means ± SD for n = 3 independent experiments.

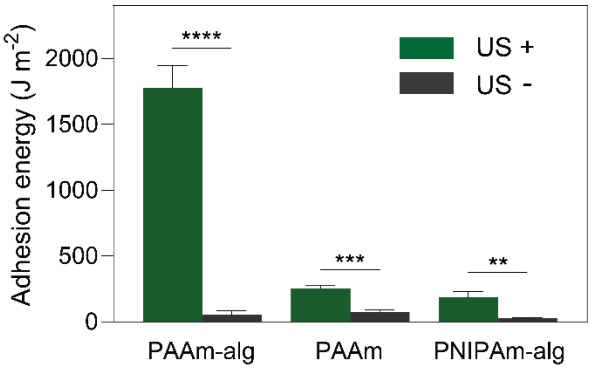

Figure S3.3. US-mediated tough bioadhesion applicable to various hydrogels, including double-network hydrogels such as PAAm-alg and PNIPAm-alg, and a single-network PAAm hydrogel. Data reported as means ± SD for n = 3 independent experiments. Statistical significance and *P* values are determined by two-sided Student's *t* test. "**" indicates $P < 0.01$; "***" indicates $P < 0.001$; "****" indicates $P < 0.0001$.

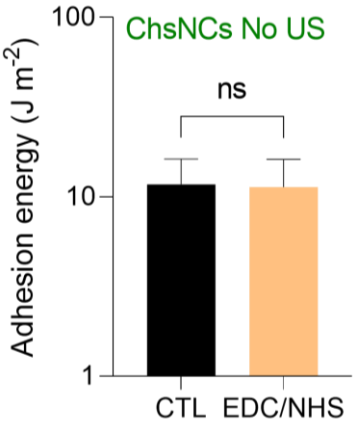

Figure S3.4. Hydrogel-skin adhesion using chitosan nanocrystals (ChsNCs) with or without EDC/NHS. CTL indicates control conditions without US treatment. Data reported as means ± SD for n = 3 independent experiments. "ns" indicates not significant. The result signals the primary constraint for ChsNC bioadhesion to be the lack of tissue anchorage, instead of covalent bonding formation.

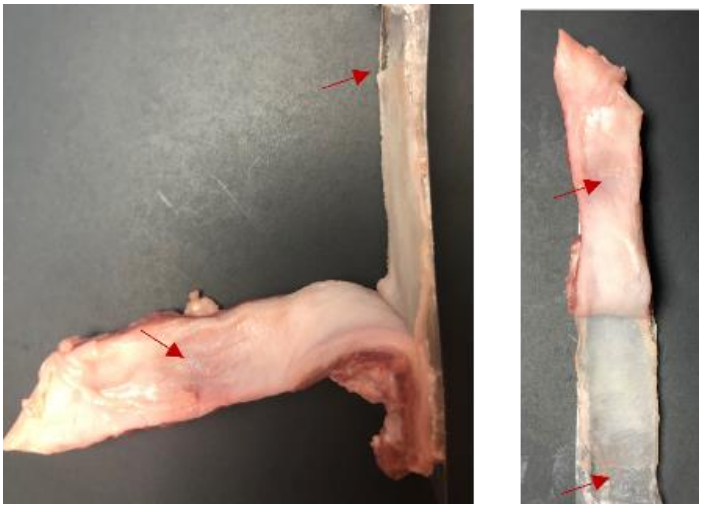

Figure S3.5. Delamination of porcine buccal membrane from the underlying tissue in 180-peeling test of the hydrogel-buccal tissue hybrid with US treatment. The hydrogel remains adhered to the buccal mucosa. Red arrows indicate delamination site.

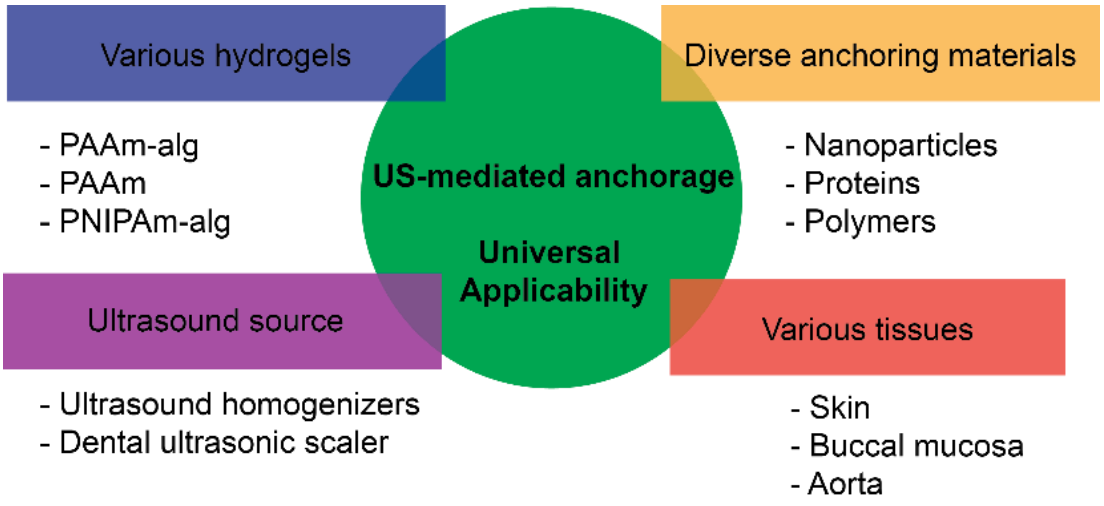

Figure S3.6. Universal applicability of the proposed US-mediated anchorage strategy demonstrated in this study.

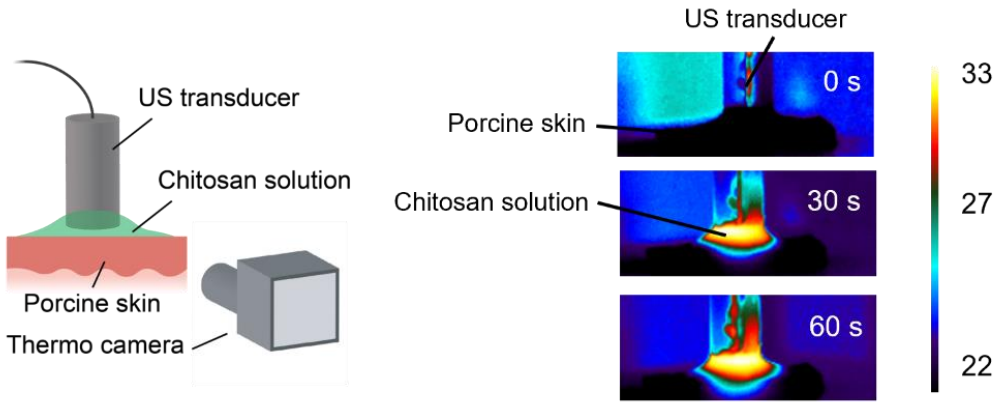

Figure S3.7. US-induced heating in the primer solution spread on skin captured by a thermo camera over time (temperature unit: °C).

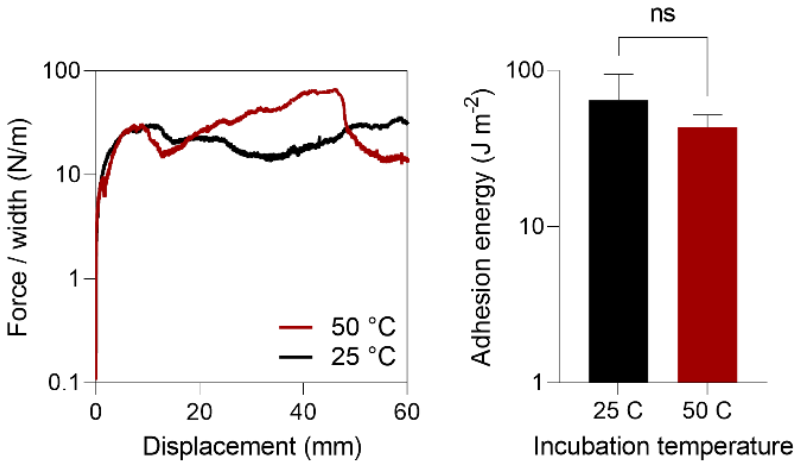

Figure S3.8. Modest effects of incubation temperature on bioadhesion. Data reported as means ± SD for n = 3 independent experiments. “ns” indicates not significant.

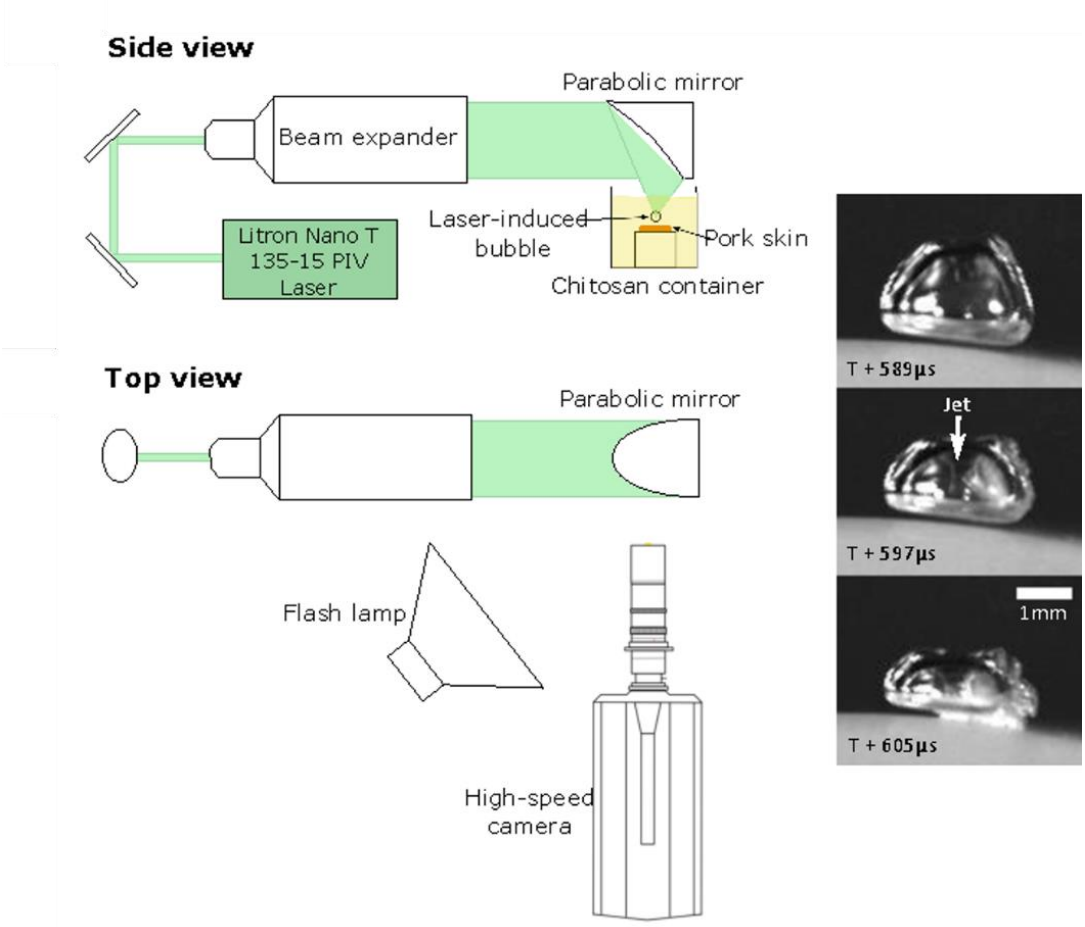

Figure S3.9. Laser-induced bubble experiments. Setup to visualize single bubble dynamics induced by a laser (Side and top views; right). Digital images of the single bubble micro-jetting (right).

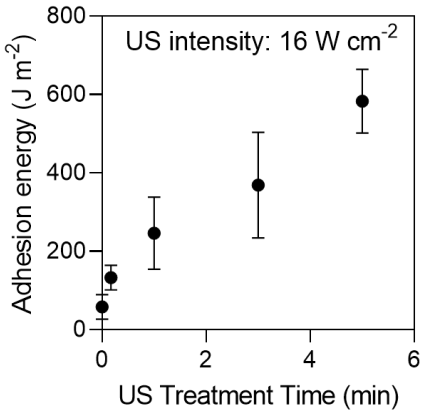

Figure S3.10. Tissue-hydrogel adhesion enhances with US treatment time. Data reported as means ± SD for n = 3 independent experiments. Data reported as means ± SD for n = 3 independent experiments.

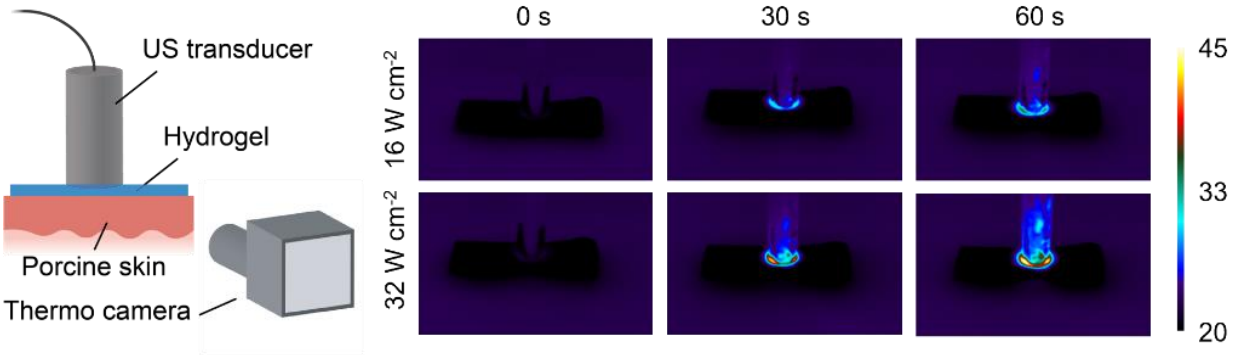

Figure S3.11. Thermo-effects of US when applied onto hydrogel-skin hybrid (temperature unit: °C).

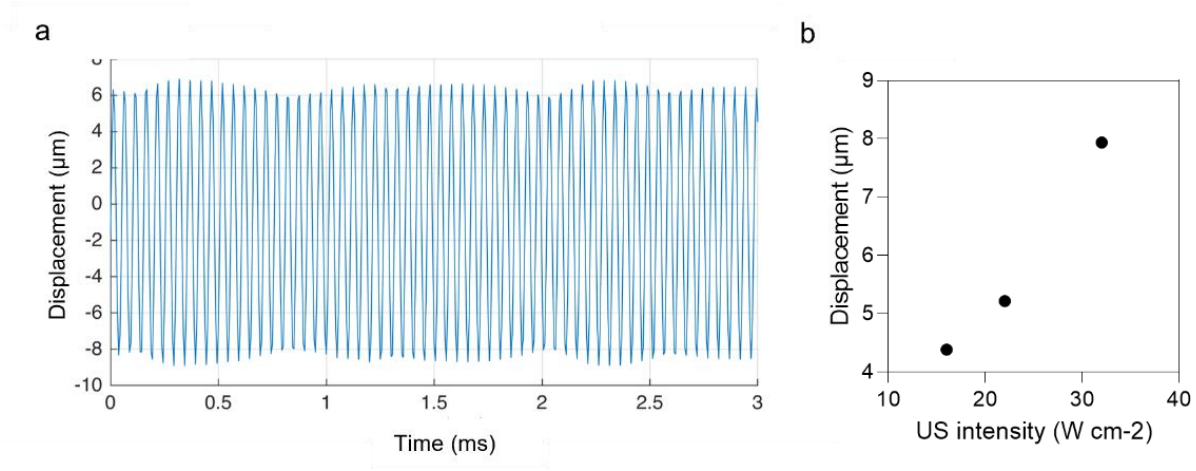

Figure S3.12. US transducer displacement. Displacement of US transducer as a function of time (a) and intensity (b).

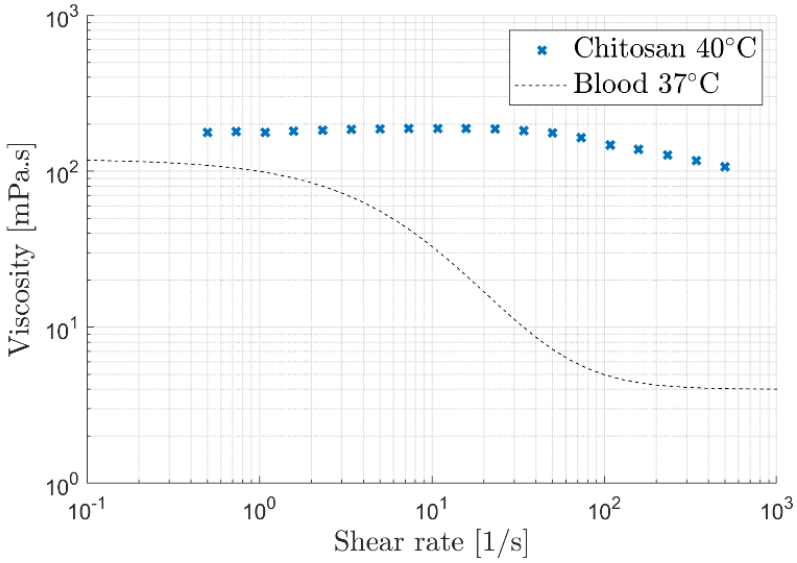

Figure S3.13. Flow curves of human blood and chitosan 2% solution.

References

1. S. Nam, D. Mooney, Polymeric Tissue Adhesives. *Chem. Rev.* **121**, 11336–11384 (2021).

2. Z. Ma, G. Bao, J. Li, Multifaceted Design and Emerging Applications of Tissue Adhesives. *Adv. Mater.* **33**, 2007663 (2021).

3. J. Li, A. D. Celiz, J. Yang, Q. Yang, I. Wamala, W. Whyte, B. R. Seo, N. V. Vasilyev, J. J. Vlassak, Z. Suo, D. J. Mooney, Tough adhesives for diverse wet surfaces. *Science*. **357**, 378–381 (2017).

4. H. Yuk, C. E. Varela, C. S. Nabzdyk, X. Mao, R. F. Padera, E. T. Roche, X. Zhao, Dry double-sided tape for adhesion of wet tissues and devices. *Nature*. **575**, 169–174 (2019).

5. K. Liu, H. Yang, G. Huang, A. Shi, Q. Lu, S. Wang, W. Qiao, H. Wang, M. Ke, H. Ding, T. Li, Y. Zhang, J. Yu, B. Ren, R. Wang, K. Wang, H. Feng, Z. Suo, J. Tang, Y. Lv, Adhesive anastomosis for organ transplantation. *Bioact. Mater.* (2021), doi:10.1016/j.bioactmat.2021.11.003.

6. J. Yang, R. Bai, Z. Suo, Topological Adhesion of Wet Materials. *Adv. Mater.* **30**, 1800671 (2018).

7. H. R. Brown, T. P. Russell, Entanglements at Polymer Surfaces and Interfaces. *Macromolecules*. **29**, 798–800 (1996).

8. A. Mahdavi, L. Ferreira, C. Sundback, J. W. Nichol, E. P. Chan, D. J. D. Carter, C. J. Bettinger, S. Patanavanich, L. Chignozha, E. Ben-Joseph, A. Galakatos, H. Pryor, I. Pomerantseva, P. T. Masiakos, W. Faquin, A. Zumbuehl, S. Hong, J. Borenstein, J. Vacanti, R. Langer, J. M. Karp, A biodegradable and biocompatible gecko-inspired tissue adhesive. *Proc. Natl. Acad. Sci.* **105**, 2307–2312 (2008).

9. X. Chen, H. Yuk, J. Wu, C. S. Nabzdyk, X. Zhao, Instant tough bioadhesive with triggerable benign detachment. *Proc. Natl. Acad. Sci.* **117**, 15497–15503 (2020).

10. J. Li, D. J. Mooney, Designing hydrogels for controlled drug delivery. *Nat. Rev. Mater.* **1**, 16071 (2016).

11. X. Ni, C. Chen, J. Li, Interfacial fatigue fracture of tissue adhesive hydrogels. *Extreme Mech. Lett.* **34**, 100601 (2020).

12. N. Artzi, T. Shazly, A. B. Baker, A. Bon, E. R. Edelman, Aldehyde-Amine Chemistry Enables Modulated Biosealants with Tissue-Specific Adhesion. *Adv. Mater.* **21**, 3399–3403 (2009).

13. C. Demené, J. Robin, A. Dizeux, B. Heiles, M. Pernot, M. Tanter, F. Perren, Transcranial ultrafast ultrasound localization microscopy of brain vasculature in patients. *Nat. Biomed. Eng.* **5**, 219–228 (2021).

14. C. Wang, X. Li, H. Hu, L. Zhang, Z. Huang, M. Lin, Z. Zhang, Z. Yin, B. Huang, H. Gong, S. Bhaskaran, Y. Gu, M. Makihata, Y. Guo, Y. Lei, Y. Chen, C. Wang, Y. Li, T. Zhang, Z. Chen, A. P. Pisano, L. Zhang, Q. Zhou, S. Xu, Monitoring of the central blood pressure waveform via a conformal ultrasonic device. *Nat. Biomed. Eng.* **2**, 687–695 (2018).

15. C. Lovegrove, High-intensity focused ultrasound shows promise for noninvasive tumor ablation. *Nat. Clin. Pract. Oncol.* **3**, 8–9 (2006).

16. C. M. Schoellhammer, A. Schroeder, R. Maa, G. Y. Lauwers, A. Swiston, M. Zervas, R. Barman, A. M. DiCiccio, W. R. Brugge, D. G. Anderson, D. Blankschtein, R. Langer, G. Traverso, Ultrasound-mediated gastrointestinal drug delivery. *Sci. Transl. Med.* **7**, 310ra168-310ra168 (2015).

17. S. Y. Yang, E. D. O'Cearbhaill, G. C. Sisk, K. M. Park, W. K. Cho, M. Villiger, B. E. Bouma, B. Pomahac, J. M. Karp, A bio-inspired swellable microneedle adhesive for mechanical interlocking with tissue. *Nat. Commun.* **4**, 1702 (2013).

18. S. Rose, A. Prevoteau, P. Elzière, D. Hourdet, A. Marcellan, L. Leibler, Nanoparticle solutions as adhesives for gels and biological tissues. *Nature*. **505**, 382–385 (2014).

19. G. Kim, V. M. Lau, A. J. Halmes, M. L. Oelze, J. S. Moore, K. C. Li, High-intensity focused ultrasound-induced mechanochemical transduction in synthetic elastomers. *Proc. Natl. Acad. Sci.* **116**, 10214–10222 (2019).

20. W. L. Nyborg, Mechanisms for Nonthermal Effects of Sound. *J. Acoust. Soc. Am.* **44**, 1302–1309 (1968).

21. Z. Yang, Z. Ma, S. Liu, J. Li, Tissue adhesion with tough hydrogels: Experiments and modeling. *Mech. Mater.* **157**, 103800 (2021).

22. A. R. Rezai, M. Ranjan, P.-F. D'Haese, M. W. Haut, J. Carpenter, U. Najib, R. I. Mehta, J. L. Chazen, Z. Zibly, J. R. Yates, S. L. Hodder, M. Kaplitt, Noninvasive hippocampal blood−brain barrier opening in Alzheimer's disease with focused ultrasound. *Proc. Natl. Acad. Sci.* **117**, 9180–9182 (2020).

23. S. Mitragotri, D. Blankschtein, R. Langer, Ultrasound-Mediated Transdermal Protein Delivery. *Science*. **269**, 850–853 (1995).

24. N. Huebsch, C. J. Kearney, X. Zhao, J. Kim, C. A. Cezar, Z. Suo, D. J. Mooney, Ultrasound-triggered disruption and self-healing of reversibly cross-linked hydrogels for drug delivery and enhanced chemotherapy. *Proc. Natl. Acad. Sci.* **111**, 9762–9767 (2014).

25. J. Yu, J. Wang, Y. Zhang, G. Chen, W. Mao, Y. Ye, A. R. Kahkoska, J. B. Buse, R. Langer, Z. Gu, Glucose-responsive insulin patch for the regulation of blood glucose in mice and minipigs. *Nat. Biomed. Eng.* **4**, 499–506 (2020).

26. J.-Y. Sun, X. Zhao, W. R. K. Illeperuma, O. Chaudhuri, K. H. Oh, D. J. Mooney, J. J. Vlassak, Z. Suo, Highly stretchable and tough hydrogels. *Nature*. **489**, 133–136 (2012).

27. T. Jin, D. Kurdyla, S. Hrapovic, A. C. W. Leung, S. Régnier, Y. Liu, A. Moores, E. Lam, Carboxylated Chitosan Nanocrystals: A Synthetic Route and Application as Superior Support for Gold-Catalyzed Reactions. *Biomacromolecules*. **21**, 2236–2245 (2020).

28. B. E. Treeby, J. Jaros, A. P. Rendell, B. T. Cox, Modeling nonlinear ultrasound propagation in heterogeneous media with power law absorption using a k-space pseudospectral method. *J. Acoust. Soc. Am.* **131**, 4324–4336 (2012).

29. E. L. Carstensen, K. Li, H. P. Schwan, Determination of the Acoustic Properties of Blood and its Components. *J. Acoust. Soc. Am.* **25**, 286–289 (1953).

Preface to Chapter 4

In Chapter 3, we focus on the interfacial adhesion between hydrogels and biological tissues, where we propose a paradigm-shifting technology to control tough bioadhesion in strength, space and time. We demonstrate its advantages over other existing hydrogel bioadhesion strategies, and its implication to be used for regenerative medicine. However, in general surgeries and situations where mechanically active tissues need to be reattached, surgical sutures are expected to be indispensable in the near future due to their orders-or-magnitude higher tensile strength for wound closure compared to hydrogel-based adhesives.

In Chapter 4, we will steer gear towards the interface between hydrogels and fiber-based biomedical devices such as surgical sutures. We propose a bioinspired surface functionalization strategy to fabricate tough gel sheathed surgical sutures with multifunctionality for advanced wound management. This new tough hydrogel coating will remedy the recognized issues with suturing, including mismatched mechanical properties with soft tissues, the resulted tissue damage, trauma, friction and drag caused by the suture fibers, and the limited therapeutic functions of traditional sutures.

We show that robust integration of tough hydrogel and surgical suture can be achieved with over 1500 J m^{-2} interfacial adhesion energy, among the highest reported in the literatures. The proposed material system design is compatible with various hydrogels and suture materials. We demonstrate the sufficient tensile strength and soft surface stiffness due to the core-sheath design. We further show that enhanced biomechanical properties, such as low tissue drag and friction, can also be obtained due to the slippery hydrogel surface. In addition, we expand the functionality of sutures via a composite approach. By including functional materials into the tough gel sheath, we explore the antifouling, antibacterial, sustained drug release, and near-infrared bioimaging functions of sutures for the diagnostic, monitoring, therapeutic management of surgical wound.

This work is published in *Science Advances* and can be cited as:

Zhenwei Ma, Zhen Yang, Qiman Gao, Guangyu Bao, Amin Valiei, Fan Yang, Ran Huo, Chen Wang, Guolong Song, Dongling Ma, Zu-Hua Gao, Jianyu Li*. Bioinspired tough gel sheath for robust and versatile surface functionalization. *Science Advances* 7.15 (2021): eabc3012.

Chapter 4 Bioinspired Tough Gel Sheath for Biomaterials Surface Functionalization

Abstract

Sutures pervade surgeries, but their performance is limited by the mechanical mismatch with tissues and the lack of advanced functionality. Existing modification strategies result in either deterioration of suture's bulk properties or a weak coating susceptible to rupture or delamination. Inspired by tendon endotenon sheath, we report a versatile strategy to functionalize fiber-based devices like sutures. This strategy seamlessly unites surgical sutures, tough gel sheath and various functional materials. Robust modification is demonstrated with strong interfacial adhesion (>2000 J m^{-2}). The surface stiffness, friction and drag of the suture when interfacing with tissues can be dramatically reduced, without compromising the tensile strength. Versatile functionalization of the suture for infection prevention, wound monitoring, drug delivery and near-infrared imaging is then presented. This platform technology is applicable to other fiber-based devices and foreseen to impact broad technological areas ranging from wound management to smart textiles.

4.1 Introduction

Sutures are a class of fiber-based device primarily to mechanically approximate tissues or attach wearable/implantable devices to human body (*1*). They are in form of either mono- or multi-filaments (i.e., braided),and designed to degrade or stay permanently in the body. A variety of materials have been invented and adopted as surgical sutures, including plastics (degradable: polyglycolide, polylactic acid; non-degradable: nylon, polypropylene), biologically derived proteins (collagen, silk), and metals (stainless steel, nitinol). The sutures have been widely used in many branches of medicine such as wound closure and anastomosis with a global market of over 5 billion US dollars (*2*). Despite the recent progress of tissue adhesives development (*3*, *4*), they will remain indispensable for general surgical procedures because of their reliable performance, ease of implementation, and the capacity to exert larger forces than any tissue adhesives (*2*).

However, the performance of existing sutures has been limited by their poor biomechanical properties and lack of functionality, which are implicated in surgical and post-surgical complications. First, sutures are made of rigid dry materials (elastic modulus >1 GPa) in contrast to soft hydrated tissues (elastic modulus <100 kPa), as they need to carry substantial mechanical

loading along the axis to approximate tissues (*5*). This mechanical mismatch is found to cause inflammation and impaired healing outcomes (*6*). Second, the rough surface of sutures, particularly for the braided sutures, can drag and rub against the contacting tissue during and after suture placement. This mechanical irritation can damage fragile tissues and those under disease conditions such as aneurysm and ulcer, leading to tissue dissection and other post-surgery complications (*7*, *8*). In addition, clinically used sutures lack advanced functionality for wound management. Thus, multifunctional sutures are in demand to perceive, report and respond to the wound healing process, for instance, delivering therapeutic to promote wound healing (*9*) and preventing surgical site infections (*10*). Such functional sutures are developed recently, which feature drug delivery or sensing capacities. But limitations to these approaches remain, including complex fabrication process, high cost, limited physical integrity, as well as the above-mentioned biomechanical constraints. These issues associated with surgical sutures are also found in other fiber-based devices, particularly those interfacing with the human body such as guidewires and smart textiles. New strategies to improve the biomechanical properties and functionality of sutures and other fiber-based devices continue to be sought.

General strategies to functionalize sutures include bulk modification and surface functionalization. The former involves bottom-up approaches to (re)produce the suture (e.g., electrospinning and melt extrusion), which may compromise the suture's strength and are inapplicable to commercially available sutures (*11*). To minimize the alteration of the bulk properties, the surface functionalization is appealing, which results in a suture coating via dip-coating/soaking (*12*, *13*), layer-by-layer deposition (*14*, *15*), grafting (*16*), and impregnation (*17*). However, the suture coating is often weak and vulnerable to fragmentation and delamination, due to the chemical inertness of suture materials and the demanding mechanical loading of the suture application (e.g., shear and compression during suturing and knotting). The mechanical failure of suture coating results in the loss of functionality (fig. S4.1, A to C) and other side effects (e.g., burst drug release for drug-eluting suture coating). Evidently, the toughness and adhesion of the suture coating is thus mission-critical and recognized as a prerequisite of any reliable functionalization.

For surface functionalization of surgical sutures, hydrogel technologies are promising in light of recent developments of tough hydrogel adhesion on various materials such as tissues (*3*), hydrogels (*18*), metals (*19*), and elastomers (*20*). These established strategies exploit pre-formed hydrogel patches to be applied on flat surfaces, and thus are not compatible with fiber-based devices as

sutures. Formation of hydrogel coating on complex structures has been recently reported, but is focused on single-network hydrogels and elastomer-based devices (*21*). Neither this strategy nor the other methods are applicable on surgical sutures due to the chemical inertness of suture materials. In addition, most adhesive hydrogels are inclusion-free and lack advanced functionality. Particularly, few work to date demonstrates wound bed monitoring and near infrared (NIR) bioimaging applications with hydrogel coatings. Further development is needed to reinvent and repurpose the hydrogel coating for sutures and other fiber-based devices.

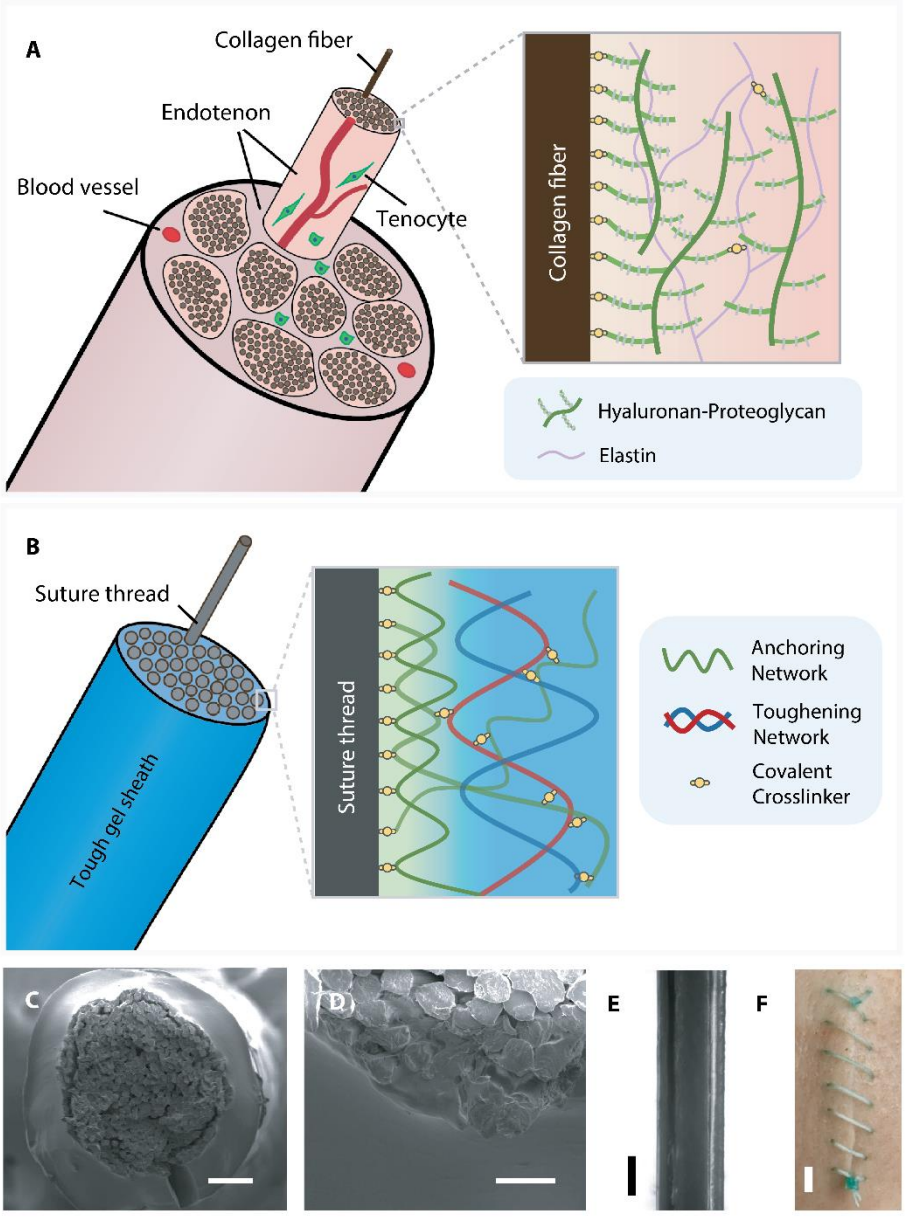

Figure 4.1. Bioinspired design of tough gel sheathed (TGS) suture. Schematics of the structural and material design of (**A**) tendon and (**B**) TGS suture. Scanning electron microscope (SEM) images of (**C**) TGS suture and (**D**) a zoom-in at the suture-sheath interface. Scale bars: 100 μm (**C**) and 25 μm (**D**). (**E**) Bright field image of TGS suture. Scale bar: 500 μm. (**F)** A continuous stitch applied on porcine skin using TGS suture. Scale bar: 1 cm.

To address the above-mentioned issues, we report a bioinspired design and fabrication method for multifunctional tough gel sheathed (TGS) sutures. Different from the previously reported methods based on surface absorption or single-network hydrogels, our strategy features a double-network tough gel sheath strongly bonded with surgical sutures for robust modification. The TGS is hypothesized to help mitigate the mechanical mismatch and irritation of sutures when interfacing with tissues, and to further provide a robust and versatile platform to functionalize commercially available sutures for advanced functionality. As a proof of principle, motivated by the clinical need of wound management, we will demonstrate the TGS sutures loaded with an antibacterial compound, pH-sensing microparticles, drugs and fluorescent nanoparticles (NPs) for anti-infection, wound bed monitoring, drug delivery and NIR bioimaging applications. This work will demonstrate that the TGS suture could unite the merits of suture fibers, tough hydrogels and functional materials by design, and thus achieve a unique combination of enhanced biomechanical properties and multiple functionality, which would be beneficial for general surgical procedures and wound management (fig. 4.1D).

4.2 Design and Fabrication of Tough Gel Sheathed (TGS) Sutures

The design of TGS suture is inspired by endotenon sheath of tendon, which encapsulates and glues collagen fibers together (Fig. 4.1A) (*22*). The endotenon sheath is mechanically tough and strongly adhesive on the collagen fibers, attributing to its double-network structure: the hyaluronan-proteoglycan network binds with the collagen fibers, while the elastin network strengthens and toughens the whole structure. The endotenon sheath not only forms a frictionless surface of the tendon, but also comprises cells and blood vessels for mass transport and repair of the tendon. Learning from the structure and function of the endotenon sheath, we propose a tough gel sheath (TGS) to modify and further functionalize commercially available sutures. To achieve the strong bonding with the suture, the TGS contains one *anchoring network* that forms covalent bonds on

the suture surface for strong adhesion and intertwines with another *toughening network* consisting of physical bonds, which can effectively dissipate energy for high toughness (Fig. 4.1B). This strategy is distinct from the surface absorption, the single-layer polymer grafting, and the hydrogel skin method that requires swelling and doping the substrate with free-radical initiators to form a single-network hydrogel coating (*15*, *16*, *21*).

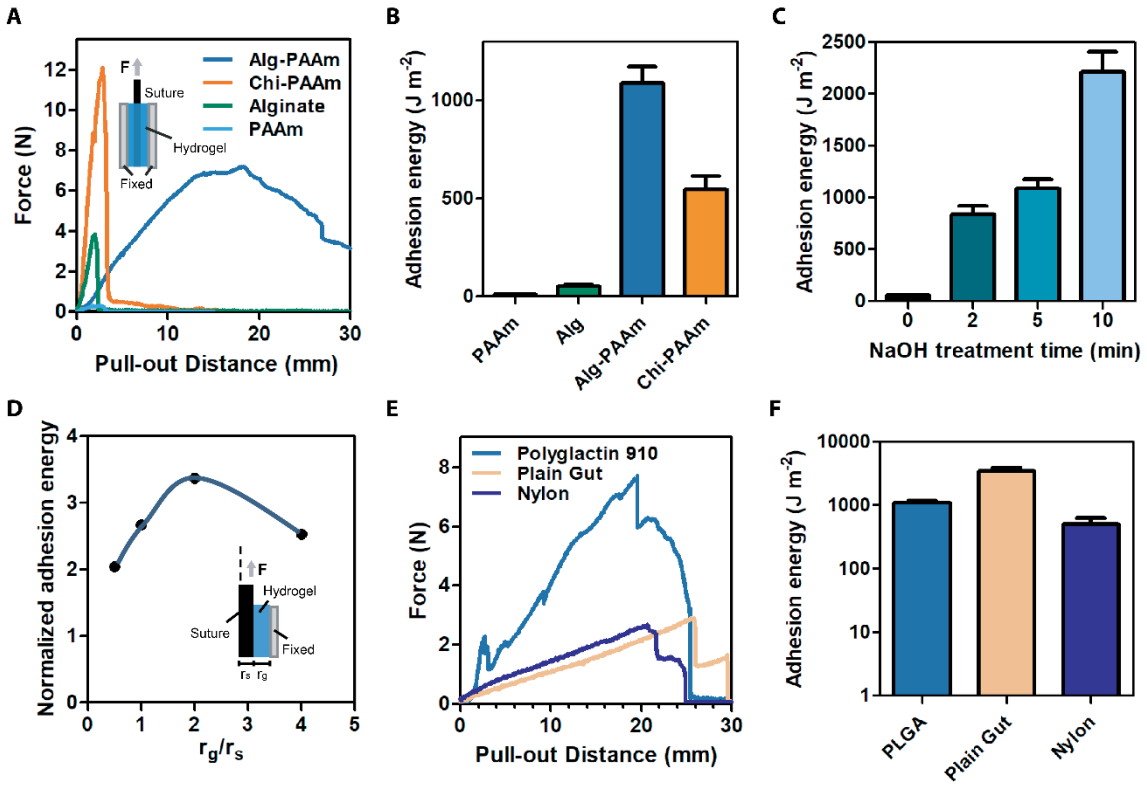

Figure 4.2. Strong adhesion of tough gel sheath and suture. Representative force-displacement curves (**A**) and the adhesion energy (**B**) measured from the pull-out tests (inset in a) of gel sheathed sutures formed with Polyglactin 910 suture and different hydrogels (PAAm: polyacrylamide; Alg: alginate; Chi: chitosan). (**C**) Adhesion energy as a function of NaOH treatment time. (**D**) FEM results of the normalized adhesion energy (Γ/Γ_0) as a function of the ratio of the sheath thickness and the suture radius (r_g/r_s). The force displacement curves of pull-out test (**E**) and the adhesion energy (**F**) of TGS sutures encompassing various suture materials, including Polyglactin 910 (PLGA), plain gut and nylon. Data reported as mean ± standard deviation for n = 3 independent experiments.

The TGS sutures are prepared directly from commercially available surgical sutures with a facile two-step method. We illustrate the essential procedure with a widely used braided surgical suture, polyglactin 910 (copolymer of 90% glycolide and 10% lactide, PLGA), and an alginate-polyacrylamide (PAAm) hydrogel that acts as the TGS due to its high toughness and excellent biocompatibility (*23*). As the pristine suture lacks the functional groups for anchoring, the suture was first treated with 1 M NaOH solution to create carboxylic acid groups on the surface, which was later primed with primary-amine-rich chitosan macromolecules and coupling reagents [1-ethyl-3-(-3-dimethylaminopropyl) carbodiimide hydrochloride (EDC) and N-hydroxysuccinimide (NHS)] to form the *anchoring network*. To form the *toughening network*, the modified suture was then inserted into a glass capillary tube filled with a precursor solution of alginate-PAAm hydrogels; after gelation overnight, the TGS suture was obtained after post-crosslinking in 0.1 M $CaCl_2$ solution (fig. S4.2). The applicability of this strategy to other hydrogels and suture materials will be presented below. Sutures of a wide range of diameters (0.01-1 mm) are used by surgeons in different surgical procedures. Our results demonstrated that the suture was robustly integrated with a thin TGS, and that the thickness was tunable with the diameter of the capillary tube (Fig. 4.1, C to E). With our current set-up, we can reproducibly fabricate 10-15 cm long TGS suture threads with consistent coating thickness (fig. S4.3A). For the long-term storage of TGS sutures, they can be freeze-dried and kept at their dry-state as other commercialized sutures, then simply rehydrated in saline solutions prior to usage (fig. S4.3B). As a demonstration of its physical integrity, a continuous stitch with secured knotting was successfully performed on porcine skin using the TGS suture (Fig. 4.1F). The in vitro biocompatibility of the TGS suture-conditioned medium is comparable to that of the control medium, showing no significant difference in the in vitro viability of human vocal fold fibroblasts after 48-hour culture (fig. S4.4).

4.3 Experimental Investigation of Strong Suture-Sheath Bonding

To interrogate the bonding between the suture and the hydrogel sheath, we invented a pull-out test to characterize the adhesion energy of suture-sheath interface. Briefly, the suture was embedded within a hydrogel cuboid, and then pulled out with an Instron machine (Model 5965), while the force F and the displacement δ were recorded (fig. S4.5). The two opposing sides of the hydrogel cuboid was glued to two acrylic sheets as rigid constraints. It was observed that the adhesion

survived at a large pull-out displacement (20 mm versus 30 mm of the adhesion interface) and that part of the tough gel matrix still attached to the suture even when it was completely pulled out (Fig. 4.2A and fig. S4.5).

An analytical model was developed and applied to calculate the adhesion energy. The strain energy density stored in the hydrogel sheath U_g can be calculated from the force-displacement curve till the point when the interface failed via $U_g = \int F(\delta)d\delta \Big/ \pi(r_{tot}^2 - r_s^2)L$, where r_s denotes the suture radius; r_{tot} denotes the summation of the hydrogel sheath thickness and suture radius; L denotes the jointed length. The critical energy release rate, i.e. adhesion energy, was calculated from U_g with the Equation (See Methods for derivation and other details):

$$\Gamma = \frac{U_g(r_{tot}^2 - r_s^2)}{2r_s} \tag{1}$$

With the above Equations, we calculated that the adhesion energy obtained from the alginate-PAAm sheathed polyglactin 910 suture was over 1000 J m^{-2} (Fig. 3.2B), which was comparable with the tough adhesion of hydrogels achieved on tissues, elastomers and metals.

To reveal the mechanism for the strong adhesion, we next delineated the effects of the *anchoring* and *toughening* networks separately. First, to evaluate the importance of the *toughening* network, the suture sheath was formed with brittle single-network hydrogels (i.e., alginate or PAAm hydrogels), which largely resembled the strategies reported previously (*13*, *21*). Without a tough matrix, the suture-sheath interface is vulnerable to rupture (adhesion energy < 50 J m^{-2}) (Fig. 4.2B). Second, to confirm the role of the *anchoring* network, we fabricated the sheathed sutures without NaOH treatment or surface priming (chitosan/EDC/NHS). Evidently, the lack of strong *anchoring* network led to very low adhesion energy (< 50 J m^{-2}) (fig. S4.6A). The result also implied that the mechanical interlocking of the hydrogel within the braided suture played a small role. The importance of amide-based interfacial bonds was further confirmed with a positive correlation between the duration of NaOH treatment and the adhesion energy (Fig. 4.2C). Over 2000 J m^{-2} adhesion energy was achieved with 10 minutes surface activation. It can be concluded that the strong adhesion is attributed to the synergy of the energy dissipation of the hydrogel matrix and the covalent bonding at the suture-sheath interface.

4.4 Finite Element Modeling of Suture-Sheath Adhesion

To further model the interfacial failure mechanism and aid the design of suture sheath, we developed a finite-element model (FEM) to simulate the pull-out process of a suture from a hydrogel sheath. The *toughening network* was characterized with the Ogden model and the Mullins model, while the *anchoring network* was modelled as cohesive elements with low (24 J m^{-2}) and high (300 J m^{-2}) intrinsic toughness values Γ_0 (*24*). Our simulation showed that the adhesion energy Γ increased with the intrinsic toughness Γ_0 (fig. S4.6, B and C), consistent with the observation of stronger adhesion after longer NaOH treatment (Fig. 4.2C). To study the effect of sheath thickness, we varied the hydrogel thickness in terms of normalized hydrogel radius r_g / r_s while keeping the intrinsic toughness Γ_0 = 300 J m^{-2}. As the adhesion energy Γ is shown to scale linearly with Γ_0 (*25*), we normalized the adhesion energy Γ by the intrinsic toughness Γ_0. Large normalized adhesion energy was observed ($\Gamma / \Gamma_0 > 2$) in all tested conditions (Fig. 4.2D), indicative of a potent toughening effect of the TGS (*23*). Interestingly, we found a non-monotonic correlation between Γ / Γ_0 and r_g / r_s. After examining the shear stress distribution along the joint interface, we interpret the observation as follows (fig. S4.7, A to D). Given a thin sheath ($r_g / r_s \leq 2$), the suture-sheath interface debonds simultaneously and the volume of energy dissipating materials increases with the thickness of the suture sheath, leading to higher adhesion energy; when the sheath is even thicker, the energy dissipation is confined around the crack tip, and thus the total amount of dissipated energy is reduced as well as the adhesion energy.

4.5 Wide Applicability of TGS Design

The design and method for the TGS sutures are applicable to a variety of surgical sutures and hydrogels. Besides the synthetic degradable PLGA suture, we have successfully fabricated the TGS sutures using naturally derived degradable plain gut sutures and synthetic non-degradable nylon sutures (Fig. 4.2, E and F) with the same method. Furthermore, the suture sheath can be formed with various hydrogels as the *toughening network*, which can interpenetrate with the chitosan-based *anchoring network*. As an example, we formed a TGS composed of a chitosan-

PAAm hydrogel. The efficacy of our method is evidenced with high adhesion energy of the sheath-suture interfaces in all the tested conditions. This study leads to a family of TGS sutures of varying chemical compositions and properties and demonstrates the versatility of the proposed design and method.

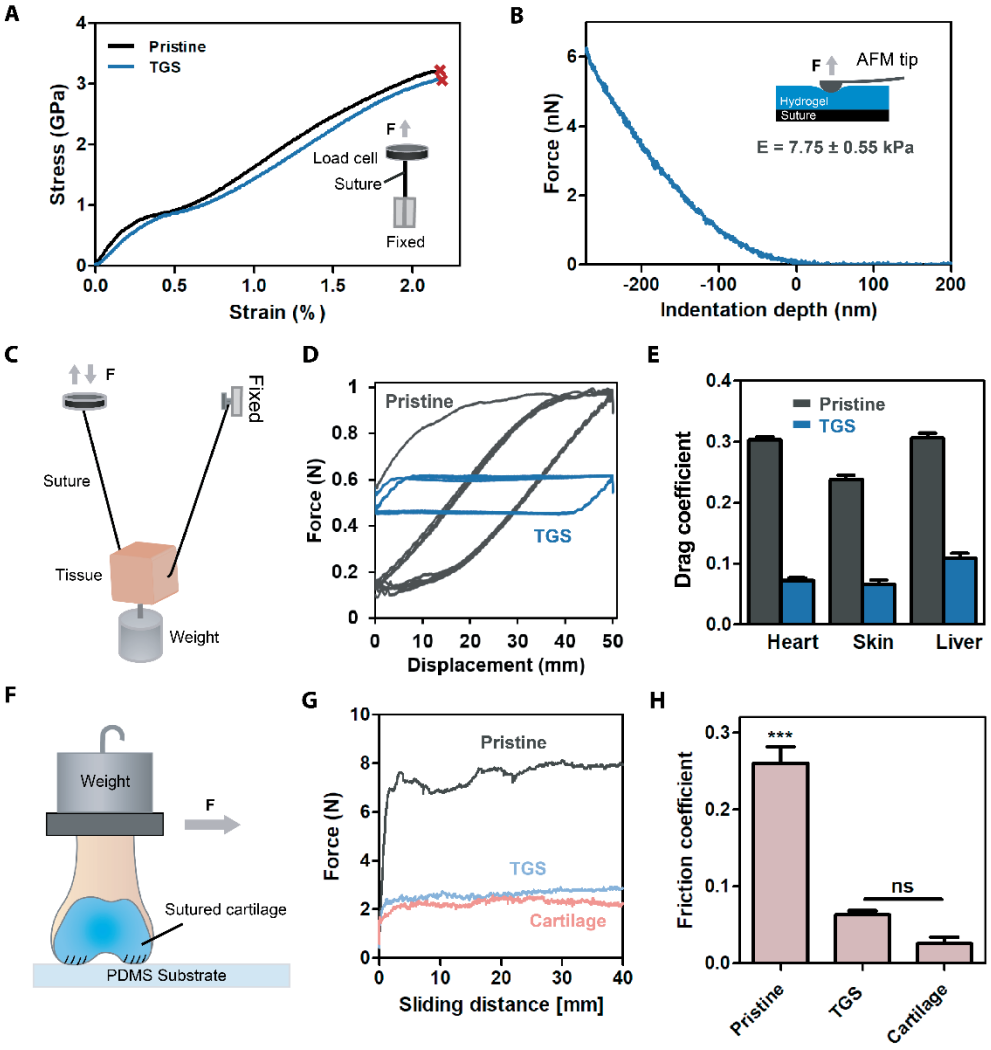

Figure 4.3. Improved biomechanical properties of the TGS suture. (**A**) Stress-strain curves of the pristine and TGS sutures (polyglactin 910). (**B**) Representative microindentation force-indentation depth curve measured on the TGS suture surface. (**C**) Schematic of the tissue drag test. (**D**) Representative drag force-displacement curves of the pristine and TGS sutures. (**E**) Drag coefficients of suture (pristine or TGS) interfacing with various tissues (heart, skin, liver). (**F**) Schematic of the ex vivo friction test of the suture placed on articular cartilage, where the PDMS

is used as substrate. Representative friction force-sliding distance curves (**G**) and the calculated friction coefficients (**H**) of intact cartilage, sutured cartilage with the pristine or TGS suture. Data reported as mean ± standard deviation for n = 3 independent experiments; *** $p < 0.001$, by two-tailed, one-way ANOVA with Holm-Sidak Post-hoc comparison.

4.6 Characterization of TGS Suture Biomechanical Properties

We next demonstrated that the intrinsic biomechanical properties of TGS sutures could help mitigate the limitations of clinically used suture materials. The core-sheath structure could provide low stiffness hydrogel surface to resolve the mechanical mismatch between the suture and local tissues, without sacrificing the tensile strength of the pristine sutures for wound closure. With carefully controlled suture hydrolysis via NaOH treatment, the obtained TGS suture retained high tensile strength (3 GPa), comparable to pristine sutures (Fig. 4.3A, fig. S8). However, prolonged surface treatment will lead to compromised suture strength, despite the enhanced interfacial adhesion (fig. S4.8, Fig. 3.2C). The surface elastic modulus of the TGS suture is around 7 kPa measured by atomic force microscopy (AFM) equipped with a cell-sized spherical probe (Fig. 4.3B), compared to ultra-high stiffness ~68 MPa of the pristine suture (fig. S4.9). The activation treatment is strictly limited to the very superficial layer of sutures, and yet provides sufficient functional groups for binding with the sheath. The mechanical mismatch between the suture and soft tissues is thus remedied by the soft hydrogel sheath, which may also mitigate the local stress concentration and enable a mechanical microenvironment favorable for tissue regeneration.

In addition to the low stiffness, TGS suture also provides a slippery surface when interfacing with the tissues, which could substantially reduce the tissue drag and friction that have been linked with microtrauma and tissue damage (*26*). When passing through the tissue, traditional sutures can drag and damage the tissue; after the placement, the rough surface of sutures, particularly braided ones, can cause constant friction and wear on the contacting tissue. This is particularly severe for tissues under constant friction and impact, such as articular cartilage, where surgical suturing has been associated with higher risk of osteoarthritis (*7*). To characterize the tissue drag, we performed a customized ex vivo drag test, mimicking the suturing process, to determine the drag coefficient of the TGS and pristine sutures on soft tissues such as skin, heart and liver (Fig. 4.3, C to E). The results show that the drag coefficients of the TGS suture are 2-3 times lower than that of pristine sutures (Fig. 4.3E). A characteristic stick-and-slip phenomenon was observed in the drag force-

displacement profile of the pristine suture, but not in the case of the TGS suture (Fig. 4.3D and fig. S4.10). We also developed a customized setup to characterize the friction induced by the sutures on porcine articular cartilage (Fig. 4.3F). Using PDMS as an artificial tissue substrate, we characterized the friction coefficient between PDMS and cartilage or sutured cartilage using the pristine or TGS suture. Our results show that friction coefficient for TGS sutures was comparable to articular cartilage, and significantly lower than the pristine suture (Fig. 4.3, G and H).

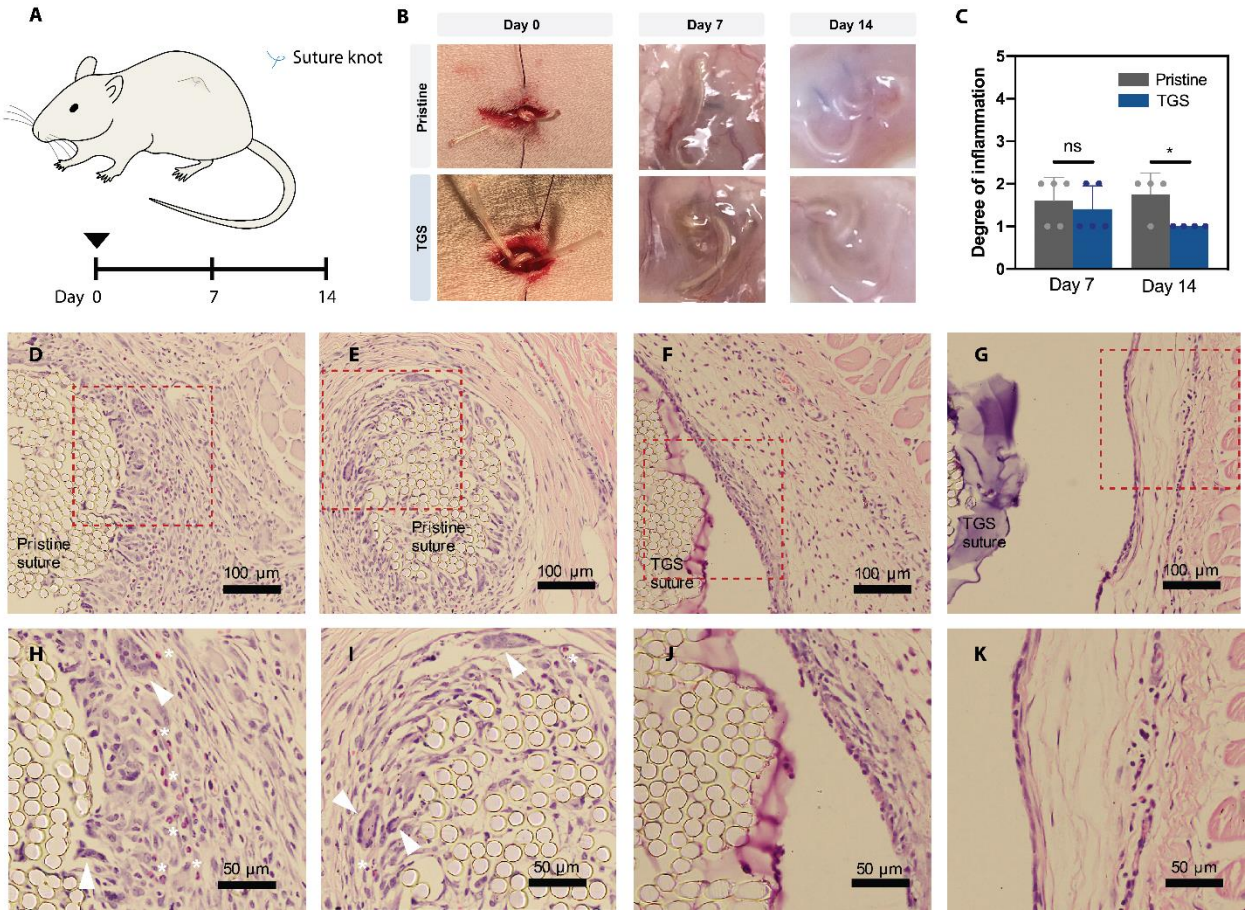

Figure 4.4. In vivo biocompatibility of pristine and TGS sutures. (A) A schematic illustration of the subcutaneous implantation of suture knots. The biocompatibility was assessed on day 7 and 14. (B) View of the suture knots implantation process and macroscopic inspection of the encapsulated suture knots on day 7 and 14. (C) Degree of inflammation of implanted pristine and TGS sutures evaluated blindly by a experienced pathologist (0, normal; 1, very mild;, 2, mild; 3, moderate; 4, severe; 5, very severe). Statistical significance and P values are determined by two-sided Student's *t*-test. "*" indicates $p<0.5$; "ns" indicates not significant. (D-K) Representative

histology images stained with haemotaxylin and eosin (H&E) of suture knot implanted for 7 days (pristine (D, H); TGS (F, J)) and 14 days (pristine (E, I); TGS (G, K)). (H-K) are histological images of higher magnification of regions interest (rectangle with dotted red lines) from (D-G). White arrows indicate foreign body giant cells; star symbols indicate proinflammatory eosinophils.

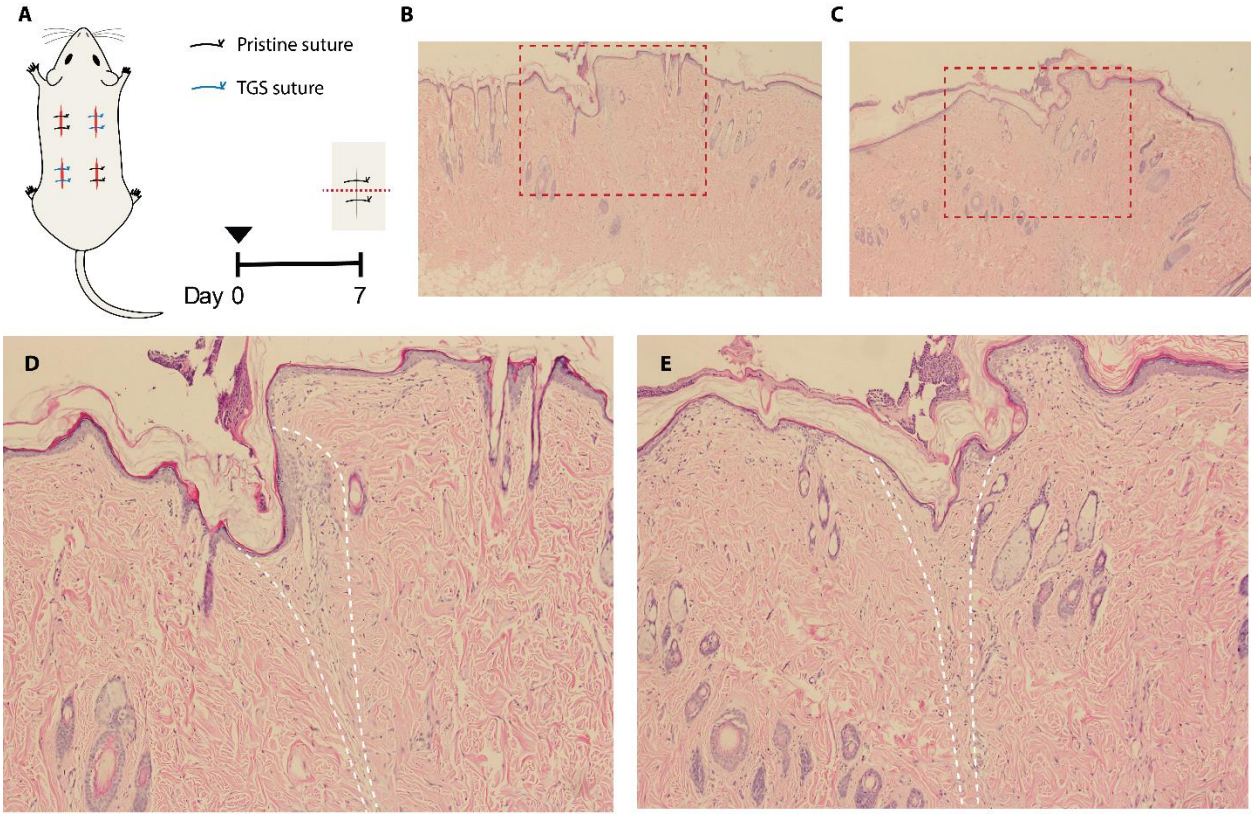

Figure 4.5. Wound healing using pristine and TGS sutures. (**A**) A schematic illustration of incision wounds closed with pristine and TGS sutures, and sections taken for histology (dotted red line) on day 7. (**B, C**) Representative histological images stained with H&E at lower maginification (40X) showing comparable wound healing outcome using pristine (B) and TGS (C) sutures, assessed blindly by an experienced pathologist (n=6). (**D**, **E**) Histological images of higher magnification (100X) of the regenerated epidermis/dermis layer (red rectangle in B and C respectively). Dashed white lines indicate wound edges.

4.7 In Vivo Biocompatibility and Wound Closure

The in vivo biocompatibility of pristine and TGS sutures were evaluated via subcutaneous implantation of the suture knots in rats for 7 and 14 days (Fig. 4.4A). No significant degradations were observed for both pristine and TGS sutures during the 2-week period (Fig. 4.4B). Histological assessment by an experienced pathologist indicate that both sutures elicit comparable mild inflammation response on day 7, while TGS sutures showed very mild to none inflammation on day 14, significantly lower than pristine sutures (Fig. 4.4C, fig. S4.11). This is evidenced with the elevated cell infiltration into the pristine suture inter-filament spacings overtime (Fig. 4.4, D and E), and the presence of foreign body giant cells and proinflammatory eosinophils within the proximity of pristine suture filaments (Fig. 4.4, H and I). For TGS sutures, no foreign body inflammatory reactions were observed on day 7 and 14. A thin capsule with minimal number of lymphocytes were identified surrounding the TGS suture knot, yet no giant cells, neutrophils, or macrophages were noticed. Exhaustive examination revealed no cell infiltration into the TGS sutures due to the nanoporosity of the hydrogel sheath, indicating a good suture-sheath integration.

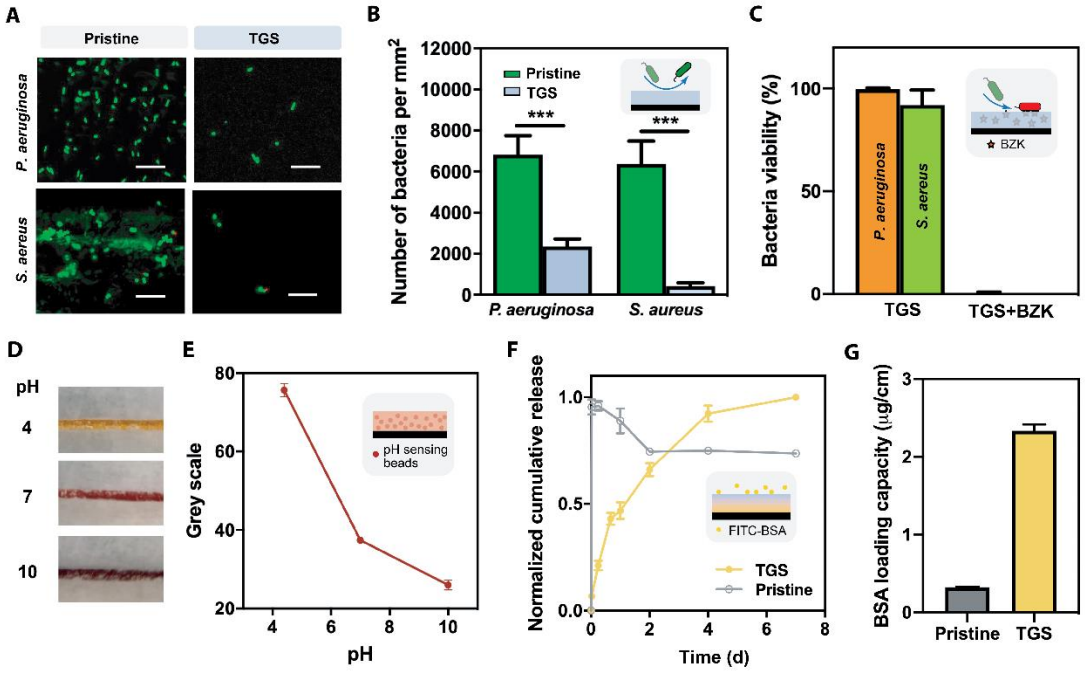

Figure 4.6. Versatile TGS suture functionalization. (**A**) Representative fluorescence images of live (green)/dead (red) assay of bacteria (*P. aeruginosa* and *S. aereus*) seeded onto the pristine or

TGS suture. Scale bar is 10 μm. (**B**) Total number of bacteria adhesion on pristine or TGS sutures. (**C**) Over 99% bacteria were killed on TGS sutures loaded with BZK. Representative images (**D**) and quantitative color change assay (reflected in grey scale) (**E**) of pH-sensing TGS suture immersed in solution with various pH levels. (**F**) 7-day normalized cumulative release profile of FITC-BSA from the pristine or TGS suture. (**G**) BSA loading capacity of pristine or TGS suture. Data reported as mean ± standard deviation for n = 3 independent experiments; * $p < 0.05$, *** $p < 0.001$, by two-tailed, one-way ANOVA with Holm-Sidak Post-hoc comparison.

To confirm the mechanical function of TGS sutures for wound closure, we further evaluated the wound healing of dorsal full-thickness incisions closed by pristine or TGS sutures (Fig 3.5A, fig. S4.12). The wounds were first assessed macroscopically on day 7, demonstrating good wound closure capability of both sutures, while no infection was observed (fig. S4.12). As expected, hydrogels on TGS sutures were dehydrated due to its exposure to the ambient environments. However, the hydrated hydrogel sheath was well-preserved beneath the wound bed (fig. S4.12), indicating reliable suture-gel integrity during the mechanically demanding suturing and knotting process and the one-week wound healing period. The potential dehydration of the hydrogel sheath for topical applications could be mitigated by applying a commercialized thin elastomer adhesive film (Tegaderm, 3M) above the wound bed if needed. Histological assessment by a blinded pathologist confirmed that all incisional wounds were healed by primary intention with minimum inflammation and fibrosis (Fig. 4.5B-E).

4.8 Versatile Functionalization of TGS Sutures

Besides the excellent biomechanical properties and biocompatibility inherent to the TGS, the functionality of the TGS suture will next be engineered through inclusion of various functional materials. It is feasible as the TGS can serve as a versatile platform, warranted by the robust modification, to readily encapsulate and deliver small payloads along with the suture to the strategic site adjacent to a wound. As a proof of principle, we will load the suture sheath with an antibacterial compound, pH-sensing microparticles, a model drug and fluorescent NPs, then demonstrate the effectiveness of the functionalization below.

The inter-filament spacing within braided sutures may attract bacteria through capillary forces and host bacteria growth. Owing to the cell-repellent nature of PAAm, the TGS suture exhibited excellent anti-fouling property with significantly lower bacteria adhesion, for both gram positive (*S. aereus*) and gram negative (*P. aeruginosa*) bacteria that are closely associated with surgical site infection (Fig. 4.6, A and B) (*27*). By further loading the TGS with an antibacterial compound (benzalkonium chloride, BZK) widely used in many consumer products, over 99% of the adhered bacteria were killed (Fig. 4.6C, fig. S4.13), thanks to the positively charged quaternary ammonium compound incorporated into the hydrogel matrix (*27*). This study demonstrates the antifouling and antimicrobial functions of the TGS suture and its potential for controlling surgical site infection.

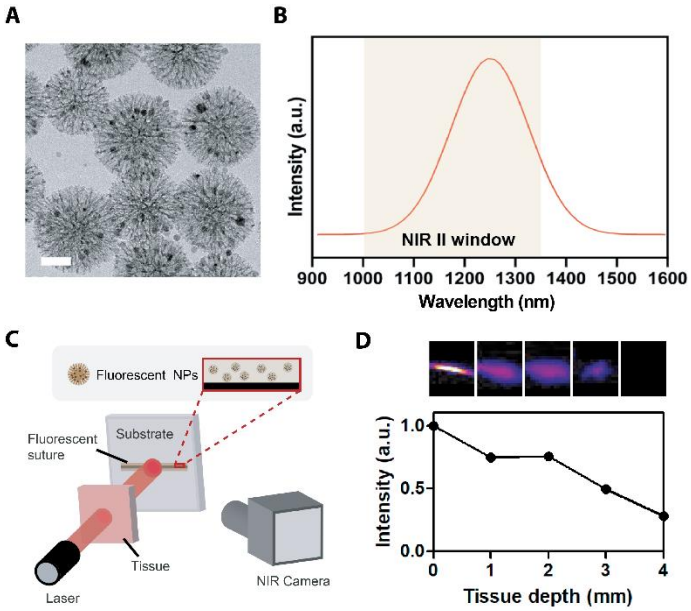

Figure 4.7. Fluorescent suture for NIR bioimaging. (**A**) Representative transmission electron microscopy (TEM) image of $mSiO_2$@PbS/CdS-Fe_3O_4 fluorescent NPs. Scale bar is 50 nm. (**B**) Fluorescent emission spectrum of $mSiO_2$@PbS/CdS-Fe_3O_4 in the NIR-II window. (**C**) Schematic of the ex vivo experimental set-up to characterize the photoluminescence penetration of fluorescent NPs-loaded TGS suture behind porcine tissue. (**D**) Representative fluorescence images (top) and normalized intensity (bottom) of the TGS sutures under tissues of varying thickness.

The suture sheath can be further functionalized to monitor the physiological signals during wound healing processes due to the strategic location of surgical sutures at the wound site. As a proof of concept, we loaded pH-sensing beads into the TGS as pH-monitoring sutures. The wound bed pH is a key indicator of the wound healing process; healthy skin is often acidic, and for wound bed exposed to body fluid, the pH is usually around 7, while the pH of chronic wounds or infected wounds could go up to 10 (*28*, *29*). Our results show that the pH-sensing sutures readily transduce the pH signal into color change, visible to naked eyes (Fig. 4.6, D and E). The monitoring could be continuous and essentially minimally invasive as the sutures naturally penetrate through the wounded tissue; the semi-permeable hydrogel sheath allows for mass exchange at the molecular level (yet not allow bacterial invasion). The new suture function would particularly benefit the monitoring of chronic wounds by non-professionals and in-time intervention when the pH level is abnormal. By integrating the antifouling and antibacterial functions, the new suture technology could be potentially used as point-of-care systems for the management of chronic wounds.

The TGS suture can also serve as a depot to deliver drugs to the wound site locally. The TGS can encapsulate the drug and regulate its release through the drug-matrix interactions. As a proof of concept, we loaded the TGS with FITC-bovine serum albumin (BSA) as a widely used model drug to form drug-eluting TGS sutures. We also dip-coated the pristine suture with the model drug as a control for comparison. A one-week cumulative release profile shows that TGS suture presents higher encapsulation efficiency and longer release period, comparing to the control suture using dip-coating strategy (Fig. 4.6, F and G). Together with the above-mentioned demonstrations, we show that the TGS platform enables the diagnostic, monitoring and therapeutic functions to address the clinical needs for wound management.

The intricate surgical procedures and delicate soft tissues call for the precise targeting and visualization of sutures during and after operation. NIR fluorescence imaging is an emerging biomedical imaging modality for use in both fundamental scientific research and clinical practice (*30*). By incorporating our recently developed NIR fluorescent NPs (*31*) (with fluorescence emission wavelength at 1250 nm in NIR-II: 1000-1350 nm, Fig. 4.7, A and B, fig. S4.14) into the TGS, we further expand the potential of our platform for deep-tissue bioimaging via a customized ex vivo set-up (Fig. 4.7C). The fluorescent NPs-loaded TGS suture exhibits bright linear fluorescence along suture with dark background captured by an NIR camera under excitation of 806 nm laser in NIR-I (700-950 nm) and the strong signal could still be observed when the suture

was covered by porcine tissue with up to 3 mm thickness (Fig. 4.7D). The intense NIR fluorescence and high contrast demonstrate the deep-tissue penetration capability of the fluorescent suture. To our knowledge, this first demonstration of fluorescent sutures with high optical transparency in the NIR biological window would facilitate minimally invasive surgeries to localize the suture during implementation and later removal, and benefit fluorescence image-guided surgery and post-surgery bioimaging/diagnostics (*32*).

4.9 Discussions and Conclusions

Sutures are among the simplest and most widely used devices in clinical medicine. Despite recent efforts to make bioactive sutures, clinically used sutures remain largely passive, mechanical devices. The obstacles toward translation, in addition to the regulatory issue, include the lack of robust modification approaches and the limited functionality so far being integrated into the sutures. To overcome these issues, we first designed and constructed the TGS on various commercially available sutures, and then engineered multifunctionality of the suture by exploiting salient attributes of hydrogel sheath such as softness, lubrication, antifouling and transparency.

By rationally designing the *anchoring* and *toughening* networks of the TGS, we achieved an extremely tough suture-sheath interface as manifested by the experimentally measured adhesion energy beyond 2000 J m^{-2}. Such an interface managed to sustain the high mechanical loading during suturing and knotting. To put this value under context, the adhesion energy based on surface absorption and single-network hydrogels in the previously reported systems is below 100 J m^{-2} (*21*). To our knowledge, it is among the toughest interface achieved with hydrogels and the first reported tough adhesion between hydrogel and fiber-based materials.

Distinctive properties of the surgical suture can emerge with the robustly integrated TGS, which were proven to mitigate mechanical mismatch and irritation of sutures when interfacing with soft tissues. This is manifested in our in vivo implantation studies of TGS sutures, suggesting minimal inflammation reactions, while pristine sutures elicit more severe foreign body response. Due to the soft hydrated nature of hydrogels, the TGS provided a soft and lubricant surface, which decreased the surface stiffness and drag/friction coefficients by a factor of 10^4 and 3, respectively, without altering the tensile strength of the suture. Moreover, the hydrated surface of TGS is inherently antifouling, evidenced by lowering the bacteria adhesion for both gram positive (*S. aereus*) and gram negative (*P. aeruginosa*) bacteria.

In addition, the TGS exhibited significant attributes such as optical transparency and permeability to support the proper function of optical functional materials. In this work, it was exemplified with the pH-sensing microparticles and the fluorescent nanoparticles for pH monitoring and NIR bioimaging, respectively. In both cases, the TGS retained the payloads effectively due to the small pore sizes. For pH-sensing, the TGS is optically transparent and fully permeable to ionic species presented in the wound bed. For NIR bioimaging, both the excitation laser and the emission light from the fluorescent nanoparticles can transmit through the hydrogel sheath without decay.

We further demonstrated the drug delivery capacity of the TGS to improve the therapeutic function of surgical sutures for advanced wound management. Our results showed that the TGS can encapsulate and release small-molecule antimicrobial compounds and protein model drugs to the wound site for infection prevention and tissue repair. The hydrogel sheath is expected to be compatible with other bioactive agents such as growth factors and cytokines owing to its hydrophilic nature. The drug loading capacity can be tuned by varying the drug concentration or the thickness of the hydrogel sheath, and the drug release kinetics can be modulated by engineering controlled release mechanisms of the hydrogel (*33*). These features make our strategy advantageous over the conventional dip-coating approach, which is limited by low loading capacity and burst release of drugs due to the lack of polymeric network to slow down the release (*11*). Smart drug delivery features could be further engineered within the TGS to enable triggered or stimuli-responsive drug release locally to the injured sites in a sustained manner to accelerate the wound healing process. By integrating bioactive reagents specific for certain application scenarios and individual patients, our method could potentially allow one to tailor surgical sutures for personalized therapies (*34*); while the tunable biophysical and biochemical niche could be further leveraged for cell encapsulation and delivery for advanced cell therapy (*35*).

TGS sutures are expected to be particularly beneficial for rejoining and reattaching mechanically active musculoskeletal tissues such as tendon. Compared with native tendon tissues, TGS sutures demonstrated much higher tensile strength, yet lowered stretchability. Thus, biomimetic approach could be further developed to optimize TGS sutures with similar mechanical properties and non-linear stress strain behaviors with native tendon tissues, providing adequate mechanical support for tendon rejoining, mitigating stress concentrations caused by traditional sutures, and applying appropriate biophysical cues to potentially accelerate tendon regeneration.

The current low-throughput production of TGS sutures limits their bench-to-bedside translational potentials. This could be resolved by adopting the industrialized dip-coating approaches, as indicated in our proof-of-concept demonstrations (fig. S4.15), although the rheological properties and polymerization conditions of the precursor solutions require further optimization.

A variety of hydrogels and suture materials are amenable to the design of TGS for robust surface functionalization. In particular, both mono- and multifilament sutures of varying diameters were successfully engineered to bond with the TGS. This strategy is auspicious for other fiber-based devices, including fibers, yarns, 3D-printing scaffolds, guidewires and continuum robots (*36*, *37*). As a demonstration, a 3d-printed polylactic acid fiber was integrated with tough gel using the strategy developed in this work as a fiber-reinforced tough aortic patch (fig. S4.16). By leveraging our surface functionalization strategy, a bottom-up approach could be adopted to design more complex functional hybrid structures for 2d smart textiles and 3d scaffolds for materials and biomedical engineering. Biodegradation properties could be introduced by designing TGS containing (triggerable) degradable crosslinkers (e.g. di-sulfide bond, matrix metalloproteinase (MMP), etc.). The broad applicability of the strategy reported here should ultimately provide a versatile basis to design and functionalize fiber-based devices that leverage new hydrogels and functional materials to evolve towards a desired form and function for different applications.

4.10 Conclusions

In summary, we reported a bioinspired design and method to robustly integrate clinically used surgical sutures, tough hydrogels and various functional materials. Strong adhesion was realized at the suture-sheath interface and substantiated with extensive experimental characterization and computational simulation. A family of TGS sutures were developed, which achieved superior biomechanical performance and multiple functionality. The TGS sutures exhibited tissue-like stiffness, low drag and friction on the contacting tissue without compromising the tensile strength. The suture sheath provided a versatile platform to merge the suture with functional materials for the diagnostic, monitoring and therapeutic functions. Applications of anti-infection, wound bed pH sensing, drug delivery and NIR bioimaging were demonstrated within a single platform for advanced wound management. The facile generation of TGS suggested an extensive design flexibility for other fiber-based devices such as textiles and fabrics. This platform is an important step toward integration of hydrogel technologies, functional materials and fiber-based devices to

develop next-generation multifunctional materials. This work would open new avenues for the development of surgical tools, wearable and implantable devices, soft robotics, fiber and textile materials.

4.11 Materials and Methods

Fabrication of TGS sutures. The essential fabrication procedure is illustrated with polyglactin 910 sutures (VICRL, 2-0, Ethicon). First, the suture was surface-treated with 1 M NaOH solution for 2 minutes, and then rinsed with deionized water before air drying. The surface-activated suture was then inserted into a glass capillary tube (World Precision Instrument, TW120-6) as a micro-reactor, which defines the thickness of tough sheath and provides a closed environment for polymerization. Chitosan of high deacetylation degree (> 95%, Lyphar Biotech) was dissolved at 2% concentration in 0.2 M acetic acid solution. EDC and NHS (Sigma) were vortexed mixed with the chitosan solution both at a final concentration of 40 mg/ml. The mixture was then injected into the capillary tube through a 25G needle (Sigma) to prime the suture surface for 10 minutes. The pre-polymer solutions for alginate-PAAm hydrogels, containing 2% sodium alginate (high molecular weight, I1G, KIMICA Corporation), 16% acrylamide (Sigma), 0.01% N,N'-methylenebis(acrylamide) (MBAA, Sigma), 0.03% ammonium persulfate (APS, Sigma), and 0.46% tetramethyl-ethylenediamine (TEMED, Sigma), and inclusions (if any; e.g., drugs and microparticles) was syringe-mixed and then injected into the capillary tube and replaced the chitosan solution. Two customized plugs with centered through-holes were 3D-printed with an Autodesk Ember desktop 3D printer and capped at two ends of the tube to enable the coaxial structure of the hybrid suture. After an overnight reaction, the sheathed suture was retrieved from the tube, and later immersed in 0.1 M $CaCl_2$ solution for 5 minutes to further crosslink the alginate before usage.

Scanning electron microscopy. The pristine or TGS sutures were frozen at -80 °C and subsequently lyophilized for 24 hours with a freeze dryer (Labconco Freezone). The freeze-dried sutures were coated with 4 nm platinum using a high-resolution sputter coater (ACE600, Leica) to increase the surface conductivity. A scanning electron microscope (FEI Quanta 450 environmental) was used to image the specimens at 5 kV and 10 mA under various magnifications.

Mechanical characterization. The pristine or TGS sutures were pulled uniaxially using an Instron machine (Model 5965; load cell: 1 kN) at 0.5 mm/s displacement rate, while the force and

displacement were recorded. The tensile strength was determined from the peak stress at failure. The sample length was 20 mm for all the tests.

Atomic force microscope. An atomic force microscope (JPK NanoWizard 3, Berlin, Germany) was used to conduct micro-indentation tests to measure the microscale Young's modulus of suture surface. Rectangular silicon cantilevers with 25 μm-in-diameter spherical beads attached as probes were used (Novascan, IA, USA). Cantilevers with a nominal spring constant of 0.6 N/m were used for testing the sheathed sutures and of 2 N/m for the pristine sutures. The spring constants of the cantilevers were determined with a thermal noise method before the experiments. Indentations were conducted at 20 different locations for each sample. The Hertzian contact model was used to calculate the Young's moduli (*38*).

Specimen fabrication for adhesion testing. Sutures with relatively thicker sheath were fabricated for characterizing the adhesion energy between the suture and the tough hydrogel sheath. Briefly, for alg-PAAm sheathed polyglactin 910 suture (VICRL, 2, Ethicon), sutures were treated with 1 M NaOH solution with various durations (2, 5, 10 minutes) or without any treatment. It was then primed with 2% chitosan solution containing 40 mg/ml EDC/NHS for 10 minutes and then placed inside a customized acrylic mold of designed dimensions (W: 30 mm; L: 50 mm; H: 3 mm), with one end sticking out of the mold. Prepolymer solution was then applied into the mold, sealed with another layer of acrylic sheet and the hybrid was allowed for full gelation overnight. The prepolymers for different hydrogel cuboids are: 2% sodium alginate, 16% acrylamide, 0.01% MBAA, 0.03% APS, 0.46% TEMED and 20 mM $CaSO_4$ for alginate-PAAm hydrogels; 2% alginate solution containing 40 mM $CaSO_4$ for alginate hydrogels; 16% acrylamide, 0.01% MBAA, 0.03% APS, and 0.46% TEMED for PAAm hydrogels; a solution containing 2.5% chitosan, 35.5% acrylamide was mixed with 21.6 μL of 2% MBAA, 135.6 μL of 0.27M APS, and 4.02 mL of chitosan gelling agent (consisted of 0.1 M Na_2HPO_4, 0.1 M NaH_2PO_4, and 0.306 M $NaHCO_3$) for PAAm-chitosan hydrogel. The other sheathed sutures were based on alginate-PAAm hydrogels, while Nylon suture (3-0, Ethilon, Ethicon) was treated with 1 M HCl for 1 hour and plain gut (6-0, Ethicon) was used as received, before surface priming and in-situ gelation as previously described.

Adhesion energy characterization. The adhesion energy between the suture and the hydrogel sheath was characterized using a customized pull-out test with an Instron machine. Two acrylic

sheets were glued onto two opposing sides of a hydrogel cuboid as rigid constraints. To apply a full constraint on the hydrogel sheaths, the backing of the suture-gel hybrid is fixed on to the bottom grip of the Instron machine, while the exposed suture end was fixed on to the upper grip. The suture was pulled out unidirectionally at a displacement rate of 0.5 mm/s, while the force F and the displacement δ were recorded. The critical energy release rate, i.e. adhesion energy, was calculated with the Equation (1).

Finite element modeling. The simulation was carried out with ABAQUS (Version 2017, Dassault Systems). The axisymmetric assumption was made to reduce the problem to two-dimensional to save the computation time (fig. S4.6, A to C). The top end of the suture is subjected to a constant loading rate $\dot{\delta} = 0.01$ mm/s, while the right edge of the hydrogel sheath is fixed in all degrees of freedoms (fig. S4.6C). The computational study provides a qualitative trend insensitive to the exact geometric parameters of the hydrogel sheath and the boundary conditions.

The hydrogel sheath was modelled as an incompressible Ogden hyperelastic material with Mullins effect to account for the mechanical dissipation. The strain energy density for the Ogden model is given by:

$$U = \frac{2\mu}{\alpha^2}(\lambda_1^\alpha + \lambda_2^\alpha + \lambda_3^\alpha - 3)$$

where U is the strain energy density, μ the shear modulus, α the fitting coefficient, λ_i the ith principle stretch ($i = 1,2,3$). The nominal stress S for a pure-shear test is then given by

$$S = \frac{2\mu}{\alpha}(\lambda^{\alpha-1} - \lambda^{-(\alpha+1)}) \tag{2}$$

The Ogden model coefficients were obtained by fitting Equation (2) to the loading paths in the pure-shear test results of the alg-PAAm hydrogel (fig. S4.6, F to H). The shear modulus μ and α were fitted to be 34.9 kPa and 1.60, respectively. The model for the Mullin's effect is given by:

$$\begin{aligned} W &= \eta\widehat{W} + \phi(\eta) \\ \phi(\eta) &= \int_1^\eta \left[(m + \beta W^m)\mathrm{erf}^{-1}(r(1-\eta)) - W^m \right] d\eta \\ h &= \frac{1}{r}\left[\mathrm{erf}\left(\frac{U}{m+\beta U} \right) - \frac{m+\beta U}{\sqrt{\pi}U}\left[1 - \exp\left[-\left(\frac{U}{m+\beta U} \right)^2 \right] \right] \right] \end{aligned} \tag{3}$$

where η is the damage variable (η = 0 and 1 represents the material in its virgin and the completely damaged state, respectively); $\widehat{W}$ the strain energy density without energy dissipation, W^m the maximum strain energy density before unloading, $\phi(\eta)$ the damage function, erf the error function. $r = 1.33, m = 27.35, \beta = 0.2818$ are fitting coefficients and were obtained by fitting Equation (3) to the hysteresis ratios h against the external work *U*, where *h* is interpreted as the ratio of the loop area to the area under the loading paths (fig. S4.6F). The suture was modelled as linear elastic with the elastic modulus of 300 GPa, measured from the slope of the stress-strain curve of the pristine suture in (Fig. 4.3A), and the Poisson's ratio of 0.3. The interface was characterized as a layer of cohesive elements, modelled with a triangular traction-separation law (fig. S4.6G). $\delta_{\max}$ and $S_{\max}$ are the prescribed maximum displacement and strength, respectively, and the area under the curve is the intrinsic work of adhesion Γ_0. The damage initiation is governed by the quadratic nominal stress criterion:

$$\left(\frac{t_n}{S_{\max}}\right)^2 + \left(\frac{t_s}{S_{\max}}\right)^2 = 1 \tag{4}$$

where t_n and t_s are the stresses in the directions normal and tangential to the joint interface, respectively. Mesh convergence tests were carried out to determine the appropriate number of elements applied in each model. In the loading regime for the case with $r_g / r_s = 1$, the results obtained with different mesh sizes were indistinguishable; in the debonding regime, the results with the smallest mesh size 0.075 mm and 0.05 mm showed a good agreement, indicating that the results were insensitive to the mesh size adopted in the current simulation (0.05 mm) (fig. S4.6H).

Derivation of energy release rate G. The schematic of the suture with hydrogel sheath simulated in FEM was shown in fig. S4.6. The radii of two-dimensional axisymmetric cross-section in the $r-z$ plane of suture and the gel are r_s and r_g, respectively, and $r_{tot} = r_g + r_s$. The two parts are adhered together with a joint length *L*.

Upon the pulling of the suture while the outer surface of the suture is fixed, the interface of the joint sustains the shear force,

$$\tau = \frac{F}{\left(2\pi r_s L\right)} \tag{5}$$

presumably the shear stress is uniform over the joined region, and the joint parts are under simple shear with shear strain γ_g and γ_s. The integration of the shear stress over the shear strain defines the strain energy density stored in the materials,

$$U = \int \tau(\gamma) d\gamma \tag{6}$$

In a quasi-static loading process, the work done by the pulling force on the suture and the hydrogel at a given δ is completely converted to the elastic energy stored in the materials. Thus, the strain energy densities in the gel and the suture also have the form:

$$\begin{aligned} U_g &= \frac{\int F(\delta_g) d\delta_g}{\pi\left(r_{tot}{}^2 - r_s{}^2\right) L} \\ U_s &= \frac{\int F(\delta_s) d\delta_s}{\pi\left(r_s{}^2\right) L} \end{aligned} \tag{7}$$

where δ_g and δ_s are the distance that the two-dimensional gel and suture sections are deformed due to simple shear along the pulling direction, and $\delta = \delta_g + \delta_s$. The shear strain in the two-dimensional hydrogel sheath γ_g and the suture γ_s can be obtained using the relation $U = U_g + U_s$,

$$\gamma_s = \frac{\delta_s}{\frac{1}{2} r_s}, \gamma_g = \frac{\delta_g}{\frac{r_g{}^2}{2r_s} + r_g} \tag{8}$$

The total potential of the system, consisting of the elastic energy stored in the materials and the potential energy by the pulling force, is given by

$$\Pi = U_s L\pi r_s^2 + U_g L\pi\left(r_{tot}^2 - r_s^2\right) - F(\delta_s + \delta_g) \tag{9}$$

During a quasi-static crack growth dc, the joint length reduces by the same amount. Thus, the energy release rate is determined by $-\partial\Pi / \left(2\pi r_s dc\right)$, or equivalently by

$$\frac{\partial \Pi}{2\pi r_s dL} \tag{10}$$

Combining Equations (8), (9) and (10) leads to

$$\begin{aligned}\Gamma = &\left[\frac{\partial U_s}{\partial \tau}\frac{\partial \tau}{\partial L}L\pi r_s^2 + \frac{\partial U_g}{\partial \tau}\frac{\partial \tau}{\partial L}L\pi(r_{tot}^2 - r_s^2)\right]\frac{1}{2\pi t_s} + \left[U_s\pi r_s^2 + U_g\pi(r_{tot}^2 - r_s^2)\right]\frac{1}{2\pi t_s} \\ &-\left[F\frac{\partial \gamma_s}{\partial \tau}\frac{\partial \tau}{\partial L}\frac{r_s}{2} - F\frac{\partial \gamma_g}{\partial \tau}\frac{\partial \tau}{\partial L}\left(\frac{r_g^{\,2}}{2r_s} + r_g\right)\right]\frac{1}{2\pi t_s} \\ &= \frac{1}{2\pi r_s}\left[U_s\pi r_s^2 + U_g\pi(r_{tot}^2 - r_s^2)\right]\end{aligned} \tag{11}$$

Because the elastic modulus of the suture is ~100000 times higher than that of the hydrogel sheath while their radii are of the same order of magnitude, the latter bears most of the strain energy. Thus, it is safe to remove the term with U_s and the expression can be further reduced to the Equation (1).

Shear stress distribution analysis from FEM. The non-monotonic correlation between Γ/Γ_0 and r_g/r_s was shown in Fig. 4.2B, i.e., it increases in the range of $2 < r_g/r_s < 4$ and decreases in the range of $r_g/r_s \le 2$. To understand the phenomenon, the magnitude of the normalized shear stress $\left|S_{shear}/S_{\max}\right|$ along the joint interface as a function of the applied displacement δ and distance z (fig. S4.6, A to C) was examined. The results for $r_g/r_s = 1$ and 4 are shown in fig. 4.6S (D and E) respectively. In both cases, $\left|S_{shear}/S_{\max}\right|$ is uniform along the interface and increases monotonically at small δ values. As δ increases to larger values, $\left|S_{shear}/S_{\max}\right|$ for $r_g/r_s = 1$ increases to 1h and then rapidly decreases to 0, indicating the joint interface debonds simultaneously after reaching the prescribed maximum strength. On the other hand, when $r_g/r_s = 4$, $\left|S_{shear}/S_{\max}\right|$ in a small region near the top reaches the prescribed strength first and then rapidly decreases to 0, hindering the uncracked region from reaching the maximum strength. Consequently, the energy dissipation is confined in the small region, leading to smaller Γ/Γ_0 with higher r_g/r_s.

Drag coefficient characterization. A customized drag coefficient characterization method, recapitulating the dragging experienced at tissue-suture interface during suturing process, was developed. We termed it drag coefficient to differentiate it from the standard friction coefficient characterization. The tissues (porcine heart, liver or heart) were cut into similar size and kept in PBS prior to testing. A 100 g of weight was attached to the tissue. Suture was then pass through the tissue. One end of the suture was affixed to a lab stand, while the other end clamped to the load cell. The position of the stand remained constant for all the samples tested. The Instron was set to cycle five times over a 50 mm distance at a speed of 3 mm/s. To interpret the data, the drag coefficient μ_d was calculated using the following formula:

$$\mu_d = (F_A - F_D)/(F_A + F_D) \tag{12}$$

where F_A denotes the average maximum (ascending crosshead) force, and F_D denotes the average minimum (descending crosshead) force.

Sutured cartilage-PDMS friction coefficient characterization. A custom-built scaffold made of aluminum t-slots was assembled for the friction coefficient testing. Porcine cartilage was purchased from local butcher shop. A PDMS sheet was fixed to an aluminum plate, which could slide freely along a trail fixed onto the bottom surface. One end of the plate was connected to an inextensible string attached to the load cell through a pully system. Two fixtures connected with an aluminum beam were inserted into the trail of the two standing frames of the scaffold, which could slide freely vertically. The top side of the cartilage was glued onto the beam, while the intact bottom side contacted with the PDMS sheet. During the test, the fixtures/beam and applied weight together induced a compressive stress to make sure the intimate contact between the cartilage and the PDMS sheet, so that the friction coefficient could be measured. The PDMS sheet was then subjected to a displacement with a constant loading rate (0.5 mm/s) and the force was recorded by the load cell. The friction coefficient μ_f was determined using the following Equation:

$$\mu_f = F_p / F_c \tag{13}$$

where F_p denotes the averaged plateau force, and F_c denotes the compressive force applied. The sutured cartilage was prepared by applying continuous stitches using pristine polyglactin 910

suture or alg-PAAm hydrogel sheathed polyglactin 910 suture onto the bottom surface of the cartilage.

In vivo biocompatibility and wound healing. All animal surgeries were reviewed and approved by the Facility Animal Care Committees (FACCs) at McGill University and the Research Institute of McGill University Health Centre. Female Sprague Dawley rats (200-300 g, Charles River Laboratories) were used for all in vivo studies. All hydrogel precursor solutions prepared for TGS suture fabrication were sterilized with 0.2-μm filters. Pristine sutures (2-0 and 5-0, Vicryl, Ethicon) were used as received. For in vivo biocompatibility assays, a small incision (typically 1 cm) was made through the dorsal subcutaneous tissue of rats and a scissors was used to create a small pocket. TGS or pristine suture (1.5-cm long) was made into a knot and implanted into the subcutaneous pocket (n=6). The incisions were then closed with the 5-0 Vicryl suture. At 7 and 14 days, animals were sacrificed, and the implanted sutures and surrounding tissues were excised and fixed in 4 % formalin for 24 hours for histological analyses. To examine the effect of TGS and pristine sutures on wound closure and healing, four 1.5-cm long full-thickness skin incision without tissue loss were created with a scalpel on the lateral dorsum of each rat. The wounds were closed using either TGS or pristine sutures (n=6) with an interrupted pattern. Rats were sacrificed after 7 days. Tissues with regions of interest were excised and fixed in 4 % formalin for 24 h for histological analyses.

Histological processing. Fixed tissue samples were placed into 70 % ethanol and submitted for histological processing and hematoxylin and eosin (H&E) staining at the Centre for Bone and Periodontal Research at McGill University. Z.G. is the Pathologist-in-Chief at McGill University Health Centre and examined all histological sections.

Antibacterial study. The bacterial strains used were the Gram-positive bacteria Staphylococcus aureus (ATCC 25923) and Gram-negative Pseudomonas aeruginosa (PAO1). Bacterial cultures were refreshed on nutrient agar from -80 ºC stocks. To grow bacterial suspensions, single colonies were transferred to Luria-Bertani (LB) broth and incubated overnight at 37 ºC and 220 rpm. Bacterial cells were harvested at logarithmic growth phase and centrifuged at 4000g for 10 min (Heraeus Multifuge X3R, Thermo Fisher Scientific, USA). The cells were resuspended in PBS and the optical density (OD) of the suspension at 600 nm was adjusted to 0.3 using a UV-visible spectrophotometer (Biomate 3S, Thermo Scientific, USA). Polyglactin 910 suture was used without any modification as pristine suture; alg-PAAm sheathed polyglactin 910 suture was used

as the TGS suture; TGS suture with loaded BZK was prepared by immersing TGS suture in 10% BZK solution overnight and subsequently washed 3 times in PBS solution before testing. Each suture sample was immersed in 1 mL bacterial suspension and incubated for 1 hour. The suture was then removed and rinsed with PBS to remove loosely attached cells. Before imaging each sample, bacteria were stained using Live/Dead BacLight Viability Kit (Molecular Probes, Inc, USA) utilizing a mixture of SYTO9 and propidium iodide. SYTO9 can cross the membrane of all bacteria in a population staining them green whereas propidium iodide only permeates the cells with compromised membranes (referred to as dead) staining them red. The samples were imaged using a confocal laser scanning microscope (LSM710, Zeiss, Germany). Multiple images were taken from each sample and the experiments were repeated three times. Viability was calculated as the percentage of live bacteria over total number of bacteria in each image.

pH monitoring. he pH sensing beads were prepared by doping mesoporous resin beads with a pH-responsive dye. Briefly, Brilliant Yellow dye (TCI, Tokyo, Japan) was dissolved in an ethanol solution (20%) at 4.5 mg/mL. Dowex 1 × 4 chloride form (Sigma) was thoroughly washed with DI water and ethanol, then added to the dye solution. The supernatant was washed several times until a clear solution was obtained. The pH sensing beads were collected and mixed with alg-PAAm prepolymer solution containing Iragure 2959 (Sigma) as photoinitiator, since APS could be absorbed by the resin. Both bulk hydrogel and suture-hydrogel hybrid were prepared under UV light (365 nm) for 1 hour. The hydrogel was immersed in solution of different pH for 5 minutes. Photo was taken, converted to 8-bit images and the grey scale of each sample was analyzed using ImageJ.

Drug release study. FITC-albumin (A9771, Sigma) was dissolved in DI water at 30 mg/ml. Pristine suture was first treated with 1M NaOH solution for 2 minutes, rinsed with DI water and air dried to increase the hydrophilicity of the suture surface. The surface activated suture was then immersed in FITC-albumin solution overnight. Suture-gel hybrid was fabricated using prepolymer solution made with FITC-albumin solution and left overnight before retrieved from the device. Both pristine sutures and suture-gel hybrids were cut into 1 cm long threads and subsequently transferred to a 12 well plate with 0.5 mL DI water in each plate and incubate in dark at 37 ºC. At each time point, a 50 µl aliquot of the solution was collected and the fluorescence intensity was measured using a plate reader. A standard curve was obtained by measuring the intensity of

different solution with different FITC-albumin concentration and used as a reference to calculate the cumulative release profile for each sample.

Synthesis and characterization of fluorescent NPs-loaded TGS sutures. The fluorescence NPs, $mSiO_2$@PbS/CdS-Fe_3O_4, were synthesized using a modified protocol reported previously (*31*). The morphology of as-prepared NPs was investigated by transmission electron microscopy (TEM, JEOL 2100F) at 200 kV equipped with a charge-coupled device (CCD) camera. Energy Dispersive X-ray Spectroscopy (EDX) was taken on specific areas during TEM measurements. Fluorescent emission spectra were acquired on a Fluorolog®-3 system (Horiba Jobin Yvon) using an excitation wavelength of 600 nm. Fluorescent NPs-loaded TGS suture was obtained by mixing the fluorescent NPs into alg-PAAm prepolymer solution prior to in-situ gelation.

NIR bioimaging. To demonstrate deep-tissue penetration property of fluorescent NPs-loaded TGS suture, a homemade setup was designed to take NIR images ex vivo, as shown in Fig. 4d. Briefly, fluorescent NPs-loaded TGS suture with length of 3 cm was fixed on a holder which covered with pieces of porcine tissue of different thickness (or without). An 806 nm laser with power density of 10 W/cm^2 was used to excite the NIR suture through the porcine tissue. Meanwhile, NIR images were recorded by a Xeva-1.7 infrared camera (Xenics Corp, Belgium) equipped with an 830 nm long-pass optical filter to block the light below 830 nm and the scattered excitation light of the 806 nm laser.

In vitro biocompatibility assay. To assess the cell compatibility of the TGS sutures, human vocal fold fibroblasts were cultured in 24 well plates at 10^6 ml^{-1} cell density in conditioned medium containing Dulbecco's Modified Eagle Medium (DMEM) (Life Technologies, ON) and supplemented with 10% fetal bovine serum, 1% penicillin/streptomycin, and 1% MEM non-essential amino acids, along with 1 cm long TGS suture or no suture as control. Cell viability was assessed using a Live/Dead viability kit (Invitrogen, L3224) after 48-hour culture, and was imaged using a confocal laser scanning microscope (LSM710, Zeiss, Germany). Live cells were shown in green fluorescence and dead cells were shown in red.

Statistical analysis. Comparative data analysis has been performed on friction coefficient characterization ((sutured) cartilage-PDMS), bacteria adhesion on pristine or TGS suture with or without BZK inclusion using a two-tailed, one-way ANOVA with a Holm-Sidak posthoc pairwise

comparison test. All statistical analyses were conducted in SigmaStat 3.5 (Systat Software Inc., San Jose, CA, USA).

4.12 Supporting Information

A

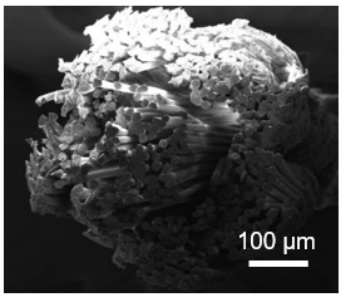

B

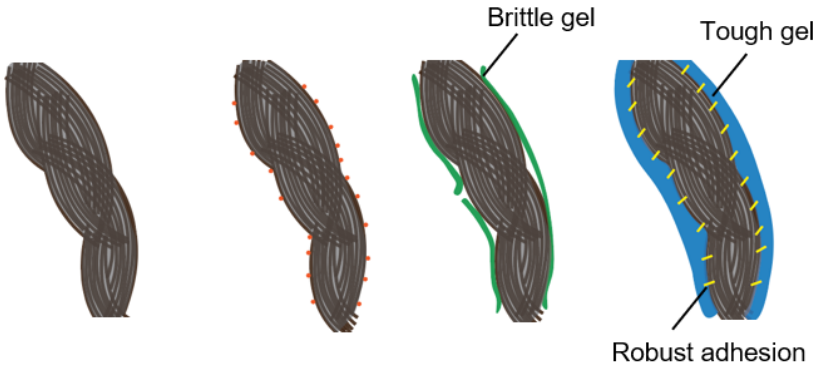

C

	Pristine	Compound deposition	Brittle gel coating	Tough gel sheath
Coating reliability	-	✗	✗	✓
High loading capacity	✗	✗	✗	✓
Robust interface	✗	✗	✗	✓
Tissue-like surface stiffness	✗	✗	✓	✓
Tissue drag prevention	✗	✗	✗	✓
Multifunction	✗	✗	✗	✓

D

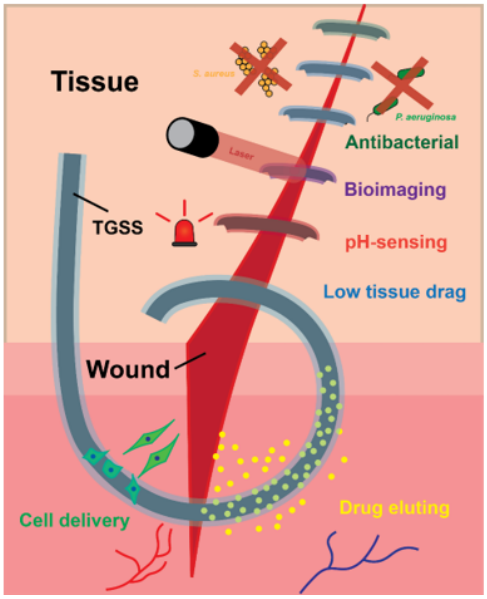

Figure S4.1. Comparison of surface engineering strategies for surgical sutures. (A) SEM image and schematic of the pristine braided suture polyglactin 910. Schematics (B) and comparison (C) of different suture functionalization strategies. (D) Proposed multifunctions of TGS suture.

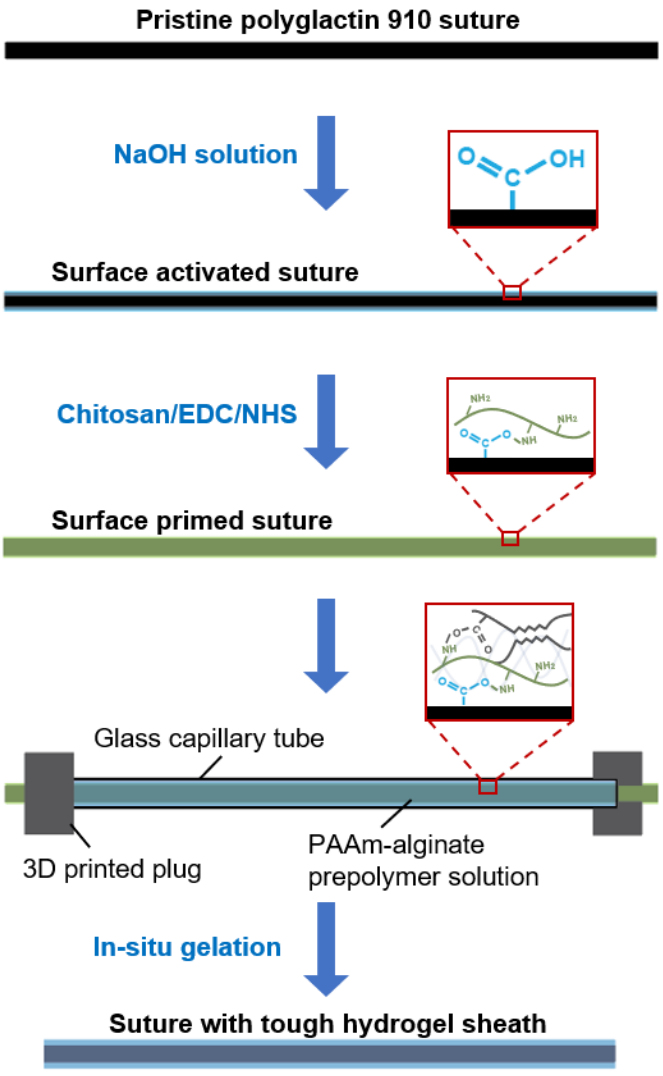

Figure S4.2. Workflow of the fabrication of alg-PAAm hydrogel sheathed polyglactin 910 suture.

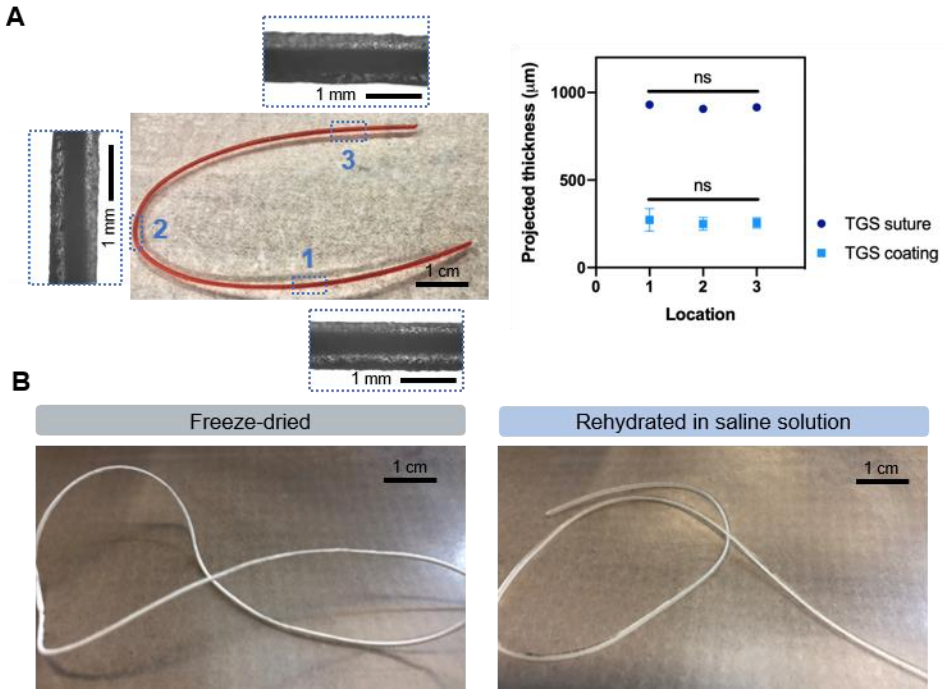

Figure S4.3. Manufacturing and storage considerations of TGS sutures. (A) Reproducible manufacturing of TGS suture with consistent thickness. "ns" indicates not significantly different. (B) Long term storage of TGS sutures as freeze-dried form (left), which can be rehydrated in saline solution (B) before usage.

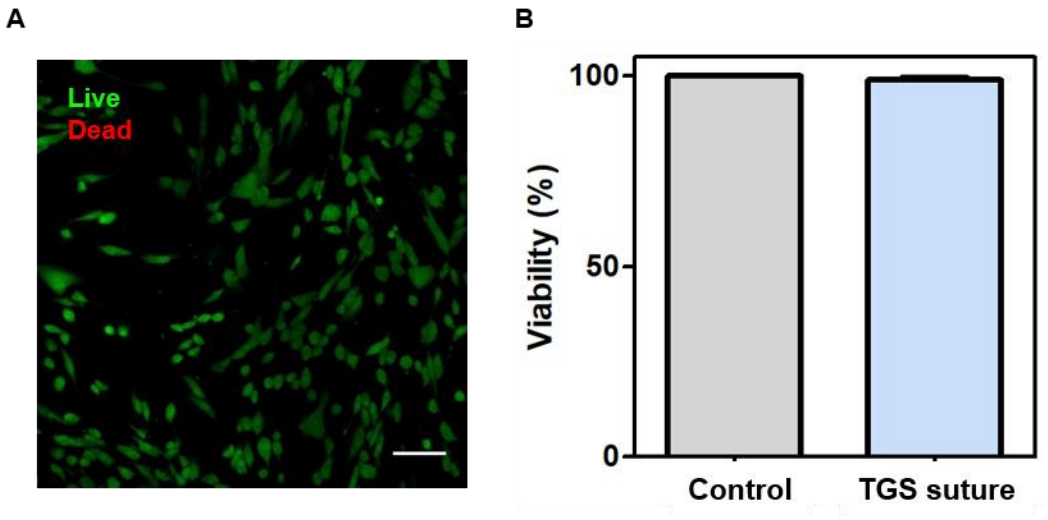

Figure S4.4. In vitro cell compatibility of TGS suture. (A) Representative fluorescent image of live/dead assay on human vocal fold fibroblasts after 24-hour culture in medium that were conditioned with TGS suture. Scale bar is 200 μm. (B) Cell viability was compared between the conditions by quantifying the percentage of live cells cultured in TGS suture conditioned medium or DMEM as control. Error bars show standard deviation; n=3.

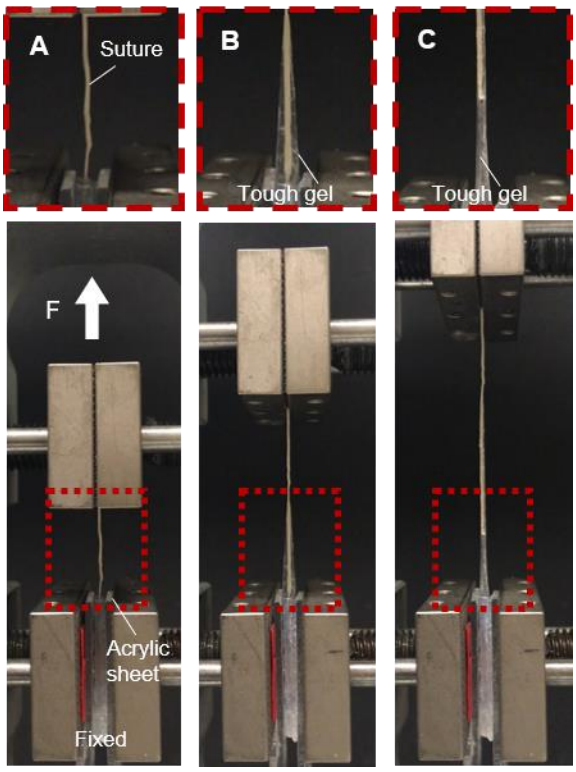

Figure S4.5. Suture pull-out test used to characterize the suture-gel adhesion energy. Representative digital images captured during the pull-out test using alg-PAAm hydrogel sheathed polyglactin 910 suture at reference state (A), debonding initiation (B), and right before fully debonding (C).

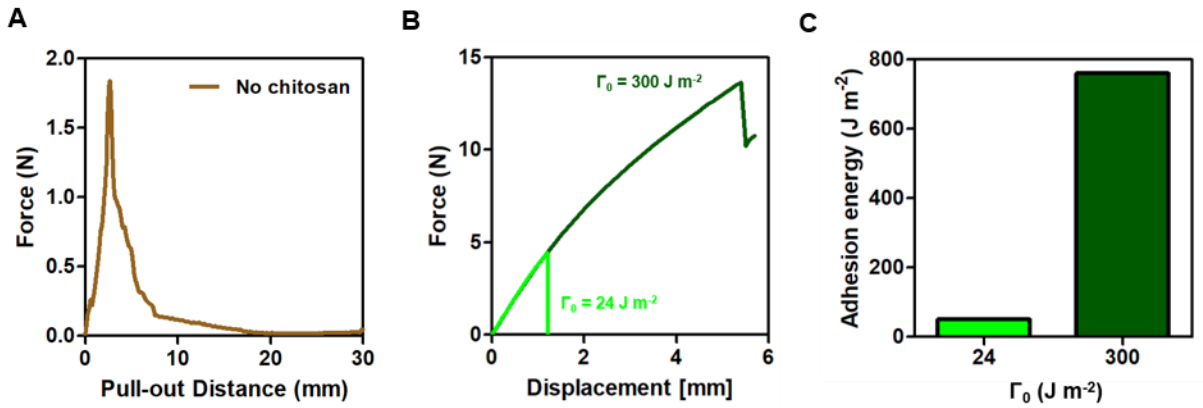

Figure S4.6. Effects of surface priming on suture-sheath adhesion. (A) Representative pull-out test result on TGS suture fabricated without chitosan priming. FEM results of the effect of Γ_0 on suture-gel adhesion energy. (B-C) FEM results of the effect of Γ_0 on suture-gel adhesion energy. Representative force-displacement curve (B) and calculated adhesion energy (C) of hydrogel sheathed suture with low (24 J m^{-2}) and high (300 J m^{-2}) Γ_0.

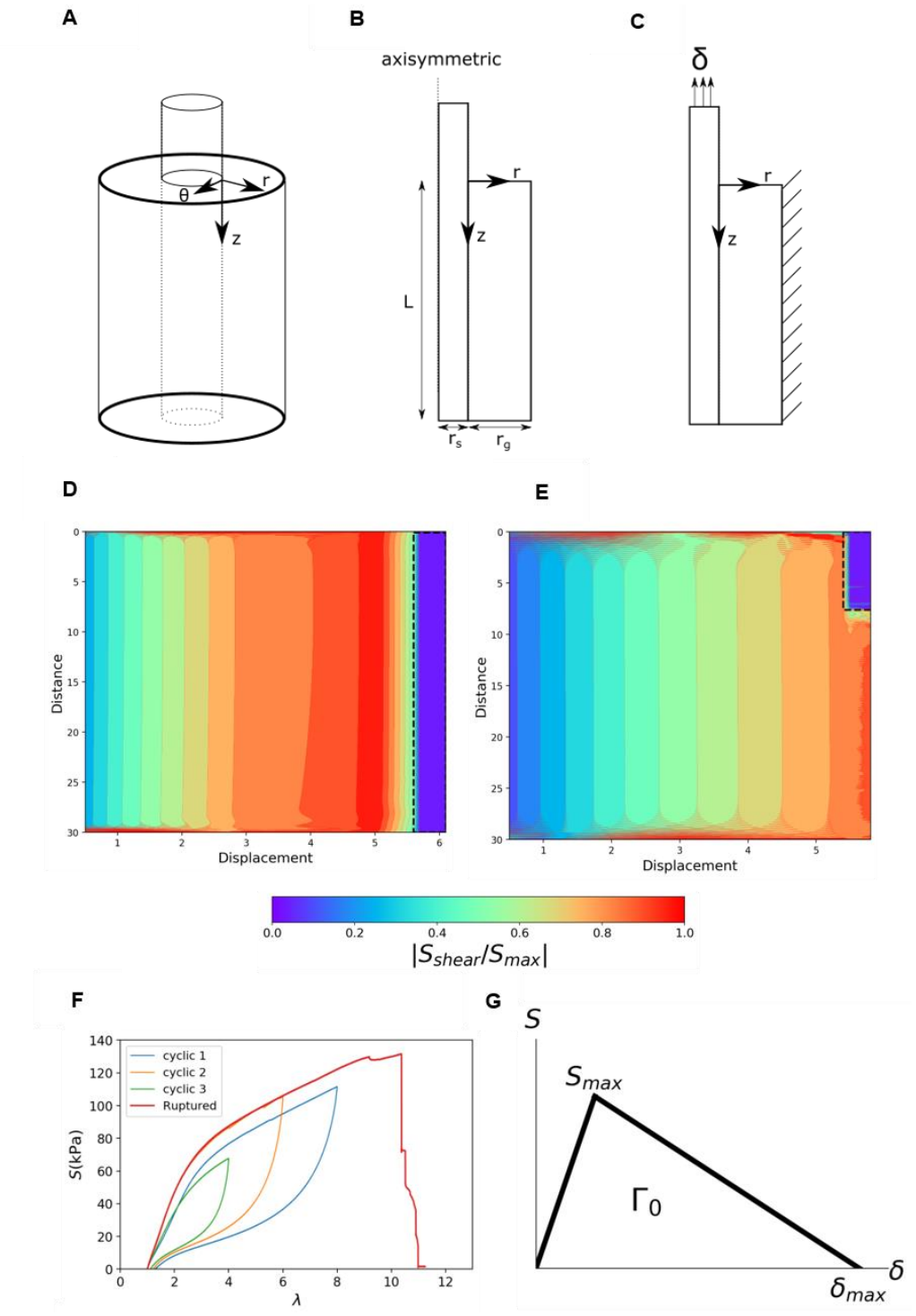

Figure S4.7. Shear stress distribution analysis from FEM. (A-C) Schematic of the suture and the hydrogel sheath used in the FEM in the 3d space (A) and 2d axisymmetric plane (B). (C) The loading condition and associated boundary condition applied to the suture-hydrogel hybrid. The

origin of the coordinates coincides with the top end of the joint interface. (D-E) Magnitude of the normalized shear stress plotted as a function of the applied displacement (δ) and the distance along the joint interface (z) for $\boldsymbol{r_g/r_s = 1}$ (D) and 4 (E). (F-H) Mechanical testing and mesh convergence study for FEM. (F) Nominal stress versus principle stretch under pure shear tests of alg-PAAm hydrogel. (G) The intrinsic work of adhesion characterized by the triangular traction-separation law. (H) Mesh convergence study for the case with

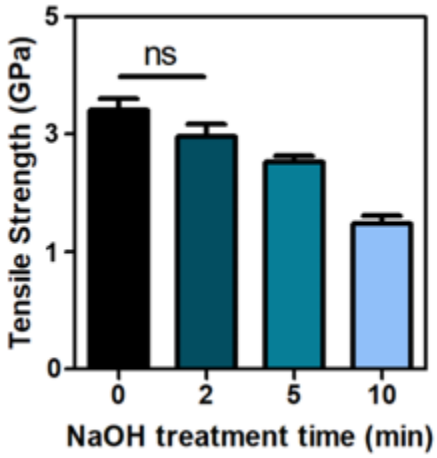

Figure S4.8. Effect of NaOH treatment on TGS suture tensile strength.

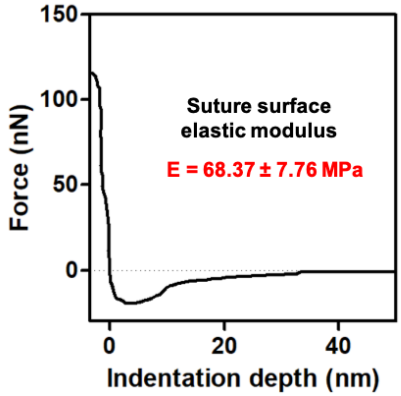

Figure S4.9. Surface elasticity of polyglactin 910 suture characterized using AFM.

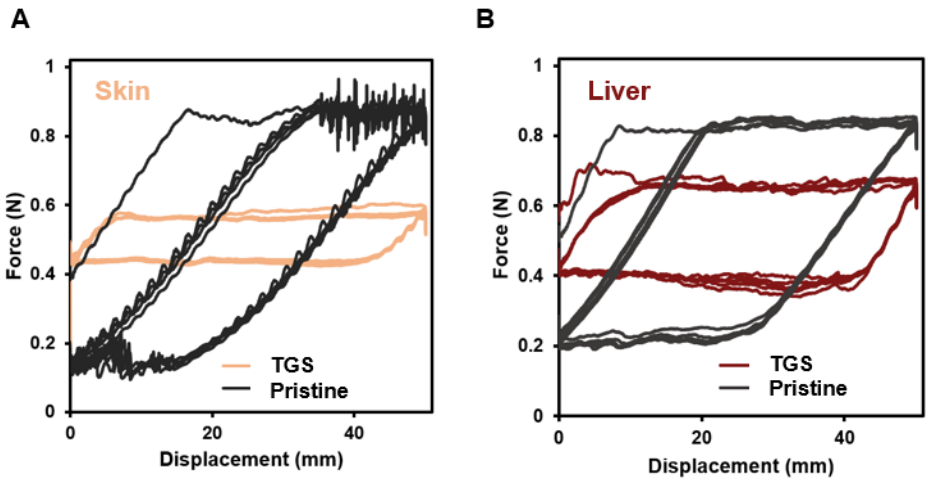

Figure S4.10. Representative drag force-displacement curves of the pristine and TGS sutures applied on porcine skin (A) and liver (B).

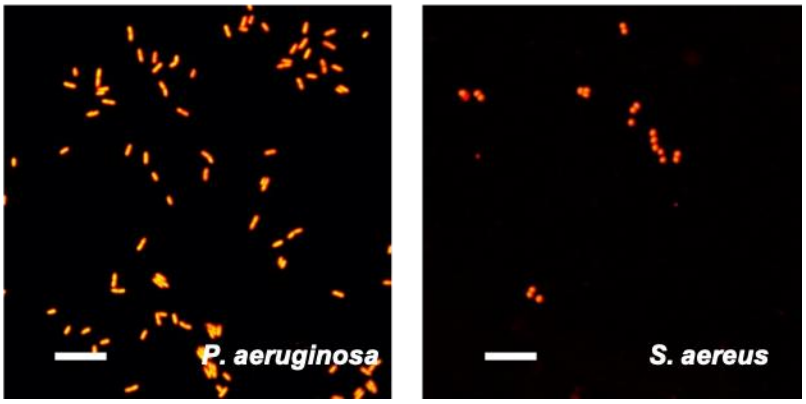

Figure S4.11. Representative figures of bacteria viability assay on TGS suture containing BZK. Scale bar is 10 μm.

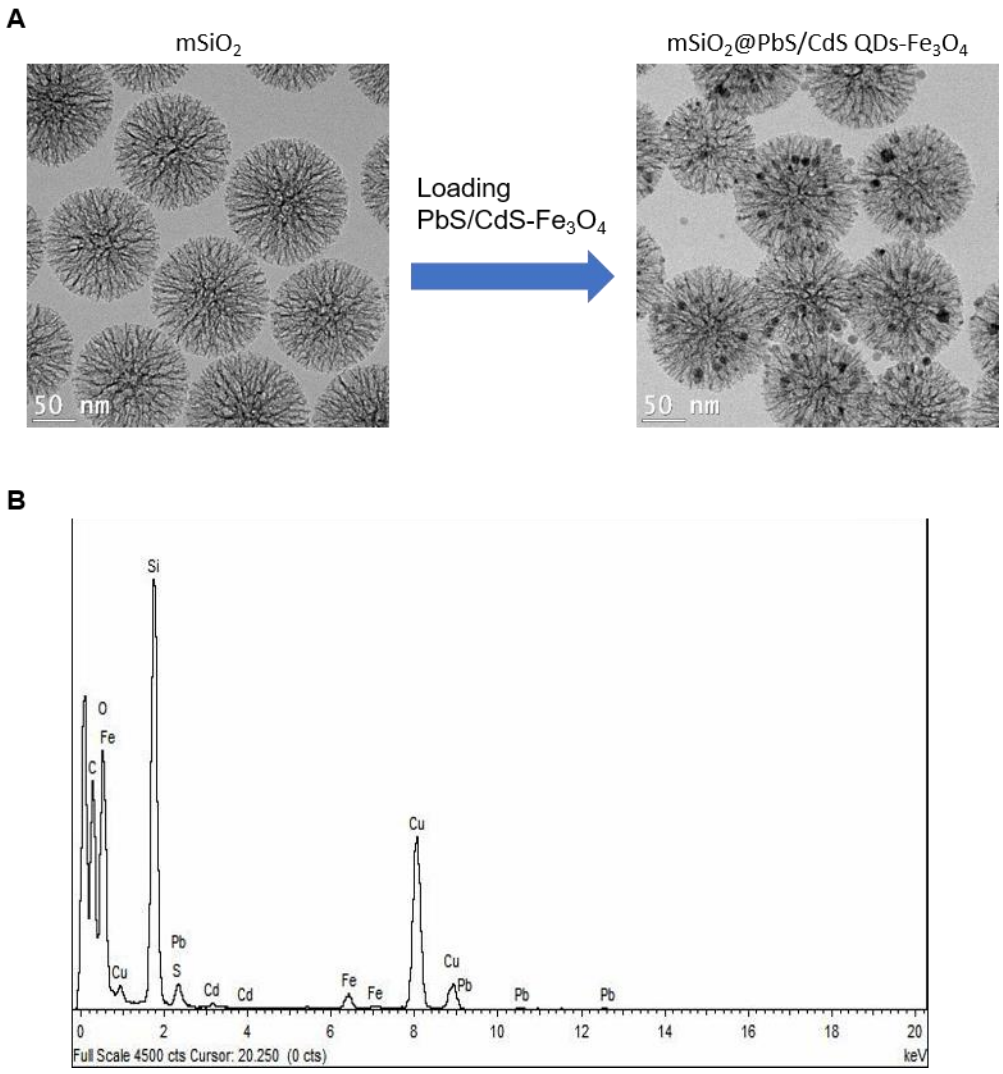

Figure S4.12. Characterization of fluorescent nanoparticles (NPs). (A) Transmission electron microscopy (TEM) images of $mSiO_2$ (left) and $mSiO_2$@PbS/CdS-Fe_3O_4 (right). (B) Energy-dispersive X-ray (EDX) spectrum of $mSiO_2$@PbS/CdS-Fe_3O_4 showing the co-existence of Si, O, Fe, Pb, Cd and S elements.

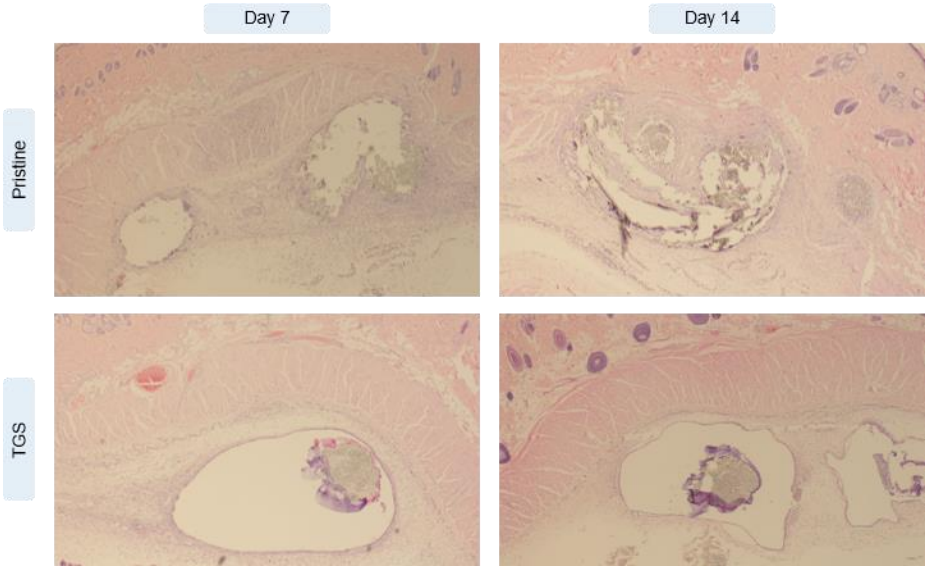

Figure S4.13. Representative overview of implantation pocket, with the dermis and suture knot (4X).

Figure S4.14. Macroscopic investigation of wound closure and healing using pristine and TGS sutures.

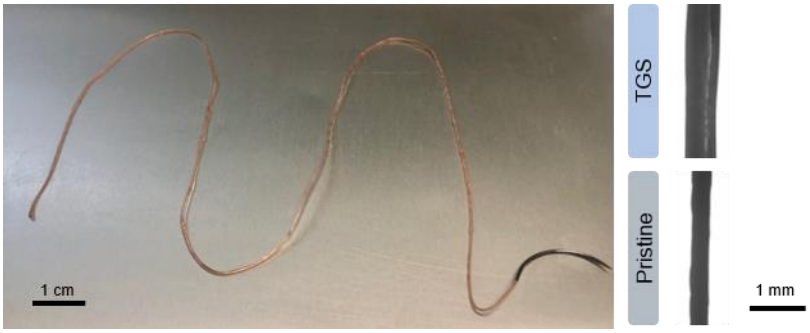

Figure S4.15. Continuous TGS suture fabrication using a dip-coating approach as a proof of concept.

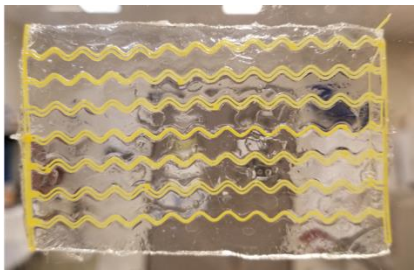

Figure S4.16. Fiber-reinforced tough gel patch. A demonstration of tough gel sheathed 3d-printed polylactic acid filaments with robust hydrogel-fiber interface.

References

1. J. V. Clough, J. Alexander-Williams, SURGICAL AND ECONOMIC ADVANTAGES OF POLYGLYCOLIC-ACID SUTURE MATERIAL IN SKIN CLOSURE. *The Lancet*. **305**, 194–195 (1975).

2. R. E. Abhari, J. A. Martins, H. L. Morris, P.-A. Mouthuy, A. Carr, Synthetic sutures: Clinical evaluation and future developments. *J. Biomater. Appl.* **32**, 410–421 (2017).

3. J. Li, A. D. Celiz, J. Yang, Q. Yang, I. Wamala, W. Whyte, B. R. Seo, N. V. Vasilyev, J. J. Vlassak, Z. Suo, D. J. Mooney, Tough adhesives for diverse wet surfaces. *Science*. **357**, 378–381 (2017).

4. H. Yuk, C. E. Varela, C. S. Nabzdyk, X. Mao, R. F. Padera, E. T. Roche, X. Zhao, Dry double-sided tape for adhesion of wet tissues and devices. *Nature*. **575**, 169–174 (2019).

5. D. E. Discher, D. J. Mooney, P. W. Zandstra, Growth Factors, Matrices, and Forces Combine and Control Stem Cells. *Science*. **324**, 1673–1677 (2009).

6. L. Van De Water, S. Varney, J. J. Tomasek, Mechanoregulation of the Myofibroblast in Wound Contraction, Scarring, and Fibrosis: Opportunities for New Therapeutic Intervention. *Adv. Wound Care*. **2**, 122–141 (2013).

7. E. B. Hunziker, A. Stähli, Surgical suturing of articular cartilage induces osteoarthritis-like changes. *Osteoarthritis Cartilage*. **16**, 1067–1073 (2008).

8. L. Shahinian, S. I. Brown, Postoperative Complications with Protruding Monofilament Nylon Sutures. *Am. J. Ophthalmol.* **83**, 546–548 (1977).

9. B. R. Freedman, D. J. Mooney, Biomaterials to Mimic and Heal Connective Tissues. *Adv. Mater.* **31**, 1806695 (2019).

10. C.-C. Chu, D. F. Williams, Effects of physical configuration and chemical structure of suture materials on bacterial adhesion: A possible link to wound infection. *Am. J. Surg.* **147**, 197–204 (1984).

11. M. Champeau, J.-M. Thomassin, T. Tassaing, C. Jérôme, Current manufacturing processes of drug-eluting sutures. *Expert Opin. Drug Deliv.* **14**, 1293–1303 (2017).

12. J. J. Elsner, M. Zilberman, Antibiotic-eluting bioresorbable composite fibers for wound healing applications: Microstructure, drug delivery and mechanical properties. *Acta Biomater.* **5**, 2872–2883 (2009).

13. M. Akbari, A. Tamayol, V. Laforte, N. Annabi, A. H. Najafabadi, A. Khademhosseini, D. Juncker, Composite Living Fibers for Creating Tissue Constructs Using Textile Techniques. *Adv. Funct. Mater.* **24**, 4060–4067 (2014).

14. L. Wang, D. Chen, J. Sun, Layer-by-Layer Deposition of Polymeric Microgel Films on Surgical Sutures for Loading and Release of Ibuprofen. *Langmuir*. **25**, 7990–7994 (2009).

15. J. S. Lee, Y. Lu, G. S. Baer, M. D. Markel, W. L. Murphy, Controllable protein delivery from coated surgical sutures. *J. Mater. Chem.* **20**, 8894–8903 (2010).

16. S. Saxena, A. R. Ray, A. Kapil, G. Pavon-Djavid, D. Letourneur, B. Gupta, A. Meddahi-Pellé, Development of a New Polypropylene-Based Suture: Plasma Grafting, Surface Treatment, Characterization, and Biocompatibility Studies. *Macromol. Biosci.* **11**, 373–382 (2011).

17. M. Champeau, J.-M. Thomassin, T. Tassaing, C. Jerome, Drug Loading of Sutures by Supercritical CO2 Impregnation: Effect of Polymer/Drug Interactions and Thermal Transitions. *Macromol. Mater. Eng.* **300**, 596–610 (2015).

18. J. Yang, R. Bai, Z. Suo, Topological Adhesion of Wet Materials. *Adv. Mater.* **30**, 1800671 (2018).

19. W. Li, X. Liu, Z. Deng, Y. Chen, Q. Yu, W. Tang, T. L. Sun, Y. S. Zhang, K. Yue, Tough Bonding, On-Demand Debonding, and Facile Rebonding between Hydrogels and Diverse Metal Surfaces. *Adv. Mater.* **31**, 1904732 (2019).

20. H. Yuk, T. Zhang, G. A. Parada, X. Liu, X. Zhao, Skin-inspired hydrogel–elastomer hybrids with robust interfaces and functional microstructures. *Nat. Commun.* **7**, 1–11 (2016).

21. Y. Yu, H. Yuk, G. A. Parada, Y. Wu, X. Liu, C. S. Nabzdyk, K. Youcef-Toumi, J. Zang, X. Zhao, Multifunctional “Hydrogel Skins” on Diverse Polymers with Arbitrary Shapes. *Adv. Mater.* **31**, 1807101 (2019).

22. P. Kannus, Structure of the tendon connective tissue. *Scand. J. Med. Sci. Sports*. **10**, 312–320 (2000).

23. J.-Y. Sun, X. Zhao, W. R. K. Illeperuma, O. Chaudhuri, K. H. Oh, D. J. Mooney, J. J. Vlassak, Z. Suo, Highly stretchable and tough hydrogels. *Nature*. **489**, 133–136 (2012).

24. H. Yuk, T. Zhang, S. Lin, G. A. Parada, X. Zhao, Tough bonding of hydrogels to diverse non-porous surfaces. *Nat. Mater.* **15**, 190–196 (2016).

25. T. Zhang, S. Lin, H. Yuk, X. Zhao, Predicting fracture energies and crack-tip fields of soft tough materials. *Extreme Mech. Lett.* **4**, 1–8 (2015).

26. G. Zhang, T. Ren, X. Zeng, E. Van Der Heide, Influence of surgical suture properties on the tribological interactions with artificial skin by a capstan experiment approach. *Friction*. **5**, 87–98 (2017).

27. A. Valiei, M. Okshevsky, N. Lin, N. Tufenkji, Anodized Aluminum with Nanoholes Impregnated with Quaternary Ammonium Compounds Can Kill Pathogenic Bacteria within Seconds of Contact. *ACS Appl. Mater. Interfaces*. **10**, 41207–41214 (2018).

28. L. A. Schneider, A. Korber, S. Grabbe, J. Dissemond, Influence of pH on wound-healing: a new perspective for wound-therapy? *Arch. Dermatol. Res.* **298**, 413–420 (2007).

29. A. Tamayol, M. Akbari, Y. Zilberman, M. Comotto, E. Lesha, L. Serex, S. Bagherifard, Y. Chen, G. Fu, S. K. Ameri, W. Ruan, E. L. Miller, M. R. Dokmeci, S. Sonkusale, A. Khademhosseini, Flexible pH-Sensing Hydrogel Fibers for Epidermal Applications. *Adv. Healthc. Mater.* **5**, 711–719 (2016).

30. G. Hong, A. L. Antaris, H. Dai, Near-infrared fluorophores for biomedical imaging. *Nat. Biomed. Eng.* **1**, 1–22 (2017).

31. F. Yang, A. Skripka, M. S. Tabatabaei, S. H. Hong, F. Ren, Y. Huang, J. K. Oh, S. Martel, X. Liu, F. Vetrone, D. Ma, Magnetic Photoluminescent Nanoplatform Built from Large-Pore Mesoporous Silica. *Chem. Mater.* **31**, 3201–3210 (2019).

32. Z. Hu, C. Fang, B. Li, Z. Zhang, C. Cao, M. Cai, S. Su, X. Sun, X. Shi, C. Li, T. Zhou, Y. Zhang, C. Chi, P. He, X. Xia, Y. Chen, S. S. Gambhir, Z. Cheng, J. Tian, First-in-human

liver-tumour surgery guided by multispectral fluorescence imaging in the visible and near-infrared-I/II windows. *Nat. Biomed. Eng.*, 1–13 (2019).

33. J. Li, D. J. Mooney, Designing hydrogels for controlled drug delivery. *Nat. Rev. Mater.* **1**, 16071 (2016).

34. B. A. Aguado, J. C. Grim, A. M. Rosales, J. J. Watson-Capps, K. S. Anseth, Engineering precision biomaterials for personalized medicine. *Sci. Transl. Med.* **10** (2018), doi:10.1126/scitranslmed.aam8645.

35. K. H. Vining, D. J. Mooney, Mechanical forces direct stem cell behaviour in development and regeneration. *Nat. Rev. Mol. Cell Biol.* **18**, 728–742 (2017).

36. J. Lee, B. L. Zambrano, J. Woo, K. Yoon, T. Lee, Recent Advances in 1D Stretchable Electrodes and Devices for Textile and Wearable Electronics: Materials, Fabrications, and Applications. *Adv. Mater.* **32**, 1902532 (2020).

37. Y. Kim, G. A. Parada, S. Liu, X. Zhao, Ferromagnetic soft continuum robots. *Sci. Robot.* **4** (2019), doi:10.1126/scirobotics.aax7329.

38. G. G. Adams, M. Nosonovsky, Contact modeling — forces. *Tribol. Int.* **33**, 431–442 (2000).

Preface to Chapter 5

In Chapter 4, we propose a bioinspired tough gel sheath as a soft biomimetic interface for the closure of soft biological tissues. The lubricating hydrogel utilized is beneficial for lowering the potential damage caused by traditional rough and stiff surgical sutures. However, various other limitations remain, including concerns of body fluid/air leakage and bacteria infiltration. For suturing mechanically active tissues such as gastrointestinal and musculoskeletal tissues, a seamless integration of sutures and native tissues is especially desired to guarantee the reliable closure of the damaged tissues.

In Chapter 5, we report a gel adhesive puncture sealing (GAPS) suture for effective tissue sealing and closure. Building upon the tough gel sheath surface functionalization strategy reported in Chapter 4, and the hydrogel-tissue adhesion mechanism in Chapter 2, we will engineer an additional adhesive layer to further strengthen the biointegration of surgical sutures and biological tissues.

We show that strong adhesion on diverse biological tissues can be achieved when GAPS sutures are applied, significantly higher than the previously reported TGS sutures or pristine sutures. To demonstrate the translation potential of the GAPS sutures, we create perforation on porcine gastrointestinal tissues ex vivo and then close the wound with GAPS or pristine sutures. We confirm the sealing capability of GAPS sutures, exemplified with the prevention of fluid leakage from the intestinal cavity where the pristine sutures fail to do so. In another ex vivo model by applying mechanically challenging cyclic tensile loading on sutured bovine meniscus flaps with complete radial tear, GAPS suture significantly reduces the gap formation between sutured tissues, indicating its advantage for repairing mechanically active musculoskeletal tissues.

This work is currently under preparation for submission:

Zhenwei Ma, Alex Nguyen, David Mazy, Christopher Chung-Tze-Cheong, Stéphanie Lamer, Farshid Ghezelbash, Zhen Yang, Yin Liu, Shiyu Liu, Benjamin Freedman, Marie-Lyne Nault*, Jianyu Li*. Gel adhesive puncture-sealing sutures for wound closure. (Under preparation) (2022)

Chapter 5 Gel Adhesive Puncture-Sealing Sutures for Wound Closure

5.1 Introduction

Surgical sutures are versatile medical devices widely used in the clinics. They are the gold-standard surgical tools for wound closure, and have been adopted to reattach teared tissue flaps (*1*), blood vessels (*2*), gastrointestinal (GI) tract (*3*) and to integrate xenografts (*4*), allografts (*5*), or other engineered scaffolds/devices with native tissues (*6*). However, despite such diverse applications, they're unable to create an immediate tight seal with surrounding tissues, which often lead to body fluid or air leakages and high risks of surgical site infection (*7–9*).

Suturing is an effective yet rather invasive wound-closure procedure, involving a series of needle penetration in and out of tissues to anchor and knot the suture. Multiple suturing roots are often implemented to lower the stress concentration caused by the fastened suture threads. Additionally, the size of the needle attached to the suture thread is almost always larger than the suture fiber diameter to allow them to successfully pass-through tissues during wound closure. The puncture hole left by needle penetration and the inability of sutures to fill up the puncture hole is another major cause of body fluid/air leakage (*10*).

Furthermore, the long-term consequence of using these stiff suture fibers is tissue damage and dehiscence due to constant fiber slicing, compression, and friction on tissues (*11–16*). The mechanical irritation is particularly problematic for wound management of abdominal tissues under high-tension (*13*), dynamic tissues under constant movements (*14*), and degenerative tissues with compromised mechanical properties in elderly and immunocompromised patients (*17*) with diminishing regenerative capacity.

Hydrogel based bioadhesives are proposed to remedy the leakage problem associated with suturing (*18–22*). However, they cannot provide comparable tensile strength as sutures, due to the fundamental limit of soft materials in strength, and thus are instructed and approved for sealing the suturing line as a supplementary measure (*23–26*). Therefore, novel wound closure devices are in great demand to efficiently seal the tissue defects, offer strong biointegration with surrounding tissues to prevent further damage, and ideally serve as a mechanically biomimetic and therapeutic interface to accelerate wound healing (*27*).

Advances in suture engineering have been made in two general directions. Increasing the mechanical properties (e.g., tensile strength) of sutures is the first direction pursued. However it remains debatable whether a even stronger suture is required, because most existing sutures for soft tissue repair have outperformed the strength of these native tissues (such as connective tissues), and the prevalent post-surgical failure mode observed is in fact tissue failure, instead of suture failure (*12*). Further improving suture strength is unfortunately unable to address the disadvantages of suturing. Another direction is to bioengineer sutures with additional drug eluting or cell delivery functions (*28–30*). These strategies have recently shown promise to therapeutically instructing tissue regeneration, but they cannot mitigate the mechanical mismatch of the suture materials and damaged tissues. To this end, our recent work proposed a bioinspired surface functionalization strategy to seamlessly unite surgical sutures with a tough gel sheath (TGS), and shows markedly reduced surface stiffness, friction, and drag of the suture when interfacing with tissues (*31*). This platform technology suggests the possibility of further seamlessly integrating sutures with biological tissues for wound closure and sealing.

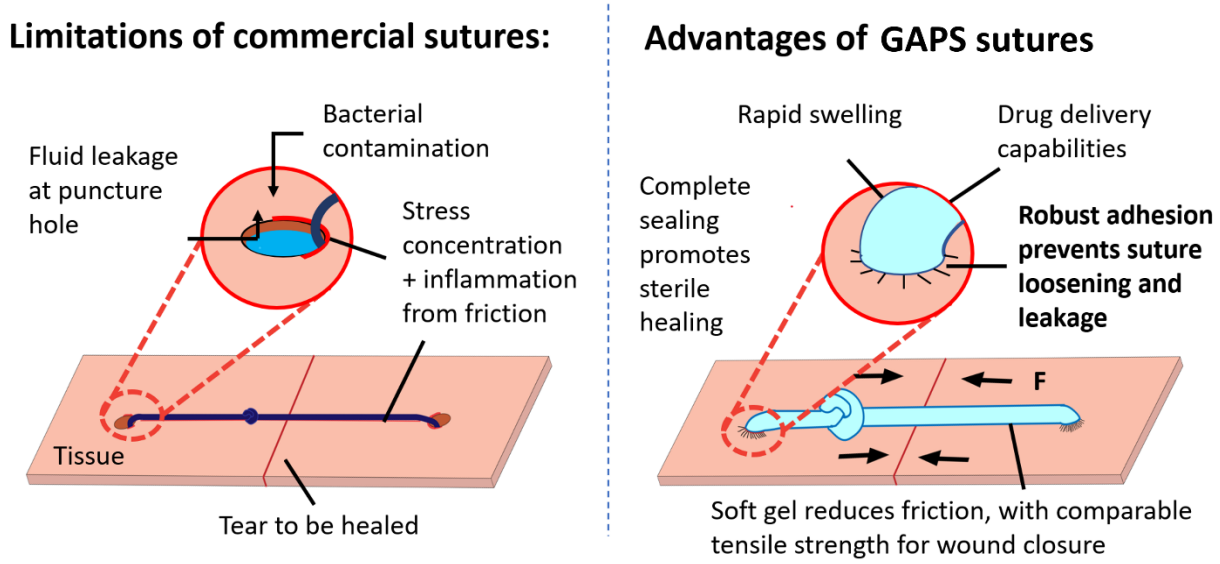

Figure 5.1. Comparison of commercial and GAPS sutures.

Therefore, to address the aforementioned issues, building upon the proposed surface functionalization strategy (*31*), here we propose a new design of gel adhesive puncture sealing

(GAPS) sutures for tissue repair and wound closure. Such sutures can retain high tensile strength for secured tissue closure, while rapidly swell and adhere to the punctured tissue to enable tight sealing (Fig. 5.1). The proposed strategy is compatible with various tissues and defect sizes by rational design of the swelling kinetics of the adhesive hydrogel matrix. We further demonstrate the translational potential of GAPS sutures and their advantages for meniscal tear repair and GI laceration sealings. Besides tissue repair, the GAPS sutures could serve as novel wound closure devices and be fine-tuned for various wound management scenarios suffered from the application of traditional sutures, such as diabetic ulcers, thoracic organ sealing, cartilage and tendon repair.

5.2 Results and Discussions

The GAPS suture consists of three components that are seamlessly and robustly integrated together: a suture fiber core of high tensile strength; a swellable, tough, soft hydrogel sheath to mitigate tissue damage and to dissipate energy; and an adhesive layer to intimately integrate the gel sheath with tissues. As a proof of concept, we coat a multifilament polyglactin 910 suture (VICRYL, 2-0), a widely used degradable surgical suture, with a thin layer of tough hydrogel (polyacrylamide-alginate; PAAm-alg); a chitosan solution with additional crosslinking reagent (EDC/NHS) will be used as the adhesive layer.

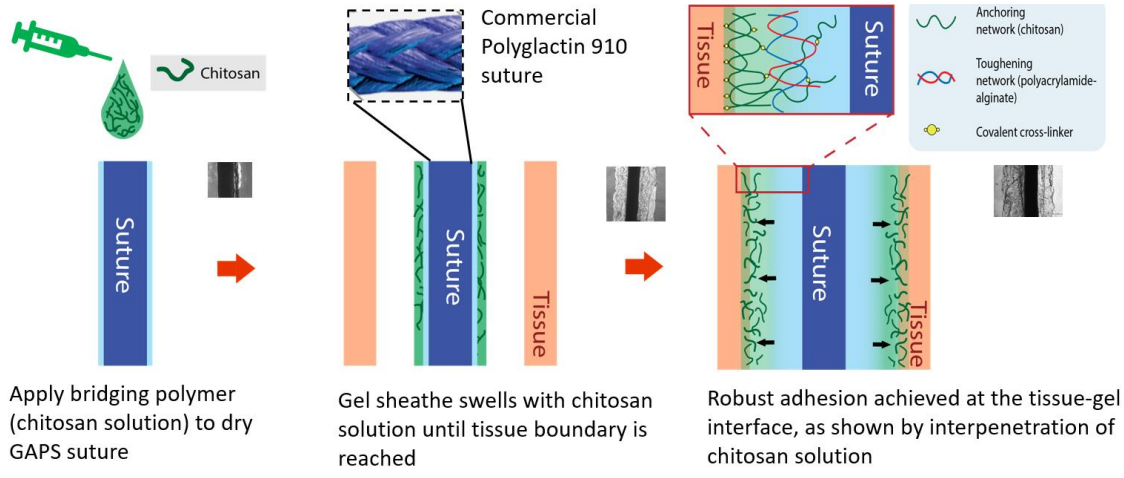

Figure 5.2. Workflow of GAPS suture application.

To apply GAPS sutures, the essential workflow is summarized in Fig. 5.2. Briefly, the GAPS suture is implemented at its dry state which presents a similar diameter to pristine sutures. This allows the easy passing of the suture inside tissues, matching the standard surgical procedure established for the specific suture. Due to the strong interfacial bonding between suture fiber and hydrogels, no delamination is observed despite dehydration. This is exemplified with the high interfacial adhesion energy and shear strength of GAPS suture at both wet and dry state. Subsequently, we apply the adhesive agents locally along the suture lines; driven by capillary forces, the agents wick spontaneously into the spacing between the suture and the tissue. The integrated gel coating rapidly swells to reach the boundary tissue defect wall. The suture-tissue adhesion then initiates and reaches its maximum adhesion energy within an hour. Due to fast swelling processes, the initiation of adhesion is as rapid as a few minutes right after the swollen hydrogel is in contact with the wall of the puncture hole, which is further enhanced with interfacial chemical reactions. Although instant bioadhesion (e.g. formed within seconds) is sometimes valued in emergency situations such as hemorrhage controls to prevent heavy bleeding (*22*), precise control of the adhesion area and timing is preferred instead (e.g. formed within several minutes). Our material system and adhesion kinetics allow sufficient operating time window for suturing, knotting, repositioning and adjustments.

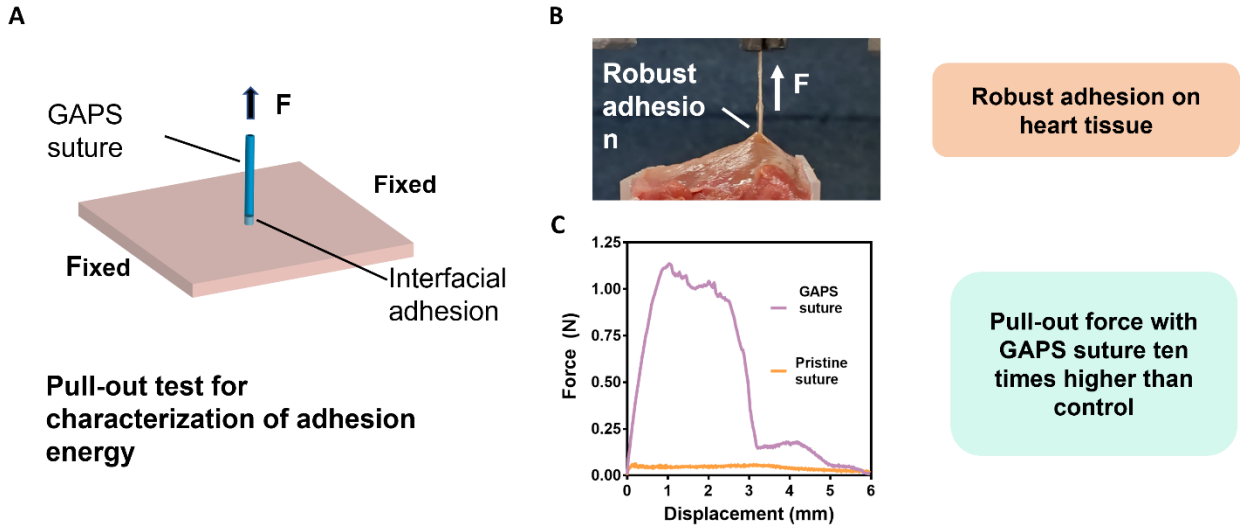

Figure 5.3. Experimental setup (A, B) and representative force-displacement curve (C) of the suture pull-out test.

Tensile strength of the sutures is the key attribute for reliable wound closure. Using a uniaxial tensile test, we show that no significant difference is observed regarding the tensile strength (~ 3 GPa) of the GAPS and pristine sutures, sufficient for most soft tissue repair. Next, we will characterize the bioadhesion property of GAPS sutures on various tissues and investigate the correlation of hydrogel swelling and tissue adhesion energy.

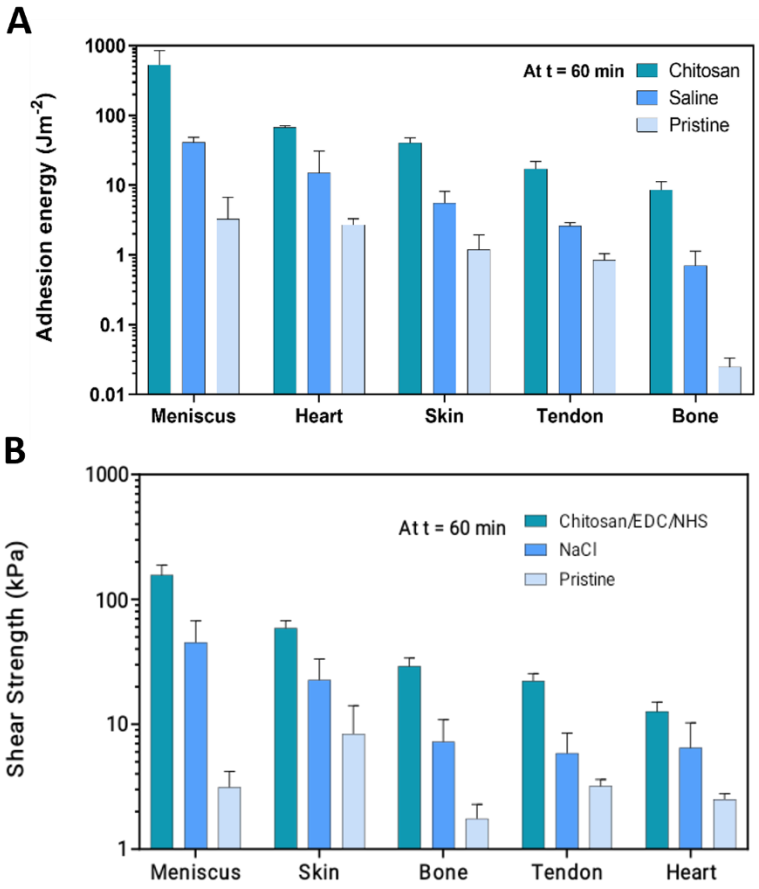

Figure 5.4. Adhesion energy (A) and shear strength (B) between pristine, TGS (NaCl), GAPS (Chitosan/EDC/NHS) and various tissues. Data reported as means ± SD for n = 3 independent experiments.

To quantify the bioadhesion property of the GAPS sutures, we design a customized pull-out test to characterize the suture-tissue adhesion (Fig 5.3A, B). Briefly, we prepare tissue specimens of the same size, then create a through-hole inside the tissue with a needle. We then apply the pristine suture, tough gel sheathed (TGS) suture(*31*) or GAPS suture at the puncture site. TGS sutures without any addition of adhesive agents (i.e., chitosan, EDC and NHS) are included to investigate how mechanical interlocking between the swollen TGS sutures and the contacted tissues contributes to adhesion. After 1-hour incubation, we pull out the suture from the defect created on the tissue specimen with an Instron machine (Fig 5.3C). The GAPS sutures are found to form robust adhesion on diverse wet porcine tissues, including skin, meniscus, tendon, heart, and bone (Fig 5.4). We notice that the heart tissue can be lifted during the pull-out testing, further indicating the strong integration of GAPS suture and its surrounding tissues (Fig 5.3B). High adhesion energy and shear strength both are observed on meniscus and tendon, potentially due to their high collagen content to form high-density amide bond between the GAPS suture and tissue surface. Lowest adhesion is observed on bones, potentially because of their low protein presentation and the low energy dissipation capacity of the rigid extracellular matrix.

As expected, only very modest tissue adhesion (< 5 J m^{-2}) is obtained with pristine sutures without any coatings on various tissues, possibly due to the dragging and friction at the suture-tissue interface during pull-out. On the other hand, the swollen TGS sutures can readily provide significantly higher adhesion energy than the pristine sutures, although their adhesion performance is still significantly lower than the GAPS ones.

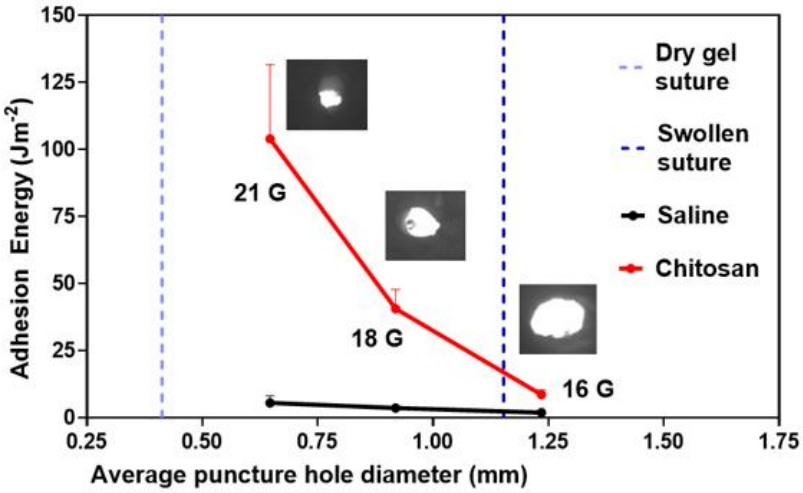

Figure 5.5. Effects of tissue defect size on GAPS suture-tissue adhesion. Data reported as means ± SD for n = 3 independent experiments.

To further investigate the bioadhesion performance as a function of the size of punctured hole in tissues, we vary the hole size with needles of different diameters (16G, 18G and 21G). After sealing the hole with GAPS sutures (Fig. 5.5), we perform pull-out testing and find that the adhesion energy decreases with the defect size. Fig. 5.5 shows that over 100 J m^{-2} adhesion energy with porcine skin can be observed when the smallest puncture hole is created, while negligible adhesion enhancement is noticed for the largest tissue defect.

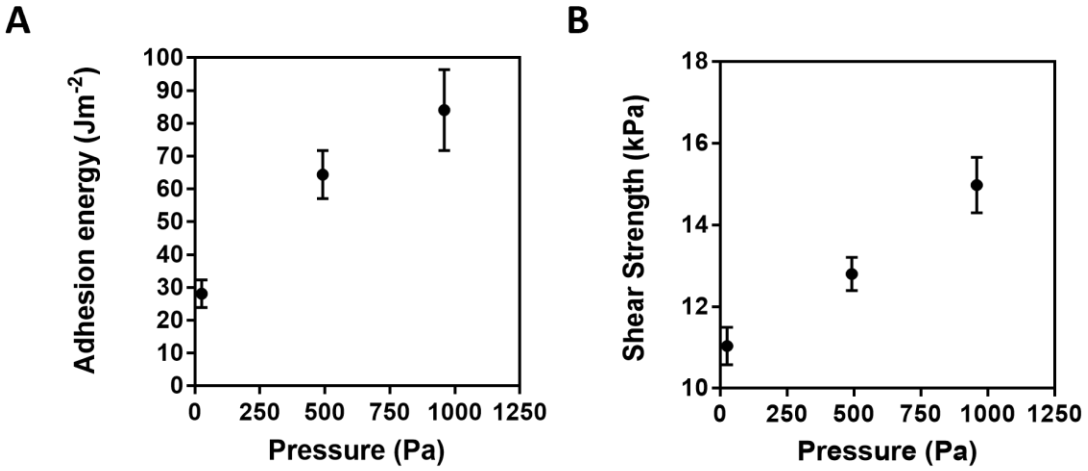

Figure 5.6. Effects of applied pressure on hydrogel-tissue adhesion energy (A) and shear strength (B) based on interfacial chemical reactions. Data reported as means ± SD for n = 3 independent experiments.

To explain the correlation between the adhesion and hole size, we hypothesize that the pressure built up at the suture-tissue interface during hydrogel swelling could mediate their adhesion on the contacted tissue area. This hypothesis is motivated by recent findings that compression (compressive strain/stress) can alter interfacial adhesion between two hydrogels (*32*). To test our hypothesis, we measure the adhesion energy between porcine skin tissues and bulk PAAm-alg based tough adhesive hydrogels when various pressure is applied. Indeed, higher applied pressure leads to markedly higher adhesion energy (Fig. 5.6 A) and shear strength (Fig. 5.6 B). However,

as indicated in Fig. 5.5, the pressure itself and the resulted mechanical interlocking does not significantly contribute to the adhesion enhancement of GAPS sutures when no chemical reactions are involved, which can be explained as follows.

In the case of tough adhesion with tissues, there are three key contributors for the overall adhesion energy: the intrinsic work of adhesion Γ_0 (energy required to break interfacial bonds between the tissue and adhesive), energy dissipation in the adhesive matrix (Γ_A), and the tissue (Γ_T)(*18*).

$\Gamma_0 = \Gamma_0 + \Gamma_A + \Gamma_T$

It has been recognized that the value of Γ_0 determines the amplification effect from energy dissipation of the adhesive matrix Γ_A (*33*). Mechanical interlocking alone does not alter Γ_0, thus it's unable to unlock the potential of matrix energy dissipation to increase adhesion (*34*). On the other hand, since the tissue defect is not perfectly smooth, when higher pressure is accumulated to conform tissue surface topography, a more intimate interaction is expected at the hydrogel-tissue interface, leading to higher effective contact area to initiate the interfacial chemical reactions, therefore increased interfacial covalent bonds formation, i.e., higher Γ_0. They all eventually contribute to the significantly amplified adhesion energy Γ.

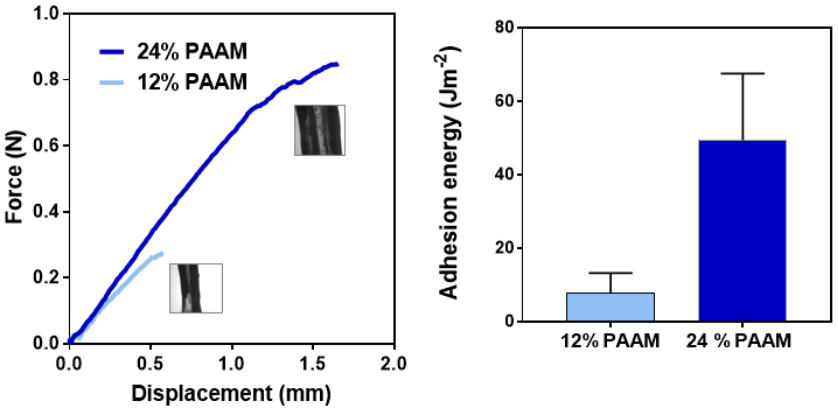

Figure 5.7. Effect of hydrogel swelling potential on GAPS suture-tissue adhesion. Data reported as means ± SD for n = 3 independent experiments.

We further hypothesize that controlling the swelling of the hydrogel matrix allows us to customize and fine-tune the interfacial adhesion profile. By engineering the swelling properties of a single-

network PAAm hydrogel, we show that when the same defect size is created on tissues, significantly higher adhesion energy is observed with the hydrogel capable to swell more (Fig 5.7). The hydrogel coating resembles the swellable packers used in oil industry for sealing the flow of downhole fluids during hydraulic fracturing (*35*). The result highlights the benefit of fine-tuning the adhesive gel layer of GAPS sutures to match various tubular tissue geometry, e.g., blood vessels for embolization, and other irregular tissue defects.

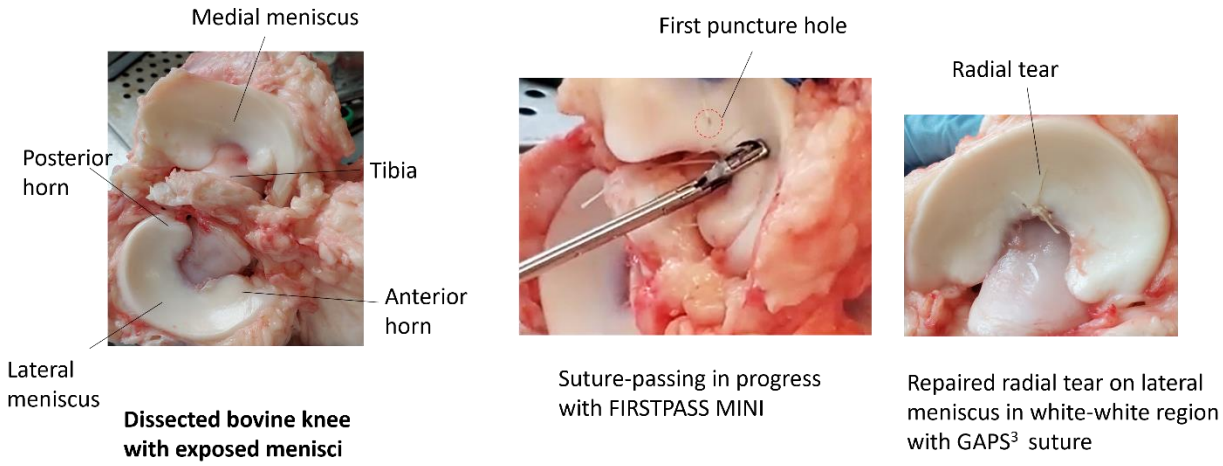

Figure 5.8. Workflow of applying GAPS sutures on bovine meniscal tear using FIRSTPASS MINI suture passer device.

Encouraged by the strong adhesion between GAPS sutures and meniscus tissue, we next establish the potential of GAPS sutures in treating meniscal tears. In the case of meniscus tear management, repairing meniscus to allow meniscal healing is greatly desired to avoid the adverse consequence of meniscectomy, including postoperative osteoarthritic changes to the knee (*36*–*39*). This application is representative among those in relation of mechanically active musculoskeletal tissues, such as meniscus and tendon. They have been proved to be challenging because of slow regeneration and the harsh biomechanical environment these tissues reside in (*40*, *41*).

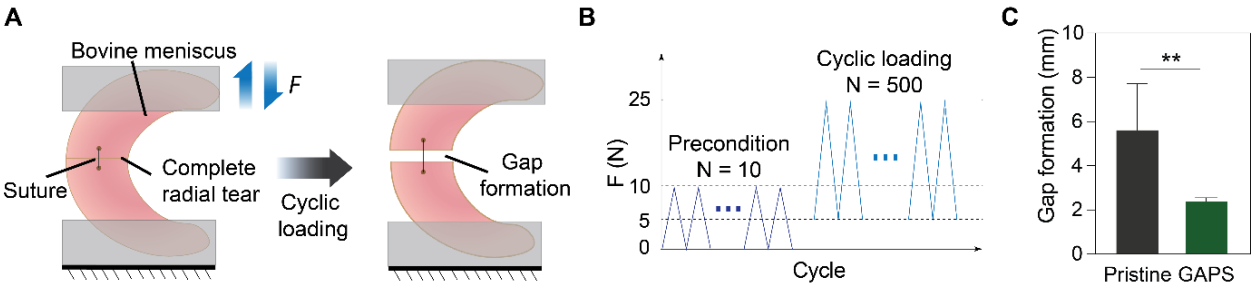

Figure 5. 9. Gap formation of sutured bovine meniscal tear using pristine, or GAPS sutures after cyclic loading. (A) Schematic of the experimental set-up for the cyclic tensile loading of the sutured bovine meniscus. (B) Loading condition of the mechanical testing. (C) Gap formation of sutured meniscus after cyclic loading. Data reported as means ± SD for n = 5 independent experiments. Statistical significance and *P* values are determined by two-sided Student's t test. "**" indicates $P < 0.01$.

In clinical practice, meniscus repairs with sutures are predominantly conducted with customized surgical devices adapted to the tight knee space (*42*, *43*). Such surgical devices have been routinely used in the operating rooms for suturing and knotting in the limited knee space for meniscus repair (*44*). To test the compatibility of these devices with our sutures, we deployed a suture passer device (FIRSTPASS MINI; Smith & Nephew) to apply the GAPS sutures onto meniscal tear created on bovine meniscus (Fig. 5.8). The successful implementation of GAPS suture with existing suture passer device suggests its applicability to other delivery devices, which offers ease of operation for surgeons to integrate the GAPS suture device into their existing workflow. This would greatly increase the translational potential of the proposed technology.

As meniscus are under constant loading, we then conduct cyclic tensile testing on the sutured meniscus. Specifically, a complete radial tear is created at the center of the freshly excised bovine meniscus. The separated tissue flaps are subsequently sutured with either pristine or GAPS sutures. All specimens are then subjected to 10 cycles of 0 – 10 N preloading, followed by 500 cycles of 5 – 25 N loading to mimic the physiological loading conditions (*45*) (Fig. 5.9 A, B). Interestingly, we find that GAPS sutures can drastically decrease the gap formation between the sutured tissues. Pristine sutures result in over 5 mm gap, while only around 2 mm is formed when GAPS sutures are implemented (Fig. 5.9 C). No deknotting, knot sliding, or elongation of the suture thread are observed.

A post-testing examination reveals the cause of gap formation to be the plastic deformation/damage of the meniscus tissues compressed by the sutures. Evidently, pristine suture fiber induces significantly deeper indentation into the tissues compared to GAPS sutures, which can be visualized using two photon microscopy. We hypothesize that the adhesive gel layer of the GAPS suture can serve as a tough yet soft interface with native meniscus tissue, markedly lower the stress concentration and damage caused by stiff pristine suture fibers. Our findings indicate that GAPS sutures can potentially mitigate the tissue damage caused by traditional sutures, lower the failure rate of meniscus repair procedures and encourage surgeons to eventually steer away from the highly invasive meniscectomy surgeries.

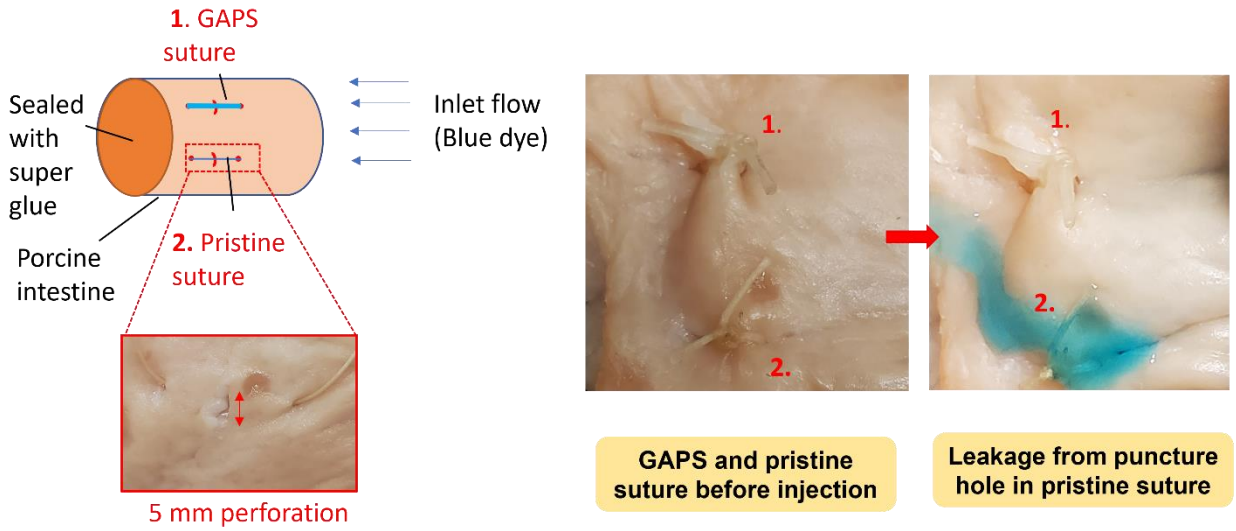

Fig. 5.10. Sealing performance of sutured intestine perforation with pristine or GAPS sutures.

Lastly, we demonstrate the advantage of GAPS suture for sealing intestinal perforation. GI perforation, including ones occur on stomach, large bowel and small intestine, can have devastating consequences of fluid leakage into the abdominal cavity, while allowing bacteria to enter the GI tract, leading to life-threatening conditions such as peritonitis. To characterize the fluid leakage prevention efficacy using sutures, we create a 5 mm diameter perforation on porcine intestine tissue. The defect is closed with either pristine or GAPS sutures. We seal one end of the intestine tube with glue, while injecting blue dye solution from the other end. We notice that no

leakage is observed when GAPS sutures is applied, but for pristine sutures, solution leakage occurred from the puncture hole (Fig. 5.10). It's worth noting that the source of the leakage is not from the perforation site, which is tightly closed by suturing and knotting. In fact, the needle punctured hole for passing sutures can still be a cause of fluid leakage which can be sealed with the newly developed GAPS suture.

5.3 Conclusion

In summary, we develop a novel suture device that can rapidly swell and adhere to diverse biological tissue for tight sealing to prevent leakage and serving as a biomimetic tough and soft interface to mitigate tissue damage caused by traditional sutures. We investigate the GAPS suture-tissue adhesion mechanism and kinetics, and validate their applications for meniscus repair and GI lesion sealing ex vivo. The novel GAPS suture device and the proposed swelling-adhesion strategy could be leveraged as an effective approach for the functionalization of other fiber-based devices, such as catheter, stent and coils, and inspire the design of novel medical devices for embolism, hemostasis and tumor treatment.

5.4 Materials and Methods

Fabrication of GAPS suture. First, the polyglactin 910 sutures (Coated VICRL, 2-0, Ethicon). was surface-treated with 1 M NaOH solution for 1 min and thoroughly rinsed with deionized water before air drying. The surface-activated suture was then inserted into a glass capillary tube (World Precision Instrument, TW120-6), which defines the thickness of gel sheath and provides a closed environment for polymerization. Chitosan powder (>95%; Lyphar Biotech) was dissolved at 2% concentration in 0.1 M HCl solution. The adhesive solution was fabricated by mixing EDC and NHS (Sigma-Aldrich) with the chitosan solution both at a final concentration of 20 mg/ml. It was then injected into the capillary tube through a 27-gauge needle (Sigma-Aldrich) to prime the suture surface for 10 min. Both double-network PAAm-alg hydrogel or single network PAAm hydrogel were prepared as the gel sheath. The prepolymer solutions for alginate-PAAm hydrogels contain 2% sodium alginate (high molecular weight, I1G, KIMICA Corporation), 16% acrylamide (Sigma-Aldrich), 0.01% N,N′-methylenebis (acrylamide) (MBAA; Sigma-Aldrich), 0.03% ammonium persulfate (APS; Sigma-Aldrich), and 0.46% tetramethyl-ethylenediamine (TEMED; Sigma-Aldrich). For PAAm hydrogel, two formulas with different monomer concentration were prepared. It contains 12% (or 24%) acrylamide, 0.02% MBAA, 0.03% APS, and 0.46% TEMED. To

fabricate the gel sheath, the prepolymer solution is injected into the capillary tube to replace the adhesive solution. After more than one-hour incubation to allow complete polymerization, the GAPS suture was retrieved from the tube and later immersed in 0.1 M $CaCl_2$ solution for 5 min, then air dried.

Characterization of suture-tissue adhesion. All tissues (porcine skin, heart, bone, intestine and bovine meniscus, tendon) used in the study were obtained from local slaughterhouse and stored -80 C before usage. The adhesion energy between the suture and the tissue sheath was characterized using a customized pull-out test with an Instron machine. Tissues specimen were cut into regular square shape with the same thickness. A puncture hole was created using needles of various sizes. Suture thread with length bigger than the thickness of the tissue was then placed inside the through-hole. For pristine sutures, the adhesion was characterized as prepared. For TGS sutures, saline (0.9% NaCl) solution was applied at the puncture site to allow the swelling of the TGS. For GAPS sutures, adhesive solution (chitosan/EDC/NHS) was applied at the puncture site to allow the swelling and adhesion of the sutures. Subsequently, two acrylic sheets were glued on the edge of the tissues as rigid constraints. The acrylic sheets are fixed on to the bottom grip of the Instron machine, while the exposed suture end was fixed on to the upper grip. The suture was pulled out unidirectionally at a displacement rate of 0.5 mm/s, while the force and the displacement were recorded. The adhesion energy was calculated using the form: $\Gamma = W_g t_g + W_t t_t$, where t is the thickness of the specimen, W is the strain energy of the sheared region under a critical load. The subscriptions stand g and t stand for the gel and the tissue, respectively.

GAPS suture for meniscal tear repair. Bovine menisci (n = 10) were dissected from bovine knees. On the menisci, a complete radial tear was performed. All specimen were separated in two groups and repaired using either pristine (n = 5) or GAPS (n = 5) with a single stitch and five knots. The repaired menisci were then clamped on an Instron machine. The specimens were cyclically preconditioned between 1 and 10 N for 10 cycles and then cyclically loaded for 500 cycles between 5 and 25 N at a frequency of 0.16 Hz. The specimens were then retrieved from the fixture and the tissue damage was first inspected by naked eyes. As shown in Figure 5.9 A, the gap formed between the tearing edges of the two tissue flaps was then measured using a caliper. The suture loop before and after testing was also measured to ensure that there was no suture elongation or loosening of the knot. To analyze the mechanical damage of sutures to the collagen fibers of the

meniscus after cyclic loading, the tissue flaps were cleared following an established protocol (*46*), then observed under a multi-photon microscope (Zeiss Axioexaminer).

GAPS suture for meniscal tear repair. Porcine intestine was cut into 3-cm long tubular specimens. One end of the intestine tube was sealed using Krazy glue. Two 5-mm diameter holes were created on the specimen juxtaposed with each other. They were sutured with either pristine or GAPS suture with a single stitch and 5 knots. Blue dye solution was prepared by mixing a concentrated blue food dye solution with water. The solution was injected into the tube using a syringe, until a leakage was observed from the sutured defects.

Reference

1. J. V. Clough, J. Alexander-Williams, Surgical and economic advantages of polyglycolic-acid suture material in skin closure. *The Lancet*. **305**, 194–195 (1975).

2. T. Mimae, T. Hirayasu, K. B. Kimura, A. Ito, Y. Miyata, M. Okada, Advantage of absorbable suture material for pulmonary artery ligation. *Gen. Thorac. Cardiovasc. Surg.* **58**, 511–515 (2010).

3. J. C. Slieker, F. Daams, I. M. Mulder, J. Jeekel, J. F. Lange, Systematic Review of the Technique of Colorectal Anastomosis. *JAMA Surg.* **148**, 190–201 (2013).

4. B. K. Milthorpe, Xenografts for tendon and ligament repair. *Biomaterials*. **15**, 745–752 (1994).

5. J. V. Novaretti, J. Lian, A. J. Sheean, C. K. Chan, J. H. Wang, M. Cohen, R. E. Debski, V. Musahl, Lateral Meniscal Allograft Transplantation With Bone Block and Suture-Only Techniques Partially Restores Knee Kinematics and Forces. *Am. J. Sports Med.* **47**, 2427–2436 (2019).

6. V. Tagliaferri, S. Ruggieri, C. Taccaliti, C. Gentile, T. Didonna, M. D'asta, F. Legge, P. Guida, G. Scambia, M. Guido, Comparison of absorbable and permanent sutures for laparoscopic sacrocervicopexy: A randomized controlled trial. *Acta Obstet. Gynecol. Scand.* **100**, 347–352 (2021).

7. R. Eickhoff, S. B. Eickhoff, S. Katurman, C. D. Klink, D. Heise, A. Kroh, U. P. Neumann, M. Binnebösel, Influence of suture technique on anastomotic leakage rate—a retrospective analyses comparing interrupted—versus continuous—sutures. *Int. J. Colorectal Dis.* **34**, 55–61 (2019).

8. G. Malapert, H. A. Hanna, P. B. Pages, A. Bernard, Surgical Sealant for the Prevention of Prolonged Air Leak After Lung Resection: Meta-Analysis. *Ann. Thorac. Surg.* **90**, 1779–1785 (2010).

9. S. Kathju, L. Nistico, L. Hall-Stoodley, J. C. Post, G. D. Ehrlich, P. Stoodley, Chronic Surgical Site Infection Due to Suture-Associated Polymicrobial Biofilm. *Surg. Infect.* **10**, 457–461 (2009).

10. J. K. Shin, M. S. Youn, Y. J. Seong, T. S. Goh, J. S. Lee, Iatrogenic dural tear in endoscopic lumbar spinal surgery: full endoscopic dural suture repair (Youn's technique). *Eur. Spine J.* **27**, 544–548 (2018).

11. D. M. Pagnanelli, T. G. Pait, H. V. Rizzoli, A. I. Kobrine, Scanning electron micrographic study of vascular lesions caused by microvascular needles and suture. *J. Neurosurg.* **53**, 32–36 (1980).

12. B. D. Owens, J. Algeri, V. Liang, S. DeFroda, Rotator cuff tendon tissue cut-through comparison between 2 high–tensile strength sutures. *J. Shoulder Elbow Surg.* **28**, 1897–1902 (2019).

13. S. P. Rodrigues, T. Horeman, J. Dankelman, J. J. van den Dobbelsteen, F.-W. Jansen, Suturing intraabdominal organs: when do we cause tissue damage? *Surg. Endosc.* **26**, 1005–1009 (2012).

14. A. J. Venjakob, P. Föhr, F. Henke, T. Tischer, G. H. Sandmann, F. Blanke, A. B. Imhoff, S. Milz, R. Burgkart, S. Vogt, Influence of Sutures on Cartilage Integrity: Do Meniscus Sutures Harm Cartilage? An Experimental Animal Study. *Arthrosc. J. Arthrosc. Relat. Surg.* **35**, 1509–1516 (2019).

15. E. B. Hunziker, A. Stähli, Surgical suturing of articular cartilage induces osteoarthritis-like changes. *Osteoarthritis Cartilage*. **16**, 1067–1073 (2008).

16. L. Shahinian, S. I. Brown, Postoperative Complications with Protruding Monofilament Nylon Sutures. *Am. J. Ophthalmol.* **83**, 546–548 (1977).

17. Y. S. Lee, J. Y. Jeong, C.-D. Park, S. G. Kang, J. C. Yoo, Evaluation of the Risk Factors for a Rotator Cuff Retear After Repair Surgery. *Am. J. Sports Med.* **45**, 1755–1761 (2017).

18. Z. Ma, G. Bao, J. Li, Multifaceted Design and Emerging Applications of Tissue Adhesives. *Adv. Mater.* **33**, 2007663 (2021).

19. J. Li, A. D. Celiz, J. Yang, Q. Yang, I. Wamala, W. Whyte, B. R. Seo, N. V. Vasilyev, J. J. Vlassak, Z. Suo, D. J. Mooney, Tough adhesives for diverse wet surfaces. *Science*. **357**, 378–381 (2017).

20. B. R. Freedman, A. Kuttler, N. Beckmann, S. Nam, D. Kent, M. Schuleit, F. Ramazani, N. Accart, A. Rock, J. Li, M. Kurz, A. Fisch, T. Ullrich, M. W. Hast, Y. Tinguely, E. Weber, D. J. Mooney, Enhanced tendon healing by a tough hydrogel with an adhesive side and high drug-loading capacity. *Nat. Biomed. Eng.*, 1–13 (2022).

21. S. O. Blacklow, J. Li, B. R. Freedman, M. Zeidi, C. Chen, D. J. Mooney, Bioinspired mechanically active adhesive dressings to accelerate wound closure. *Sci. Adv.* (2019), doi:10.1126/sciadv.aaw3963.

22. H. Yuk, J. Wu, T. L. Sarrafian, X. Mao, C. E. Varela, E. T. Roche, L. G. Griffiths, C. S. Nabzdyk, X. Zhao, Rapid and coagulation-independent haemostatic sealing by a paste inspired by barnacle glue. *Nat. Biomed. Eng.* **5**, 1131–1142 (2021).

23. Dennis Christopher, Sethu Swaminathan, Nayak Sunita, Mohan Loganathan, Morsi Yosry (Yos), Manivasagam Geetha, Suture materials — Current and emerging trends. *J. Biomed. Mater. Res. A.* **104**, 1544–1559 (2016).

24. A. A. Milne, W. G. Murphy, S. J. Reading, C. V. Ruckley, Fibrin sealant reduces suture line bleeding during carotid endarterectomy: A randomised trial. *Eur. J. Vasc. Endovasc. Surg.* **10**, 91–94 (1995).

25. W. D. Spotnitz, Fibrin Sealant: The Only Approved Hemostat, Sealant, and Adhesive—a Laboratory and Clinical Perspective. *ISRN Surg.* **2014**, 203943 (2014).

26. J. A. Rousou, Use of Fibrin Sealants in Cardiovascular Surgery: A Systematic Review. *J. Card. Surg.* **28**, 238–247 (2013).

27. B. R. Freedman, D. J. Mooney, Biomaterials to Mimic and Heal Connective Tissues. *Adv. Mater.* **0**, 1806695.

28. R. E. Abhari, J. A. Martins, H. L. Morris, P.-A. Mouthuy, A. Carr, Synthetic sutures: Clinical evaluation and future developments. *J. Biomater. Appl.* **32**, 410–421 (2017).

29. F. Alshomer, A. Madhavan, O. Pathan, W. Song, Bioactive Sutures: A Review of Advances in Surgical Suture Functionalisation. *Curr. Med. Chem.* **24**, 215–223 (2017).

30. M. Champeau, J.-M. Thomassin, T. Tassaing, C. Jérôme, Current manufacturing processes of drug-eluting sutures. *Expert Opin. Drug Deliv.* **14**, 1293–1303 (2017).

31. Z. Ma, Z. Yang, Q. Gao, G. Bao, A. Valiei, F. Yang, R. Huo, C. Wang, G. Song, D. Ma, Z.-H. Gao, J. Li, Bioinspired tough gel sheath for robust and versatile surface functionalization. *Sci. Adv.* **7**, eabc3012 (2021).

32. J. Yang, R. Bai, Z. Suo, Topological Adhesion of Wet Materials. *Adv. Mater.* **30**, 1800671 (2018).

33. T. Zhang, H. Yuk, S. Lin, G. A. Parada, X. Zhao, Tough and tunable adhesion of hydrogels: experiments and models. *Acta Mech. Sin.* **33**, 543–554 (2017).

34. Z. Yang, Z. Ma, S. Liu, J. Li, Tissue adhesion with tough hydrogels: Experiments and modeling. *Mech. Mater.* **157**, 103800 (2021).

35. S. Cai, Y. Lou, P. Ganguly, A. Robisson, Z. Suo, Force generated by a swelling elastomer subject to constraint. *J. Appl. Phys.* **107**, 103535 (2010).

36. F. W. Roemer, C. K. Kwoh, M. J. Hannon, D. J. Hunter, F. Eckstein, J. Grago, R. M. Boudreau, M. Englund, A. Guermazi, Partial meniscectomy is associated with increased risk of incident radiographic osteoarthritis and worsening cartilage damage in the following year. *Eur. Radiol.* **27**, 404–413 (2017).

37. W. Wilson, B. van Rietbergen, C. C. van Donkelaar, R. Huiskes, Pathways of load-induced cartilage damage causing cartilage degeneration in the knee after meniscectomy. *J. Biomech.* **36**, 845–851 (2003).

38. M. Doherty, I. Watt, PaulA. Dieppe, LOCALISED CHONDROCALCINOSIS IN POST-MENISCECTOMY KNEES. *The Lancet*. **319**, 1207–1210 (1982).

39. I. D. McDermott, A. A. Amis, The consequences of meniscectomy. *J. Bone Joint Surg. Br.* **88-B**, 1549–1556 (2006).

40. G. Nourissat, F. Berenbaum, D. Duprez, Tendon injury: from biology to tendon repair. *Nat. Rev. Rheumatol.* **11**, 223–233 (2015).

41. H. Kwon, W. E. Brown, C. A. Lee, D. Wang, N. Paschos, J. C. Hu, K. A. Athanasiou, Surgical and tissue engineering strategies for articular cartilage and meniscus repair. *Nat. Rev. Rheumatol.* **15**, 550–570 (2019).

42. G. R. Barrett, K. Richardson, C. G. Ruff, A. Jones, The effect of suture type on meniscus repair. A clinical analysis. *Am. J. Knee Surg.* **10**, 2–9 (1997).

43. E. Farng, O. Sherman, Meniscal repair devices: a clinical and biomechanical literature review. *Arthrosc. J. Arthrosc. Relat. Surg.* **20**, 273–286 (2004).

44. G. Y. Nakama, Z. S. Aman, H. W. Storaci, A. S. Kuczmarski, J. J. Krob, M. J. Strauss, Different Suture Materials for Arthroscopic Transtibial Pull-out Repair of Medial Meniscal Posterior Root Tears: A Human Biomechanical Study. *Orthop. J. Sports Med.* **7**, 2325967119873274 (2019).

45. Y. H. D. Lee, J. Nyland, R. Burden, D. N. M. Caborn, Cyclic Test Comparison of All-Inside Device and Inside-Out Sutures for Radial Meniscus Lesion Repair: An In Vitro Porcine Model Study. *Arthrosc. J. Arthrosc. Relat. Surg.* **28**, 1873–1881 (2012).

46. M.-T. Ke, S. Fujimoto, T. Imai, SeeDB: a simple and morphology-preserving optical clearing agent for neuronal circuit reconstruction. *Nat. Neurosci.* **16**, 1154–1161 (2013).

Chapter 6 Discussions

This thesis proposes various material system and apparatus to enable and control interfacial tough adhesion between biomaterials, biological tissues and biomedical devices. These novel materials design strategies have significantly expanded the material repertoire of tough adhesives, enriched the fundamental understanding of adhesion mechanisms, and suggested promise of clinical applications of these platform technologies for the repair and regeneration of mechanically active biological tissues. However, there are still multiple limitations of the proposed technologies, which demand further optimization and improvement, and are discussed herein. Following the proposed multifaceted adhesive design strategy detailed in Chapter 2, I discuss these aspects in the following categories: adhesive substrate, adhesive layer, adhesive matrix, external apparatus, translational potential, and future work.

6.1 Adhesive Substrate

The main focus of this thesis is placed upon a selected list of biological tissues substrate and suture surface. Strong adhesion is demonstrated on various tissues such as skin, buccal mucosa, tendon, meniscus and aorta. These tissues are of particular interest due to their large surface area, demanding mechanical functions, and recognized barrier effects. Tough bioadhesion are critically important for their reliable performance and/or has been challenging to form. With carefully designed adhesive material system, over 1000 J m^{-2} adhesion energy is achieved at those interfaces, among the highest reported in the literature (*1–3*). Additionally, with US mediated anchorage approach, we managed to significantly increase the intrinsic work of adhesion between hydrogel and biological tissues up to 60 J m^{-2}, which is even higher than when chemical reaction is used (*4*). However, this value is still markedly lower than the fatigue fracture threshold at the bone-tendon/ligament/cartilage interface (around 800 J m^{-2}) (*5*). Such high fatigue fracture threshold of hydrogel adhesion has been realized on synthetic materials (*6*), but the reported method is not biocompatible. Further efforts need to be dedicated to elevating the obtainable intrinsic work of adhesion to a level closer to or even higher than the highly fatigue-resistant biointerface inside the human body. This will allow us to expand the use of bioadhesives to reattach mechanically challenging bone-tendon or bone-ligament junctions, and to eventually replace invasive surgical procedures such as suturing. Regarding the obtained strong hydrogel coating on fiber-based medical devices such as surgical sutures, robust adhesion has been demonstrated on PLGA,

collagen and nylon. However, the main anchoring mechanism is still limited to carbodiimide chemistry. To further expand the tough adhesive functionalization for various other suture materials, other covalent bonding chemistry and physical anchoring strategies need to be explored. Although the aforementioned suture materials have found versatile usage for general surgeries, they're not the popular options chosen by orthopaedic surgeons to reattach meniscus, tendon or ligament. For example, FiberWire® Suture (Arthrex), constructed of a multi-strand, long chain ultra-high-molecular-weight polyethylene core with a braided jacket of polyester, is in fact the gold-standard suture materials due to their high strength and abrasion resistance. They're not compatible with the surface activation strategy proposed in the thesis. Innovative surface functionalization chemistries need to be adapted to enable the tough gel sheath formation on these suture materials.

6.2 Adhesive Layer

Throughout the thesis, chitosan is selected as a model anchoring adhesive material, due to the highly positively charged polymer chain which serves as an almost perfect interfacial bonding material for many negatively charged tissue surface and alginate within the polyacrylamide-alginate hydrogel matrix routinely used in the present study. Indeed, the toughest adhesion energy is achieved for both hydrogel-tissue and hydrogel-suture interface, compared to any other adhesive layer used in the thesis. This is consistent with previous pioneering work from Mooney and Li (*1*, *7*). Chitosan can also readily form a physical gel upon pH changes (*8*, *9*). The carbodiimide chemistry is also sensitive to pH (*10*). As a result, the adhesion relying on these interactions are also highly pH-dependent, leading to various levels of obtainable interfacial adhesion energy. It's expected that the adhesion formed using chitosan polymer within a relatively acidic environment (e.g., pH < 4.5) is rather low. However, this biochemical environment is quite common in gastrointestinal tissues and in diseased tissues (such as cancer). Chitosan has been suggested to accelerate haemostasis (*11*); consequently, these highly charged biopolymers are not very hemocompatible, causing concerns regarding their thrombus-inducing potential and their long-term implantation in cardiovascular systems. Thus, alternative adhesive layers need to be developed to address the limitations of these biopolymers. As discussed in Chapter 2, a class of mussel-inspired adhesives which relies on catechol chemistry have shown promise to be used as bioadhesives on diverse wet surfaces (*12*). The inclusion of catechol chemistry into the adhesive

layer design may potentially offer an eligible solution for robust adhesion in harsh underwater environment such as in blood or acidic environment (*13*, *14*).

6.3 Adhesive Matrix

In the thesis reported above, the highly stretchable and tough double network polyacrylamide-alginate (PAAm-alg) hydrogel is selected as a model adhesive matrix, due to its high toughness to effectively dissipate energy (*15*) and being soft enough to be compatible with the surface roughness of various biological tissues (*1*). The PAAm-alg hydrogel and its particular combination with the adhesive layer, chitosan/EDC/NHS, has been reported previously to achieve tough adhesion on diverse wet surfaces, and was recently applied for enhanced tendon healing (*16*). The proposed US-mediated anchorage approach in this thesis eliminates the need of using EDC/NHS and the non-orthogonal carbodiimide chemistry. Among the hydrogel matrix tested, PAAm-alg outperformed all other hydrogels, including another double-network hydrogel PNIPAm-alg and a single network hydrogel PAAm. Similar performance is observed for the reported TGS suture, where the highest suture-hydrogel adhesion energy is realized when PAAm-alg hydrogel is used, compared to double-network PAAm-chitosan hydrogel, and single-network PAAm and alginate hydrogel. It is hypothesized that this is mainly due to the high toughness of the PAAm-alg hydrogel matrix (>5000 J m^{-2}) compared to all other reported hydrogels used in the thesis. However, based on some of my preliminary studies, toughness alone does not dictate the obtainable adhesion energy, and the author has yet to enable even higher adhesion energy (e.g. over 2000 J m^{-2}) for hydrogel adhesion on biological tissues. As a matter of fact, merely increasing the toughness of PAAm-alg by increasing calcium concentration, lower bioadhesion is obtained (data not shown). The "side-effects" of increasing PAAm-alg toughness via the physical crosslinking of alginate is an increase in hydrogel stiffness, which is hypothesized to decrease its conformability to tissue substrate, and subsequent ineffective interfacial interactions through the adhesive layer. Many biological tissues such as skin and tendon have high toughness and energy-dissipation capability. Intuitively, these biological "tough composite hydrogels" seem to be the best candidate as adhesive matrix (*17*). However, while trying to adhere two pieces of skin or two tendon flaps with an adhesive layer (chitosan/EDC/NHS), only very modest adhesion can be achieved (data not shown). This further support the critical significance of the proposed material system design where all elements of the adhesive system and their interactions contribute to the obtainable adhesion energy.

Future studies may include the design and optimization of tough composite hydrogel possessing both extremely high toughness and tissue-mimetic surface softness, two seemingly contradictory properties.

Other limitations of the PAAm-alg used in the studies are their non-degradability, non-injectability and low fatigue-resistance. Degradability is an important consideration for implantable bioadhesives design to prevent the need of secondary surgeries to retrieve the administered adhesives when they're no longer needed. Degradable tough adhesives have been recently developed by incorporating degradable crosslinkers into the PAAm-alg matrix, such as poly(ethylene glycol) diacrylate (PEGDA) or hyaluronic acid methacrylate (HAMA) (*18*). Still, careful optimization of the degradation profile of the hydrogel adhesives is required to accommodate the mechanical requirement for the regeneration timeframe of the targeted tissues. An injectable tough adhesive is highly desired to realize the minimally invasive delivery of adhesives for the repair of internal organs. Up to now, no literature has been reported to enable the injectability of PAAm-alg without biocompatibility concerns. The monomer (acrylamide) for the fabrication of PAAm-alg is highly neurotoxic, and the polymerization reaction is very oxygen sensitive. To address the concerns of the usage of PAAm-alg, the author has recently developed an injectable adhesive that can toughen when exposed to body fluid. This work is in preparation for patent application and is thus not included in the thesis. Although PAAm-alg can effectively dissipate energy for tough adhesion under monotonic loading, it suffers from a common "disease" of polymeric materials, fatigue, due to the usage of the calcium-mediated physical crosslinking of alginate to enable the background hysteresis (*19*). Future investigations are needed to engineer fatigue-resistant adhesive matrix (*19–21*) with compatible fatigue-resistant adhesive layer to achieve fatigue-resistant bioadhesion.

6.4 External Apparatus

The proposed US-mediated bioadhesion approach has demonstrated markedly higher spatial control of the tough bioadhesion, but the resolution of the controllable adhesion remains low (centi-meter level) and is mainly limited by the size of the US transducer probe available in the lab. To be applied in delicate surgical procedures which requires micro-meter accuracy, the use of focused US should be explored. These focused US devices have been widely adopted in the clinics for tumor ablation (*22*) and to breach the blood-brain barrier for controlled drug delivery (*23*). By

leveraging the focused US to locally generate cavitation microbubble, one may precisely control the anchoring location of the primer materials and the subsequent precision bioadhesion. Additionally, the current US set-up used in the thesis is rather bulky, future US source can be customized with more elegantly designed piezo electric elements array and more operation flexibility regarding the US frequency, duration and intervals (*24*).

The proposed temporal control of the tough bioadhesion relies on a unique biopolymer, gelatin, and the thermal effects generated from the US transducer. The achievable adhesion energy is indeed significantly higher (over 200 J m^{-2}) compared to controls, but they're still markedly lower than other anchoring primer materials used in the study, such as chitosan polymer (>1000 J m^{-2}) and chitosan nanocrystals (> 500 J m^{-2}). It is hypothesized that the main difference is the presentation of the available primary amine groups on the polymer chain, which can form strong electrostatic interactions with both the hydrogel and the tissue. On the other hand, the upper critical solution temperature (UCST) of gelatin is around 30-35 °C, which is lower than the body temperature. In this thesis, as a proof of concept, the gelatin used is compatible with tough bioadhesion on skin surface which presents a temperature of around 34 °C. However, to be applied as implantable adhesives, further modification is required to adjust the UCST of gelatin to be above 37 °C.

Current fabrication of the TGS suture is low-throughput, due to the usage of capillary tube microreactors. The continuous fabrication of such suture can be potentially realized through carefully controlled rheological modification of the momnomer solutions to form thin coating on sutures with defined thickness, and/or use ultraviolet (UV) light to trigger rapid reaction. The use of microfluidics technologies to directly fabricate tough gel sheathed suture fibers could also be a promising solution (*25*).

6.5 Translational Potential

For US-mediated bioadhesion, only limited short-term biocompatibility tests are performed using a rodent model. Because of the drastic physiological and anatomical difference between rat and human, further validation and optimization on large animal and human cadaver is needed in the near future to identify the safety threshold of the applied US intensity, frequency, and duration. Regarding the translational potential of the proposed technologies, this thesis provides some limited proof-of-concept demonstrations of the capability of our functional adhesives for the

diagnostic, monitoring, and therapeutic intervention of a closed wound. For the advanced wound management functions demonstrated in the thesis, all the experiments were conducted in a carefully designed and controlled ex vivo environment. Further in vivo studies are required to test the proposed multifunctionality of the sutures when encountered in a complex biochemical and biomechanical environment. To explore GAPS sutures for meniscus repair, a preliminary study of repairing a complete radial tear has shown advantages over traditional sutures. However, in vivo investigations in small and big animals are demanded to confirm the actual therapeutic benefits of utilizing the newly developed surgical sutures for the repair of mechanically active biological tissues, such as tendon, meniscus and ligament.

Finally, the proposed tough adhesive functionalization on surgical sutures is in fact a compromise made partially due to the translational considerations regarding the indispensable role of these fiber-based devices widely applied in various surgeries. With a hope of eventually completely replacing relatively invasive surgical sutures with bioadhesives, disruptive technologies are in desire to address the aforementioned limitations of the material system design of adhesive substrate, adhesive layer, adhesive matrix and external apparatus.

6.6 Future Work

Building upon the proposed multifaceted adhesive hydrogel device design, there exists ample opportunities to further customize and engineer novel biomaterials and devices for biomedical applications. Examples include tendon repair, bleeding control and cancer treatment. The high-level summary and key hypotheses of these ongoing and future work are detailed below.

6.6.1 Tendon mimetic tough adhesive surgical suture for tendon repair

Tendon repair remains a major challenge for sport medicine due to tendon's demanding mechanical requirements and low healing capacity. For centuries, surgical sutures have been ubiquitously used for tendon rejoining and tendon-bone reattachment due to their high tensile strength and ease of operation. Numerous suturing techniques and anchoring devices have since been developed for the accountable integration of adjacent tendon/ligament/bone tissues.

However, sutures often cause significant stress concentration at the suturing roots, which is severed under constant loading, inducing additional tissue damage, gap formation, and even re-rupture. Alternative biomaterials have been recently developed to address these issues. In particular,

hydrogels have shown great promise for soft tissue repair because of their customizable chemical and mechanical properties, therapeutic functions and biocompatibility.

Inspired by the composite structure of tendon consisting of well-integrated collagen fibers and endotenon sheath, we recently developed a TGS suture with robust suture-gel interface (>2000 J m^{-2}), high tensile strength (GPa) and soft surface (kPa). The slippery TGS suture surface can readily support gliding, and can be functionalized with a tissue-adhesive surface on-demand, which can potentially lower stress concentration caused by traditional sutures and prevent gap formation thanks to the suture-tendon biointegration.

The TGS can be further engineered with antibacterial, drug delivery, pH sensing, and bioimaging functions for advanced wound management. By combining the merits of both suture and hydrogel, TGS sutures are expected to mitigate current limitations of commercialized sutures, while introducing paradigm-shifting therapeutic intervention for enhanced tendon repair.

6.6.2 Hemostatic suture for effective bleeding control

An unmet need for suturing during cardiovascular surgery is to control bleeding/leakage of blood vessels. To this end, an ideal suture should induce localized clotting to avoid bleeding/leakage at suturing roots. The development and evaluation of such sutures, termed as hemostatic sutures, is a valuable extension of this thesis work.

Based on the sheathed suture technology developed here, I plan to further engineer the hemostatic potential of the hydrogel sheath, capable of releasing coagulant thrombin to induce faster clotting, and/or with incorporated functional compounds to accelerate the intrinsic blood clotting cascade. A key hypothesis is that these sutures could induce clotting during suturing more effectively, and that the intrinsic design could localize clotting events, avoiding displaced clots into circulation that may induce micro-thrombosis and life-threatening complications such as stroke. Such sutures could make surgical procedures like anastomosis faster and safer, and mitigate postsurgical complications such as anastomotic failure.

The expected outcomes of this project include (1) novel hemostatic surgical sutures to mitigate complications like bleeding in general surgical procedures; (2) technological advancement in coating and functionalization of miniaturized biomedical devices; (3) understanding and controlling of blood-material interactions, particularly localized blood clotting.

6.6.3 Bioresponsive immunotherapeutic adhesive suture device to prevent pancreatic cancer recurrence

Beyond tissue repair applications, another promising research direction for the new surgical suture is cancer treatment. Pancreatic ductal adenocarcinoma (PDAC) is the 4th leading cause of cancer-related death; more than 5,000 Canadians die from this notorious disease every year. Surgical resection is the only potentially curative treatment option, however, with a median survival of less than 2 years due to high disease recurrence rate. Incomplete resection, particularly residual tumor at the surgical cutting and reconstruction site, is one of the major causes of local tumor recurrence and metastasis. Systemic administration of immunomodulatory therapeutics (e.g., anti-CD47) has been suggested to be a promising treatment strategy, but was recently shown to be associated with severe blood disorders. This issue calls for the invention of next-generation drug-eluting devices to locally manage PDAC to prevent tumor recurrence and metastasis.

Traditional sutures are usually used as passive mechanical devices to close up surgical wound and to attach remaining pancreas to the small intestine after tumor resection. I recently developed a multifunctional suture with sensing capability and high drug loading capacity at wound sites. I thus hypothesize that by engineering such smart suture devices that can mechanically and biologically integrate with tumor tissues, sense the microenvironment of residue tumor growth, and on-demand and locally deliver drugs blocking the “don’t eat me” signals expressed by cancer cells, we can trigger patient’s innate and adaptive immune system to eliminate the residue tumor, preventing both local tumor recurrence and distant metastasis after surgery. This proposed suture device is potentially applicable to all other malignancies that have a high local recurrence rate thus revolutionize cancer patient surgical care.

Chapter 7 Conclusion and Remarks

The motivation driving this thesis work centered around addressing the unmet challenges of engineering robust and versatile tough adhesion and integration of (1) synthetic hydrogels and biological tissues; (2) biomedical device and synthetic hydrogels; (3) biomedical device and biological tissues.

In this thesis, by leveraging clinically used ultrasound, I proposed a paradigm-shifting technology to achieve chemical-reaction-free tough bioadhesion with unprecedented spatiotemporal controllability. I thoroughly investigated its adhesion mechanism and demonstrated the potential of the platform for transdermal drug delivery. Next, I developed a bioinspired design of tough hydrogel sheath that can achieve the strong integration of diverse fiber-based materials and various hydrogels. This novel surface functionalization strategy mitigates the adverse mechanical properties of traditional biomedical devices, and unlocks their potential for advanced wound management. Finally, I invented a novel swellable and bioadhesive suture device based on the proposed interfacial adhesion mechanism. I studied the mechanism and kinetics of the swelling-adhesion at the hydrogel-tissue interface, and suggested their advantages in meniscal tear repair and intestinal lesion closure.

Taken together, the work presented in this thesis exemplifies and highlights the significance of multifaceted design in biomaterials innovation and biointerface science studies. By merging disciplines of mechanics, chemistry and biology, I proposed the design principles of next-generation biomedical adhesives, discovered the unrecognized role of ultrasound in manipulating bioadhesion, and attempted in translating the newly developed biomaterials/devices for regenerative medicine.

This is just the beginning towards understanding the complex interfacial science and applying the acquired knowledge for real-world applications. With the goal of an ultimate integration of synthetic materials and biological system, I'll dedicate my career to solving *tough* clinical issues with *tough* biomaterials design.

References

1. X. Zhao, X. Chen, H. Yuk, S. Lin, X. Liu, G. Parada, Soft Materials by Design: Unconventional Polymer Networks Give Extreme Properties. *Chem. Rev.* **121**, 4309–4372 (2021).

2. Z. Ma, G. Bao, J. Li, Multifaceted Design and Emerging Applications of Tissue Adhesives. *Adv. Mater.* **33**, 2007663 (2021).

3. J. Li, A. D. Celiz, J. Yang, Q. Yang, I. Wamala, W. Whyte, B. R. Seo, N. V. Vasilyev, J. J. Vlassak, Z. Suo, D. J. Mooney, Tough adhesives for diverse wet surfaces. *Science*. **357**, 378–381 (2017).

4. H. Yuk, C. E. Varela, C. S. Nabzdyk, X. Mao, R. F. Padera, E. T. Roche, X. Zhao, Dry double-sided tape for adhesion of wet tissues and devices. *Nature*. **575**, 169–174 (2019).

5. J. Chen, D. Wang, L.-H. Wang, W. Liu, A. Chiu, K. Shariati, Q. Liu, X. Wang, Z. Zhong, J. Webb, R. E. Schwartz, N. Bouklas, M. Ma, An Adhesive Hydrogel with "Load-Sharing" Effect as Tissue Bandages for Drug and Cell Delivery. *Adv. Mater.* **32**, 2001628 (2020).

6. X. Chen, H. Yuk, J. Wu, C. S. Nabzdyk, X. Zhao, Instant tough bioadhesive with triggerable benign detachment. *Proc. Natl. Acad. Sci.* **117**, 15497–15503 (2020).

7. B. R. Freedman, O. Uzun, N. M. M. Luna, A. Rock, C. Clifford, E. Stoler, G. Östlund-Sholars, C. Johnson, D. J. Mooney, Degradable and Removable Tough Adhesive Hydrogels. *Adv. Mater.* **33**, 2008553 (2021).

8. B. R. Freedman, A. Kuttler, N. Beckmann, S. Nam, D. Kent, M. Schuleit, F. Ramazani, N. Accart, A. Rock, J. Li, M. Kurz, A. Fisch, T. Ullrich, M. W. Hast, Y. Tinguely, E. Weber, D. J. Mooney, Enhanced tendon healing by a tough hydrogel with an adhesive side and high drug-loading capacity. *Nat. Biomed. Eng.*, 1–13 (2022).

9. S. Mitragotri, Healing sound: the use of ultrasound in drug delivery and other therapeutic applications. *Nat. Rev. Drug Discov.* **4**, 255–260 (2005).

10. F. Duck, T. Leighton, Frequency bands for ultrasound, suitable for the consideration of its health effects. *J. Acoust. Soc. Am.* **144**, 2490–2500 (2018).

11. S. Nam, D. Mooney, Polymeric Tissue Adhesives. *Chem. Rev.* **121**, 11336–11384 (2021).

12. X. Ni, C. Chen, J. Li, Interfacial fatigue fracture of tissue adhesive hydrogels. *Extreme Mech. Lett.* **34**, 100601 (2020).

13. J. Liu, S. Lin, X. Liu, Z. Qin, Y. Yang, J. Zang, X. Zhao, Fatigue-resistant adhesion of hydrogels. *Nat. Commun.* **11**, 1071 (2020).

14. S. O. Blacklow, J. Li, B. R. Freedman, M. Zeidi, C. Chen, D. J. Mooney, Bioinspired mechanically active adhesive dressings to accelerate wound closure. *Sci. Adv.* (2019), doi:10.1126/sciadv.aaw3963.

15. A. Fatimi, P. Chabrot, S. Berrahmoune, J.-M. Coutu, G. Soulez, S. Lerouge, A new injectable radiopaque chitosan-based sclerosing embolizing hydrogel for endovascular therapies. *Acta Biomater.* **8**, 2712–2721 (2012).

16. J. Yang, R. Bai, Z. Suo, Topological Adhesion of Wet Materials. *Adv. Mater.* **30**, 1800671 (2018).

17. S. A. Madison, J. O. Carnali, pH Optimization of Amidation via Carbodiimides. *Ind. Eng. Chem. Res.* **52**, 13547–13555 (2013).

18. B. Guo, R. Dong, Y. Liang, M. Li, Haemostatic materials for wound healing applications. *Nat. Rev. Chem.* **5**, 773–791 (2021).

19. C. Guyot, M. Cerruti, S. Lerouge, Injectable, strong and bioadhesive catechol-chitosan hydrogels physically crosslinked using sodium bicarbonate. *Mater. Sci. Eng. C.* **118**, 111529 (2021).

20. H. Lee, B. P. Lee, P. B. Messersmith, A reversible wet/dry adhesive inspired by mussels and geckos. *Nature*. **448**, 338–341 (2007).

21. A. H. Hofman, I. A. van Hees, J. Yang, M. Kamperman, Bioinspired Underwater Adhesives by Using the Supramolecular Toolbox. *Adv. Mater.* **30**, 1704640 (2018).

22. J.-Y. Sun, X. Zhao, W. R. K. Illeperuma, O. Chaudhuri, K. H. Oh, D. J. Mooney, J. J. Vlassak, Z. Suo, Highly stretchable and tough hydrogels. *Nature*. **489**, 133–136 (2012).

23. Z. Yang, Z. Ma, S. Liu, J. Li, Tissue adhesion with tough hydrogels: Experiments and modeling. *Mech. Mater.* **157**, 103800 (2021).

24. W. Zhang, J. Hu, J. Tang, Z. Wang, J. Wang, T. Lu, Z. Suo, Fracture Toughness and Fatigue Threshold of Tough Hydrogels. *ACS Macro Lett.* **8**, 17–23 (2019).

25. S. Lin, J. Liu, X. Liu, X. Zhao, Muscle-like fatigue-resistant hydrogels by mechanical training. *Proc. Natl. Acad. Sci.* **116**, 10244–10249 (2019).

26. J. Ni, S. Lin, Z. Qin, D. Veysset, X. Liu, Y. Sun, A. J. Hsieh, R. Radovitzky, K. A. Nelson, X. Zhao, Strong fatigue-resistant nanofibrous hydrogels inspired by lobster underbelly. *Matter*. **4**, 1919–1934 (2021).

27. C. Lovegrove, High-intensity focused ultrasound shows promise for noninvasive tumor ablation. *Nat. Clin. Pract. Oncol.* **3**, 8–9 (2006).

28. A. Abrahao, Y. Meng, M. Llinas, Y. Huang, C. Hamani, T. Mainprize, I. Aubert, C. Heyn, S. E. Black, K. Hynynen, N. Lipsman, L. Zinman, First-in-human trial of blood–brain barrier opening in amyotrophic lateral sclerosis using MR-guided focused ultrasound. *Nat. Commun.* **10**, 4373 (2019).

29. S. Li, J. Xu, R. Li, Y. Wang, M. Zhang, J. Li, S. Yin, G. Liu, L. Zhang, B. Li, Q. Gu, Y. Su, Stretchable Electronic Facial Masks for Sonophoresis. *ACS Nano* (2022), doi:10.1021/acsnano.1c11181.

30. X. Hu, M. Tian, N. Pan, B. Sun, Z. Li, Y. Ma, X. Zhang, S. Zhu, Z. Chen, L. Qu, Structure-tunable graphene oxide fibers via microfluidic spinning route for multifunctional textiles. *Carbon*. **152**, 106–113 (2019).